# Radiometric dating and stratigraphic reassessment of the Elliot and Clarens formations; near Maphutseng and Moyeni, Kingdom of Lesotho, southern Africa

Ms. Zandri Rademan, 16964063

Thesis presented in partial fulfilment of the requirements for the degree of Masters of Science at

University of Stellenbosch
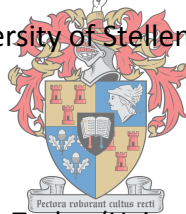
Supervisor: Dr. R. T. Tucker (University of Stellenbosch)

Co-advisor: Dr. E. M. Bordy (University of Cape Town)

Department of Earth Sciences

Faculty of Science

RSA

December 2018

DECLARATION

By submitting this dissertation electronically, I declare that the entirety of the work contained herein is my own, original work, that I am the sole author thereof (except where explicitly otherwise stated), that reproduction and publication thereof by Stellenbosch University will not infringe any third-party rights and that I have not previously in its entirety or in part submitted it for obtaining any qualification.

Date: December 2018

ACKNOWLEDGEMENTS

I am profoundly grateful to my family and friends for supporting me every step of the way. A very special thank you goes to my parents, who offered me financial, logistical and emotional support without which this project would not have been a success. Thank you to my mother for believing in me and supporting me through numerous emotional breakdowns. Thank you to my father for offering up his valuable time to become my field assistant, aiding with vital solutions to problems I was too blind to see and lending a critical eye when needed. Thank you to my brother who kept a sense of humour when I had lost mine. Ek is verskriklik lief vir julle. A heartfelt thank you goes to my horses, who kept me grounded and sane throughout this entire experience. Lastly, but most importantly, may all of the glory go to the Lord our God.

ABSTRACT

The Elliot and Clarens formations (Stormberg Group) of the Karoo Supergroup famously preserve not only a dynamic suite of depositional environments spanning the Late Triassic to Early Jurassic, but also boast a diverse assemblage of trace and body fossils. Due to the nature of these assemblages spanning the globally correlative Triassic-Jurassic Boundary (TJB) and end-Triassic Extinction Event (ETE), the accuracy of temporal placement and correlation via the stratigraphic framework is paramount. Yet, a distinct lack of robust temporal framework and inconsistencies between the bio-, magneto- and lithostratigraphic records persist. This project sought to provide localized context for three key fossil-bearing localities (southwestern Lesotho), which could thereafter be applied both at a regional and global scale. In-depth facies, palaeocurrent and architectural element analyses illustrated an overall increase in palaeoclimatic aridity, as evidenced by the change in depositional system from the meandering fluvial dominated lower Elliot Formation to the aeolian Clarens Formation. Detrital zircon geochronology ascertained a temporal framework ranging from the Norian to Pliensbachian (216.7-190.5 Ma) Elliot Formation to the Sinemurian to Pliensbachian (190.5-186.7 Ma) Clarens Formation. These temporal constraints also support the presence of a regional paraconformity at the lower and upper Elliot contact. The geochronology additionally indicated a shared source provenance of recycled grains from the Cape Supergroup and older Karoo strata, interspersed with direct source inputs from proximal magmatic/metamorphic provinces. Ultimately, the greater temporal and palaeoecological resolution provided by this study promotes the better understanding of the early Mesozoic history of southern Gondwana and lays the foundations for future geochronological investigations.

Table of Contents

List of Figures

List of Tables

1   INTRODUCTION

The Elliot Formation primarily became famed for its world-renowned continental 'red-bed' successions, which hosts some of the world's key Triassic-Jurassic fossil material. A distinct disparity pertaining throughout the various groups of taxa hosted in the Late Triassic and Early Jurassic sedimentary units indicated the probable palaeoecological influence of the Triassic-Jurassic Boundary (TJB) and end-Triassic Extinction Event (ETE; Olsen and Galton, 1984; Smith and Kitching, 1997; Lucas and Hancox, 2001; Knoll, 2004; Knoll, 2005; Olsen et al., 2011; McPhee et al., 2017). Contention regarding the precise TJB location within the stratigraphic record is prevalent, especially within the southern hemisphere (e.g., Turner, 1999; Bordy et al., 2004a, b, c; Smith et al., 2009; Sciscio et al., 2017a; McPhee et al., 2017). Opportunities to resolve this uncertainty lies within the Elliot and Clarens formations of the Stormberg Group, which are particularly abundant in the more eroded, outcrop-rich western Lesotho. Resultantly, the three primary study localities of this investigation are in Quthing (Moyeni), Masitise and Maphutseng—all of which are prominent for hosting an abundance of well-preserved, fossil-rich Elliot and Clarens outcrops (Fig. 1; 2). Altogether, a total of nine (9) key sites were established throughout the study areas, providing a large range of lateral and vertical morphologies used in this study (Fig. 2).

The Karoo Basin of southern Africa contains a clastic sedimentary rock record spanning the Late Carboniferous-Early Jurassic (Fig. 1). The Karoo Supergroup provides key information on the geochronological, litho-, bio- and magnetostratigraphic record of southern Africa (e.g., Du Toit, 1939; 1954; Haughton, 1969; Kitching, 1977; Smith, 1990; Johnson et al., 1996; Bangert et al., 1999; Rubidge, 2005; Johnson et al., 2006; Barbolini, 2014; Sciscio et al., 2017a; Viglietti et al., 2018). The upper part of the Karoo succession, the Stormberg Group, is particularly abundant in Late Palaeozoic-very early Mesozoic trace and body fossil assemblages, currently used in the schematic

biozonation schemes of the region (e.g., Ellenberger, 1970; Kitching and Raath, 1984; Olsen and

Galton, 1984; Lucas and Hancox, 2001; Knoll, 2004; Knoll, 2005).
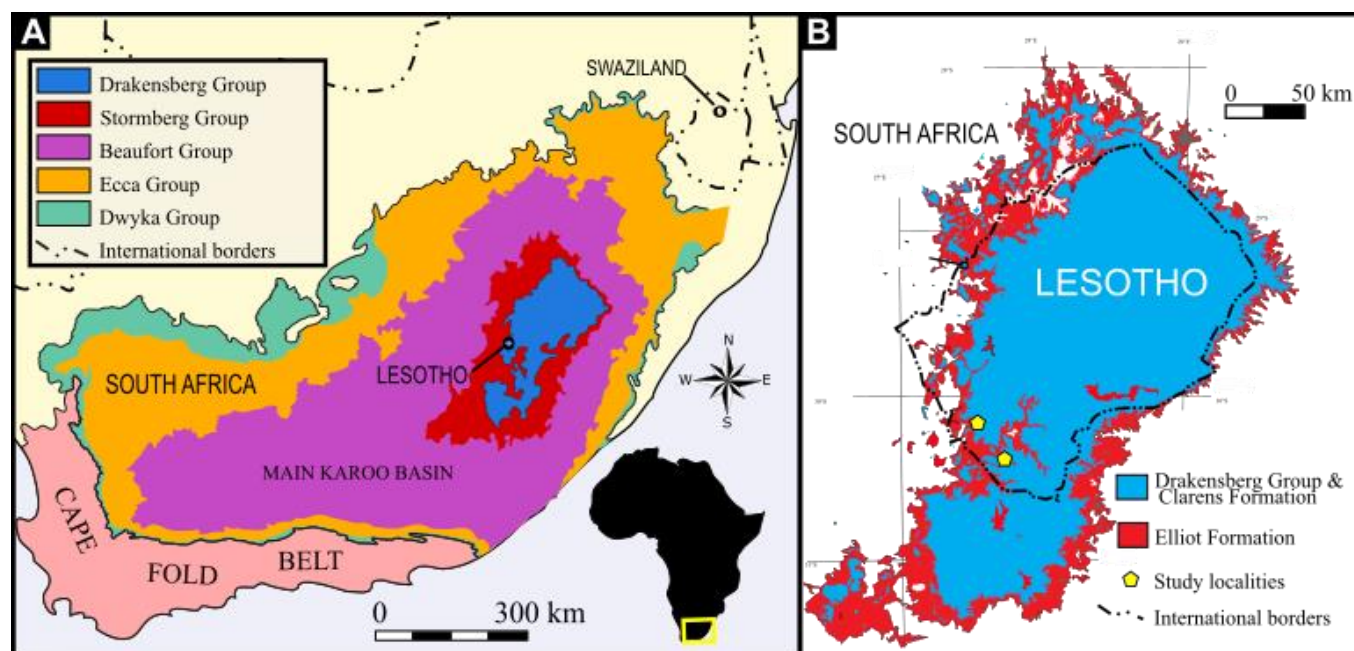
Fig. 1: The Kingdom of Lesotho's Stormberg Group elements host some of the world's most famous palaeontological finds. Figures A and B show more exact locations of this study's sites within the Kingdom of Lesotho. Figures modified after Bordy et al. (2004b).

The Karoo Supergroup extends over a period in which two global mass extinctions have been

identified in the fossil record across the Permian-Triassic (PTB ~251.0 Ma) and the Triassic-Jurassic

(TJB ~201.3 Ma) boundaries. These events are marked by the global extinctions of several taxonomic

groups, marine and terrestrial biota alike—at rates far higher than regular background levels of

taxonomic turnover (Sepkoski, 1982). Colbert (1958) and Newell (1963) provided some of the first

accounts of the biological turnover in both terrestrial and marine strata across the TJB, however

these preliminary reports of biodiversity changes were found to coincide with the end-Triassic

extinction (ETE) event—which predated the TJB. Further concrete work on the ETE has been sparse,

however has recently become increasingly more widespread (Hallam, 2002; Tanner et al., 2004;

Whiteside et al., 2010; Blackburn et al., 2013; Wotzlaw et al., 2014; Kent, et al., 2017). The TJB and

ETE placements are commonly associated with biostratigraphic, geochemical, chronostratigraphic

and palaeomagnetic shifts (e.g., Raup and Sepkoski, 1982; Beerling and Berner, 2002; Tanner et al.,

2004; Blackburn et al., 2013; Wotzlaw et al., 2014; Kent, et al., 2017). Both ichnofossil and body

fossil material, in conjunction with recently attained magnetostratigraphic profiles, have aided in providing a tentative global correlative TJB placement within the Elliot Formation (Kitching and Raath, 1984; Olsen and Galton, 1984; Anderson et al., 1998; Rubidge, 2005; Sciscio et al., 2017a). The biozonation of the richly fossiliferous Elliot Formation by Kitching and Raath (1984) has been reviewed by various authors in the past three decades (Lucas and Hancox, 2001; Knoll, 2004: 2005; Sciscio et al., 2017a), however no prominent changes have been made since. This is mainly due to the lack of radiometric dates for the entire Stromberg Group. The age of the latter is mainly inferred by the U-Pb derived data from the overlying Drakensberg Group (Duncan et al., 1997; Jourdan et al., 2005). The lack of a well-constrained stratigraphic framework beckons for further temporal resolution. The need for absolute age controls has recently become more prevalent, with advances in detrital zircon geochronology proving that global stratigraphic correlations solely based on largely lithostratigraphic dependent biostratigraphic correlations are tenuous at best (Fildani et al., 2003; Surpless et al., 2006; DeCelles et al., 2007).

Hence. this study primarily aims to crucially expand and refine the Elliot and Clarens chronostratigraphic framework through radiometric U-Pb (LA-ICPMS) detrital zircon dating, providing local absolute maximum depositional ages. The geochronology also provides a novel look into Stormberg Group sedimentary provenance, dispersal patterns and tectonic resolution, further improving the quality of original lithological and palaeocurrent derived provenance and tectonic patterns presented by the likes of Botha (1968), Eriksson (1983; 1985), Visser (1984), Johnson (1991), Smith et al. (1993), Catuneanu et al. (1998), Turner (1999) and Bordy et al. (2004a, b, c, d). Localised sedimentological analyses seek to provide further detailed resolution to the regional exposures of Elliot and Clarens units, reinvestigate the stratigraphic position of the ichnologically significant study sites and possible lateral continuity of marker units, previously studied by Bordy (2004a, b, c, d), Smith et al. (2009) and Bordy and Eriksson (2015). Subsequent robust palaeoenvironmental reconstructions further determine basinal sediment source patterns and provenance.

This study provides much needed accurate geochronological context, correlative palaeoenvironmental interpretations, provenance patterns and relevant palaeoecological changes for Late Triassic-Early Jurassic fossil-rich sediments. Ultimately, this study facilitates high-resolution investigations of individual bone-bed and ichno-sites in southern Africa, allowing for further resolution and correlation studies in both local and global Triassic-Jurassic stratigraphic, magnetostratigraphic, biostratigraphic and geochronological records. The increased temporal resolution will aid in marking temporal changes regarding the palaeo-fauna and -flora across the TJB, both locally and globally. Absolute age controls of the local litho- and biostratigraphy will additionally aid in marking relevant palaeoecological changes and biotic adaptations prior and synchronous to the Early Jurassic in southern Africa.
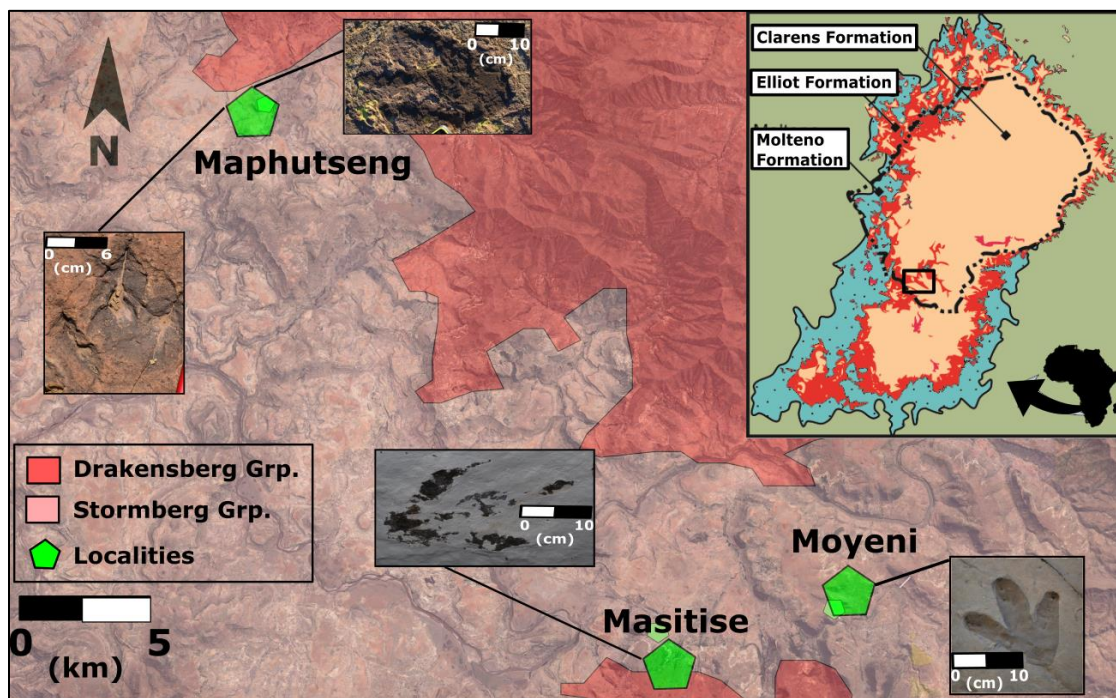
Fig. 2: Regional geological map of the Kingdom of Lesotho. Green markers illustrate the positions of the three main data collection localities, namely Quthing (Moyeni), Masitise and Maphutseng. Modified after Council of Geoscience's Online Simplified Geological Map of South Africa, Google Earth (2018) and Bordy et al. (2004b). Note: inserted trackway images show approximate locations for known and new trackway sites.

2   GEOLOGICAL BACKGROUND

2.1   Basin Setting

The understanding of the tectonic model of the Karoo Basin has varied greatly over the last four decades. The impressive Karoo Basin deposits (covering several hundred thousand square kilometres) was described by Rust (1975) as a tectono-sedimentary basin. This train of thought was further modified to include an orogenic model (sans subduction) as suggested by Hälbich (1983) and a continent-continent collision model (including southward subduction) by Winter (1984). The majority of authors however tend to agree upon a retro-arc foreland basinal system model (Lock, 1978; Lock, 1980; de Wit et al., 1988; Johnson, 1991; Cole, 1992; Catuneanu et al., 1998; Hansma et al., 2016).

The retro-arc foreland basin model was refined by extensive studies by Visser (1984; 1986; 1989; 1990; 1992), de Wit and Ransome (1992), Johnson et al. (1997), Catuneanu et al. (1998) and Catuneanu (2004) and is the best supported model for the resultant Pan-Gondwanian fold and thrust belt, the Cape Fold Belt (CFB). The CFB formed during the Cape orogeny as a direct result of the Late Carboniferous-Early Triassic northward shallow-angle subduction of the Carboniferous Panthalassan palaeo-Pacific beneath the southern Gondwana convergent margin (Fig. 3) (Lock, 1978; de Wit et al., 1988; Johnson 1991; de Wit and Ransome, 1992; Johnson et al., 2006; Tankard et al., 2009). A further indicator of subsidence, from a stable passive to an active margin, includes the development of a magmatic arc at the southern Gondwana subduction (Pysklywec and Mitrovica, 1999). The breakup of Gondwana in the Early Jurassic subsequently resulted in the fragmenting of the CFB in the early Mesozoic (Catuneanu et al., 1998; 2005). The Karoo Basin subsidence was likely brought on by the wide-scale lithostratigraphic uplift associated with the Mid-Carboniferous development of Pangea, illustrated by the bio- and lithostratigraphically derived unconformable contact (~23 Ma) between the uppermost Witteberg Group (Cape Supergroup) and overlying Dwyka

Group (Karoo Supergroup) contact (Visser, 1990; Streel and Theron, 1999; Gradstein et al., 2004; Catuneanu, 2005; Tankard et al., 2009).

Although the retro-arc foreland basin model has widely been considered by the likes of Johnson (1991), Cole (1992), Catuneanu et al. (1998; 2005) and Isbell et al. (2008), challenging models and hypotheses have questioned the inconsistencies associated with this primarily flexural tectonic sourced, compressional retro-arc, orogenic load CFB model (Fig. 3). A few of these models include: a thin-skinned folding model (Lindeque et al., 2011), thick-skinned thrusting (Paton et al., 2006), the subduction-induced mantle flow controlled basinal crustal uplift model and subsequent fault dominated subsidence (Tankard et al., 2009; Tankard et al., 2012) and lack of sutures and horizontal lineations to account for the retro-arc models (Tankard et al., 2009). A thermal anomaly driven updoming and pre-Karoo volcanism crustal extension model was suggested by Turner (1999), which took into account the fining upward sequences in the upper Karoo, Stormberg Group's continental sediments. The Stormberg Group, however, also shows at least two separate coarsening upward sequences throughout its stratigraphy (Bordy et al., 2004b, d). A general lack in Karoo lithologies' standardized radiometric age constraints and incomplete bio-records limit the resolution for these tectonic interpretations (Turner, 1999).

The continental main Karoo Basin, described by Catuneanu et al. (1998) as the Karoo Foreland Basin, developed as a response to supralithospheric flexural loading in the CFB, whereby basinal fill was derived from the CFB (Hälbich, 1983; Cole, 1992; Johnson et al., 2006). Basinal fill, which was originally thought to be connected to a single subsiding basin, is interpreted as the interplay amongst varying degrees of tectonically controlled subsidence and sedimentation rates of varying hierarchical levels (Rust, 1959; Rust, 1975; Turner, 1975; Cole 1992; Veevers et al., 1994). The Karoo Basin unconformably overlies the Namaqua-Natal Metamorphic Belt toward the south and west and the Archean Kaapvaal Craton towards the north. Consequently, the contact of the Kaapvaal Craton

and Namaqua-Natal Metamorphic Belt underlies the current day Kingdom of Lesotho (e.g.,

Barthelemy and Dempster, 1975; Barthelemy, 1976; Schmitz and Rooyani, 1987).
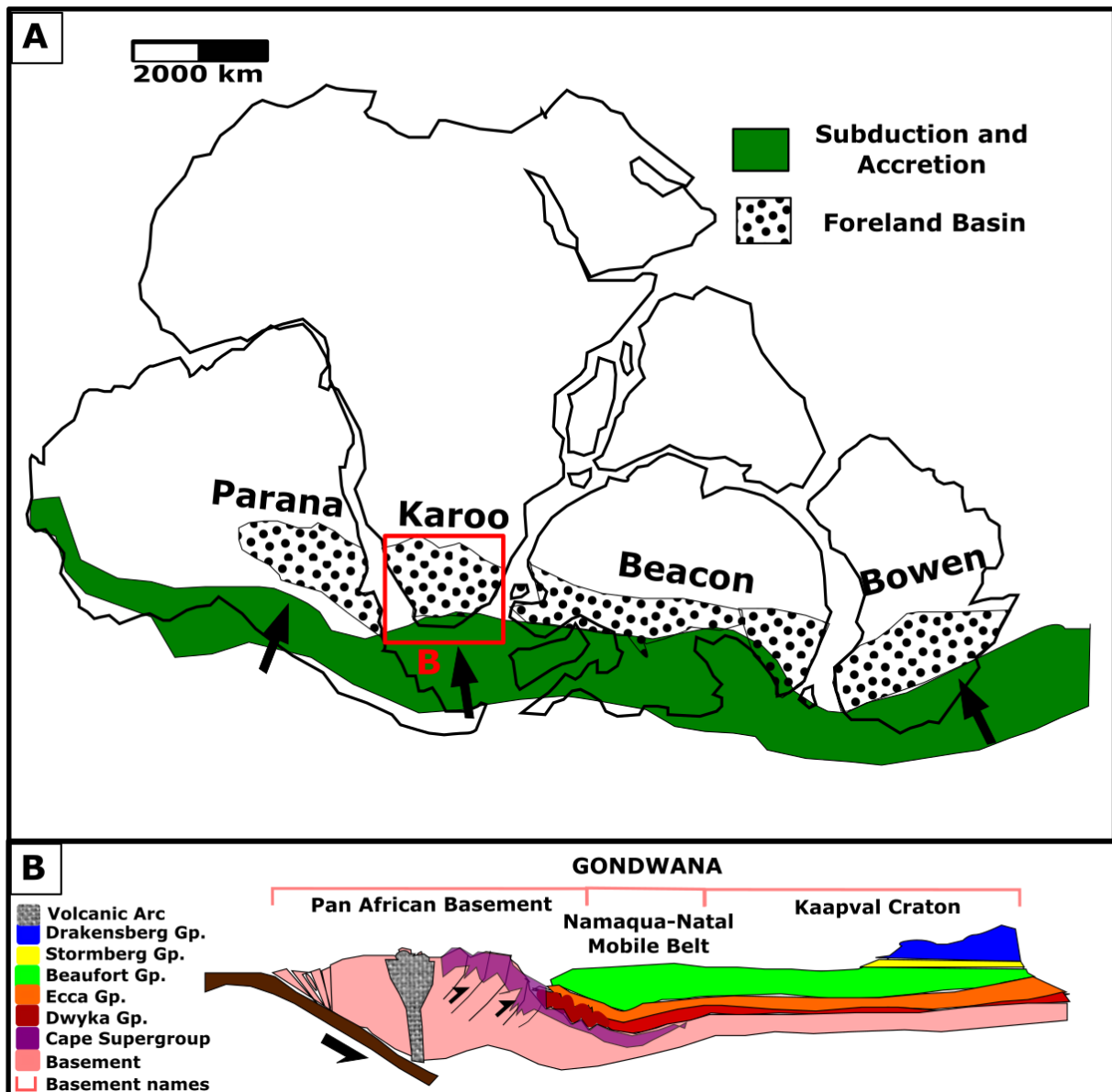
Fig. 3: Palaeogeography of Gondwana (A) and cross-sectional reconstruction along its southern margin (B), clearly illustrates the subduction from S to N. (A) The foreland systems are a result of the back-arc infill of the subducting and accreting southern margin. This subduction resulted in the fold-thrust compressional belt associated with the Cape Fold Belt of southern Africa (modified after de Wit, 1992; Turner, 1999; Catuneanu, 2004). (B) The Karoo Basin of southern Africa is schematically simplified in a SW-NE cross-section to present the formation of the Karoo retro-arc foreland basin. Illustration not to scale and vertically exaggerated (modified after Catuneanu et al.,1998; Woodford and Chevallier, 2002; Catuneanu, 2004).

The supracrustal loading orogen (CFB) of the favoured retro-arc foreland basin model presents

the partitioning of the foreland system into the foredeep, forebulge and back-bulge (Fig. 4). These

flexural provinces form part of the main contributing constituents of the Karoo Basin subsidence

(Catuneanu et al., 1998; Pysklywec and Mitrovica, 1999; Catuneanu et al., 2002; Catuneanu, 2004; Catuneanu et al., 2005). The final fluvial-aeolian dominated sequence of the first-order orogenic unloading of the Karoo Basin, the Stormberg Group, was deposited on the distal forebulge of the overfilled phase of the foreland basin (Fig. 4) (Catuneanu et al., 1998; Catuneanu, 2004; Hancox, 1998 [Unpublished]). Periods of flexural uplift within the overfilled Stormberg Group basinal deposition resulted in hiatus periods in an otherwise foresag dominated fluvial deposition (Fig. 4).

According to the foreland basin model, the upper Karoo hosts a total of four unconformities (Cole, 1992; Anderson and Anderson, 1993; Veevers et al., 1994; Johnson et al., 1997). Two distinct unconformities within the Stormberg Group include a third-order, ~12 Ma event at the base of the Molteno Formation (~223.0 Ma; referred to as the 'Mid-Triassic Lacuna' and 'Ladinian Gap') and a second-order event at the Molteno-Elliot formations contact (~215.3 Ma). These unconformities were found to closely correlate to syntectonic orogenic unloading hiatuses, likely associated with two small orogenic tectonic events (Hälbich et al., 1983; Cole, 1992; Gresse et al., 1992; Anderson and Anderson, 1993; Veevers et al., 1994; Catuneanu et al., 1998; Bordy et al., 2005; Blewett and Phillips, 2016). These tectonic events are puntuated with upward coarsening sequences, attributed to the increase in proximal topographic slopes (flexural subsidence) and fluvial depositional energy (Catuneanu, 1998; Bordy, et al., 2004a). Another notable unconformity within the Stormberg Group includes the paraconformity within the Elliot Formation (Bordy et al., 2004a, b, c, d; Bordy and Eriksson, 2015).
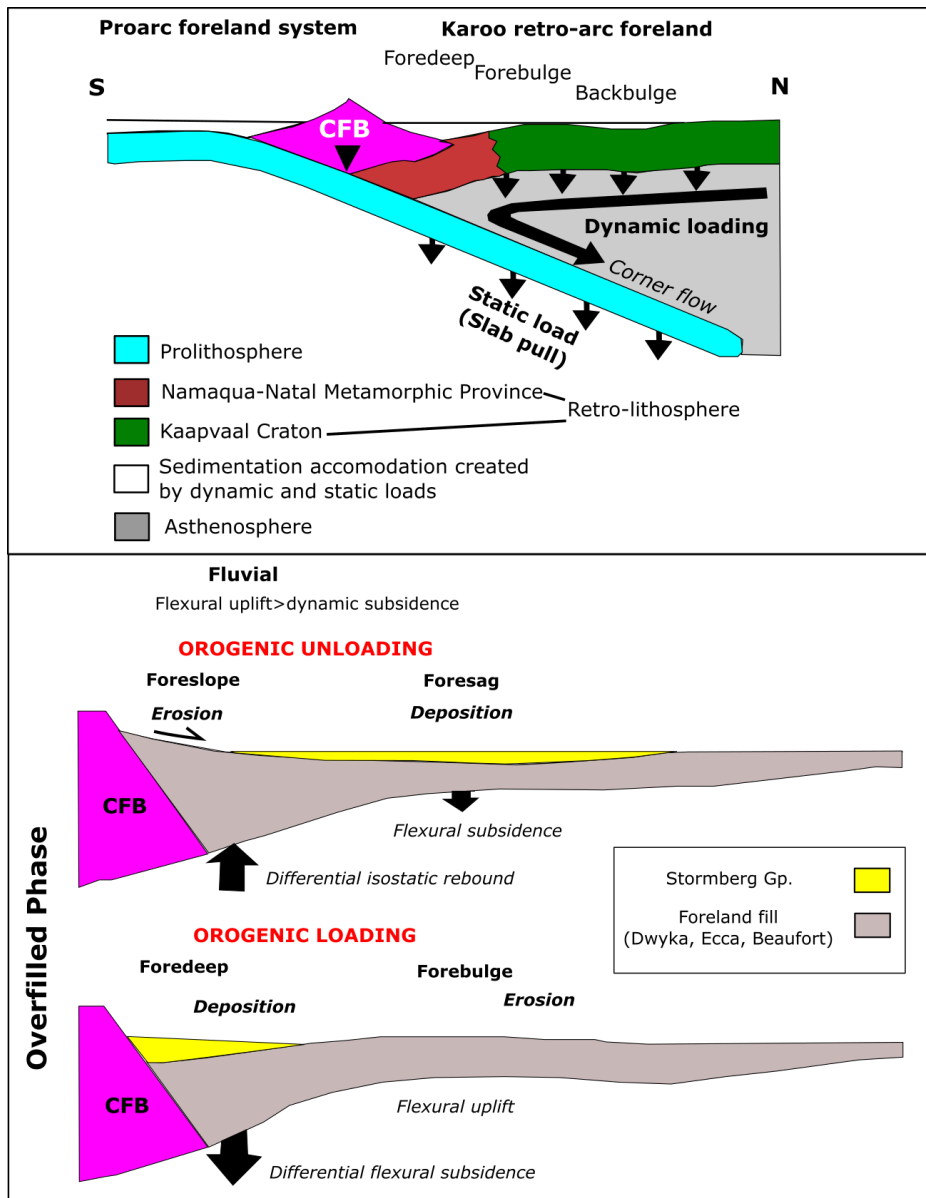
Fig. 4: A composite overview of the formation of the Karoo retro-arc foreland system the associated tectonic controls. The figure also illustrates schematic diagrams of the overfilled phase Stormberg Group deposition and the corresponding effects of flexural uplift and dynamic subsidence with regard to foreland fill patterns. Figures modified after Catuneanu et al. (1998) and Catuneanu (2004).

The various units of the famous Karoo Supergroup form an amalgamated system of diverse depositional facies. The first-order basinal deposition of the Karoo Supergroup has been linked as a direct response to two main allogenic controls, namely climate and tectonism. Intra-basinal tectonic controls of the Karoo Basin, in conjunction with a gradual, increasingly arid, climatic shift from the Late Carboniferous-Early Permian to Early Jurassic allowed for the variation in sedimentary provenance (e.g., Tankard et al., 1982; Visser, 1991; Cole, 1992; Catuneanu et al., 1998; Catuneanu et al., 2005). These deposits range from the oldest, Late Carboniferous glacial Dwyka Group (Visser,

9

1986; Cole, 1992; Johnson, 1994) to the conformably overlying deep to marginal marine Ecca Group (Johnson, 1976; Visser and Loock, 1978; Cole, 1992; Smith et al., 1993; Johnson, 1994; Rubidge et al., 2000). The Ecca Group diachronously regressed toward the overfilled phase, predominantly fluvio-lacustrine dominated, Permian-Triassic Beaufort Group (Johnson, 1966; Johnson, 1976; Visser and Loock, 1978; Turner, 1985; Smith, 1987; Smith, 1990; Smith et al., 1993; Johnson and Le Roux, 1994; Smith, 1995; Neveling, 2004) and finally, the unconformably overlying, increasingly arid, fluvial-aeolian dominated Triassic-Jurassic Stormberg Group (Visser, 1984; Eriksson, 1981; Eriksson, 1986; Bordy and Catuneanu, 2001; Bordy et al., 2004a, b, c, d; Bordy and Eriksson, 2015). The Stormberg Group interstitially presents numerous periods of tectonically driven hiatuses, smaller frequent periods of pedogenesis and pre-Karoo Large Igneous Province (LIP) Early Jurassic extensional tectonism features through palaeocurrents, normal faults and provenance indicators (Bordy et al., 2004a, b, c, d; Bordy et al., 2005; Bordy and Eriksson, 2015). These sediments present the final-phase deposition and are capped by the rifting induced Drakensberg Group extrusions (183.0 Ma), forming part of the massive Early Jurassic Karoo LIP (Johnson, 1994; Duncan et al., 1997; Marsh et al., 1997).

2.2   Stormberg Group

The Stormberg Group comprises of the Molteno, Elliot and Clarens formations, constituting of fluvial to aeolian dominated sedimentary facies. These deposits host crucial biostratigraphically significant fossiliferous units, used primarily in global correlations to units pertaining within the Late Triassic-Early Jurassic (Kitching and Raath, 1984; Olsen and Galton, 1984; Lucas and Hancox, 2001; Knoll, 2004; Knoll, 2005). The Stormberg Group stratigraphically represents the youngest deposited sedimentary strata of the Karoo Supergroup, unconformably underlain by the Beaufort Group and capped by the Drakensberg Group (Turner, 1969; Cole, 1992; Catuneanu et al., 1998). The sedimentary units are subdivided according to variations in grain size, structures, lithologies, associated biotic components, colour analyses and facies architecture. This lithological tripartite subdivision includes the lowermost, coarse-grained meandering and braided stream facies

dominated Molteno formation, the finer grained meandering stream and flood basin to aeolian facies dominated Elliot Formation (subdivided into the upper and lower Elliot) and the primarily aeolian derived thick cross-bedded sandstone beds of the Clarens Formation (Haughton, 1924; Beukes, 1970; Rust, 1975; Eriksson, 1981; Turner, 1983; Visser, 1984; Eriksson, 1986; Smith, 1990; Johnson, 1991; Anderson et al., 1998; Bordy et al., 2004a, b, c, d).

The Stormberg Group exposures are limited to the central to north-eastern Lesotho Highlands. This spatial distribution was originally attributed to the gradual decrease in syndepositional supply during the deposition of the unit in the Late Triassic and Early Jurassic (Cole, 1992). However, this theory was later revised due to the discovery of xenoliths from the Stormberg and Drakensberg Groups found within kimberlite pipes west and south-west of the current day exposures. Thus, lateral continuity of the Stormberg Group could be confirmed (Hanson et al., 2009). The units within this group tend to show very little changes in facies associations along its lateral extent. These units hold important climatic features from the worldwide Late Triassic-Early Jurassic boundary (TJB) extinction event and post boundary faunal and floral diversification, with palaeodepositional changes noted from the fluvial and coal-bearing Molteno to the aeolian Clarens Formation (Eriksson,1985; Bordy et al., 2004a, d). Based on palaeocurrent datasets, the Upper Karoo sediment sources were found to originate primarily from southern, south-eastern and minor western sources (the latter only valid for the uEF and Clarens Formation), with previous works linking the sediment input to plausible sources of the CFB and older Karoo Supergroup sediments (Catuneanu et al., 1998; Bordy et al., 2004a, b; Bordy and Head, 2018 (In Press)).

2.2.1   Elliot Formation

The continental 'red-beds', formally known as the Elliot Formation, forms part of the mid- to upper-Stormberg Group. The Elliot Formation is famous for not only its rich fossiliferous beds, but also the gradual aridification in palaeoclimatic conditions highlighted by a distinct variance in fluvial deposition associated with the Triassic-Jurassic Boundary (Du Toit, 1954; Visser and Botha, 1980;

Kitching and Raath, 1984; Smith, 1990; Bordy et al., 2004a, b, c). The Elliot Formation consists primarily of continental maroon and less common green mudstones and siltstones, alternating with fine- to medium-grained competent sandstones deposited by fluvial, lacustrine and aeolian systems (Botha, 1968; Le Roux, 1974; Johnson, 1976; Eriksson, 1983; Smith et al., 1993; Johnson et al., 1996; Bordy et al., 2004a, b, c, d). The beds of the Elliot Formation and overlying Clarens units are slightly tilted (<5°) throughout the field sites, with a negligible effect on stratigraphic thickness and internal structures. The Formation shows relative thicknesses ranging from ~460 m in the south to ~70 m in the northern basin (Bordy et al., 2004c).

There is a reasonably large database of dinosaur fossils and trackways within the Elliot Formation of Lesotho, based primarily on work done by Ellenberger (1970). Focused sedimentological lithological and concurrent basin-wide facies interpretations of the Elliot Formation were attained by Bordy et al. (2004a, b, c, d). The Formation shows two distinct units with local and regional differences in provenance, petrography and sedimentary structures (including facies assemblages and denudation patterns), namely the lower Elliot Formation (lEF) and upper Elliot Formation (uEF) strata (Smith, 1990; Bordy et al., 2004c). Bordy et al. (2004a, b, c, d), made major contributions with regard to refining the uEF and lEF units' variances. The informal subdivision of the lEF and uEF, lithological differences aside, is also shown by a definite difference in the modern-day geomorphology of the units (ie., slope angles becoming steeper over the uEF; Bordy et al., 2004c; Bordy and Eriksson, 2015).

2.2.1.1 lower Elliot Formation

Architectural elements within the lEF include: lenticular, multi-storey, pinched out (laterally discontinuous) sandstone bodies with maximum thicknesses ranging from 20 to 25 m and mudstone units from 20 to 30 m (Bordy et al., 2004c). Some mudstone units, which intercalate with the sandstone units, reportedly reach thicknesses of ~100 m (Eriksson, 1985; Smith, 1990). The lEF lithologies, especially the mudstones, are represented by various lighter shades of red and mottlings

of grey, green, yellow and purple. Sandstone beds often form laterally accreting bodies (lateral accretion), separated slightly with generally fining-upward successions, along with units dominated by trough and planar cross-stratification, some massive beds and lastly, less common low angle cross-stratification (Visser and Botha, 1980; Eriksson, 1983; Eriksson, 1985; Turner, 1986; Bordy et al., 2004a, c). The lEF sandstone petrography, in comparison to the uEF, consists of predominantly coarse-grained units with comparatively less feldspar-rich compositions (Botha, 1968; Visser and Botha 1980; Bordy et al., 2004a, c). Structures in the mudstone of the lEF of Lesotho are rare, so the mudstones are mostly massive or rarely horizontally laminated (Bordy et al., 2004a, c). Pedogenic alterations, which are abundant in the uEF, are rarer in the lEF and include: small irregular mottles, desiccation cracks and rare calcareous glaebules (Bordy et al., 2004a, c). South African samples, which are generally of a higher quality than Lesotho's outcrops, have however shown rhythmically bedded, laterally continuous tabular units.

Previous palaeoenvironmental interpretations of the lEF units are concurrent with one another; stipulating that the rhythmically bedded units present proof of fairly fixed meandering flows and extensive floodplain deposits (Botha, 1968; Le Roux, 1974; Visser and Botha,1980, Eriksson, 1983; Eriksson, 1985; Smith, 1990; Smith et al., 1993; Bordy et al., 2004a, c). The provenance study of the unit, based on palaeocurrent directional data and petrography, also provide evidence of a low sinuosity, meandering fluvial system, sourced from south and south-western sources, likely the CFB (Bordy et al., 2004b).

2.2.1.2   upper Elliot Formation

Bordy et al., (2004c) provided evidence that the uEF lithologies have higher percentages of feldspar grains, compared to the lEF lithologies, which may be attributed to an increased aridity and/or source overprint. Lithologies of the uEF also displayed a distinct deep red/maroon and sporadic light grey mottled colouring. Further distinctive variations include the sandstone

morphologies of the uEF and lEF, whereby the uEF units tend to generally be finer grained and comparatively more sorted than those of the lEF (Bordy et al., 2004c).

Distinct architectural elements within the uEF include: alternating sheet sandstone bodies (5.0-6.0 m thick) and thick, pedogenically altered 0.5-10m mudstone units (Visser and Botha, 1980; Visser, 1984; Eriksson, 1983; Eriksson, 1985; Bordy et al., 2004a, b, c, d). Bordy et al. (2004c) found that the frequency of sandstone bodies gradually increases upwards in the stratigraphy and are internally separated by semi-horizontal (laterally extensive) erosional surfaces, lacking in larger basal irregularities. In the uppermost part of the uEF, amalgamated lenses of sandstones of cumulative thicknesses up to 15.0m in places occur. Within the more massive sandstone bodies, rare trough cross-stratification, small scale water escape structures (ball and pillow), mud-drapes, desiccation cracks and various bioturbation features are also present. High-angled cross-bed reworking of sandstone bodies provided evidence of an increased dominance in aeolian depositional controls throughout the uEF, as suggested by Botha (1968), Visser and Botha (1980) and Visser (1984).

The distinctive hallmark of the uEF is the inclusion of a relatively laterally extensive, 1.5 m thick, pedogenic glaebule conglomerate unit (massive to slightly bedded) (Bordy et al., 2004c). Clasts are often polymictic, range in size from granule- to pebble-sized and well-rounded. Clast compositions often include carbonate and septarian nodules and other clasts, including: mudstone and sandstone fragments, fossil bones, teeth and occasional small quartz clasts. Angular clasts are less common and often very fine to fine sandstone derived (Bordy et al., 2004c). This paedogenic glaebule conglomerate, apart from being a distinct marker unit, is palaeontologically unique as it also hosts the vast *Tritylodon* Acme (or Assemblage) Zone (TAZ), originally identified by Kitching (1979) and later discussed in biostratigraphic detail in Kitching and Raath (1984). This marker is thought to present a period of mass-wasting and general accumulation of distal reworked bone fragments, mostly comprising of *Tritylodon sp.* material (Smith and Kitching 1997; Bordy et al., 2004c). Although Kitching and Raath (1984), as well as Smith and Kitching (1997), suggested lateral

14

continuity of the TAZ, Moodley (2015 [Unpublished]) disproved this notion, as the paedogenic nodule conglomerates are not restricted to association with the TAZ only within the uEF. That being said, the TAZ undoubtedly lies within the *Massospondylus* Range Zone (Kitching and Raath, 1984). The TAZ reportedly also directly overlies a large nodule horizon, which often times is thought to be associated with the TJB through relative globally approximated time scales (Smith and Kitching, 1997). The TAZ palaeodepositional environment falls under a semi-arid palaeosol (loess), with its typical pedogenic features falling under immature calcic vertisols, with an estimated sedimentation rate of 50 000 years by process of a rapid base-level drop (Smith and Kitching, 1997; Bordy et al., 2004c; Smith et al., 2009).

The generalized palaeoenvironmental interpretation of the sandstone bodies within the uEF, which consist of laterally persistent sheet sandstones, are typical of sheetflood deposits (Botha, 1968; Visser and Botha, 1980; Bordy et al., 2004c). The more channelized facies of the upper uEF are produced by successive streamfloods. The mudstones are massive but horizontal laminations are more common than in the lEF. Mudstones also include provide evidence of loessic type pedogenic alteration features, calcareous surfaces, calcretized root surfaces, calcareous concretions, large-scale calcretized and clay-lined shrinkage cracks and irregular, light grey mottles (Visser and Botha, 1980; Smith, 1990; Bordy et al., 2004a, c). On a finer scale, the various pedogenic alteration features and desiccation cracks in the mudstones also suggest that calcareous palaeosol horizons were common throughout the uEF. The transitional palaeoenvironmental character of the uEF is supported by the presence of pedogenic glaebule conglomerates associated with storm surge deposition. Lenticular sandstone bodies of the uppermost uEF were characterized by frequent crevassing and the various sizes of asymmetric, channel-shaped deposits, with laterally accreted layers were identified as shallow secondary sinuous channels of a floodplain (Smith, 1990; Anderson et al., 1998; Bordy et al., 2004a, c, d). Provenance studies indicate that the subarkoses in the UEF were sourced from a south-westerly as well as westerly direction (Bordy et al., 2004b).

2.2.2   Clarens Formation

The Clarens Formation concordantly overlies the fluvio-aeolian uEF. The Clarens lithologies consist of predominantly yellowish, fine-grained, cross-bedded quartz arenite successions, typical of aeolian dune deposits (Beukes, 1970; Eriksson, 1979; Eriksson, 1981; Eriksson, 1986; Turner, 1986; Smith, 1990; Holzförster, 2007). The occasional presence of larger trough cross-bedded sets of sandstones and siltstones likely resulted due to interdune deposits (Turner, 1986). Channel-fill sandstones occur within the southern edge of the basin, and form upward-coarsening (fine- to medium-grained) sucessions of trough- and cross-laminated sandstones (van Dijk et al., 1978; Eriksson, 1986; Holzförster, 2007). These channel fills are interpreted as meandering streams and associated floodplains, most likely situated within the distal alluvial-fan morphology (van Dijk et al., 1978; Eriksson, 1986). Some smaller-scale playa-lake and ephemeral stream deposits resulted in horizontal stratification, sand volcanoes, ripples and dewatering structures within fine- to very fine sandstone and siltstone units. Interesting structures within the Clarens include: a wide-variety of dinosaur footprints, invertebrate trails, mudcracks, gypsum crystallization, runzel marks, scour marks and fossilized roots. Formation bed thicknesses vary from 300 m to 100 m (Du Toit, 1954).

Initial works on the Clarens done by Haughton (1924; 1969), Du Toit (1939) and Stockley (1947) defined the Clarens as a one-dimensional, typically 'dry' aeolian dunal dominated sequence. Further facies analyses, however, displayed a distinct difference in deposits in the drier aeolian based northern basin exposures and the more 'wet' interdunal environments, typified by complex playa and ephemeral stream environments, toward the south (Beukes, 1970; Eriksson, 1981; Eriksson, 1986; Turner, 1986; Holzförster, 2007). The Clarens palaeoenvironments are more in line with ephemeral wet desert depositional patterns (Beukes, 1970; Holzförster, 2007), where distal alluvial and wet desert facies in the north-northeast interacted with typical drier central aeolian desert facies in an overall arid basinal system (Eriksson, 1979). Models of the aeolian deposition in the northern basin suggest a model of large merging alluvial fan systems, propagating from southern

16

and eastern source areas into the dry central basin (van Dijk et al., 1978; Eriksson, 1981; Eriksson, 1986; Smith, 1990; Bordy and Catuneanu, 2001).

2.2.3   Biostratigraphy of the Stormberg Group

The Karoo Basin hosts some of the best-preserved and most diverse biota, including macro- and micro-palaeobotanical remains, vertebrate and invertebrate body and trace fossils. The Stormberg Group shares this biotic diversity, punctuated by an abundance of Triassic and Jurassic fossil material, including: 1) palaeobotanical petrified wood and megaplants (Anderson and Anderson, 1983; Anderson and Anderson, 1993; Anderson and Anderson, 1995); 2) invertebrate fossils, especially abundant in the Molteno Formation (van Dijk, 1978; Rieck, 1973, Rieck, 1974; Anderson et al., 1998); 3) palaeoenvironmentally significant ichnofossils (Ellenberger, 1970; Turner, 1978; Raath et al., 1990; Gow and Latimer, 1999; Marsicano et al., 2009; Smith et al., 2009; Wilson et al., 2009; Sciscio et al., 2017b), and; 4) body fossils (Kitching and Raath, 1984; Olsen and Galton, 1984; Hancox and Rubidge, 1997; Ray and Chinsamy-Turan, 2002).

The Stormberg Group draws great interest for palaeontological studies in order to provide better constraints for its biostratigraphy, geochronology and palaeoenvironmental interpretations (e.g., Olsen and Galton, 1984; Hancox and Rubidge, 1997; Barrett et al., 2009). This review excludes the Molteno Formation, with its focus on the Elliot and Clarens formations, which host one of the greatest ecological events in the earth's geological and biological history, namely the biological turnover thought to be associated with the ETE and TJB (Colbert, 1958; Olsen and Sues, 1986). In this way, the Late Triassic and Early Jurassic continental rock record retains proof of the origin of the radiation of the dinosaurs, as well as the general transition from the dominance of therapsids in the Late Permian-Early Triassic to the rise of the earliest dinosaurs and mammals (Late Triassic-Jurassic).

The change in fauna assemblages as a result of the radiation within the Elliot Formation was first noted by Haughton (1924). This change was typified by the dominance of large-bodied sauropodomorph dinosaurs in the lEF, systematically gravitating toward smaller-bodied dinosaurs

toward the top of the stratigraphy. Following this classification, whereby 'large' bones were automatically thought to indicate Upper Triassic lEF strata and smaller material to be diagnostic of Lower Jursssic post-lEF rocks, persisted, often disregarding variations in morphology and diversity. Further and more recent body-fossil discoveries of large dinosaur taxa from the uEF; however, disproved the theory that body-size changes in dinosaurian species were wholly synonymous to the aridification trend in the upper Stormberg (e.g., Yates et al., 2010; McPhee et al., 2015; 2017; Sciscio et al., 2017b). Olsen and Galton (1977) were the first to compile and publish a comprehensive continental vertebrate body and trace fossil chart from which Olsen et al. (1982) first assigned the Norian-Rhaetian age to the lEF. This was refined in Olsen and Galton (1984); ultimately providing a Carnian–Norian age to the lEF units.

Lesotho is famous for its abundant vertebrate trackway sites, the most extensive of which were initially discovered and systematically described by Ellenberger et al. (1963; 1964; 1967) and Ellenberger (1970; 1972; 1974). More recent vertebrate trackway works in Lesotho highlight diverse morphological variations—predominantly in tridactyl therapod trackways, including those by Smith et al. (2009), Wilson et al. (2009), Marsicano et al. (2014), Bordy et al. (2015), Sciscio et al. (2016), Abrahams et al. (2017), Sciscio et al. (2017b) and Bordy et al. (2017a). The Maphutseng, Masitise and Moyeni trackway sites remarkably host an abundance of well-preserved footprints, whereby current diversity includes: the lower Moyeni *Neotrisauropus*-type (=*Grallator*) and *Moyenisauropus*-type dinosaurs, *chirotheroid*-type basal crurotarsal archosaurs, a *Episcopopus*-type tetrapod; and the Maphutseng *Deuterosauropodopus major*, *Trisauropodiscus aviforma* and *Pentasauropus maphutsengi* trackways (Ellenberger, 1972; Smith et al., 2009; Wilson et al., 2009; Marsicano et al., 2009; Bordy et al., 2015 [Poster]). The floodplain fines above the Lower Moyeni trackway site also hosts three samples of what was classified as '*Massospondylus*' (Smith et al., 2009). The uEF exposures at Masitise has also produced, withstanding the footprints found within the Masitise Cave house, remains of *Massospondylus sp.* as noted by Knoll (2002b) and two *Lesothosaurus* skull remains (Knoll, 2002a, b). Maphutseng also hosts the 'Maphutseng bone-bed', well-known for

hosting an abundance of lEF fossils, in particular a rich diversity of sauropodomorphs (Ellenberger and Ellenberger, 1956; Gauffre, 1993; Knoll, 2004).

The first southern African biozonation scheme of the Triassic and Jurassic is attributed to Ellenberger (1970), who subdivided the Stormberg and Drakensberg Groups into 14 zones based exclusively on ichnfossil occurrences. The lEF, uEF and Clarens Formation coincides with Ellenberger (1970)'s A4, A5, A6 and B1, B2, B3 terminology respectively. Kitching and Raath (1984), incorporating works by Haughton (1924), Ellenberger (1970), Cooper (1982) and others, generated a more refined and mainly vertebrate fossil based biostratigraphic subdivision of the Elliot and Clarens formations (Fig. 5). The two biozones includes the *Euskelosaurus* Range Zone for the lEF and *Massospondylus* Range Zone for the uEF and basal Clarens Formation (Fig. *5*).
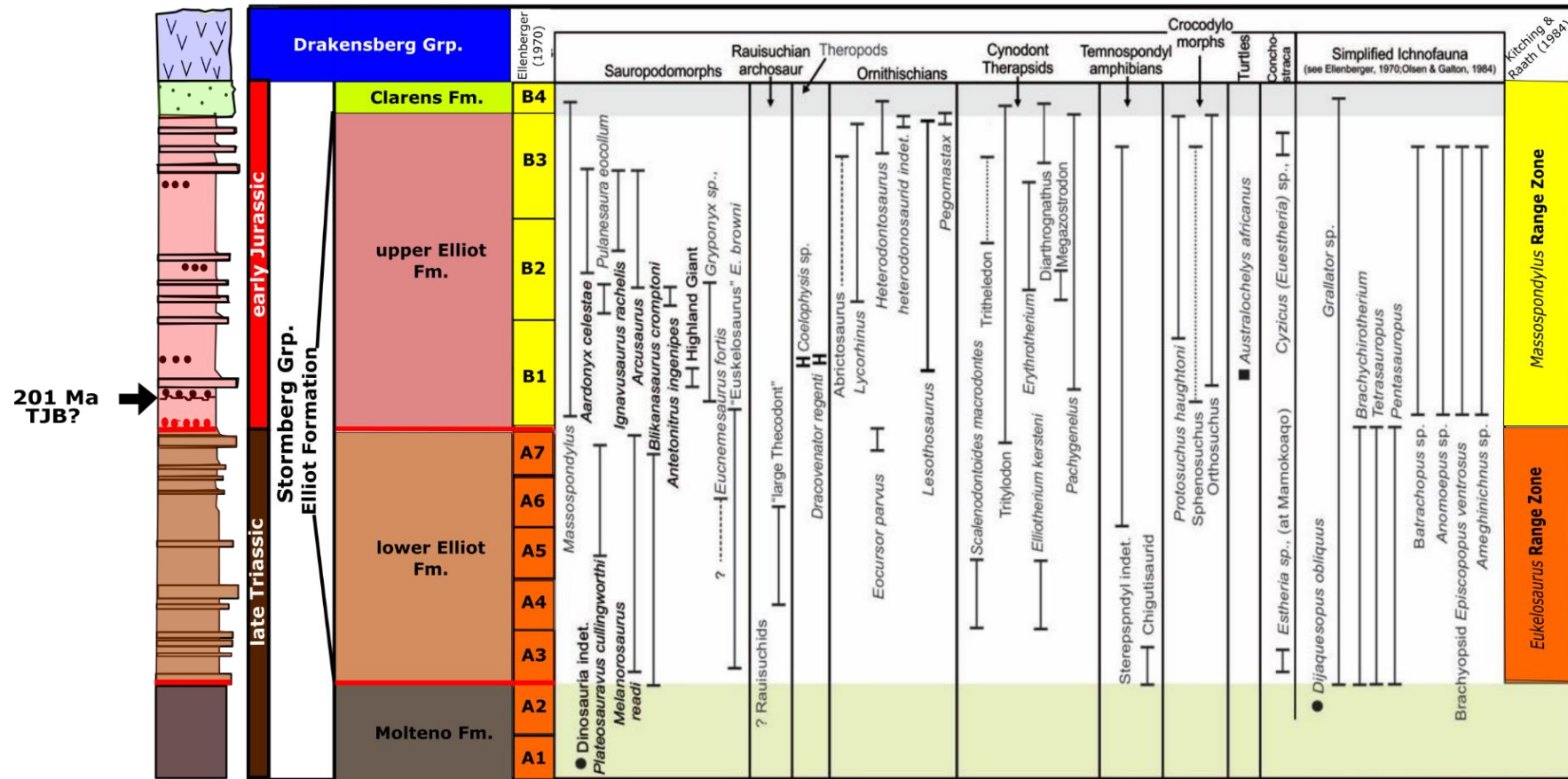
Fig. 5: Compilation of the biostratigraphy, lithostratigraphy and biozonation scheme of the Stormberg Group based on revisions by Kitching and Raath (1984), Olsen and Galton (1984), Lucas and Hancox (2001), Knoll (2004; 2005). Lithostratigraphy modified after Bordy et al. (2004a, b, c), Bordy et al. (2005), Holzförster (2007) and Smith et al. (2009). Biozonation Range Zones modified after Kitching and Raath (1984) and Ellenberger (1970). Figure modified after Sciscio et al. (2017a). Note: red lines indicate the unconformal contacts described by Bordy et al. (2004a, b, c, d) and Bordy et al. (2005).

In short, the lEF "*Euskelosaurus*" Range Zone of Kitching and Raath (1984) was proposed to indicate the interval largely dominated by an assemblage of large prosauropods. A recent study by McPhee et al. (2017) reanalysed the large sauropodomorphs findings, especially in the lEF, and concluded that valid genera included *Blikanasaurus*, *Plateosauravus*, *Eucnemesaurus* and *Melanorosaurus*. Other vertebrates that form a part of this assemblage includes cynodonts, putative 'rauisuchian' and Late Triassic tetrapod dominated ichnofossils (including the Maphutseng trackway site reassesed in this study; Olsen and Galton, 1984; Lucas and Hancox, 2001; Knoll, 2004). This assemblage is comparable to similar beds in the Los Colorados Formation (Argentina), Trossingen Formation (Germany) and the Rock Point sequence of the Chinle Formation (Lucas and Hancox, 2001). However, the Late Triassic lEF remains pervasively incomplete, making assemblage correlations difficult (McPhee et al., 2017).

The uEF and basal Clarens Formation "*Massospondylus*" Range Zone in contrast hosts a variety of *Massospondylus* remains that have (to date) not been identified within the lEF (McPhee et al., 2017). This exclusivity thus still supports the initial subdivision implemented by Kitching and Raath (1984). The Lower Jurassic uEF also hosts a taxonomically and morphologically diverse assemblage of 'prosauropods', heterodontosaurid, fabrosaurid basal ornithischian dinosaurs, cynodonts, tetrapods, mammals and basal crocodylomorphs and turtles (Olsen and Galton, 1984; Smith and Kitching, 1997; Knoll, 2005; McPhee et al., 2015; McPhee et al., 2017). The Clarens Formation, as with the uEF, hosts a number of Early Jurassic dinosaurian fossils and trackways (10 recorded), which play a vital role in local and global correlation studies (Ellenberger, 1970; Tasch, 1984; Kitching and Raath, 1984; Knoll, 2005; Sciscio, 2015 [Unpublished]). These relatively diverse beds have been correlated to other Lower Jurassic strata including the Lufeng Formation (China) and Glen Canyon Group (USA; Olsen and Galton, 1984; Butler, 2005; Knoll, 2005; Yates, 2005; Irmis, 2011; McPhee et al., 2015; McPhee et al., 2017).

2.3   Temporal Setting

The Karoo Supergroup hosts an amazing georecord. An array of in-depth biostratigraphic studies have provided ample biostratigraphic global age correlations and are, in conjunction with lithostratigraphy, the primary age determining techniques utilised throughout the Karoo Supergroup (e.g., Rieck, 1973; Rieck, 1974; Rieck, 1976a, b, c; Olsen and Galton, 1984; Kitching and Raath, 1984; MacRae, 1988; Cairncross et al., 1995; Rubidge et al., 1995; Smith, 1995; Hancox and Rubidge, 1996; Catuneanu et al., 1998; Rubidge, 2005). Direct radiometric age dating, in contrast, has been sparse, with a few intermittent volcanogenic member and detrital zircon radioisotopic dates obtained from the Karoo Supergroup (Fig. 6). The primary reason for this sparsity is the result of the lack of access to radiometric dating technology. Recent advancements in the accessibility and accuracy of the technology allowed for the sudden increase in geochronological age dating within southern Africa.

2.3.1   Elliot and Clarens age constraints

Current age constrains of the Elliot and Clarens formations are limited to globally comparative and biostratigraphically significant body fossils and ichnofossils, as well as a recent magnetostratigraphic study by Sciscio et al. (2017a). The fossil assemblages of the Elliot and Clarens formations, when correlated to other Triassic-Jurassic strata, suggest a Late Triassic (Norian to Rhaetian) age for the lEF and Early Jurassic (Hettangian to Pliensbachian) age for the uEF and Clarens Formation (Kitching and Raath, 1984; Lucas and Hancox, 2001; Yates and Kitching, 2003; Bordy et al., 2004c; Knoll, 2004; 2005). Stormberg Group elements have no radioisotopic dates as yet, the lack of which is consistently noted by authors, including Turner (1999), Smith et al. (2009), Sciscio et al. (2017) and McPhee et al. (2017). Despite the lack of radiometric age dates of the Elliot and Clarens formations, the capping Drakensberg Basalts (forming a part of the Early Jurassic Karoo LIP), with an age of 183.0 ±1.0 Ma, provide a useful uppermost age for the Stormberg Group (Duncan et al., 1997; Jourdan et al., 2005; Jourdan et

al., 2007). The end of the uppermost Clarens sedimentation is commonly thought to be coeval

with the onset of flood basalt volcanism (Drakensberg Group; Bordy and Head, 2018 (In Press)).
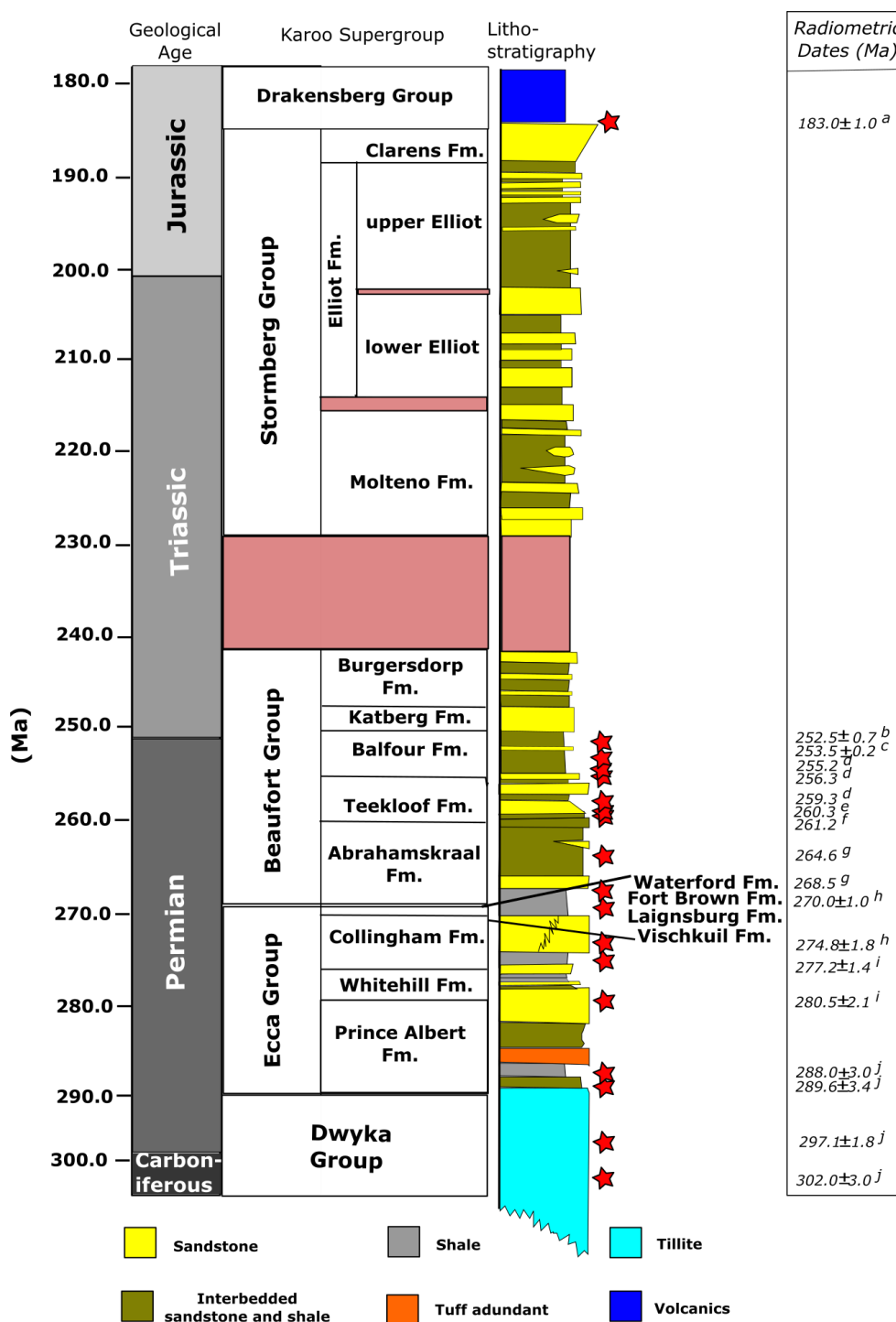
Fig. 6: A basic chronostratigraphic framework of the Karoo Supergroup. Type section used was the eastern basinal (24⁰E) section. Age and lithostratigraphic relative scale derived from Stollhofen et al. (2000), Catuneanu and Elango (2001), Gradstein et al. (2012). Radiometric age compilation (red stars) based on; a. Duncan et al. (1997); b. Coney et al. (2007), c. Gastaldo et al. (2015), d. Rubidge et al. (2013), e. Day et al. (2015), f. Lanci et al. (2013), g. Turner (1999), h. Fildani et al. (2007), i. Werner (2006) and j. Bangert et al. (1999). The lithostratigraphic column is a compilation of significant lithologies occurring throughout the Karoo Supergroup, based off Leith (1970), van Vuuren (1972), Johnson (1976), Christie (1981), Catuneanu and Elango (2001), Flint et al. (2011), Hancox and Götz (2014), Bordy and Eriksson (2015). Column not to scale. Stratigraphic hiatus: pink shaded box.

Biostratigraphic correlations of the lEF presented distinct assemblage similarities in relation to the Late Triassic Los Colorados Formation (Argentina), Germany and upper Chinle Formation (N. America; Lucas and Hancox, 2001; Yates, 2003; Yates and Kitching, 2003; Yates, 2007a, b; McPhee et al., 2014; Martinez et al., 2015). The predominance of Norian ichnofaunas and prosauropods provided reasoning that suggested the lEF is not older than the Late Triassic, Norian (Lucas and Hancox, 2001; Knoll, 2004). However, others researchers such as Gauffre (1993) constrained the prosauropod-rich lEF as Early Carnian. A larger diversity of tetrapods within the uEF and Clarens Formation, alongside distinguishing ichnofossils, prosauropods, heterodontosaurid, basal ornithischian dinosaurs, cynodonts, basal crocodylomorphs and turtles and ichnofossils, permits its correlation to other Lower Jurassic deposits (e.g., Glen Canyon Group, USA and Lufeng Formation, China; Kirkland et al., 2014; Suarez et al., 2017). This provides ample evidence of an Early Jurassic, specifically Hettangian-Sinemurian age (Ellenberger, 1970; Kitching, 1977; van Dijk, 1978; Kitching and Raath, 1984; Olsen and Galton, 1984; Smith and Kitching, 1997; Lucas and Hancox, 2001; Butler, 2005; Yates, 2005; Knoll, 2005; Yates, 2005; Sertich and Lowen, 2010; Irmis, 2011; Apaldetti et al., 2011; McPhee et al., 2015).

Although scattered, reworked tuff and bentonite beds do occur throughout the Elliot Formation (e.g., Schmitz and Rooyani, 1987; Bordy and Abrahams, 2016), however no systematic radiometric dating has been done on these volcanogenic deposits. One such bed includes the Pronksberg Mountain bentonite, within the uEF strata, which only provided highly reworked detrital zircons and thus proved to be of limited stratigraphic importance (Bordy and Abrahams, 2016). A more recent magnetostratigraphic study by Sciscio et al. (2017a) provides a refined temporal framework for the Elliot Formation and associated TJB and ETE. Using global magnetostratigraphic correlations, Sciscio et al. (2017a) refined the age range of the Elliot Formation from a basal ~213 Ma to an uppermost age of ~195-190 Ma. This age range thus falls well within the initial biostratigraphically derived Norian to Hettangian-Sinemurian age range of the Elliot Formation.

2.3.2   End-Triassic Extinction Event and Triassic-Jurassic Boundary

The end-Triassic Extinction event (ETE) predates the Triassic-Jurassic Boundary (TJB) by a few 100 000 years, with the ETE having occurred at 201.6 ±0.02/0.2 Ma and the TJB at 201.3 ±0.2 Ma (Olsen et al., 2011; Lindström et al., 2012; Blackburn et al., 2013; Cohen et al., 2013; Kent et al., 2014; Wotzlaw et al., 2014; Kent et al., 2017; Lindström et al., 2017). The ETE marks the lesser understood extinction event punctuated by sudden marine productivity loss and terrestrial faunal and floral species turnover (Olsen and Galton, 1977; Olsen et al., 1987; Raup and Sepkoski, 1982; Olsen et al., 2002a, b). The ETE is considered as one of the 'big five' extinction events over the Earth's Phanerozoic Era, however the magnitude of the event is unclear (Olsen and Galton, 1977; Raup and Sekoski, 1982; Olsen et al., 1987; Erwin, 1998; Pálfy et al., 2000; Pálfy et al., 2001; Ward et al., 2001; Hallam, 2002; Zeigler and Geissman, 2008; Blackburn et al., 2013). This uncertainty around the magnitude of the ETE and stratigraphic position of the TJB is linked to the low number of complete and dated sections, ages constrained using reliable dating methods, problematic global correlations and missing lowest (LO) and highest (HO) occurrences (Tanner et al., 2004).

The effects of the ETE within marine systems included abrupt shifts in the size and composition of biota, in particular the extinction of conodonts (very few persisting into the Hettangian), the absence of many ammonoids (*Chohstoceras rhaeticum* and *C. merum*) and changes in the brachiopod and radiolarian communities (Pálfy et al., 2007; Pálfy, 2008). Radiometric U-Pb zircon dating of the LO, HO and first occurrence (FO) of ammonoid zones, including: *Choristoceras marshi*, *Psiloceras planorbis*, *Psiloceras spelae spelae* and *Psiloceras spelae tirolicum*, is used to determine the TJB position within the marine stratigraphy (Pálfy et al., 2000; Tanner et al., 2004; Hillebrant and Krystyn, 2009; Schoene et al., 2010; Wotzlaw et al., 2014). Along continental sections, boundary sections are not easily correlated due to palaeobotanical and vertebrate provincialism, climatic variations and gaps in the biostratigraphic record (Tanner et al., 2004). Rarities can however easily be dated using biostratigraphic

correlations and geochronology. Within the continental fauna, the ETE has been marked by the extinction of many tetrapods, lowest occurrence (LO) of *Eubrontes* tridactyl therapod trackways and the abrupt change in floral compositions, which extends to the TJB (Lucas and Tanner, 2007). Recent studies have also suggested a diversification of sauropodomorph and theropod morphologies across the Triassic-Jurassic boundary worldwide (Ward et al., 2001; Olsen et al., 2002; Lucas et al., 2006; McPhee et al., 2015; McPhee et al., 2017).

The Triassic-Jurassic Boundary (TJB) and end-Triassic extinction event (ETE) have been the subject of various global studies, whereby astrochronological studies including: magnetostratigraphic, geochronological, lithostratigraphic and biostratigraphic analyses, have provided a means to global correlative studies (Olsen et al., 2011; Blackburn et al., 2013). Comparisons of the Newark-Hartford Basins astrochronology and geomagnetic polarity time scale (APTS) have proven to be cotemporaneous with marine successions of the: Carnian-Norian boundary, Norian-Rhaetian boundary, TJB, Hettangian-Sinemurian, and according to Kent et al. (2017), the radiometric temporal framework of the Pucara Basin, Peru (Olsen et al., 2011; Kent et al., 2014). This makes the Newark-Hartford Basin a primary source of temporal framework used in basinal TJB correlations.

Despite the questions surrounding the magnitude of the ETE, high rates of diversity loss (and radiation), both marine and terrestrial can only be justified through assessing the forcing mechanisms of the ETE, which are also in dispute (Raup and Sepkoski, 1982). Some of the popular forcing mechanisms (not necessarily mutually exclusive) include: sea level change and ocean anoxia (Newell, 1967; Hallam and Wignall, 1999; Richoz et al., 2012), climate change (Tanner et al., 2001; Beerling and Berner, 2002; Galli et al., 2005), bolide impact in the Late Triassic 210 ±4 Ma Manicouagan crater (Olsen et al., 2002a,b; Tanner et al., 2008) and the 201.2 ±2 Ma Rochechouart crater (Schmieder et al., 2010), and methane hydrate release (Pálfy et al., 2001). However, the most commonly supported cause is the extensive Central Atlantic

Magmatic Province volcanism (Rampino and Stothers, 1988; Marzoli et al., 1999; Wignall, 2001; Wignall, 2005; Hesselbo et al., 2002; Whiteside et al., 2010; Blackburn et al., 2013). Further studies would aid in providing resolution with regard to the causes, magnitudes, effects of the proposed mass extinction event, nature of the biotic turnovers and post-event dinosaur radiations.

A general lack in completeness in the Elliot Formation's vertebrate fossil assemblages make the precise allocation of the ETE and TJB positions (and their biostratigrahic global correlation) difficult; however, recent studies by McPhee et al. (2017) and Sciscio et al. (2017a) have offered further refinement on the southern African ETE and TJB. The ETE within the Elliot Formation is closely correlated to the lEF and uEF contact, as suggested by: the global polarity chron EF6.1r correlation by Sciscio et al. (2017a), the uEF related climate change driven *Massospondylus* radiation (e.g., Langer et al., 2010; McPhee et al., 2017), and Kitching and Raath's (1984) biozonation scheme.

The actual position of the Triassic-Jurassic boundary within the Stormberg Group has not been successfully determined to date. However, the TJB has been corroborated by several past and recent studies focused on resolving its placement via globally correlative biostartigraphic records, palaeomagnetic and palynological work within the Elliot Formation (Kitching and Raath, 1984; Bordy et al., 2004a, b, c, d; Barbolini, 2014; Sciscio, 2017a). Many studies in the northern hemisphere have determined plausible TJB positions within individual basinal stratigraphies (e.g., Newark Basin, Fundy Basin and Argana Basin) (Hesselbo et al., 2007; Pálfy et al., 2007; Pálfy, 2008; Lindström et al., 2012; Blackburn et al., 2013).

The southern African TJB, throughout previous biostratigraphic studies, was implied to be coincident with the *Euskelosaurus* and *Massospondylus* biozomes contact, which in turn was broadly correlated to the lithostratigraphic contact of the lEF and uEF (Fig. 7) (Kitching and Raath, 1984; Smith and Kitching, 1997). Furthermore, Bordy et al. (2004a, b, c, d), who never

27

attempted to date these units, has shown that the contact of the lEF and uEF is an unconformity and marks a basin-wide change in fluvial style and provenance. The biostratigraphically argued notion of the lEF being Upper Triassic and the uEF being Lower Jurassic, however, was questioned by Smith et al. (2009), whose study focused on the famous lower Moyeni trackway site (Lesotho) situated within the uEF. Due to the trackway's position within the stratigraphy, it is correlatively considered a Lower Jurassic site, however, some ichnotaxa appear to be uniquely Triassic based, bringing into question the validity of the biostratigraphic regime as well as the position of the TJB at the lEF-uEF contact (Marsicano et al., 2009; Smith et al., 2009; Wilson et al., 2009). The magnetostratigraphic study by Sciscio et al. (2017a) interestingly placed the TJB within the lower part of the uEF (Fig. 7), primarily based on the correlation with works by Hüsing et al. (2014) and others. This shift of the TJB position within the lithostratigraphic scheme of the Elliot Formation could offer new insights into biota diversities.
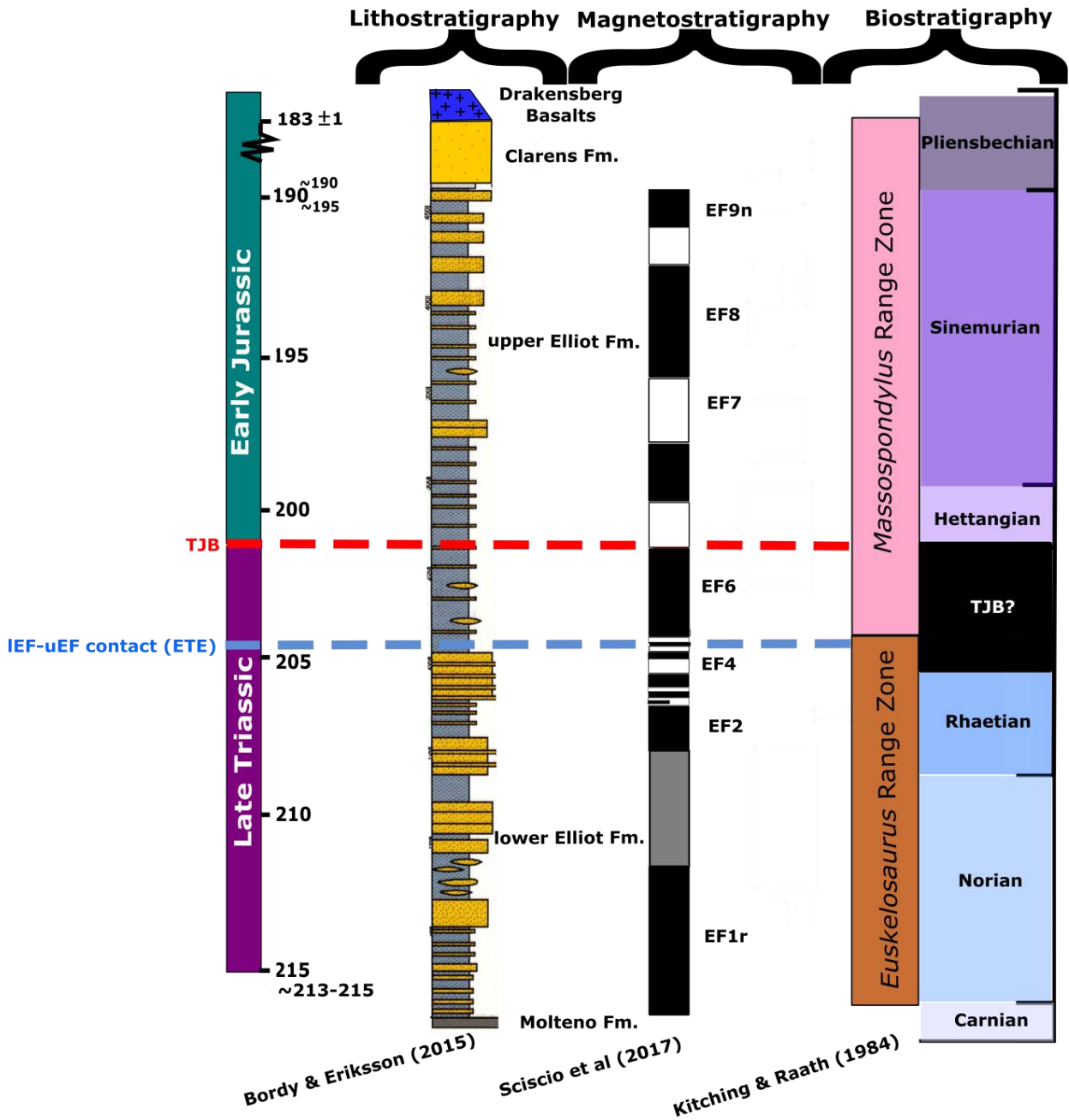
Fig. 7: Simplified composite stratigraphy outline based on previous works of both biostratigraphy (Kitching and Raath, 1984; Lucas and Hancox, 2001; Bordy et al., 2004a; Knoll, 2004;2005) and magnetostratigraphy (Sciscio et al, 2017a), with focus on the Elliot Formation. Diagram modified from Sciscio et al., 2017a. General lithostratigraphy from Bordy and Eriksson (2015) Holostratotype A (Barkly Pass; Eastern Cape).

3 METHODOLOGY

In order to establish a geochronological framework of the fossiliferous Elliot and Clarens Formations, a truly multidisciplinary approach in both data collection and analysis was required. The applied techniques ranged from sedimentological, litho- and chronostratigraphic analyses, and were used to collect and process the data.

3.1 Sedimentological Analysis

This study focused on three study sites, Quthing (Moyeni), Masitise and Maphutseng that occurs within the southwestern portion of Lesotho (Fig. 8). Data collection was initiated with sedimentological analyses of well-exposed units in the Elliot and Clarens formations along 9 traverses. Field data collected along each traverse included: 1) lithological and facies descriptions; 2) nature of upper and lower bounding surfaces; 3) lateral continuity; 4) scale and thickness of units; and 5) sedimentary and biogenic structures.

Sedimentary facies and architectural element interpretations were based on the systematic coding established by Miall (1977; 1985; 2014) and modified works by Eriksson (1981; 1983; 1985; 1986), Bordy et al. (2004a, c) and Hölzforster (2007). Facies were analysed at centimetre-scale vertically, and metre-scale laterally. The latter was needed to establish the lateral extent of bounding surfaces of architectural elements and significant fossil bearing marker units. Bounding surface order interpretations were based on the fluvial hierarchical classification scheme by Allen (1983) and Miall (1985) and aeolian hierarchical classification by Brookfield (1977).

The facies analysis also included the recording of the grain size, rounding, sorting and mineralogical composition of units by aid of a hand lens. Bed thicknesses were measured by the use a of Jacob staff, tape measure and Krantz compass (magnetic declination set at -24.44⁰) to accurately determine vertical thicknesses of beds through trigonometric means. However, the most frequently utilised method for bed thickness readings was by the use of a GPS (Garmin Etrax 10

degree-minute-seconds) set on the WGS 1984 (WGS84) datum with a <15 m (95%) positional

accuracy. Decimetre/metre scale waypoints, including elevation, were recorded electronically with

the GPS along traverse sections. Cross-checking of the obtained vertical distances with the Jacob

staff and the GPS showed no significant differences between these two approaches.

Palaeocurrent indicators were measured using the Krantz compass and techniques for uni-

and bi-directional linear (trend) and planar (restored strike and dip) indicators described in Potter

and Pettijohn (1977). Readings were taken from architectural elements with strong palaeoflow

indicators, including ripples, flute casts, channel orientations, surficial channel axis indicators, trough

cross-bedding, pinstripe laminations (aeolian) and parting lineations. Unique marker beds,

highlighted by distinct lithologies, fossil material and bed morphologies, were studied with regard to

lateral continuity and associated facies (Smith and Kitching, 1997; Smith et al., 2009; Bordy et al.,

2015 [Poster]). Unit colours, both weathered and unweathered, were allocated using the Munsell

Soil Colour Chart (2009) and Geological Rock Colour Chart (Munsell Color, 2009). Bioturbation

intensity was also calibrated using the bioturbation index (BI) by Bann et al. (2008). Indicative

bioturbidity, ranging from BI 0 (none) to BI 6 (intense), was allocated to each facies assemblage (FA).

3.2   Sampling

Data analysis consisted of age determinations via U-Pb LA-ICPMS detrital zircon ($ZrSiO_4$)

dating methods using samples collected from Quthing (Moyeni), Masitise and Maphutseng (Fig. 8).

Systematic sampling was conducted to provide comprehensive stratigraphic relationships. Sampling

ranged from the lowermost exposed lithologies (Quthing and Masitise: lower uEF and Maphutseng:

lEF) to the top-most lithologies (Clarens Formation in all areas). Direct sampling was also done for

select horizons that host fossils and trackways at Quthing (Q2; lower Moyeni trackway), Masitise

(Mas1; Masitise Cavehouse Trackway) and Maphusteng (Map2; Maphutseng Trackway Surface and

underlying bonebed). Although systematic sampling was done on every of the total nine traverses

studied; eight representative samples were selected in Quthing and six in Maphutseng for detrital

geochronological analyses (Table 1). The samples were extracted in bulk (± 3 kg) from freshly

exposed, un-weathered fine-grained sandstones and siltstones. The careful sampling of silty material

from basal units (troughs and splay units) allowed for the direct sampling of plausibly heavy element

rich sediment, where settling is expected (Mange and Maurer, 1992).

Locality	Sample Name	Field Sample #	GPS (deg,min,sec)		Elevation	Stratigraphic Position
			South	East	metres a.s.l.	
Quthing	Q1	Q1S1S1&Q1S1S2	30°23'43.5"	027°41'29.2"	1465	upper Elliot (lower)
Quthing	Q4	Q1S4S1&Q3S7S1	30°23'39.3"	027°41'20.0"	1509	upper Elliot (mid)
Quthing	Q7	Q1S12S2&Q2S2S1	30°23'27.8"	027°41'17,4"	1677	uppermost Clarens
Quthing	Q2	Q2S1S1&Q2S10S1	30°23'41.0"	027°41'35.2"	1496	upper Elliot (Trackway)
Quthing	Q6	Q2S2S3&Q4S1S2	30°22'53.6"	027°42'43.1"	1654	basal Clarens
Masitise	Mas1	Q3S2S1&Q3S3S1	30°24'20.1"	027°38'30.2"	1571	basal Clarens (Trackway)
Quthing	Q3	Q3S4S1&Q3S5S1	30°23'13.5"	027°42'31.7"	1479	upper Elliot (mid lower)
Quthing	Q5	Q4S4S2&Q4S4S3	30°22'57.3"	027°42'46.0"	1602	upper Elliot (mid upper)
Maphutseng	Map2	M1S1S3&M1S1S4	30°12'46.1"	027°28'50.8"	1534	lower Elliot (Trackway)
Maphutseng	Map1	M3S1S1&M3S2S1	30°12'42.5"	027°29'49.9"	1460	lower Elliot
Maphutseng	Map6	M4S1S2&M4S1S3	30°14'19.9"	027°30'47.7"	1752	basal Clarens
Maphutseng	Map5	M4S4S1&M4S5S1	30°14'15.6"	027°30'37.9"	1671	upper Elliot
Maphutseng	Map4	M4S10S1&M4S10S2	30°14'20.4"	027°30'11.7"	1533	lEF-uEF contact
Maphutseng	Map3	M4S12S1&M4S12S2	30°14'21.9"	027°38'10.3"	1501	lower Elliot

Table 1: List of the fourteen (14) samples collected for U-Pb LA-ICPMS detrital zircon geochronology, including field locality, GPS (GWS84) coordinates and elevation above sea level (metres).
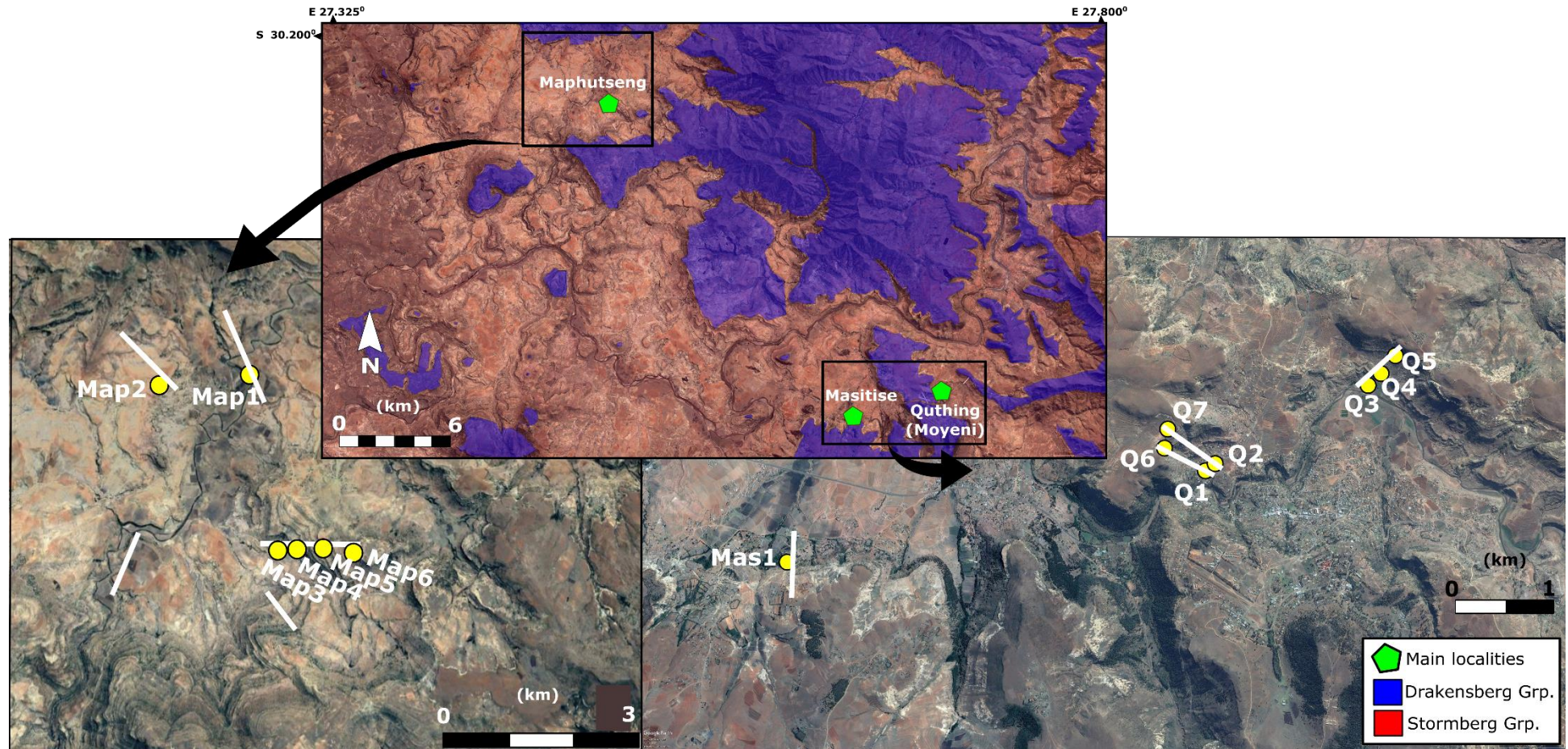
Fig. 8: Yellow markers denoting the geographical positions of the fourteen (14) samples selected for U-Pb LA-ICPMS detrital zircon geochronology from a total of 130 samples collected from various traverses (white lines) in Quthing (Moyeni), Masitise and Maphutseng. Landsat regional base maps sourced from Google Earth (2018).

3.3   Zircon separation and data processing

Sample preparations involved the separation of detrital zircons from all collected rock samples (Table 2). All samples were prepared and analysed at the Central Analytical Facility (CAF), University of Stellenbosch. The zircon extraction process involved the primary crushing (using a jaw crusher), milling (in a tungsten carbide disc mill) and subsequent sieving to reduce grain sizes to <350 μm. Thereafter, each sample was washed and panned to separate the denser heavy minerals (PH) from the lighter minerals (PL) and clay-sized fraction. The PH fraction subsequently underwent magnetic separation of the: 1) undesired ferromagnetic minerals (FM) and non-ferromagnetic material using a simple hand-held magnet; and, 2) non-magnetic (NM) and paramagnetic (PM) fractions using the FRANTS Barrier Magnetic Separator at currents ranging from 0.4-1.5 A at a slope of 10˚. The NM fraction, which includes the detrital zircons, then underwent heavy liquid separation using Tetrabromoethane (TBE), whereby the specific gravity of TBE (2.85-2.87) allows for the settling of these slightly denser zircon grains.

Laboratory & Sample Preparation	
Central Analytical Facility, Stellenbosch University (CAF)	
Sample type / mineral	Detrital zircons
Sample preparation	Conventional mineral separation techniques, zircons mounted, 2.54 cm resin mount and in-situ in thin section, 1 µm polish to finish
Mount conductive coater	Edwards S150A Sputter Coater, Gold (Au), 40mA, 3min
Imaging	CL MERLIN FE-SEM, 11 nA, working distance 9.5 mm
Laser ablation system	
Make, model & type	Resonetics Resolution ME-S155, ArF Excimer ATL Atlex
Ablation cell & volume	Laurin Technology S155 dual volume cell
Laser wavelength	193 nm
Pulse width	< 5 ns
Fluence	2.0 J/cm-2 (measured with external energy meter above sample cell)
Repetition rate	9 Hz/ zircon
Spot size	25 µm
Sampling mode / pattern	25 µm single spot analyses
Cell carrier gas	100% He, Ar and N2 make-up gases combined into Nylon 10 tubing
Pre-ablation laser warm-up (background collection)	3 cleaning shots followed by 15 seconds background collection
Ablation duration	15 seconds
Wash-out delay	15 seconds
Cell carrier gas flows	325 ml/min He
ICP-MS Instrument	
Make, Model & type	Thermo Finnigan Element2 single collector HR-SF-ICP-MS
Sample introduction	via Nylon 10 tubing
RF power	1350 W
Make-up gas flow	920 ml/min Ar & 4 ml/min N2
Detection system	Single collector secondary electron multiplier
Masses measured	202, 204, 206, 207, 208, 232, 233, 235, 238
Integration time per peak	4 ms
Total integration time per reading	0.1 sec (represents the time resolution of the data)
Sensitvity	30000 cps/ppm Pb
Dead time	6 ns
Data Processing	
Gas blank	15 second on-peak
Calibration strategy	GJ-1 used as primary reference material, Plešovice & M127 used as secondary reference materials (Quality Control)
Reference material info	GJ-1 (Jackson et al. 2004), Plešovice (Sláma et al. 2008), M127 (Nasdala et al. 2008; Mattinson 2010)
Data processing package used /Correction for LIEF	Iolite data reduction software was used to process data
Mass discrimination	Standard-sample bracketing with 207Pb/206Pb and 206Pb/238U normalized to reference material GJ-1
Common-Pb correction, composition and uncertainty	204-method, Stacey & Kramers (1975) composition at the projected age of the mineral, 5% uncertainty assigned
Uncertainty level & propagation	Ages are quoted at 2-sigma absolute, propagation is by quadratic addition. Reproducibility and age uncertainty of reference material and common-Pb composition uncertainty are propagated.
Quality control / Validation	M127: Concordia age = 528±6 Ma (2s+A31:B40, MSWD = 1.2), Plešovice: Concordia age = 340±2 Ma (2s, MSWD = 1.03)

Table 2: Analytical techniques and criteria used in the ICP-MS detrital zircon geochronology at CAF labs (University of Stellenbosch).

The remnant zircon grains were then selected via a hybrid selection protocol, which involved hand-picking zircons at random from the greater population within a field of view. Care was taken to select the most pristine grains. For each sample, an average of ~200 grains were set in a 25 mm epoxy (SpeciFix-40) resin puck and subsequently polished using: 1) a MD-Dac Satin Woven Acetate Polishing Cloth (3.0 µm) for 10 minutes with a DiaPro-Dac3 Suspension; and, 2) a MD-Dac Synthetic Short Nap Polishing Cloth (1.0 µm) with a DiaPro-Nap B1 Suspension for an additional 10 minutes. With the cores and rims of each zircon exposed, each puck was imaged using a ZEISS MERLIN Field Emission Scanning Electron Microscope (SEM) at the Electron Microbeam Unit of CAF. Prior to imaging, each polished mount was coated in conductive gold, using the Edwards S150A Gold Sputter Coater. The high-resolution SEM images were taken at a set analytical working distance of 9.5mm for clear focused images, 20 kV acceleration voltage and a 11 nA probing current. Both the Backscattered Electron Detector (BSD) and Cathodoluminescence (CL) detector were used to systematically image the samples to document individual zircon cores, microstructures, cracks, inclusions, zonations and other complexities within the grains, as well as produce accurate zircon maps. Individual zircon crystal morphologies are particularly vital for sample point mapping and temporal data interpretations. These zircon grain morphologies were studied in accordance with Gärtner et al. (2013) and Pupin's (1980) classification criteria.

Utilising the zircon maps, ablation grain selection included an unbiased selection of both igneous and metamorphic grains of pristine condition (no cracks/inclusions/complexities), as well as cores or well-preserved rims. Apatite grains were also identified and justly disregarded. From each sample, approximately 100 grains were ablated with the Resolution M-50-SE Excimer laser interfaced with an E2 SF ICP-MS. Spot sizes were set at 30 µm, with an average down-hole depth of approximately 10-15 µm. Adequate laser focus and alignment was ensured by means of test shots done on grains not included in the analyses. Shot timings were also set to 15 seconds, with a 15 second wash-out delay. A sequence included a maximum of 400 selected grains, to which lab-preferred internationally recognized standards were added intermittently. For every 30 'unknowns'

there were: 1) three/two GJ1 standards (602-605 Ma; Jackson et al., 2004); 2) one Plesovice standard (337 Ma; Sláma et al., 2008); and, 3) one M127 standard (527 Ma; Nasdala et al., 2008; Mattinson, 2010). The methods and standards used in this project were similar to those described in Frei and Gerdes (2009). The precision of the standards' respective ages (ID-TIMS ages), produced during the subsequent data reduction phase acted as a necessary quality control mechanism for the 'unknown' samples ages.

The raw output data from the laser ablation phase was processed and formatted using the Iolite data processing software's (IgorPro) data reduction scheme (DRS; Table 2). The DRS allowed for the correction of down-hole fractionation errors, as well as resultant Pb-loss corrections (Hellstrom et al., 2008; Paton et al., 2010). The data set was then exported and refined in Excel, ensuring discordant data outside the >20 % concordance bracket was separated from the concordant ages. This discordance, as described by Schoene (2014), is likely a result of: 1) mixing of cores and younger overgrowth; 2) common lead (Pb) contamination; 3) Pb loss (especially within the grains <250 Ma); and, 4) errors in analytical technique (instrument drift). Concordant data from each sample was then plotted in Concordia diagrams (at 2σ error) and further modelled and analysed using the Excel enabled Isoplot package (Ludwig, 2003). The primary objective of this study is to provide a greater temporal constraint utilising the youngest maximum depositional ages of the detrital Elliot and Clarens samples (Cawood and Nemchin, 2001; Cawood et al., 2007; Cawood et al., 2012). A combination of various age determining methods was used to attain a more precise maximum youngest depositional age, namely: 1) Youngest Single Grain (YSG); 2) Youngest Detrital Zircon Grain (YDZ); 3) TuffZirc age extractor; 4) Weighted Mean Average (YC2σ); 5) Weighted Mean Average (YC1σ); 6) Youngest Graphical Detrital Zircon Peak (YPP); and, 7) Average Youngest Detrital Zircon (Weighted Average). A number of works have dedicated significant time toward refining the methodology, such that a statistically reliable maximum youngest depositional age can be derived (Dickinson and Gehrels, 2009; Lawton and Bradford, 2011; Robinson et al., 2012; Tucker et al., 2013; Tucker, 2014 [Unpublished]).

The least rigorous method, the YSG, involves the selection of the youngest detrital zircon ($^{206}Pb/^{238}U$) within the sample population. Although this method does provide the youngest maximum depositional age for the specific sample, the single data point introduces statistical bias, resulting in data inaccuracies (Dickinson and Gehrels, 2009). The remaining methods (YPP, YDZ, YC1σ, YC2σ, weighted average, TuffZirc) are thus needed to provide a more rigorous age determination. The YPP method uses the youngest graphical peak recorded on a population histogram. This is the first peak comprising of a population of ≥8 zircon grains, at bin sizes of 30 zircons, along an age-probability plot, produced in ISOPLOT (Dickinson and Gehrels, 2009; Ludwig, 2009). YDZ is an ISOPLOT procedure used to derive the youngest detrital zircon ages from the sample population using a Monte Carlo Statistical analysis (Dickinson and Gehrels, 2009; Ludwig, 2009). The weighted mean average (YC2σ & YC1σ), derived in the AGE PICK Excel programme, takes into account both internal and external error of a youngest population. The youngest population, for the means of this study applies to a minimum clustering of three grains (≥3) to achieve a robust maximum depositional age for both 2σ and 1σ error (Dickinson and Gehrels, 2009; Jones et al., 2009). The ISOPLOT generated Weighted Average test comprises of an inverse variance-weighted average, which utilizes ages and associated errors, providing a means to clustering a batch of grains (Ludwig, 2009). The final, least sensitive test, is an ISOPLOT algorithm, TuffZirc age extractor (+8), which implements a statistical method of determining the youngest coherent population of zircons based on Pb-loss and inheritance associated error and discordance (Ludwig, 2009; Spencer et al., 2016). Together, the seven methodologies are correlated to provide statistically robust maximum youngest depositional U-Pb ages.

4   RESULTS

4.1   Facies Analysis

Outcrop based facies mapping of the nine traverses, collectively from Quthing (Moyeni), Masitise and Maphutseng, aided the identification of thirteen (13) lithofacies (Table 3). Distinct groupings of lithofacies codes, together with subsequent diagnostic architectural elements, provided a basis from which six (6) distinct facies assemblages (FA) were derived (Table 4; 5). Boundary surfaces primarily range from 1st to 3rd order surfaces (Table 5).

Facies Code	Lithofacies	Sedimentary Structures	Interpretation
Gcm	Pedogenic glaebule conglomerates: ranging from clast to matrix supported; Granule- to pebble-grade clasts, one boulder sized clast; polymictic clasts: glaebules, sandstone, bone fragments and quartz pebbles; poorly sorted; sub-angular to rounded	Rare clast orientation; palaeosol (loessic debris); massive; clast-supported (Gcm)	Lag deposits/debris flows
Gh	Pedogenic glaebule conglomerates: ranging from clast to matrix supported; Granule- to pebble-grade clasts, one boulder size clast; polymictic clasts: glaebules, sandstone, bone fragments; quartz pebbles; poorly sorted; sub-angular to rounded	Rare clast orientation; palaeosol (loessic debris); horizontally stratified (Gh)	Lag deposits
Sc	Clast-rich sandstones; granule-pebble sized clasts, intraclasts consists of mudstone/siltstone	Intraclasts	Hyperconcentrated flood-flow deposits/ scour fills
St	Fine- to medium-grained sandstone and siltstone	Trough cross-bedding	Dunes/lower-flow regime
Sm	Fine- to coarse-grained sandstones	Massively bedded; lack of internal structures; mudcracks; desiccation cracks; dewatering (slump) structure; fractured and altered as a result of a dense network of dykes in the Clarens Formation only; pedogenic alteration (vertical structures)	Rapid deposition of hyperconcentrated flows (no traction)
Sr	Fine-grained sandstones	Ripple cross-laminated; 3D ripples; flute casts	Ripples (lower-flow regime)
Sp	Medium- to fine-grained sandstones and siltstones	Planar cross-bedded	Dunes/lower flow regime
Sl	Fine- to medium-grained sandstones and siltstones	Low angle (<10°) cross-bedded; parting lineations	Humpback/washed-out dunes/ antidunes
Sh	Fine to medium-grained sandstone	Horizontally laminated mudcracks; scour marks; parting lineations; dewatering structures	Planar bed flows (lower- and upper-flow regime)
Fr	Siltstone and mudstone	Ripple cross-laminated; 3D ripples	Ripples (lower-flow regime)
Fsm	Fine-grained clay-silty mudstones, coarser silty-sand dominated mudstones	Massive; pedogenic alteration (especially in the uEF); calcareous infill; blocky weathering	Settling and/or waning flow (low energy)
Fl	Fine-grained clay-silty mudstones	Horizontally laminated	Low energy settling
P	Pedogenic alterations	Calcareous infills; desiccation cracks	Palaesol

Table 3: Relevant lithofacies codes used for the Elliot and Clarens formations of the Quthing (Moyeni), Masitise and Maphutseng localities. Facies codes modified from Miall (1977;1985; 1996; 2014).

Architectural Element	Major Lithofacies	Sedimentary Structures	Geometry
Floodplain Fines (FF)	Fsm, Fl, Fr and P	Some rare ripple structures, pedogenic alteration (glaebules, spheroidal weathering, calcareous infill), forms peds, nodules, root traces, fossilised wood, <1cm thick laminae, fossils	Thick (5-20 m) massively bedded to rarer horizontally/ripple cross-laminated mudstones, reddish-brown in colour
Channels (CH)	St, Sp, Sl, Sh, Fm	Trackways, intraclasts, parting lineations, less common dewatering structures, asymmetric ripples, flute casts, load casts, fossils	Asymmetrical and rarer symmetrical channel shaped units, one steep cutbank, often scour based, approximately 10-20 m wide, stacked in places, situated within thick mudstone units, sharp lower bounding surface, gradual coarsening up, sandy-silty channel fills, lenticular shaped sand bodies, laterally continuous
Lateral accretion (LA)	Sp, St, Sm and to a lesser degree Sh, Sl, Fsm	Imbricated clasts, parting lineations, asymmetric 3D ripples, root traces, trackways	Wedges and sheets with internal lateral accretion surfaces (point-bars/lateral bars), channel migration, laterally pinches out within ±2 m of the channel body
Channel Wings (CW)	Sp, St, Sm, Fsm	Ripple marks	Lateral pinching out of channels, 1 m thick
Scour Hollow (HO)	St, Sl, Sr	Ripple marks	Scoop-shaped concave-up hollow with an asymmetric sandstone/siltstone fill
Levees (LV)	Fl, Sm, Fsm, Fr	Pedogenic alterations, ripples	Thin sheets of fines associated with CH fill and sandy bedform deposits, accreted units of greyish-green massive mudstone units, some interfingering units of thin siltstones (commonly associated with CS), pinches out, 1.0 cm thick laminae
Crevasse Splay (CS)	Sm, Sh, Fsm, Sr, Fr, P	Coarser clasts, pedogenic alterations, fossil and trace material	<1m thick tabular/ lenticular sandstone and siltstone bodies, sharp basal boundary, fining upward, 3rd order
Sandy Bedforms (SB)	Sm, Sp, Sl	Load casts, massive	±1.5 m thick semi-horizontal concave-up lower-bounding CH surfaces, massive sheets, fining upward
Ephemeral Lake (LC)	Fl, P with less common Fr and Sh	Desiccation cracks, ripples, some pedogenic alterations	Thin successions or individual bodies 1.0-0.3 m thick lensoidal bodies consisting of 0.8 cm mudstone laminae interbedded with some thin sandstone and siltstone units (LS), does not exceed 2 m lateral extent
Laminated Sandsheets (LS)	Sm, Sh, Sl, Sr, P and rare Sp & Sc	Mud drapes, parting lineations, ripples, rare soft-sediment deformation, pedogenic alteration, desiccation cracks, carbonate infill, load casts, trackways	Sharply bounded, multistorey, thick beds of sand sheets (approximately 0.5-2.0 m high), laterally continuous, whitish appearance at times in silt-/sandstone (calcareous inclusions)
Debris Flow (DF)	Gcm, Gh, P, Sc	Clast supported, glaebules, granule-boulder sized clasts	Lenses and non-laterally continuous irregular beds, thickness varies from 0.5-1.5 m
Aeolian Dunes (AD)	Sp, Sm, Sh, Sr and rare Fsm	Mudcracks, desiccation cracks, soft sediment deformation, 3D ripples, pinstriping, burrows, trackways, frosted qtz grains	Aeolian dune cross-bedded sandstone wedges and sheets, set thicknesses: 5-15 m

Table 4: List of architectural elements found throughout the lEF, uEF and Clarens Formation.Interpretations based off Miall (1985; 1996; 2014), Bordy et al. (2004a), Eriksson (1981; 1983; 1985; 1986) and Hölzforster (2007).

Facies		Facies Type	Major Lithofacies	Bounding Surfaces	Unweathered & weathered colour	Formation	Architectural Element	Depositional Environment
		I (Mudstone dominated)	Fsm, Fl, Fr and P	0th to 2nd	(UW): 5GY 5/2 & 5Y 8/4 & 5YR 5/2 (W): 10R 5/4 & 5R 4/6 & 10R 4/6 &10GY 5/2 & 10Y 5/2	lEF & uEF	FF, LV	Overbank reworked and pedogenically altered floodplain fines
		II (Thick sandstone units)	St, Sp, Sl, Sh, Sm, Sr, Fsm, Fl, Fr	1st to 3rd	(UW): 10YR 8/6, 10Y 7/4 & 5GY 5/2 (W): 10YR 4/2 & 5Y 8/4 & 5Y 7/6 & 10GY 5/2 & 10Y 5/2	lEF & uEF	CH, LA, CW, HO, SB, LS and minor LV &FF	Meandering channel deposition with periods of high and low energy flow variations
		III (Lenticular sandstones and siltstones)	Sm, Sh, Fsm, Fr, Sr, P	1st to 2nd	(UW): 5GY 5/2, (W): 10YR 7/4 & 5Y 7/6	lEF & uEF	CS	Overbank lenticular deposits
		IV (Thick cross-bedded sandstone)	Sp, St, Sm, Sh, Sr and rare Fsm	1st and 3rd	(UW): 5Y 8/4 (W): 10 YR 8/6	Clarens	AD	Aeolian dune deposits
		V (Intercalated sandstones, siltstones and mudstones)	Fl, Sm, Sp, P, Sl, Sr, Fr and rare Sh, Sc , St	0th to 3rd	(UW): 5Y 8/4 & N6 & N9 (W): 10 YR 8/6 & 10Y 8/2 & N9	uEF & Clarens	LC, LS and minor CH & FF	Interdunal aeolian sandsheets; wet aeolian/minor backswamp consisting of playa lakes and intermittent flashflood sheet flows.
		VI (Conglomerate)	Gcm, Gh, P, Sm, Sh, Sc, Sl	2nd to 3rd	(UW): 10YR 7/4 & 10YR 6/6 (W): 10R 4/2 & 10YR 2/2	uEF	DF, LS	Denudation of floodplain palaeosols during flooding (debris flow)
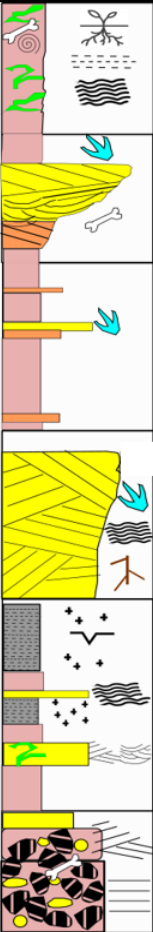
Legend:

- Mudstone
- Siltstone
- Glaebules
- Evaporites
- Bonebed
- Trackways
- Pedogenic alteration
- Calcareous infill
- Planar cross bedded (Sp)
- Sandstone
- Claystone
- Desiccation cracks
- Semi-horizontal burrows
- Rootlets
- Horizontally stratified (Gh)
- Qtz clasts
- Trough cross bedded (St)
- Horizontally laminated (Sh; Fl)
- Ripple cross laminated (Fr;Sr)
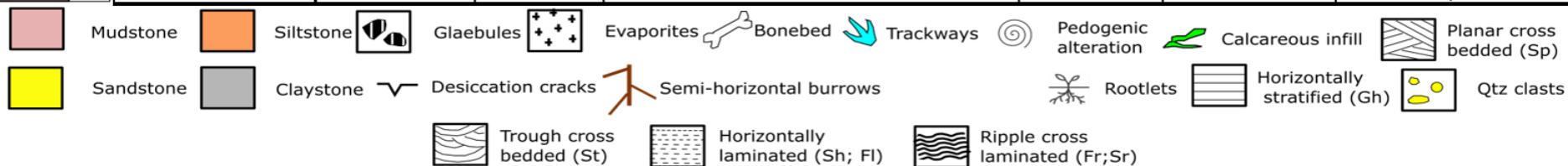
Table 5: Facies assemblage (FA) compilation based on facies codes and lithofacies architectural elements. A basic illustrated lithofacies overview is also provided for each FA. Modified after Miall (2014), Bordy et al. (2004a), Eriksson (1981; 1983; 1985; 1986) and Hölzforster (2007).

4.1.1   Facies Assemblage I (Mudstone dominated):

4.1.1.1   Description

The mudstone dominated Facies Assemblage 1 (FA 1) occurs throughout the uEF and lEF fluvial deposits. The following facies codes were identified in order of most to least abundant: Fsm, Fl, Fr and P (Table 3). FA 1 lithofacies comprise of mud and clay sized particles, with some variation occurring occasionally with the inclusions of silty-mudstone lenses and intraclasts. A unique, easily distinguishable feature of these pedogenically altered mudstones is the reddish-maroon oxidation with more minor intercalated greyish-green units. Unweathered mudstone units range from predominantly grey mudstones (5GY 5/2) to typical grey-yellow (5GY 5/2 and 5YR 5/2) colour schemes. Whereas, the weathered units display the charactersitic reddish colour range and an array of greyish-greens, including: 10R 5/4, 5R 4/6, 10R 4/6, 10GY 5/2 and 10Y 5/2.

The thick units of FA 1 comprise predominantly of massively bedded mudstones and more minor horizontal and ripple-cross laminations. Pedogenic alteration is noted throughout almost all of the units, including structures such as calcareous infill, nodules, peds, irregular mottling and abundant root traces. The horizontal laminae that have been preserved occur sporadically and are <1 cm thick in the reddish-oxidized units. Conversely, the greyish-green units host a better preservation of ~1 cm thick horizontal laminations and 0.2 cm thick ripple cross-laminations. Intraclasts (small pebbles: ~0.8 cm in diameter) occur proximal to the pedogenically altered horizons.

Bed thicknesses vary greatly, however generally tend to range in thickness from 5.0 to 20.0 m. These very thick units typically do illustrate an undulating thickness throughout their lateral extents; however, ultimately remain continuous. On the other hand, the more greyish-green mudstone subunits are not laterally continuous, generally interfingering the other mudstone units, laterally pinching out within 4.0-26 m and tend to be no thicker than 1.2 m. The bounding surfaces of FA 1 beds comprise of 1st to 2nd order fine scale laminae and coset contacts. Overlying beds often

form 3rd order convex up, sharply eroded boundaries, whereas lower bounding surfaces often comprise of gradational 1st to 2nd order boundaries. FA 1's thick successions of fine-grained maroon and greenish-grey beds can be attributed to a combination of two overbank architectural elements, namely: floodplain fines (FF) and levees (LV), respectively. Body and trace fossils are hosted within these beds, including an abundance of roots, stumps and body fossils (complete; fragments; tarsal digits; teeth). Bioturbation preservation within the mudstones of this study's localities are limited (BI 0).

4.1.1.2   Interpretation

The thickly bedded fine material, lack of internal features (Fsm) and minor horizontal and ripple-cross laminations of FA 1 suggest low-energy suspension settling associated with cohesive floodplain fines (FF) and associated overbank levees (LV). Evidence for less cohesive, medium-energy floodplains was also found in rarer massive and horizontally laminated silt-rich mudstones and siltstones. Thus, this clay and mud dominated FF and LV fraction, alongside its proximity to channel (CH) elements and pedogenically altered state is interpreted to represent the large-scale overbank deposits of an extensive fluvial system (Fig. 9). Previous Elliot Formation palaeoenvironmental interpretations described a similar fluvial dominated system with extensive floodplain coverage (Botha, 1968; Visser and Botha, 1980; Eriksson, 1983; Eriksson, 1985; Smith et al., 1993; Bordy et al., 2004c).

Three distinct floodplain types were noted throughout the FA 1 Elliot exposures, including: 1) rarer meandering fluvial-lateral migration floodplains, with an outward (laterally) and upward fining deposits (Leopold and Wolman, 1957; Jackson, 1976; Nanson, 1980; Nanson and Croke, 1992); 2) more abundant laterally stable single channel floodplains characteristic of low-energy environments, dominated by a high proportion of vertically accreted suspended-load overbank material (Beckinsale and Richardson, 1964; Macklin, 1985; Croke, 1991 [Unpublished]; Nanson and Croke, 1992); and, 3) anastomosing river floodplains (inorganic floodplains) of semi-arid ephemeral rivers with extensive

overbank muds preservation as pedogenic aggregates. These pedogenic overbank muds are found to be closely associated with single channels are dominant throughout the uEF (Nanson et al., 1986; 1988).

The thick FF elements were deposited over long periods of time, with seasonality driven markers supported by the distinct diagenetic oxidation of ferruginous silicates and clay minerals present in the material. The oxidated reddish-maroon habit and clear palaeosol indicators (cubic peds, nodules, soil horizon formation, rhizoliths, calcareous infill) present seasonally fluvial driven overbank fines accumulation, punctuated by extended drier periods (Fig. 10). These 'drying periods' of depositional waning lead to the development of palaeosols (loessic soil and laterite oxisols) in conjunction with an associated biogenic influx and become more apparent as we move further up in the Elliot Formation (Fig. 9). Conversely, greenish-grey mottling dominates the grey mudstone units of the intercalated LV deposits and are indicative of a higher-clay content and comparatively smaller amounts of non-oxidized iron-rich minerals (Merriman et al., 2003). The sustained greyish colouring with some overlying mottling suggests a water saturated reduced section, which can be ascribed to seasonal fluctuations in water table rise and fall (van Breeman, 1988; Schwertmann and Taylor, 1989; Schwertmann, 1993).

LV element internal structures also display definite variations in depositional energies, contrasting between higher energy horizontally laminated and lower shallow ripple cross-laminated beds (Allen, 1970; Reineck and Singh, 1973; Singh, 1972). The horizontally laminated deposits predominantly occur as a result of more rapid and turbulent sedimentation associated with seasonal flooding, whereas ripple cross-laminated and FF deposition occur during river flow subsidence (drier periods). These variations in sedimentation ultimately illustrate the symbiotic effect fluvial channels have on bank and overbank deposits (Fig. 9; Allen, 1965; Smith, 1983; Bridge, 1984; Farrell, 1987).
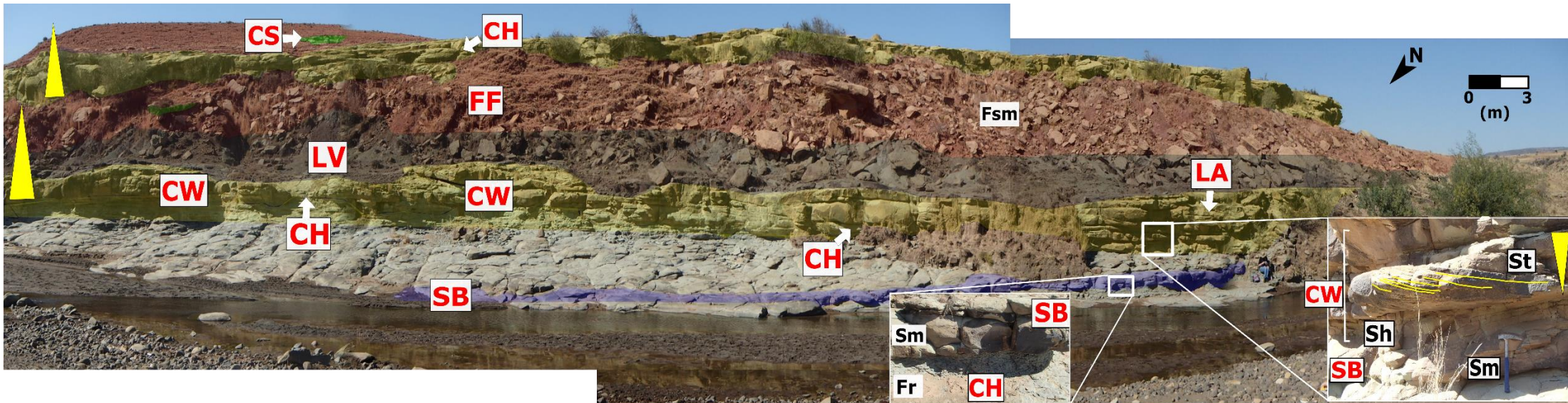
Fig. 9: Outcrop along Traverse 9, Maphutseng. Depositional facies and associated lithofacies structures of beds are highlighted. Yellow prisms present grain size succession, which in turn shows a upward fining succession. Lowest exposed surface displays a CH feature, sharply overlain by a SB, which in turn is overlain by upward coarsening CH and their associated CW and LA. There is one main CH alongside a smaller secondary CH. CH bedfills provide typical proof of concave up lower boundaries and 2nd order upper bounding surface. The CH suite is directly accompanied by LV fines and overbank FF. The boundary between the LV and FF is of a 1st order nature. The FF also display typical massive bedding. The FF in turn is again eroded and capped by a single CH bed. The entire sequence is capped off by gradational overbank FF, with interstitial lensoidal CS.

4.1.2   Facies Assemblage 2 (Thick sandstone units):

4.1.2.1   Description

Major sandstone bodies are relatively common throughout the lEF and uEF (Table 5). FA2 comprises of the following lithofacies, in order from most to least abundant: St, Sp, Sl, Sh, Sm, Sr, Fsm, Fl and Fr (Table 3). These FA 2 bodies gradually coarsen upwards (inverse grading), often transitioning from basal finer-grained siltstone, mud-dominated siltstones and less common mudstones to coarse- to medium-grained (arkose-feldspathic litharenite) sandstones. Rare intercalated individual mudstone and silty-mudstone lenses also occur throughout FA 2. Unweathered exposures range in colour from the pale yellowish orange (10YR 8/6) and greenish yellow (10Y 7/4) of sandstone and siltstone beds, to the dusky yellow green (5GY 5/2) for the finer grained interspersed mudstones. Weathered units show distinct colour variety amongst the yellow-brown sandstone and siltstones (10YR 4/2; 5Y 8/4; 5Y 7/6) and greyish green mudstones (10GY 5/2; 10Y 6/2).

Sand-silt bodies are predominantly trough cross-, planar cross- and massively bedded. Individual units host internal structure variations, including: cross-bedding (planar- and trough-) with angles of repose ranging between 20-33° and laminae/bed thicknesses ranging from 0.3 to 11.6 cm; massively bedded siltstone and mudstone units with no internal structure preservation; low-angle planar cross-bedded units with lower angles of repose (up to 18°) and lamination thicknesses <0.8 cm. Rarer instances of ripple cross-bedded and horizontal laminated fine-grained sandstones and siltstones include bed/laminae thicknesses <4 cm.

Interesting internal microfeatures include: basal bed intraclasts, rip-up clasts, dewatering structures and load casts. More common microfeatures comprise of 3D sinuous ripples (both surficial and cross-bedded) with RI and RSI values ranging from 3.3-26.7 (majority: 8-9) and 2.3-5.2, respectively, minor flute casts and scour marks, suggestive of water-wind current type deposition (Fig. 10). Mud drapes and parting lineations between sub-sets are suggestive of periods of low flow-

energy associated settling of fines. All of these features provide ample palaeocurrent indicators.

Rare soft sediment deformation is noted in the form of small-scale dewatering structures (Lowe,

1975).
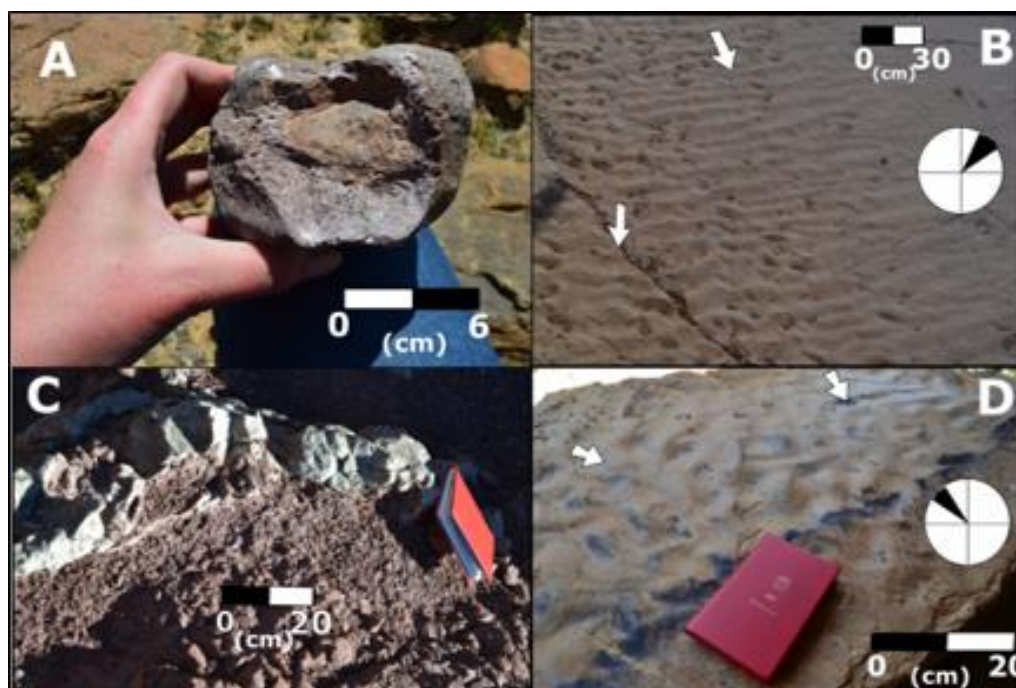
Fig. 10: Various structures found throughout the stratigraphy. (A) Irregular maroon/grey nodule from the uEF of Maphutseng, Traverse 8; (B) Relatively linear 3D ripples on the lower Moyeni trackway site depositional bar in the uEF (NE palaeocurrent); (C) Calcretized palaeosols within the FF of the uEF; (D) 3D wind ripple surface of the Clarens Formation (NW palaeowind). Note: palaeocurrent indicated in B and D with white arrows.

Beds feature sharp basal erosional boundaries, where concave-up and scoured 3rd order

boundaries dominate. Bounding surfaces range from 1st to 3rd order throughout the various FA 2

units, progressively changing from erosion dominated 3rd order basal contacts to finely-bedded (and

laminated) 1st order boundaries proportional to gradationally coarsening deposits. The topmost

contact often occurs with FA 1 or FA 3 fines, forming a 2nd order sharp contact. FA 2 subset beds

range in thickness from 0.3 m to 10.0 m and are relatively laterally continuous, with approximate

lateral extents ranging between lensoidal bodies with traceable extents <20 m to regionally

continuous bed sets.

Within FA 2, a total of eight (8) architectural elements collectively make up the major sand-

silt dominated bed sets, namely (from most abundant to least); channel elements (CH), lateral

accretion elements LA, channel wing elements (CW), scour hollows (HO), sandy bedform deposits

47

(SB), laminated sandsheets (LS), minor levee (LV) and minor floodplain fines (FF). The bedform

morphologies range from sheets, lenses to wedges. Scour hollows (HO) often form the basis of the

CH deposition, forming concave-up scours filled with trough and planar cross-bedded sandstone and

siltstone CH beds. These elements show thick asymmetric channel shaped beds with one steep

cutbank and another gentle adjacent point bar bank. Symmetrical units with two gently sloping

banks and resultant concentric fill tend to be rare (Gibling, 2006; Miall, 2014). The main CH units

show a wide variety of thicknesses, from thin unconfined ribbon-like sheets (0.6-2.0 m) to thick

amalgamated multi-storey successions (<10 m). The CH bodies themselves are generally not laterally

extensive (0.8-1.6 m), however associated elements, including CW and LA provide greater lateral

extents (Fig. 11).
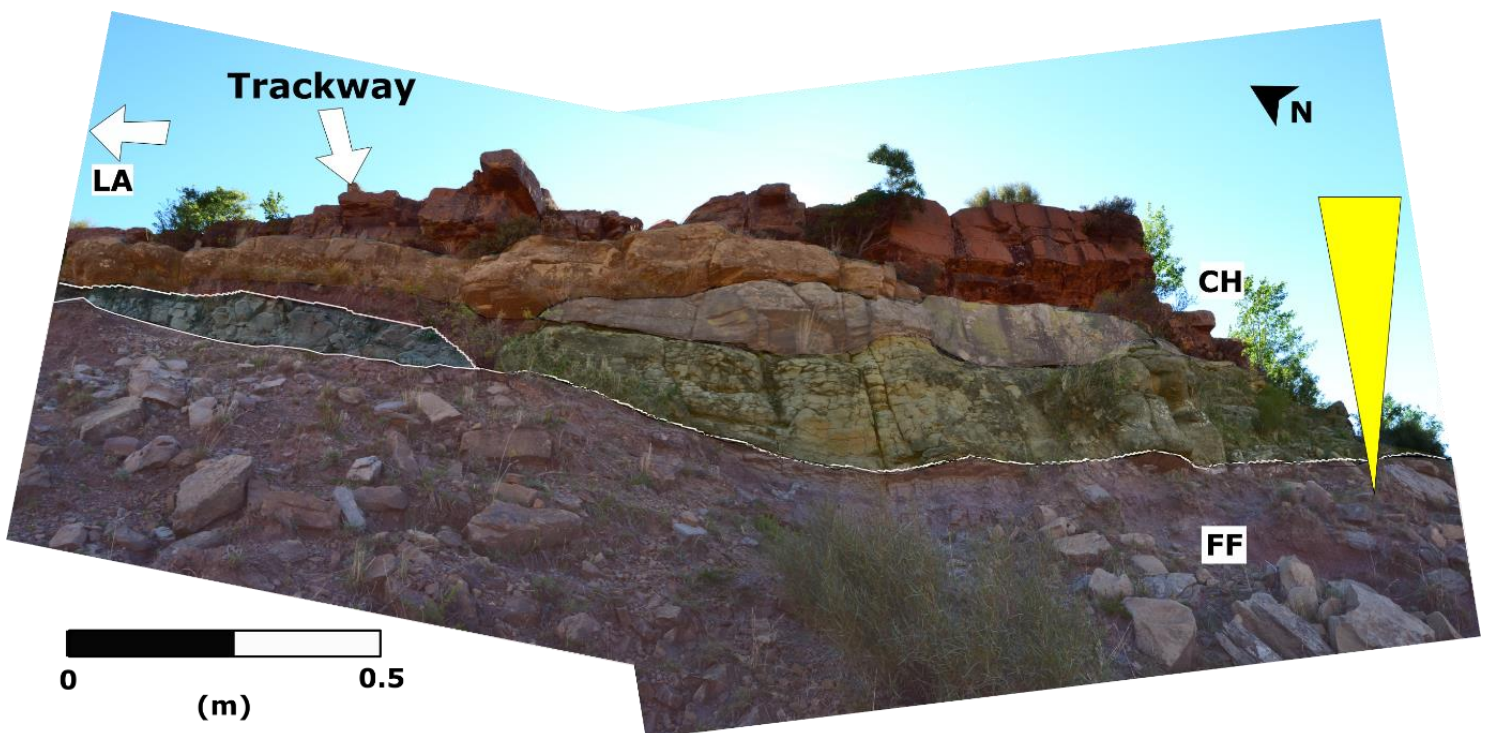
Fig. 11: An illustration of a multi-storey channel stack found in the lEF of Maphutseng, adjacent to the famous Maphutseng bonebed (in FF below) and trackway surface at the top. The channel geometry is asymmetric with successions of trough cross-stratified accretions comprising of a mixed fill. The lowermost concave-up yellow highlighted bed consists of a mud-dominated siltstone. The grain size increases upwards and gradually becomes medium-grained sandstone at the uppermost, trackway bearing layer of the succession (coarsening up). Bar migration to the East was along lateral accretion surfaces.

Directly associated with the CH sandstone units are accreted wedges and sheets that

laterally extend and pinch out to form laterally accreted beds (LA; Fig. 12) and channel wings (CW).

CW elements occur exclusively with channels (CH) and interconnect secondary channels to main channel bodies, gradually pinching out within 2.0 m of the main channel body. LA elements have toe to crest heights ranging from 0.4 to 2.3 m and continuous lateral extents, with only a few accretions ending within <20 m of the main CH body. Laminated sandsheets (LS) often form part of the multi-storey complexes ranging in thicknesses of 0.5-2.0 m and are laterally continuous up to 10 m. Semi-horizontal SB elements also form minor inclusions in FA 2 complexes, with individual units often ~1.5 m thick with very little lateral extent (<2 m). Rare instances of LV and FF deposits often occur as non-laterally extensive lenses (<1 m thick) intercalated with other FA 2 subunits.

An abundance of recorded and new Early Jurassic-Late Triassic trackways was found on the associated channel bar fill elements, including LA, CW and LS (Fig. 12). FF and LV mudstones also show evidence of pedogenic alteration by way of irregular mottling (suggesting a relatively immature palaeosol), calcareous infill, nodules, peds and root traces. Bioturbation preservation throughout FA 2 elements of this study was limited to individual burrows (BI 1).

4.1.2.2   Interpretation

FA 2 (major sandstone and siltstone) beds describe meandering fluvial channel deposits. The association of CH, LA, CW, LS, SB architectural elements in multi-storey complex to simple sheet-like units provides ample consensus regarding a meandering flow-type setting (Fig. 9; Allen, 1965; Walker, 1976; Friend, 1983; Miall, 1984; Fielding, 2006; Gibling, 2006; Miall, 2014). With regard to the CH unit thickness and width readings, they are categorized using Gibling (2006) as fixed narrow to broad ribbons and mobile multi-storey succession sheets. CW thinly bedded planar cross-bedding and trough cross-bedding are continuous (have the same bedding planes) with beds thickest within the CH (Hirst, 1991). CH and CW loads occur as either bedload-rich (dominantly sand-rich) deposits, or, a mixed load constituting of a higher percentage of suspended material alongside the bedload. Resultant channel mixed load fill ranges from muds, siltstones, coarse- to fine-grained sandstone and preserve heterolithic bank and bed accretions (Fig. 11; Galloway, 1981; Schumm, 1981).

Associated lateral accretions (LA) are the result of low-flow energy lateral accretion of material along the point bar throughout channel migration, confirmed by the upward fining succession within the subunits (Allen, 1965; Blatt et al., 1972; Reineck and Singh, 1980). This meandering river migration-offset is established by the indicative toes of the LA derived channel bars and the predominance of planar cross-bedding, similar to LA bedding descriptions in Allen (1968) and Singh (1972) (Fig. 12).
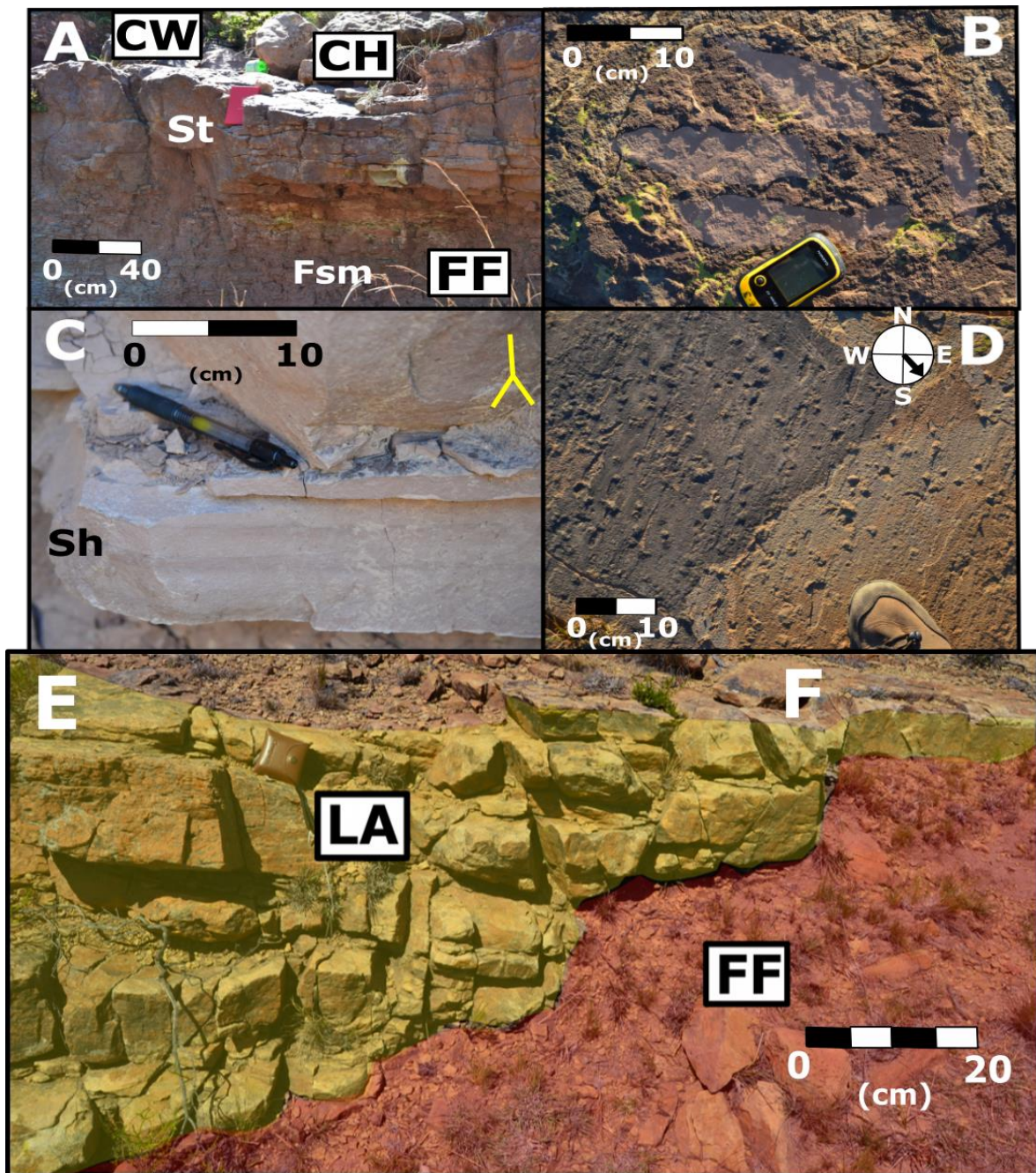
Fig. 12: (A) Narrow channel (CH) ribbon in the uEF of Traverse 1; (B) Footprint of a tetrapod trackway in the lEF, discovered in this study along Traverse 6 in Maphutseng; (C) Rare horizontally laminated sandstone in a crevasse splay (CS) deposit in the uEF along Traverse 1, Moyeni; (D) preservation of parting lineations and pebble sized intraclasts; (E) Annotated outcrop displaying typical lateral accretion wedges within the uEF of Traverse 7, Maphutseng.

Intermittent periods of increased flow energy are described by the relatively thick, silty-sandstone LS beds (Miall, 1977, 1984; Rust, 1978; Tunbridge, 1981; Tunbridge, 1984; Sneh, 1983). Sandy bedforms (SB) are also a product of channel aggradation as a result of individual flood events, evidenced by the predominant basal load cast preservation, massive bedding and fining upward SB and LS subsets (Miall, 1985). SB beds are closely associated with the concave-up lower bounding surfaces of broader, unconfined channels. Deposition thus occurs as individual flood events throughout the progressive abandonment of these channels, as evidenced in Fig (9). The rarer lenses of FF and LV fines within the thick meandering fluvial successions of FA 2 are associated with limited natural levee overbank deposits and the gradational upward fining deposits above lateral point bars (Fig. 12; Allen, 1968; Coleman, 1969; Reineck and Singh, 1973; Smith, 1983; Farrell, 1987).

Although the majority of FA 2 defining architectural elements are present throughout the Elliot Formation, some morphological variations between the lEF and uEF major siltstones and sandstones are evident. With regard to the distribution of FA 2 thick major sandstone/siltstone bodies, an abundance is noted throughout the lEF, whereas the uEF shows further spaced out, more intermittent occurrences of FA 2 successions. River morphologies throughout the Elliot Formation range from unconfined ribbons/sheets, straight to meandering channels with secondary channel associations, fixed channel deposits, mobile meandering channel sets and anastomosing characteristics, respectively (Friend, 1983). Channel sets display a mobile multistorey succession dominated deposition, related to laterally unstable meandering rivers, more commonly associated with the lEF (Gibling, 2006). Non-channelised (unconfined) ribbons and sheets provide proof of floodplain and aeolian set ephemeral sheetfloods throughout the Elliot, especially prevalent toward the upper portion of the uEF (Eriksson, 1979; Turner, 1981; Hogg, 1982; Stear, 1983; Tunbridge, 1984; Stear, 1985; Kelly and Olsen, 1993; Miall, 1996; Fielding, 1999; Giblling, 2006; Hampton and Horton, 2007). SB elements, concentrated within the lEF, are commonly associated with sand-dominated river systems, suggesting a higher prevalence of sand-dominated fluvial deposits in the lEF (Allen, 1968; Southard, 1971; Harms et al., 1975; Harms et al., 1982).

4.1.3   Facies Assemblage 3 (Lenticular sandstones and siltstones):

4.1.3.1   Description

Lenticular (and rarer tabular) sandstone and siltstone units abundantly occur throughout the Elliot Formation and are closely associated with FA 1, 2 and 5 deposits (Table 5). FA 3 comprises of the following lithofacies, in order from most to least abundant: Sm, Sh, Fsm, Fr, Sr and P (Table 3). FA 3 comprises predominantly of clay-rich siltstone and fine-grained sandstone bodies. Basal boundaries of FA 3 bodies are gradational and fine upwards (inversely graded) from clay-rich siltstone to fine-grained sandstone. Units also display lateral fining from fine-grained sandstones to more distal clay-rich siltstones. Unweathered colours are predominantly greyish yellow (5Y 8/4), whereas in contrast, more weathered units display an array of orange-yellows (10YR 7/4 and 5Y 7/6).

Internal structures (or lack thereof) are dominated by massively bedded units, as well as less common horizontal laminations and ripple cross-laminations. Horizontal laminations/beds and ripple cross-laminations have thicknesses between 0.5-1.5 cm. Some rarer pebble sized intraclasts and planar- and low angled-crossbedding, with 0.3 cm thick laminations, predominantly occur within the siltstone units.

Sandstone and siltstone units often occur as non-laterally extensive lenses (<10 m), with thicknesses of up to 1.0 m, but usually ranging between 0.3-0.8 m. However, in the uEF these beds tend to be more tabular and continuous. Bounding surfaces range from 1st order mudstone laminations, to 2nd order upper bounding surfaces for sandstone and siltstone units. FA 3 is composed of one main architectural element, namely crevasse splays (CS). The lenticular CS units are interestingly intercalated with FA 1 elements and located proximal to FA 2 CH elements, representing a definite association with overbank deposits (Fig. 9; 13).

Both fossil and trace material are hosted within and on the top surfaces of these units. Pedogenic alteration by way of internal structure loss (massively bedded) as well as the presence of

columnar ped structures, carbonate rhizoliths, calcification and rarer spheroidal weathering is prevalent in the CS siltstone units.

4.1.3.2   Interpretation

In comparison to both modern- and ancient-facies analogues, these tabular and lenticular siltstone and fine-grained sandstone units, with their close association with overbank-type deposits, are directly comparable to crevasse splays (CS) (Frazier and Osanik, 1961; Bernard and Major, 1963; Harms et al., 1963; Allen, 1968; Coleman, 1969; Reineck and Singh, 1971; Smith, 1983; Farrell, 1987; Eberth and Miall, 1991; Mjøs et al., 1993; Sarti et al., 2001; Pranter et al., 2009).

The CS elements are a result of the decreased, load capacity driven, overbank deposition associated with channel bank (levee) breaks (Bridge and Demicco, 2008). Lateral material grading provides proof of varying suspended material and flow energies along these fan-shaped splays, with the coarsest material occurring adjacent to channel bodies and laterally fining to clay-rich mudstones at the distal ends (Smith et al., 1989). Crevasse splays, as suggested by Millard et al. (2017), require large proportions of relatively coarse-grained suspended sediment and an associated steep slipface along which the crevasse splay flows away from its source channel. The rarer planar cross-bedding and low-angled planar units occur as a result of scouring by secondary channels and smaller distal interfingering slipfaces, associated with the larger main splay bodies (O'Brien and Wells, 1986). Previous works have suggested that crevasse splay dimensions are not directly related to channel flow or size. In fact, varying lateral extents, including the laterally continuous tabular crevasse splay units and less extensive lenticular splay units, are primarily controlled by floodplain drainage capabilities and suspended material type (Millard, 2013). The direct correlation between wide-spread crevasse splays and well-drained FA 1 floodplains (FF) coupled with intermediate silt to fine-sand grain sizes confirm the presence of well-drained floodplains, especially prevalent throughout the uEF. On the other hand, coarser sands found in the lenticular, less laterally extensive, splays are a likely result of limitations produced by poorly-drained floodplains (Fig. 9). The clay-rich

fraction, pedogenic alteration stuctures (columnar ped structures, carbonate rhizoliths, calcification) and massive bedding preserved within these beds can be classified as loessic siltstone beds, which are especially abundant within the uEF. This concurs with previous loessic bed classification provided by Smith and Kitching (1997). The most prominent variation between FA 3 successions in the lEF and uEF is the greater concentration of laterally extensive, tabular CS elements within the uEF, whereas the lEF hosts a relatively even proportion of both lenticular and tabular units.
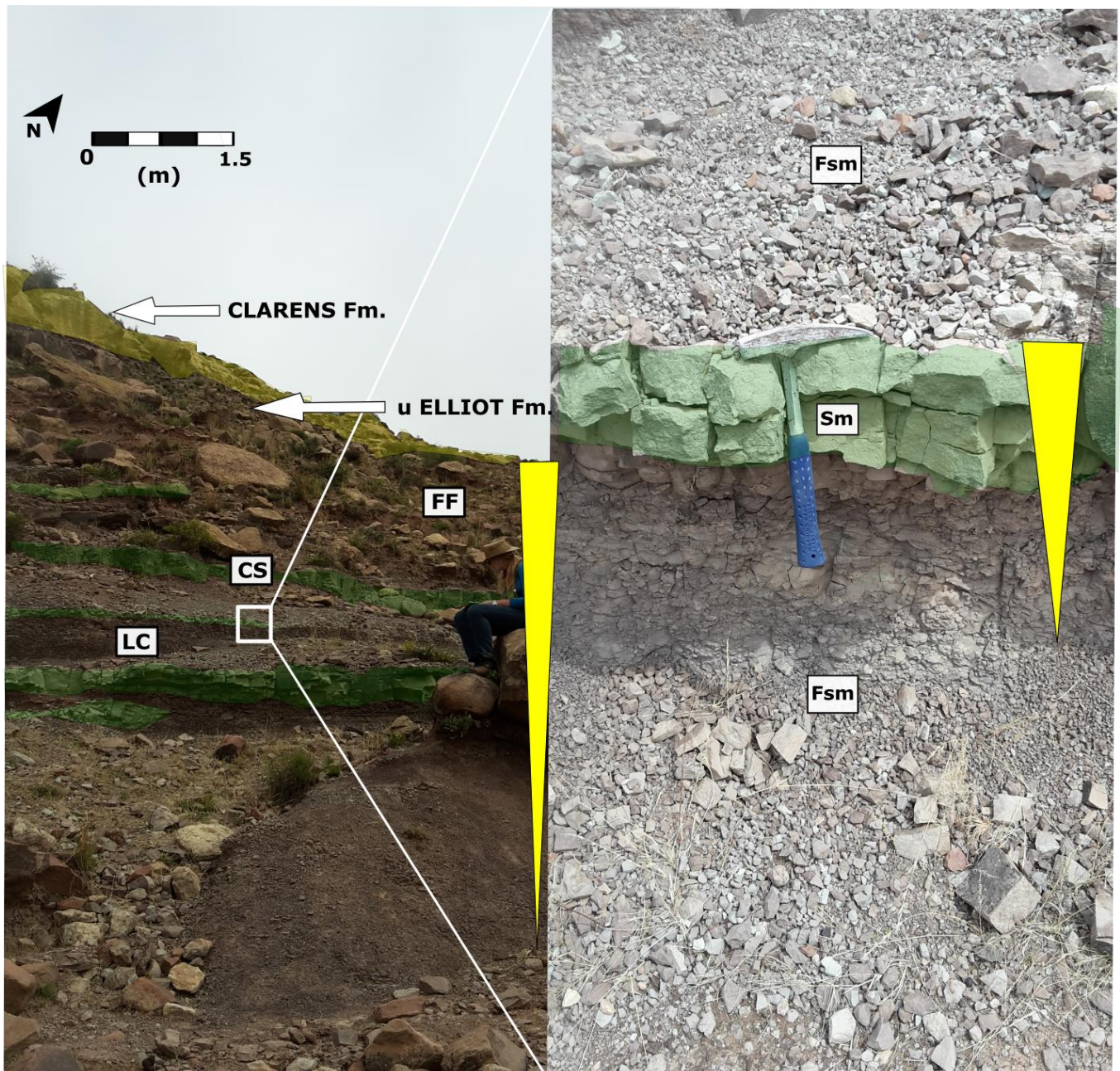
Fig. 13: FA 3 and 5 features along Traverse 2 in the uEF of Moyeni. Note the internally massive and lenticular geometry associated with the CS (green) and interbedded LC beds. Also note the coarsening upward trend of the aeolian Clarens Formation deposits.

54

4.1.4   Facies Assemblage 4 (Thick cross-bedded sandstone):

4.1.4.1   Description

Distinct, laterally extensive thickly cross-bedded sandstone successions (FA 4) constitute the majority of Clarens Formation exposures. FA 4 is composed of the following lithofacies, from most to least abundant: Sp, Sm, Sh, Sr and rare Fsm (Table 3). The assemblage comprises predominantly of fine- to medium-grained arenites and rarer carbonate-rich cemented siltstones and mudstones. Sandstone grains are characteristically moderately to well-rounded and well-sorted. The units display the typical unweathered greyish yellow (5Y 8/4) and more weathered pale yellowish orange (10 YR 8/6) sandstone colours commonly associated with the Clarens Formation.
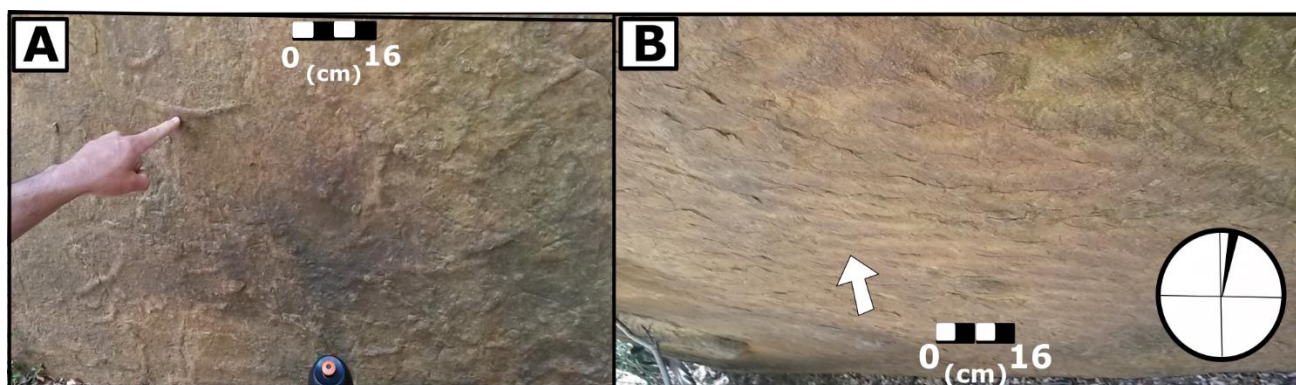
Fig. 14: Sedimentary structures within the AD, Clarens Formation. (A) Burrow cast networks in a fallen block in Masitise; (B) Sinuous 3D wind ripples (15⁰) on an aeolian dune (AD) unit. Note: palaeowind direction indicated with a white arrow.

The most distinct internally preserved lithofacies of the Clarens Formation are the thick successions of planar cross-bedded sandstone wedges and planar tabular subunits. Apart from cross-bedded sandstones, the sandstone and siltstone beds also host massively bedded subunits (no internal preservation), horizontal laminations, ripple cross-laminations and massive silty mudstones. The various cross-bedded foresets provided a 27-30° angle of repose range and internal subunit laminae tend to be 0.8 cm thick. FA 4 beds also host an array of distinguishing features, all pointing toward arid climes with occasional paedogenic alterations present, including; desiccation cracks, soft sediment deformation, 3D sinuous asymmetrical ripples (RI: 26.7; RSI: 1.7-3.6), grainflow cross-laminae, pinstriping and frosting on quartz grains (Fig. 10A; 10D; 14).

Bed thicknesses of the tabular and wedge dominated unit successions range from 5.0 m (commonly planar tabular units) to 15.0 m. Units are laterally extensive (>20.0 m); however, a general lack in continuous Clarens Formation bearing outcrops at the study localities (due to weathering) made the verification of exact lateral extents difficult. FA 4 cross-bedded units can be subdivided into individual subunit wedges and sheets, which host 1st to 3rd order boundaries.

Fossils and trace fossils are common in aeolian dune (AD) beds, including tridactyl trackways, bone fragments and burrows (Fig. 15). Burrows recorded within the units of this study are fairly sparse with networks often being sub-horizontal and classifiable as BI 2 (Fig. 14).

4.1.4.2 Interpretation

The Clarens Formation is renowned for its aeolian fluvio-dunal deposits (Haughton, 1924; Du Toit, 1939; Stockley, 1947; Eriksson, 1981; Eriksson, 1986; Holzförster, 2007). The distinct FA 4 arenite and siltstone bed morphologies and associated structures are interpreted as successions of aeolian dune (AD) architectural elements belonging to aeolian dominated deposition. The main defining and typifying feature of these AD deposits is the predominance of large-scale planar cross-bedding. Comparisons to the sandstone characterisation criteria by Glennie (1970), Margolis and Krinsley (1971) and Kocurek and Dott (1981) provide a definite aeolian dune (AD) element classification, supported by the: well-sorted and -rounded nature of the quartz arenite sandstones (mature aeolian deposition); 'frosted and pitted' surficial textures on single quartz grains that is related to aeolian deposition; grainfall laminae (pinstriping); and, grainflow cross-stratification representing transport. Further aeolian depositional setting defining structures include the high angle of repose (27-30°) within the cross-bedded units, which; although not the theoretically ideal 34° angle of dry sand as stated by Glennie (1972) and Turner (1980), still falls well within the usual realistic ranges of 25-34° found in global AD deposits. Ripple structures associated with FA 4 units are relatively asymmetrical (RSI: 1.7-3.6) and ripple index values >15 confirm wind driven deposition (RI: 26.7; Tanner, 1967).
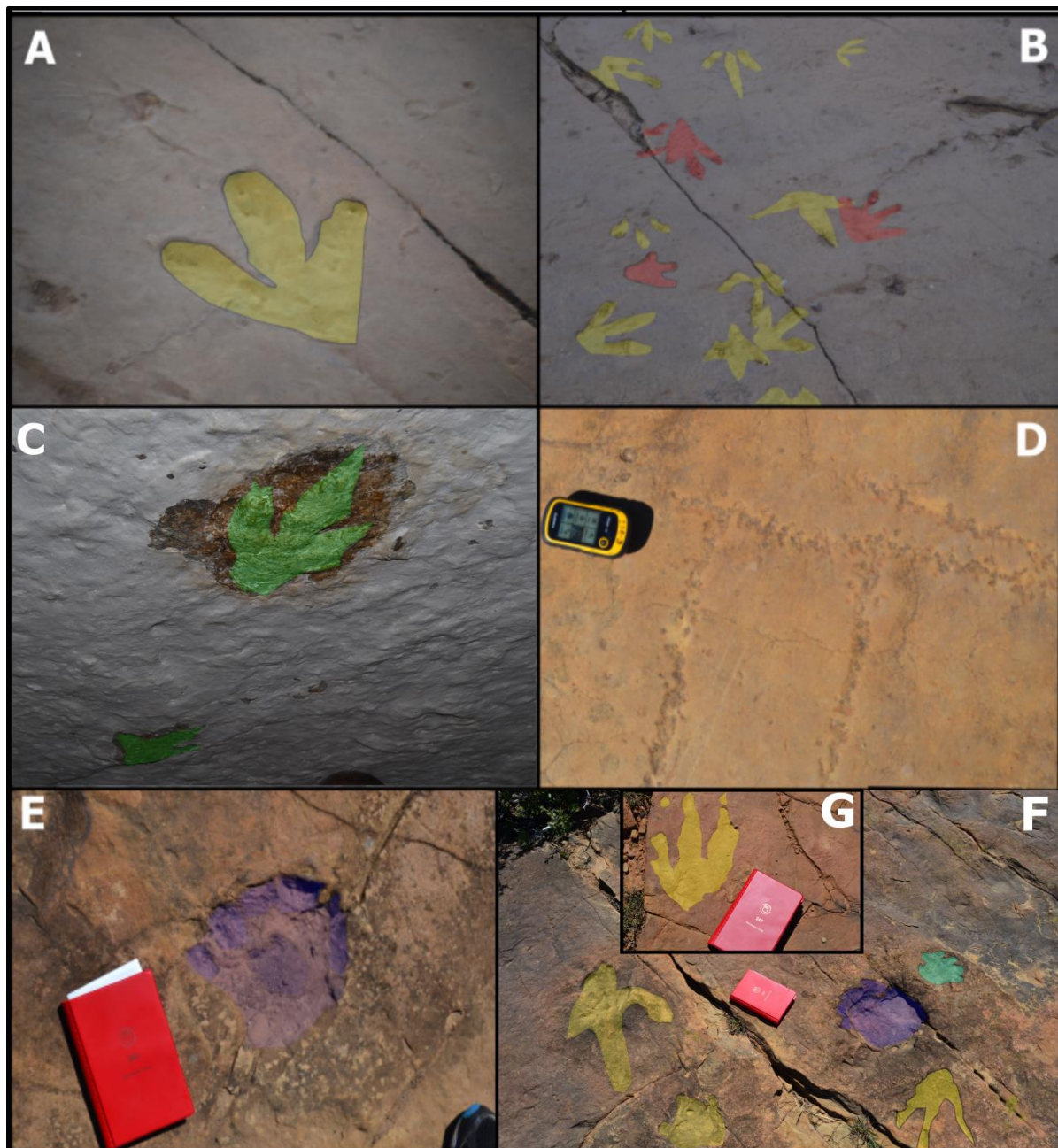
Fig. 15: Various trace fossils of the Clarens and Elliot formations. Tridactyl footprint (A) and a portion of trackway (B) at the lower Moyeni trackway site (also see Ellenberger, 1974; Smith et al., 2009; Marsicano et al., 2009; Wilson et al., 2009); (C) Tridactyl bipedal trackway on the roof of the Cave House, found at the upper Elliot-Clarens contact of Masitise; (D) Invertebrate trackways in the uEF at Masitise; note the various tiny parallel-impressions implying multiple leg sets of the same trackmaker; Various tracks on the Maphutseng trackway surface, including: tetradactyl (blue and green; E and F) and tridactyl (yellow; F and G) trackways. Also note the variance in track preservation with differing substrates.

Utilising Glennie's (1970) system for the tentative interpretation of attitude and interrelation of foresets—a system of interfingering AD elements and interdune areas, reactivation surfaces, 2nd order bounding dune migration surfaces and superimposition surfaces are prevalent throughout FA 4. The definite classification of FA 4 as dry aeolian dune deposits of an arid, wind-blown aeolian setting is comparable to Eriksson's (1986) Facies 4 interpretation.

4.1.5   Facies Assemblage 5 (Intercalated sandstones, siltstones and mudstones):

4.1.5.1   Description

Distinct lenses of minor interbedded sandstone, siltstone and mudstone units occur throughout the Elliot and Clarens formations. FA 5 comprises of the following lithofacies, in order from most to least abundant: Fl, Sm, Sp, P, Sl, Sr, Fr and rare Sh, Sc, St, Fsm (Table 3; Fig. 16; 17). Sandstone facies are generally classified as fine-grained quartz to arkosic arenites. Siltstone lithofacies are mud and silt dominated, with calcareous clay inclusions not uncommon. Mudstones also display high proportions of calcareous clay contents, alongside otherwise mud dominant compositions, producing a distinct white-grey appearance. Unweathered sandsheets and siltstones displayed a yellow grey colour, 5Y 8/4, typical of arenites, however weathered units ranged between more greenish/reddish yellows (10YR 8/6; 10Y 8/2) and whites (N9). Mudstones are easily distinguished due to their calcareous-rich, 'white-grey' colour, which tends to alter from grey (N6) to white (N9) with the addition of weathering (Fig. 13; 17).

The majority of sandstone and siltstone facies lack internal structures and are massively bedded. However, planar crossbedding, horizontal laminations, low-angle and ripple cross-bedding are also commonly preserved (Fig. 16). Cross-bedding occurs at a 30° angle of repose and thicknesses in lamination and bedding planes range between 0.3-0.7 cm and ~1.5 cm, respectively. Rarer instances of small-scale clast-rich and trough cross-bedded sandstones have also been noted. The sandsheets often host mud drapes and parting lineations, presenting periods of increased fines settling as a result of decreased flow-energy. The sandsheets also host rarer soft-sediment deformation and periodic drying in the form of desiccation cracks. Ripples are a common feature found in both mudstone lenses and sandsheets. Sandsheet ripple morphologies annotate largely wind dominated characteristics, including; RI ranges of 3.3-8.0 and RSI values equivalent to 1.7. Lensoidal mudstone units are dominated by horizontal laminations (0.8 cm thick) alongside interstitial silty mudstone/siltstone massive and horizontal laminations. Ripple cross-laminated

mudstone preservation occurs rarely. Interesting features include: calcareous infill and desiccation cracks (Fig. 17).

Sandsheet thicknesses range between 0.5-2.0 m and are relatively laterally continuous, extending up to 20 m with gradational lateral pinch outs. Mudstone and siltstone bodies are not laterally extensive and form lensoidal bodies that extend up to 2 m maximum (Fig. 13). These bodies are also thin, with 0.3 m being the average bed thickness. Bounding surfaces within FA 5 sequences generally range from 0th order gradational to 3rd order sharp contacts. Individual sandsheets tend to have a sharp lower boundary (rapid deposition), whereas mudstone and siltstone units are relatively gradational.

FA 5 consists of two primary architectural elements, namely laminated sandsheets (LS) and ephemeral lakes (LC). Rare inclusions of channel elements (CH) and floodplain fines (FF) occur intermittently. Lateral pinching, bed thickness and sharp basal boundary of sandsheet units are all indicative of laminated sandsheets, previously described by Tunbridge (1981) and Sneh (1983). Calcareous-rich mudstone lenses, occurring throughout overbank sequence deposits, describe deposition within ephemeral flood lakes (LC). The LC and LS units of FA 5 often interfinger with more laterally continuous aeolian dune (AD; FA 4) beds.

A variety of trace fossils occur on the surfaces of the LS units (Fig. 15). Pedogenic alteration is prominent in almost all of the FA 5 architectural elements. LS and LC units largely comprise of milky white carbonate-rich clays, carbonate rhizoliths (LC especially) and calcified fissures. The predominance in lack of preserved internal structures for LS units also suggest a plausible pedogenic reworking.
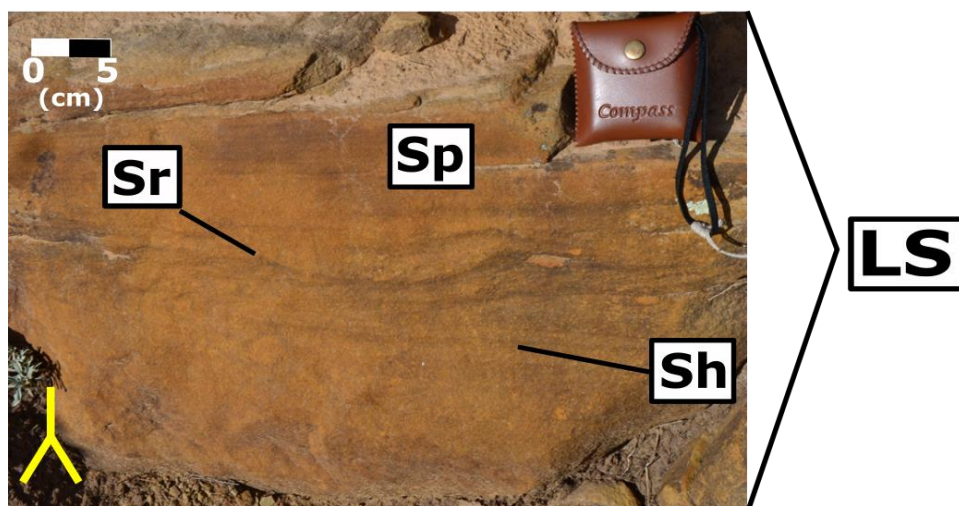
Fig. 16: Annotated image of a typical lithofacies associated with LS sandsheet beds in FA 5; including ripple cross-laminations, planar cross-laminations and horizontal laminae.

4.1.5.2 Interpretation

The combination of architectural elements, structures and pedogenic alterations in FA 5 point toward an interdune-type setting, including wet aeolian sandsheets and playa lakes.

The LS element bed morphologies (sharp basal boundary; gradually pinches out; relatively thinly bedded), internal structures, wind-dominated ripples and mudcracks all suggest a relatively rapid deposition succeeded by drying conditions. Flashfloods between dune, interdune and wet-aeolian environments of the uEF and Clarens Formation are thus the most likely mechanisms of the sandsheet deposition (Rust, 1978; Eriksson, 1981; Tunbridge, 1984; Miall, 1985; Stear, 1985; Eriksson, 1986; Sneh, 1983; Kelly and Olsen, 1993; Bordy et al., 2004a; Hampton and Horton, 2007). The presence of pedogenic alteration products within these beds, as well as surficial mudcracks additionally point toward drier periods. Associated pedogenically altered, more massive siltstone beds point toward the accumulation of loessic material within the increasingly aeolian conditions (Smith and Kitching, 1997).

The calcareous LC successions point to perennial, low-relief, low-energy lakes within topographic depressions in alluvial plains, sourced by flooding events (Nichols, 1999; Blomeier et al., 2003). Distinct preservation of desiccation cracks and pervasive calcretization are products of periods of aridity, increasingly noted further up in the uEF and Clarens formations (Donovan, 1975;

Kitching and Raath, 1984; Astin, 1990; Astin and Rogers, 1991; Nichols, 1999; Bordy et al., 2004c).

These playa lake deposits and intermittent flashflood sheet flows also host rarer ephemeral simple

channel deposits (CH elements) and interbedded backswamp FF units. The general increase in playa

lake (LC) and loessic siltstone LS unit abundance toward the uppermost uEF and Clarens Formation

highlights the gradual increase in palaeoclimate aridity, which lies in accordance with previous

palaeoenvironmental reconstructions (Kitching and Raath, 1984; Eriksson, 1986; Smith and Kitching,

1997; Bordy et al., 2004a, c).
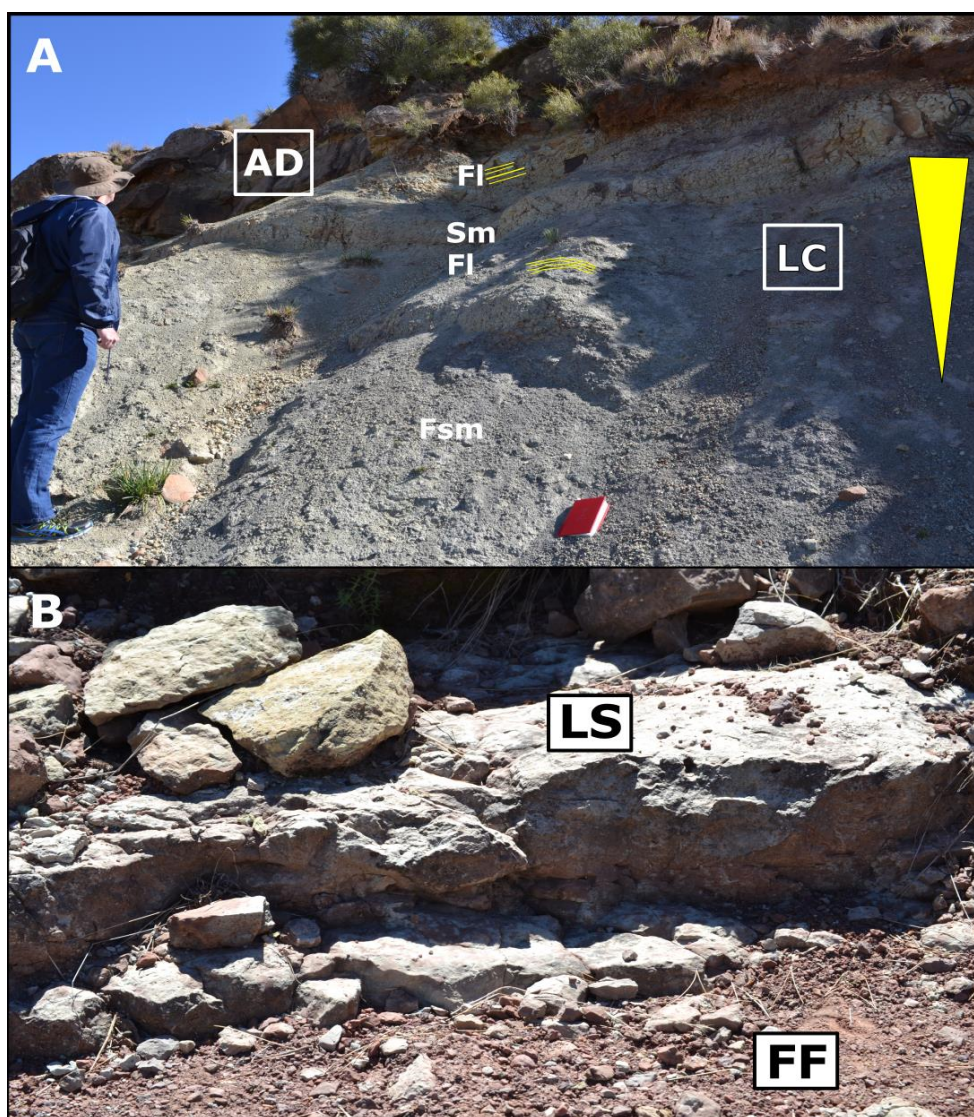
Fig. 17: (A) Typical lithofacies associated with mudstone-rich ephemeral playa lake deposition (LC) at the basal Clarens Formation of Traverse 2, Moyeni. Note: red fieldbook used as scale (19.0 cm); (B) Pervasive calcretization of loessic LS beds in the uEF of Traverse 1, Moyeni.

4.1.6   Facies Assemblage 6 (Conglomerate):

4.1.6.1   Description

Limited to the uEF of Maphutseng, a single, yet vital, outcropping of relatively thick conglomeratic facies interbedded with fine-grained pedogenically altered sandstone facies constitutes FA 6. The main lithofacies associated with FA 6 lithologies include: Gcm, Gh, P, Sm, Sh, Sc and Sl (Table 3). The conglomerate beds range from clast to matrix supported, poorly sorted composition, sub-angular to rounded clasts, rare clast imbrication and an oligomictic clast population. Clasts range in size from coarse-grained sand (0.1-0.2 cm) to granules (0.2-0.4 cm) to pebbles (0.4-6.4 cm), with one boulder (27.0 cm) sized clast. The clast compositions range from a predominance of pedogenically sourced calcareous nodules (glaebules), quartz pebbles, sandstone and mudstone clasts. Interbedded sandstone units are fine-grained with a high percentages of rock fragment inclusions and clay fractions. FA 6 beds display greyish to yellowish orange unweathered colours (10YR 7/4; 10YR 6/6), whereas the more weathered units (particularly the conglomerate matrix) range between greyish red and yellowish brown (10R 4/2 and 10YR 2/2).

Although the main applicable lithofacies is massive and clast-supported (Gmm), rudimentary horizontal stratification does occur (Gh; Fig. 18). Interbedded sandstone facies are often massively bedded and calcretized. Sandstone facies more rarely host internal structures such as horizontal laminations and low-angle cross-bedding. Intraclasts are commonly hosted at the basal sections of the sandstone beds.

The thick lobe of conglomeratic and minor sandstone beds range in individual thicknesses from 0.2 to 1.5 m and the total bed thickness undulates along the lateral extent, with the thickest part analysed for this study. The distinct FA 6 units host relatively sharp 2nd order and erosional 3rd order boundaries. Taking the grain distributions, internal structures and bed morphologies of the interbedded polymictic, para- and ortho-conglomerates and mud-rich sandstone units into consideration, the FA 6 succession includes debris-flow (DF) and laminated sandsheet (LS)

architectural elements. Although FA 6 beds preserve a definite pedogenic character and bone fragments, it does not host any bioturbation (BI 0).

4.1.6.2   Interpretation

Floodplain degradation (denudation of floodplains) likely resulted in the formation of gullies, which were consequtively filled with the FA 6 debris transport material, including: floodplain palaeosols, reworked palaeosol glaebules, sandstone and mudstone fragments and quartz pebbles. Gullying as a result of flooding, as seen in a lot of the modern deposits in Lesotho, specifically Maphutseng, allowed for this high energy traction transport flood event deposition (Fig. 19; Nemec and Muszynski, 1982; Rydgren, 1988; Grab and Deschamps, 2004). The thinly interbedded, massive, calcretized LS units are interpreted as primarily pedogenically altered infill during intermittent periods of little fluvial flooding. The periods between the high-energy events (conglomerate deposition) provided ideal circumstances for finer-grained wind and/or fluvial driven loessic-type material deposition and rudimentary paleosol production within the gully-type deposits. This floodplain denudation facies assemblage interpretation is shared with similar interpretations by Smith and Kitching (1997) and Bordy et al. (2004a, c).
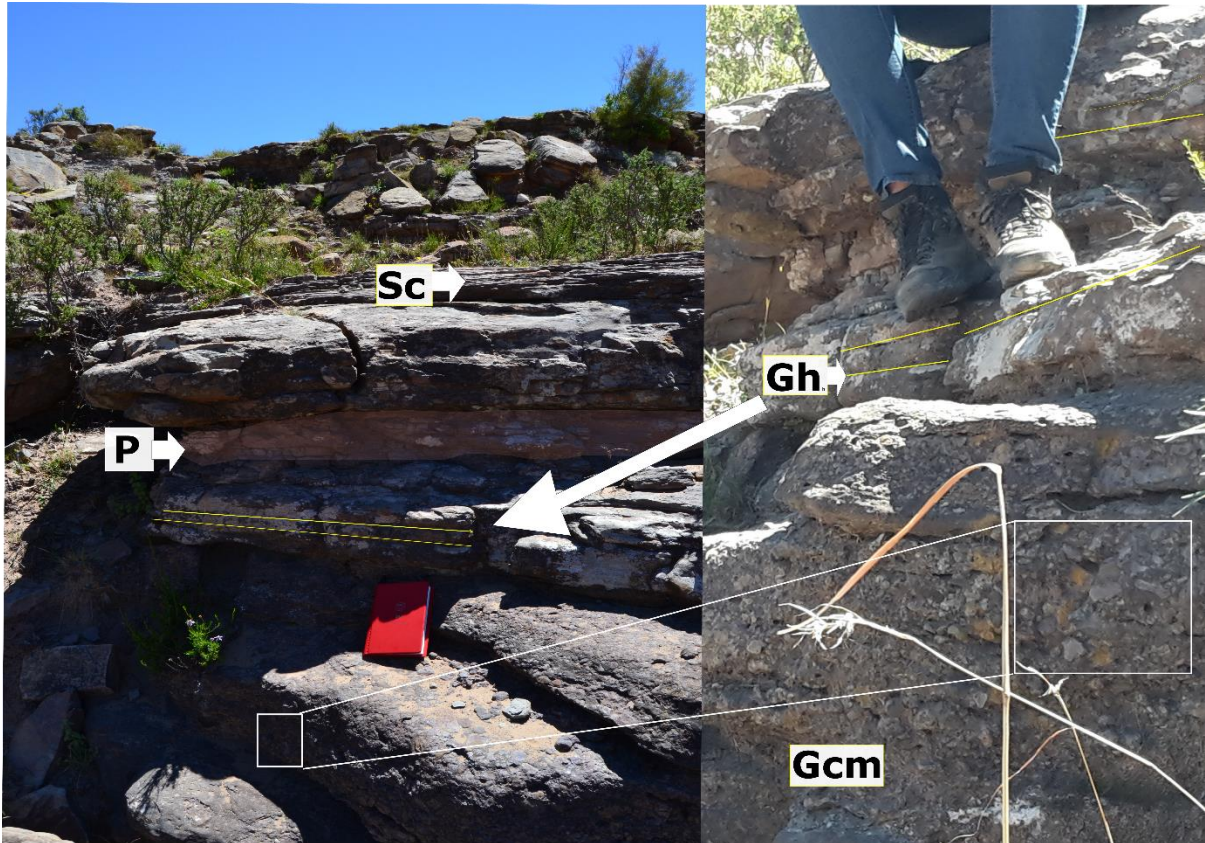
Fig. 18: The clast supported carbonate nodule conglomerates of the uEF, Maphutseng. These units are massively bedded (Gcm) as well as horizontally bedded (Gh; shown by yellow lines). Pedogenically altered sandstone units cap these conglomerate beds. Note the pedogenic glaebule pebble sized clasts easily distinguishable in the white outline.

Fig. 19: Modern day analogue of the FA 6 depositional environment during the formation of the uEF units at Maphutseng. Note the gullying cutting into the floodplain palaeosols (denudation) as well as the deposited material from traction transport dominated flood events (coarser material) and lower energy ephemeral streams and wind deposition (finer overlying material).

4.2   Stratigraphy

Intensive sedimentological analyses of individual traverses in conjunction with palaeontology, internal and external bed structures provided the basis for detailed lithostratigraphic interpretations (Fig. 24). A total of nine (9) stratigraphic sections were used in determining lithostratigraphic correlations spanning from the lowermost lEF to the uppermost Clarens. The nine sections include: Traverse 1 and 2 of lower Moyeni, Traverse 3 of Masitise, Traverse 4 of Moyeni and Traverses 5 to 9 of Maphutseng and surrounds (Fig. 20; 21).
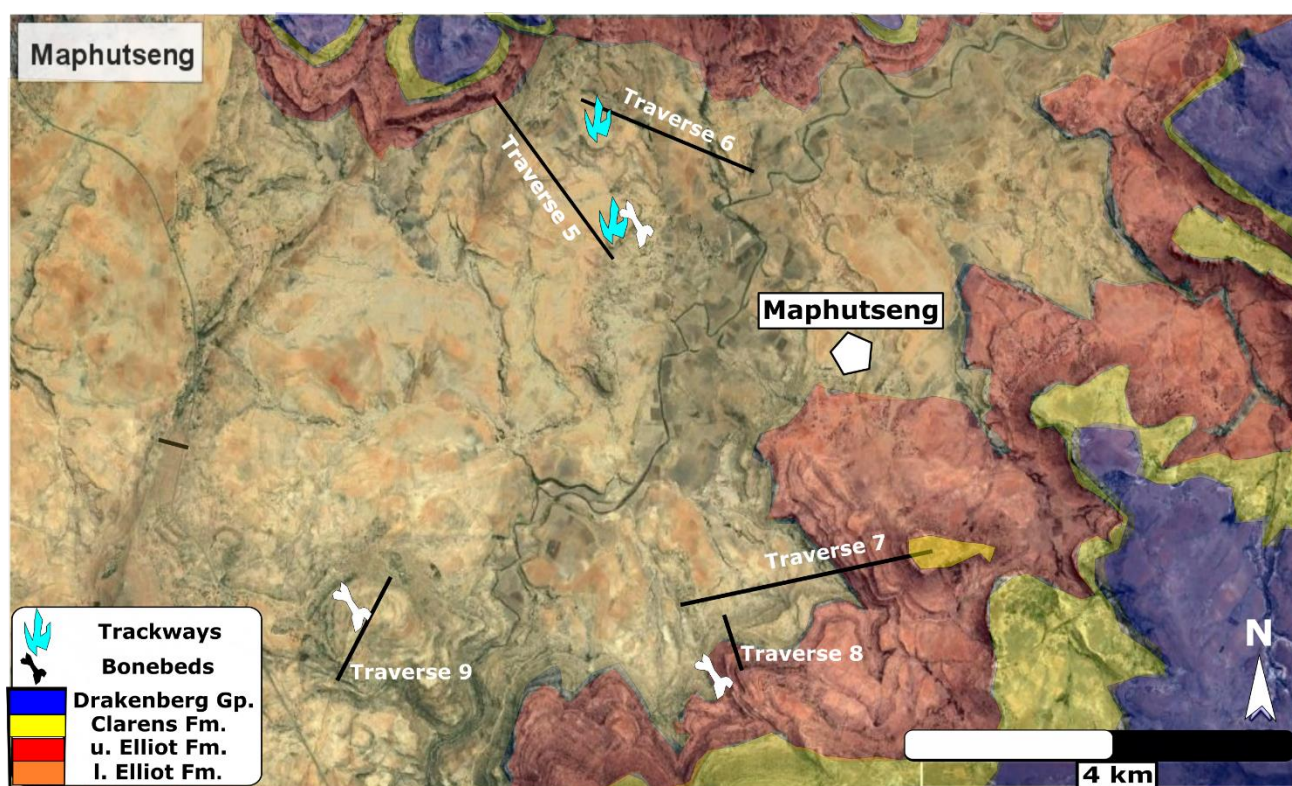
Fig. 20: Map illustrating the paths along which each traverse was studied in Maphutseng. Formation boundaries extrapolated from in-field identifications and Google Earth Images. Base map sourced from Google Earth (2018).
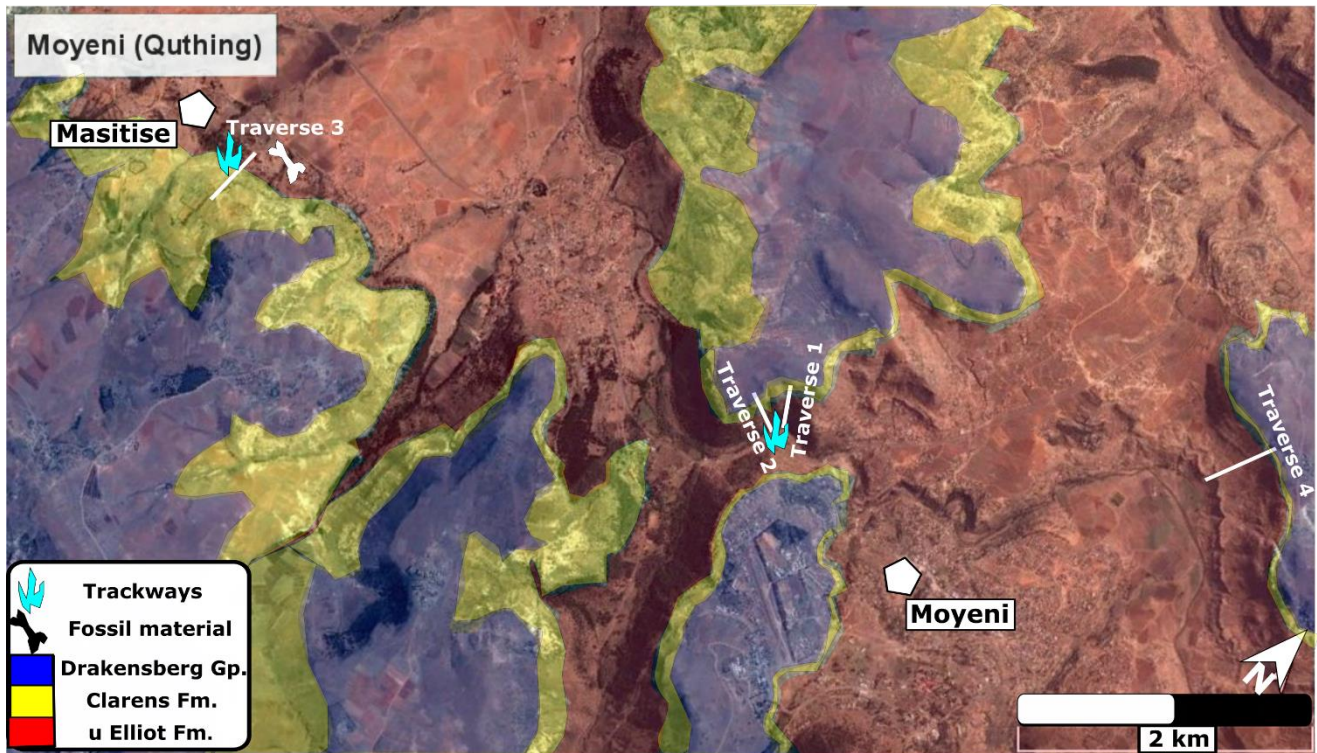
Fig. 21: Map illustrating the paths along which each traverse was studied in and near Quthing (Moyeni; Traverse 1, 2, 4) and Masitise (Traverse 3). Formation boundaries extrapolated from in-field identifications and Google Earth Images. Base map sourced from Google Earth (2018).

The detailed stratigraphic and sedimentological studies of the Elliot and Clarens formations were typified by grain size and colour variations, facies architecture and geomorphologiy. The most noticeable lithostratigraphic differences between the Elliot and Clarens are the variations in slope and general geomorphology of the outcrops (Fig. 22; 23; 24; 25). A distinct, noticeable change in lithology and geomorphology was found at the lEF and uEF contact at Maphutseng (the only site where this contact was mapped in this study). This contact provides the local counterpart of the regionally traceable feature, described in Bordy et al. (2004a, b, c) across the Stormberg basin.

A variety of facies assemblage combinations discussed in Table (5) occur intermittently throughout the various stratigraphic traverses recorded in this study. These assemblage clusterings pertain to distinct depositional settings associated with either the lEF, uEF and Clarens Formation. Distinct marker beds were also used in extrapolating lateral continuity between beds. Varying local thickness and continuity variations of facies assemblages and marker layers were noted; however,

further lateral extent and basin wide stratigraphic correlations for the sake of describing intra-

formational complexity was beyond the scope of this study.
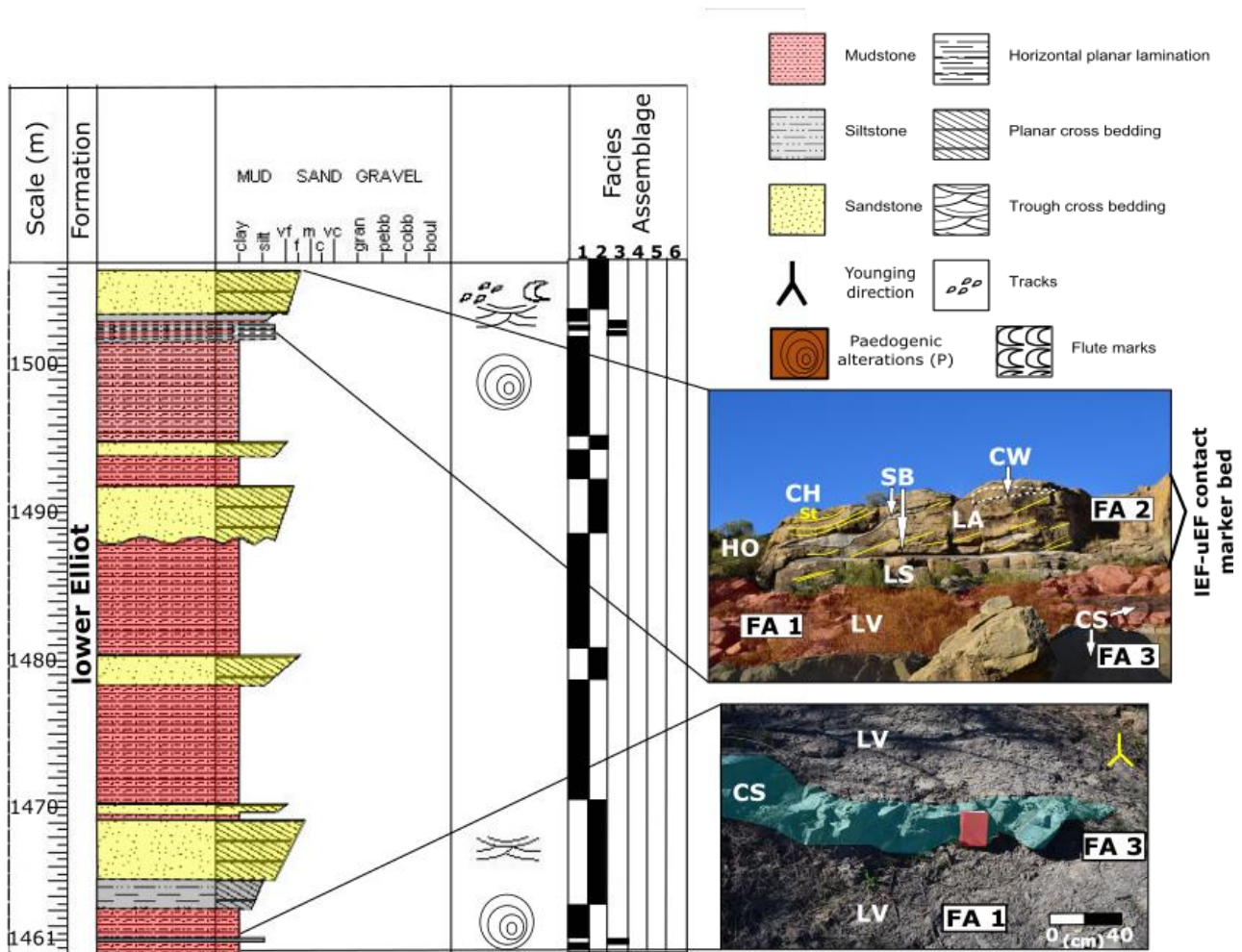
Fig. 22: Annotated stratigraphy of Traverse 6 at Maphutseng, highlighting some of the important architectural elements of the lEF.

4.2.1   lower Elliot Formation

The lEF outcrops are limited to the Maphutseng study area and exposures are restricted to the

mid- to upper section of the lEF; the lowermost lEF unit and underlying Molteno Formation contact

were not mapped. The lEF informally pertains over the basal (lower) segment of the overall Elliot

Formation. It comprises predominantly of thick, relatively continuous beds of fine- to medium-

grained fluvial channel associated sandstone and siltstone elements of FA 2. These thick sandstone

bodies (FA 2) are interbedded with thick, relatively massive grey to reddish-brown mudstones

belonging to FA 1 (FF and LV). The thick mudstone units of FA 1 have undulating bed thicknesses but

remain relatively laterally continuous. The interbedded nature of the more resistant, multi-storey, moderately-grained sandstones and less resistant mudstones result in prominent continuous tabular sandstone dominated terraces. The high ratio of channel sandstone bodies to fines in the lEF, comparatively show 'gentler' sloping outcrop profiles than the 'steeper' uEF outcrop profiles, which are dominated by finer sandstones and more abundant mudstones.

Outcrops of lenticular CS-dominated FA 3 occur proximal to CH elements, interspersed throughout the massive overbank (FA 1) deposits (Fig. 22). FA 3 facies are not as abundant as FA 2 and FA 1, and aside from the unit directly associated with the lEF-uEF contact marker layer, are not laterally continuous. These facies rather form lenses throughout FA 1 deposits. Rare instances of finely-laminated whitish-grey ephemeral lake (LC) and laminated sandstone (LS) dominated (FA 5) lenses are commonly associated with the backswamp deposits of the extensive pedogenically altered FA 1 siltstones and mudstones. Sandy bedforms (SB) belonging to FA 2 are unique to the lEF fluvial dominated deposits, associated with periodic higher energy flood events throughout the lEF.

FA 1 and FA 2 floodplain fines (FF), levees (LV) and fluvial channel (CH), LA, CW, HO, LS, SB, LV elements are relatively laterally continuous and often form traceable tabular to massive units (Fig. 22). Smaller FA 2 deposits do, however, tend to pinch out within ~10 m of the main CH body. Bed thicknesses in the lEF range between ~20 m thick massive FA 1 mudstones, 2.0 to 10 m thick FA 2 amalgamated, multi-storey channel stacks, to rarer 0.3 m thick ephemeral lake lenses. FA 2 channel sandstones dominate the lEF successions, with the majority of the channel wings and lateral accretions pinching out within 20 m of the main and secondary channel bodies. In contrast, the multi-storey FA 2 unit (undulating thickness) situated directly below the lEF-uEF contact forms a regionally distinct continuous bed. This bed occurs in sharp contrast with the directly overlying pedogenic mudstones of the basal uEF, validating previous associations of a stratigraphic gap to the contact (Bordy et al., 2004a, c; Bordy and Eriksson, 2015). In Fig (26), this distinct FA 2 marker bed

68

can be seen to closely follow the lEF-uEF contact (dotted line), and although it varies in thickness,

the unit remains laterally continuous throughout the local stratigraphy.
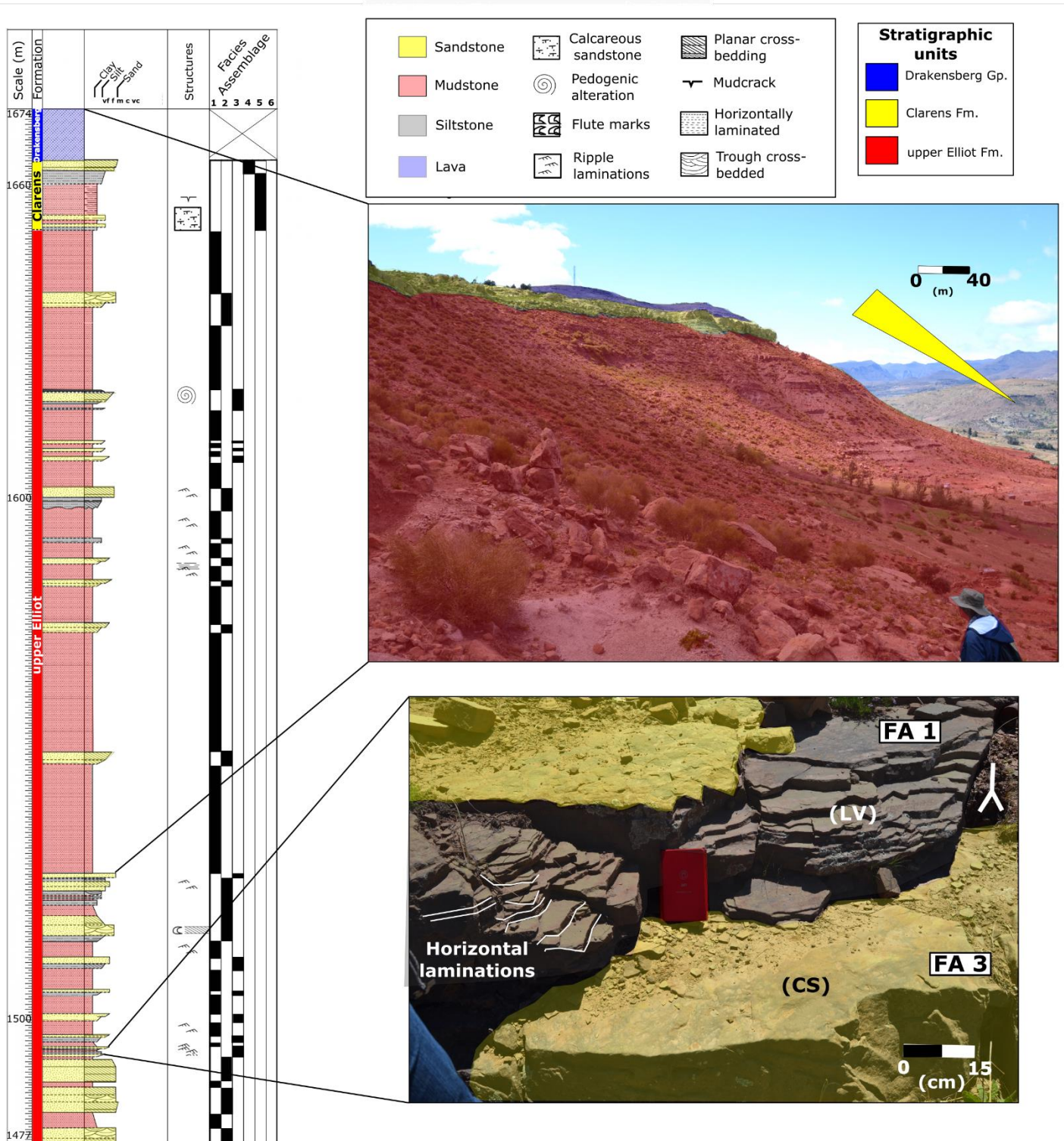
Fig. 23: Annotated stratigraphy of Traverse 4 at Moyeni (Quthing), highlighting some of the important elements and geomorphological features identified in the uEF and Clarens Formation. Yellow triangle indicates upward coarsening from the uEF to the Clarens

69

4.2.2   upper Elliot Formation

Stratigraphically, the uEF directly overlies the lEF and is exposed at all the study areas (Quthing, Masitise and Maphutseng). The uEF, similar to the lEF, hosts mudstones interbedded with fine-grained sandstones; however, predominantly comprise of relatively continuous deposits of FA 1 pedogenically altered, reddish-maroon floodplain fine (FF) mudstones (Fig. 23; 24). Rare instances of FA 1 greenish-grey LV units are limited to the basal uEF. The thick mudstone units and interbedded, coarser-grained, sandstone sheets make the topographical relief of the uEF units much steeper than the underlying lEF and form characteristic terraced slopes (Fig. 23). Units of siltstone and fine-grained sandstone are prevalent throughout the uEF and consist of relatively continuous to lenticular FA 3 CS elements interbedded with thicker FA 1 mudstones (5.0-20 m). Other units include, intercalated FA 5 whitish-grey LC mudstones, FA 2 asymmetrical ribbon-channel sandstone elements (CH, LA, CW, HO, LS), FA 2 unconfined sheetfloods and FA 5 laminated sandsheets (LS).

Although FA 2 and FA 3 units occur intermittently throughout the uEF, a marked increase in aridity is inferred from the increase of units with aeolian affinity: FA 5 and FA 4 (Fig. 24; 26). Increased loessic siltstone (FA 5) facies, unconfined ephemeral sheetfloods (FA 2 and FA 5), desiccation cracks, playa lake (LC) elements, pedogenic alteration, calcretized units and interspersed aeolian dune units (FA 4) provide evidence of increased aridity in the uEF successions. This gradual increase in up-sequence aridity is further evidenced through the decrease of thick, coarser grained, complex, stacked meandering fluvial FA 2 successions and increase of single, unconfined ribbon-type CH elements (ephemeral sheetfloods). Inversely, lenses of interbedded silty-sandstone rich CS (FA 3) deposits increase in abundance up-sequence.

A single bed, comprising of carbonate glaebule-rich conglomerates (FA 6), is limited to the uEF at Traverse 5 in Maphutseng. Similar carbonate nodule conglomerate beds, with or without reworked bone fragments, are considered one of the most diagnostic rock types in the uEF. They were first recognized as potential index rocks of the post-lEF strata by Ellenberger et al. (1964; p. 323-324) and

repeatedly described from the uEF by Bordy et al. (2004a; 2017b), Sciscio et al. (2017a, b) and McPhee et al. (2017). Although this uEF index bed at Maphutseng shows thickness variations ranging between 0.5-1.5 m laterally, its occurance is significant as it offers lithostratigraphic correlation with other uEF outcrops found regionally in South Africa and Lesotho (Ellenberger et al., 1964; Bordy et al., 2004a; 2017b; Sciscio et al., 2017 a, b; McPhee et al., 2017). Overall, the exposed stratigraphic thickness of the uEF varies from 186 to 251 m between the various traverses of this study (Fig. 26).

4.2.3   Clarens Formation

The Clarens Formation conformably overlies the uEF and presents a distinct change from the underlying uEF fluvial and lake deposits with aeolian influences to more arid aeolian deposits (Fig. 25). These deposits include thick stacks of fine- to medium-grained cross-bedded sandstones (AD), with some interbedded pedogenically altered loessic sandsheets (LS), carbonate-rich mudstones and siltstones (LC) and rare ephemeral channels (CH).

The definition of the basal contact of the Clarens beds in the literature varies greatly, with the vast majority of authors utilising the uppermost maroon mudstones of the uEF or basal section of the first thick cross-bedded sandstones as the contact (Eriksson, 1986; Bordy and Eriksson, 2015). This study, however utilised the relatively distinct gradational contact between the uppermost uEF FA 1 mudstones and overlying FA 5 mudstones as the contact boundary (Fig. 25). This ~1 m thick distinctly greyish-white weathered FA 5 mudstone and siltstone dominated unit is traceable in the four Clarens outcrops from this study and sharply overlain by the first FA 4 cross-bedded AD sandstone units (Fig. 25; 26). The overlying cross-bedded AD sandstones, however are not always as laterally consistent as the underlying greyish-white FA 5 unit, making the basal FA5 unit contact a more reliable marker of the basal Clarens contact.

The Clarens Formation predominantly hosts thick, single tabular sheets to stacked wedges (foresets) of aeolian dune (AD) beds (FA 4). These AD beds, although not laterally continuous, are the dominant lithologies of the Clarens Formation and form distinct marker units with regard to their

71

pale-yellow colouring, relative competence and lateral abundance, and contained aeolian structures (e.g. large-scale cross-bedding; wind ripples; migration toes of foresets; Fig. 24). These dune sets consist of thicknesses ranging between 5.0 to 30 m. The intermittent <1 m thin lenses of laminated sandsheets and mudstones (FA 5) represent ephemeral 'wet' interdune deposition. The Clarens Formation thicknesses range from 12 m at Traverse 4 to 56 m at Traverse 3 across a lateral distance of 7.4 km near Quthing. Interestingly, the FA 5-unit thicknesses inversely relate to the FA 4 thicknesses. To illustrate, the thicker successions of FA 4 in Traverse 3 are associated with the thinnest FA 5 lenses, whereas comparatively, the thinnest total FA 4 units at Traverse 4 coincidingly have the thickest total successions of FA 5 units (Fig. 26). The Clarens Formation deposition has a sharp contact with the overlying basalts of the Drakensberg Group.
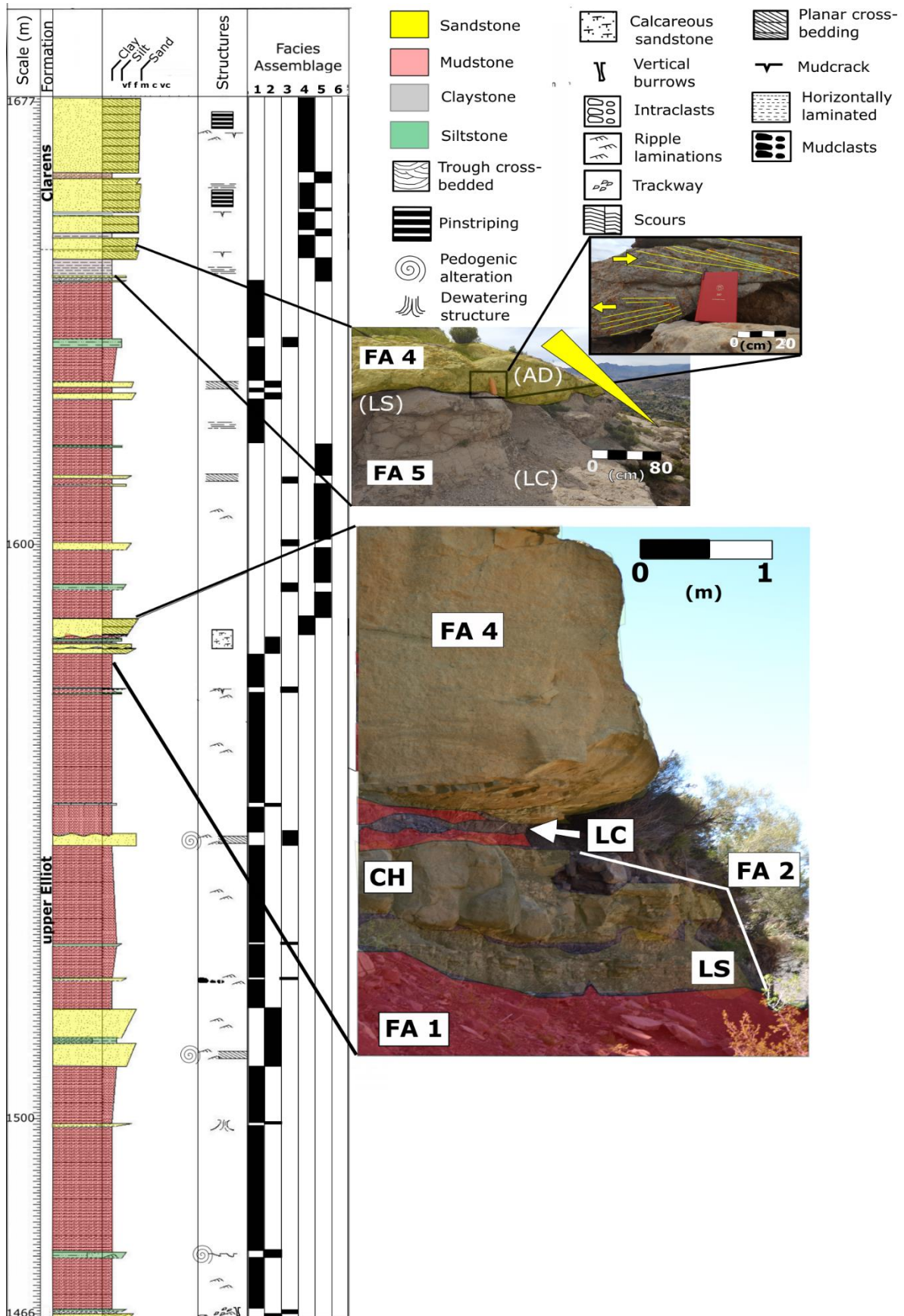
Fig. 24: Stratigraphic column of Traverse 1 at Moyeni (Quthing), illustrating the typically FA 1 dominated uEF coarsening up into the overlying FA 4 and FA 5 dominated Clarens Formation. Note: yellow arrows annotate the contrasting directions of AD element migration on the uppermost Clarens exposures.
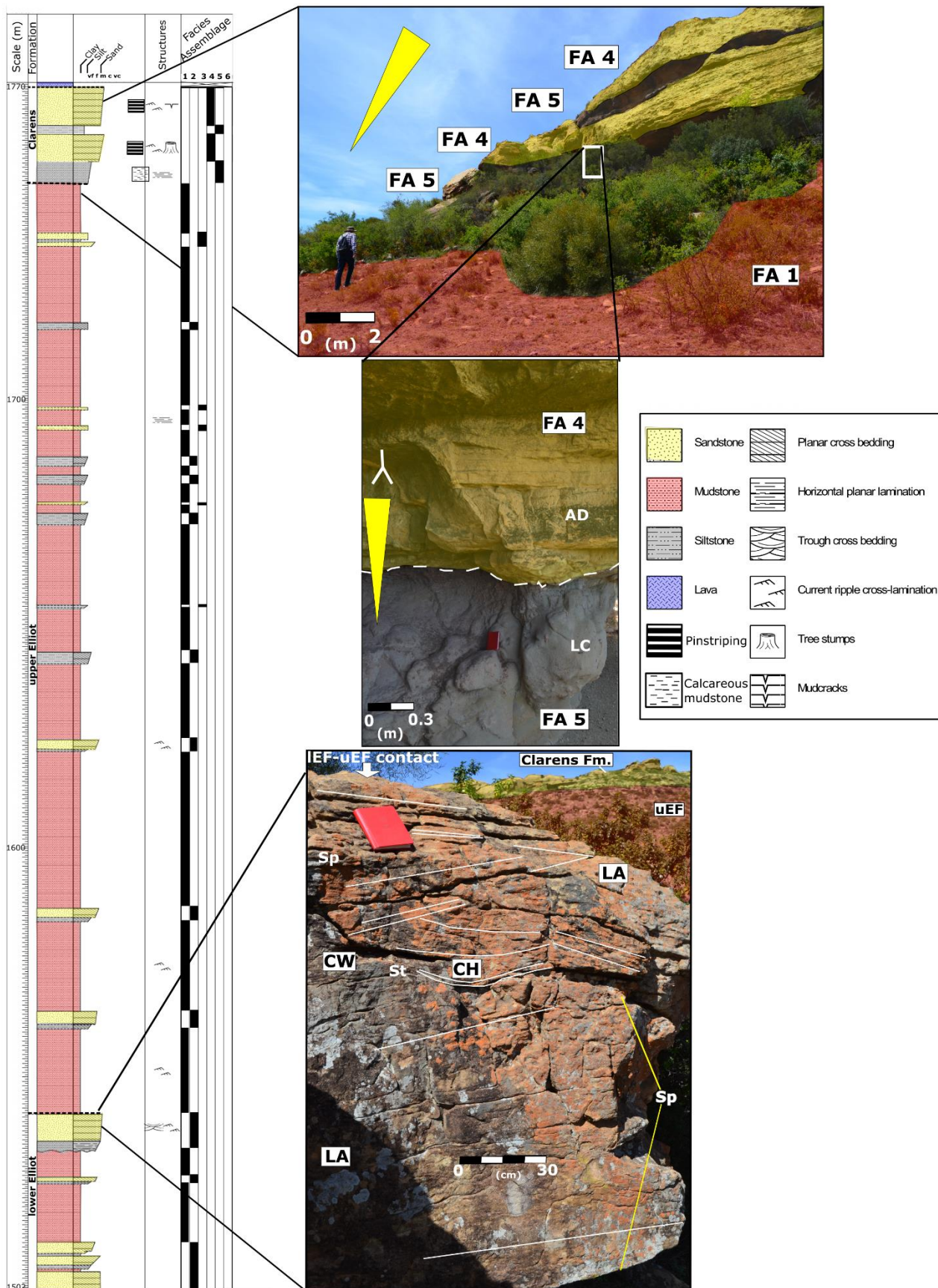
Fig. 25: The stratigraphic interpretation of Traverse 7 at Maphutseng; spanning from the lEF to Clarens Formation. Special emphasis is placed on the variation of dominant facies assemblage associations at the uEF and Clarens Formation contact and lEF-uEF contact marker bed.

Fig. 26: Correlation diagram illustrating the local major facies, marker bed units and trackway/bonebed locales. The cross-section was taken from NW (A) to SE (A') of the three-main study areas, including eight of the total nine traverses recorded. The stratigraphy ranges from the basal lEF (Maphutseng) to the capping Drakenberg basalts. Note: dotted lines depict the lEF-uEF and uEF-Clarens Formation contact.

4.2.4   Palaeocurrents

Palaeocurrent data was measured from various palaeocurrent indicators, including: ripples (both 2D and 3D), lateral accretion surfaces, foresets of planar and trough cross-bedded strata, parting lineations, axis of trough structures (in map view) (Fig. 10B; 10D; 12D; 14B; 27). A total of twenty-nine (29) palaeocurrent readings were recorded throughout the various traverses (Fig. 28; 29; Table 6). Of the 29 readings, seven (7) belong to the lEF, seventeen (17) belong to the uEF and five (5) readings were taken for the Clarens Formation.

Palaeocurrent	Traverse	Stratigraphic unit	Palaeocurrent indicator
157	1	uEF	Ripples (current)
5	1	Clarens	Crossbedded foresets
52	2	uEF	Ripples (current)
36	2	uEF	Ripples (current)
113	2	uEF	Ripples (current)
113	2	uEF	Ripples (current)
136	2	uEF	Ripples (current)
15	3	Clarens	Ripples (wind)
15	3	Clarens	Crossbedded foresets
154	4	uEF	CH trough
146	4	uEF	CH trough
69	4	uEF	LA surface
62	4	uEF	LA surface
64	4	uEF	LA surface
64	4	uEF	LA surface
70	4	uEF	CH trough
192	4	uEF	Ripples (current)
120	5	lEF	CH trough
59	5	lEF	CH trough
62	5	lEF	LA surface
36	5	lEF	LA surface
20	5	lEF	Scour marks
156	5	uEF	Ripples (current)
127	6	lEF-uEF	Parting lineations
323	7	Clarens	Ripples (wind)
323	7	Clarens	Crossbedded foresets
210	8	uEF	Ripples (current)
66	9	lEF	LA surface
236	9	lEF	CH planar axis

Table 6: Palaeocurrent readings taken throughout the study areas.
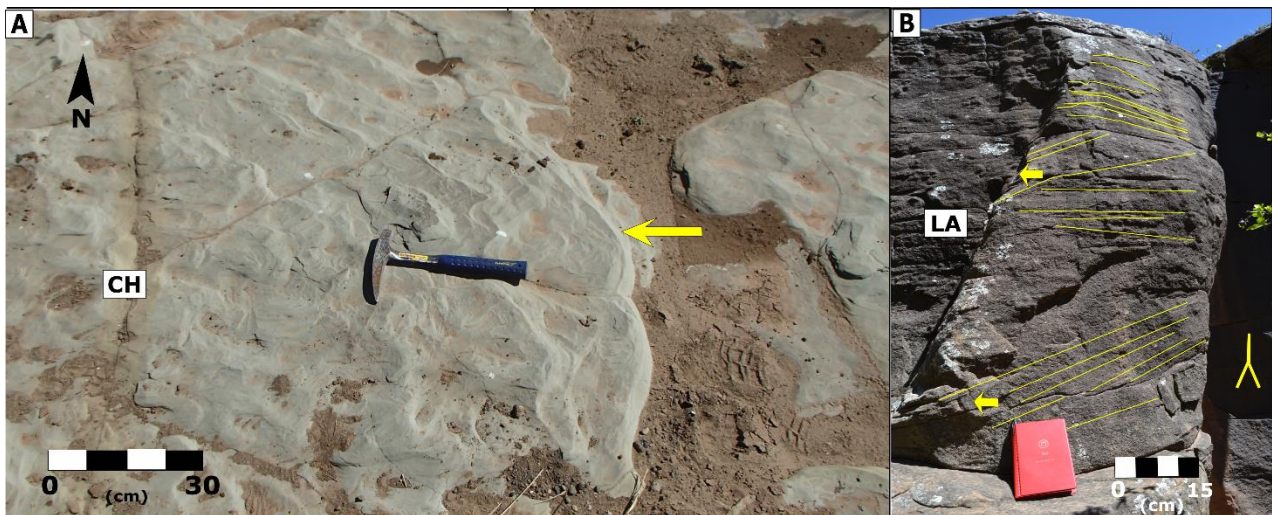
Fig. 27: (A) The top surface section of a channel in the lEF of Traverse 9, Maphutseng; (B) Yellow lines indicate the planar cross-bedding of a LA unit within the uEF of Traverse 4, Moyeni (Quthing). Note: associated palaeocurrent reading directions indicated by the yellow arrows.
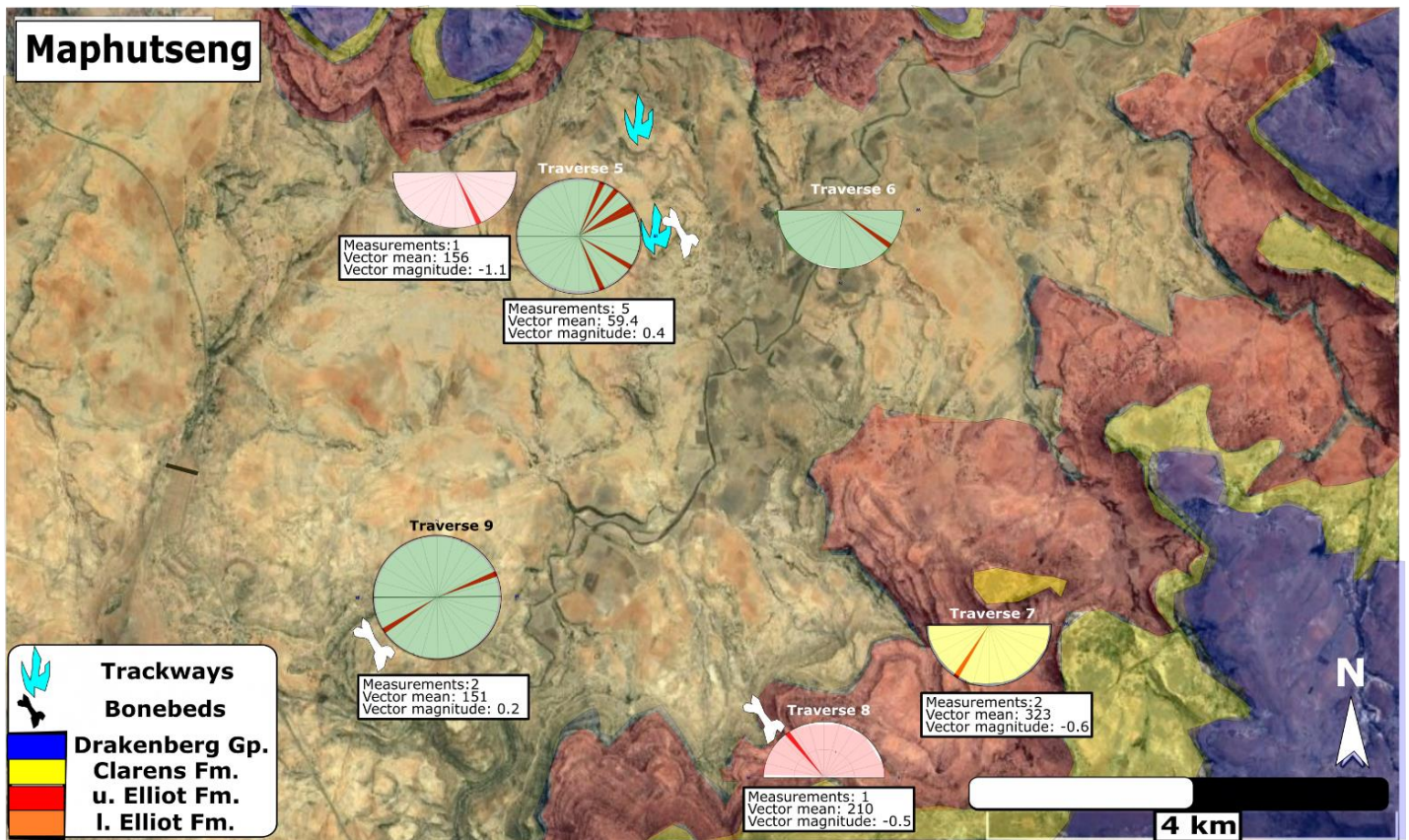
Fig. 28: The geographical distribution of the total palaeocurrent readings taken for each traverse within the Maphutseng field area. Note: the green rose diagrams illustrate lEF palaeocurrents, the pink uEF and the yellow, Clarens. Basemaps sourced from Google Earth (2018).
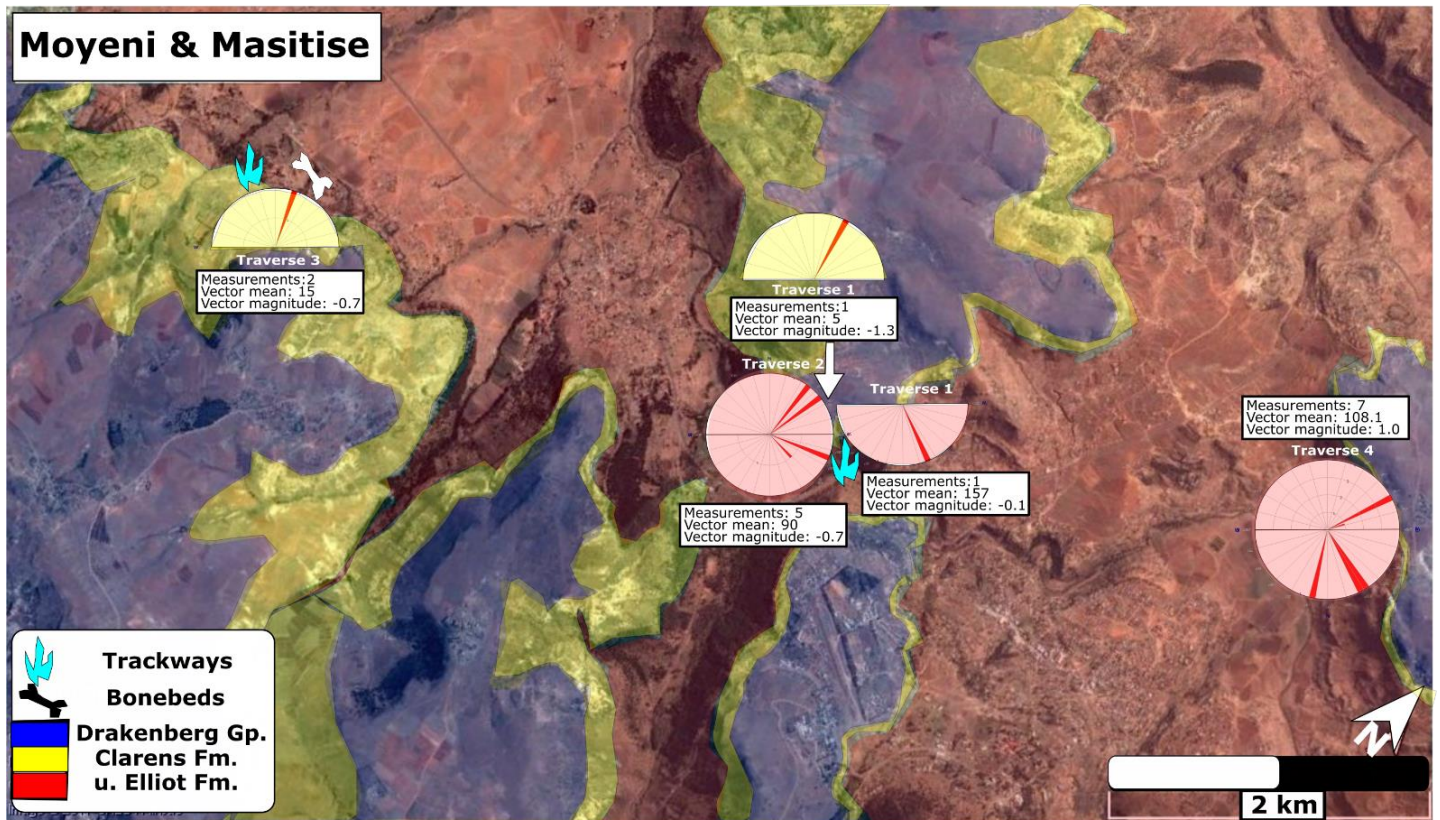
Fig. 29: The geographical distribution of the total palaeocurrent readings taken for each traverse within the Moyeni (Quthing) and Masitise field areas. Note: the pink rose diagrams illustrate uEF palaeocurrents, whereas the yellow represents the Clarens Formation. Base maps sourced from Google Earth (2018).

The 29 palaeocurrent readings taken from the lEF, uEF and Clarens Formation at the study

sites present very limited opportunities for assessing the overall palaeocurrent trends of these units.

This is because the low number of the measurements that could be obtained in this study is

statistically insignificant, according to Miall (1996) and Tucker (2011), for meaningful comparison to

the previously established regional trends (e.g. Beukes, 1970; Bordy et al., 2004b). The lEF

palaeocurrent readings (Maphutseng) present NE directed channel flows and were taken from

channel structures (lateral accretion surfaces, trough cross-bedded strata and axes and parting

lineations). Some channel migrations result in alternate flows, to the SE and SW, recorded within the

lower exposed lEF units of Maphutseng. The uEF, both in Maphutseng and Quthing (Moyeni),

presents palaeocurrent readings dominated by SE (n=8; 6 of which were taken from ripples and

ripple cross-laminations) directed flows, with some SW variation suggesting some meandering in the

lower uEF fluvial channels. The uEF units of Quthing, however, show a further prevalence of

intermittent NE palaeocurrent flows (n=6; 2 of which were taken from ripple structures), suggesting

a potential separate source input for uEF units of Quthing. The Clarens Formation outcrop palaeocurrent indicators largely consist of wind derived ripples and planar cross-bedded foresets in Quthing and Masitise. These indicators (n=4; 1 of which was taken from ripples) indicate a palaeowind direction from SSW to NNE. Outcrops in Maphutseng, on the other hand, yielded n=2 measurements (1 of which was sourced from ripple structures), which show NE to SW palaeowind directions.

4.3   U-Pb (LA-ICPMS) detrital zircon analysis

Fourteen (14) samples were selected from the 9 traverses at Maphutseng, Masitise and Moyeni, respectively. For this study, a total of 1250 individual zircons were ablated, of which 1020 grains (81.6%) were concordant. The remaining 18.4% grains fell outside the >20 % concordance bracket.

Utilising Gärtner et al. (2013) and Pupin's (1980) zircon grain morphology classification criteria, external zircon structures ranged from well rounded, asymmetrical grains to more symmetrical, completely un-rounded, doubly terminated grains. The grain elongation also varied from elongate 'needle-like' grains to short stubby grains, which; along with grain roundness and symmetry, were used to describe the grain subtypes as predominantly S- and P- type morphologies. Surface structures that mar the zircon grains of this study, include fractures, cracks and collision marks. Internal features of the zircon grains are dominated by igneous precursor euhedral oscillatory zoning and less common metamorphic precursor grains with complex internal structure (Ireland and Williams, 2003).

Interestingly, the aforementioned rounded and complex metamorphic grains tend to also display a higher grain luminescence in CL images. This being a distinct example of Th concentration variation found in metamorphic (low Th/U) and magmatic (high Th/U) grains. The majority of grains host oscillatory zoning, pertaining to an abundance of magmatic sources (Fig. 30). The minor (2.6%) complex, rounded grains of metamorphic origins (Th/U <0.1) are concentrated in the Cambrian, Proterozoic and Archean populations (Williams and Claesson, 1987).

4.3.1   Sample descriptions
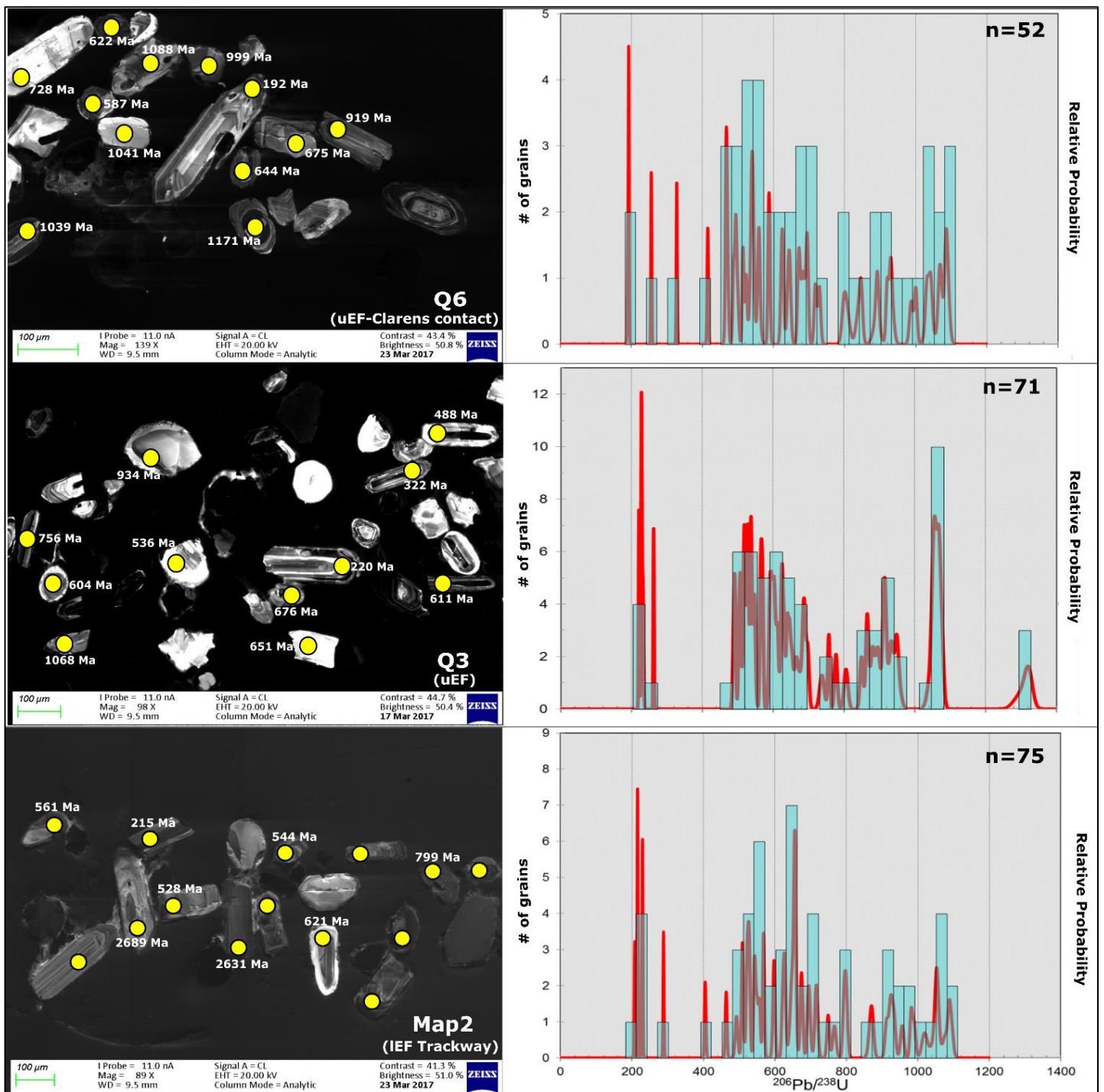
Fig. 30: Three samples from each of the three main stratigraphic subdivisions, illustrating the varying grain morphologies, their associated individual grain concordant ages (Ma) and entire sample age density plots. Note the population distributions of the density plots are all similar, with the vast majority of grains belonging to the Cambrian-Neoproterozoic (485-800 Ma). SEM images display a predominance of magmatic. oscillatory zoned grains, grain rounding, pristine S and P shape preservation, fragmenting, elongate prismatic grains and cracks. The yellow demarcations show spot size and shot positioning. Interesting to note is the very large grains >200µm are often the youngest grains.

4.3.1.1   Map2

Sample Map2 was collected from the trackway site within the lEF of Maphutseng. The majority of this sample, similar to all of the other samples, is dominated by magmatic grains (95.7%) and the remaining 4.3% belong to metamorphic origins. The metamorphic grains show complex internal structures and are very rounded. The grains within this sample all fall between 40.0-200.0 μm in length, however, the largest grain is 250.0 μm. 92.8% of these grains fall into the 150.0- 200.0 μm range. Seventy (70) concordant ages were used in this sample, whereby 19% of the analysed grains comprise of core shots and the remaining 81%, rim shots. Grain clusterings show four (4) definite populations, with fourty eight (48) grains falling outside of these populations (Fig. 30). The youngest and most abundant population occurs in the Cambrian-Neoproterozoic (509.2-568.7 Ma) comprises of 17% (n=12) of the overall grains. The two Neoproterozoic populations include the 621.7-656.7 Ma and 793.0-799.5 Ma accumulations of 14% (n=10) and 4% (n=3) of the total sample grains, respectively. The oldest population consists of a Mesoproterozoic (1052.0-1053.0 Ma) and makes up 4% (n=3) of the total grains (Table 7). The youngest grain determination resulted in: 1) YSG= 208.1 ±2.6 Ma; 2) YDZ= 208.3 ±5.3 (-6.1) Ma; 3) TuffZirc (8)= 655.2 ±1.5 Ma; 4) YC2σ (3)= 524.1 ±8.8 Ma; 5) Weighted Average (8)= 656.0 ±6.1 Ma; 6) YPP= 210.0 Ma and; 7) YC1σ (3)= 524.1 ±6.7 Ma.

As a result of the overall low input density of younger detrital grain input seen throughout all of the samples, the mean of the more sensitive test derived ages (YSG, YDZ and YPP) present a more realistic representation of the average youngest maximum depositional age. Other (less sensitive) tests, influenced by the abundant Cambrian-Neoproterozoic detrital grain samples distribution, were not included unless otherwise stated. Taking this into account, the average youngest maximum depositional age of Map2 is 208.8 Ma.

L. Jurassic (174-201 Ma)		Carboniferous (298-358 Ma)		Cambrian (485-541 Ma)		Paleoproterozoic (1600-2500 Ma)	
Triassic (201-252 Ma)		Devonian (358-419 Ma)		Neoproterozoic (541-1000 Ma)		Archean (2500-4000 Ma)	
Permian (252-298 Ma)		Silurian & Ordovician (419-485 Ma)		Mesoproterozoic (1000-1600 Ma)		Preferred Age	
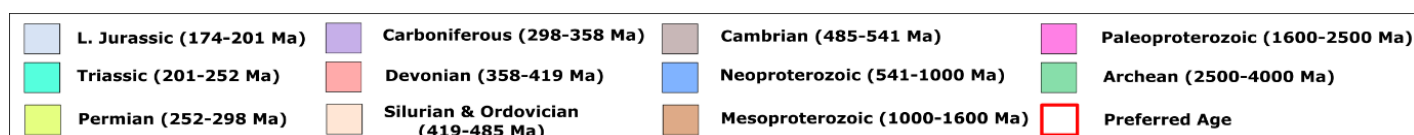
Fig. 31: Legend used to highlight the detrital grain age distribution for each sample table in Section 4.3.

						Map2												
				RATIOS								AGES [Ma]						Conc.
Analysis	U [ppm][a]	Pb [ppm][a]	Th/U[a]	206/204	207Pb/235U[b]	2 σ[d]	206Pb/238U[b]	2 σ[d]	rho[c]	207Pb/206Pb[e]	2 σ[d]	207Pb/235U	2 σ	206Pb/238U	2 σ	207Pb/206Pb	2 σ	%
A_007.FIN2	385	231	0,65455	50	0,2299	0,0062	0,03282	0,00042	0,33983	0,0508	0,0013	209,7	5,1	208,1	2,6	216	55	96
A_008.FIN2	730	523,9	0,78219	340	0,2395	0,0044	0,03401	0,00033	0,40815	0,05114	0,00086	217,8	3,6	215,6	2	236	37	91
A_010.FIN2	519	281,9	0,56898	1160	0,2423	0,0046	0,03415	0,00036	0,34093	0,05124	0,00096	220	3,8	216,4	2,2	240	40	90
A_011.FIN2	226,1	74,3	0,37948	128	0,2524	0,0088	0,03612	0,00054	0,21179	0,051	0,0017	227,8	7,1	228,7	3,3	212	72	108
A_013.FIN2	485	302	0,67629	810	0,2549	0,0048	0,03629	0,00033	0,2652	0,05137	0,00097	230,2	3,9	229,8	2,1	245	41	94
A_014.FIN2	472	296	0,55297	380	0,3334	0,0062	0,04577	0,00039	0,29404	0,0533	0,001	291,7	4,7	288,5	2,4	325	41	89
A_015.FIN2	133,3	120,2	0,46362	-20	0,494	0,013	0,06486	0,00067	0,20958	0,055	0,0014	406,5	8,7	405	4	393	56	103
A_016.FIN2	317	669	1,14826	480	0,602	0,015	0,07461	0,00076	0,45085	0,0598	0,0013	479,1	8,6	463,8	4,6	570	46	81
A_017.FIN2	59,6	90,8	0,77047	77	0,634	0,032	0,0794	0,0012	0,003088	0,0589	0,0031	495	20	492,6	7,3	510	110	97
A_018.FIN2	248	308	0,57056	670	0,674	0,011	0,0822	0,00073	0,28165	0,05939	0,00097	522,1	6,9	509,2	4,4	564	36	90
A_019.FIN2	93,2	192	0,93026	153	0,659	0,02	0,0823	0,0011	0,1023	0,0582	0,0018	512	12	509,4	6,5	511	68	100
A_021.FIN2	96,6	113,3	0,50828	210	0,68	0,019	0,08426	0,00092	0,15806	0,0585	0,0016	525	11	521,4	5,5	517	59	101
A_022.FIN2	308,2	223	0,34069	400	0,682	0,014	0,08468	0,00097	0,40203	0,0587	0,0011	526,9	8,6	524	5,8	542	42	97
A_023.FIN2	397,6	432,3	0,50704	470	0,696	0,013	0,0853	0,001	0,4096	0,0595	0,001	535,6	7,8	527,4	6,1	573	38	92
A_024.FIN2	131,6	256	0,86246	350	0,685	0,016	0,08546	0,00089	0,37395	0,0582	0,0012	528	9,5	528,5	5,3	513	47	103
A_025.FIN2	227	250	0,50617	370	0,708	0,016	0,08772	0,00089	0,30075	0,0588	0,0012	542,2	9,5	542	5,3	546	48	99
A_026.FIN2	95,6	282,2	1,23431	450	0,719	0,017	0,08819	0,00093	0,31473	0,0593	0,0015	549	11	544,7	5,5	550	54	99
A_027.FIN2	269,6	727	1,20401	430	0,727	0,013	0,0891	0,001	0,16157	0,059	0,0012	554	7,9	550,4	5,9	553	44	100
A_028.FIN2	187	491	1,05348	320	0,745	0,015	0,09028	0,00093	0,29961	0,0597	0,0012	564,2	8,9	557,1	5,5	571	46	98
A_029.FIN2	386,8	161,6	0,17865	630	0,756	0,011	0,09207	0,00079	0,55505	0,05955	0,00076	571,1	6,2	567,7	4,6	580	28	98
A_030.FIN2	251,7	476,2	0,77990	450	0,755	0,012	0,09225	0,00083	0,41537	0,05972	0,00092	569,8	7,1	568,7	4,9	578	33	98
A_031.FIN2	284,3	340,8	0,50405	530	0,808	0,018	0,097	0,0012	0,28348	0,0609	0,0014	600	10	597	7,2	621	48	96
A_032.FIN2	129	159,9	0,50233	400	0,81	0,016	0,09718	0,00092	0,25773	0,0601	0,0012	600,8	9,2	597,8	5,4	585	43	102
A_033.FIN2	165,3	435	1,03690	307	0,841	0,019	0,1013	0,0011	0,29037	0,0604	0,0013	618	11	621,7	6,2	596	49	104
A_034.FIN2	101,62	117,2	0,45788	286	0,852	0,022	0,1022	0,001	0,15865	0,0605	0,0016	623	12	627	6,1	602	59	104
A_035.FIN2	257,4	600	0,88345	940	0,864	0,02	0,1022	0,0012	0,37996	0,0613	0,0013	630	11	627,3	7,2	630	47	100
A_041.FIN2	69,1	146,5	0,84891	81	0,9	0,035	0,105	0,0017	0,14096	0,0627	0,0022	648	19	643,4	9,8	659	79	98
A_042.FIN2	76,9	230,7	1,05514	-140	0,943	0,027	0,1057	0,0011	0,33139	0,0644	0,0017	671	14	647,5	6,6	719	58	90
A_043.FIN2	80	180,1	0,83375	200	0,904	0,028	0,1068	0,0012	0,35772	0,0608	0,0017	650	15	654,1	7,3	610	63	107
A_044.FIN2	385,7	526,5	0,47576	1280	0,94	0,018	0,1069	0,0013	0,49842	0,0637	0,001	671,6	9,3	654,4	7,6	727	34	90
A_046.FIN2	128,8	232,9	0,64907	287	0,941	0,019	0,10715	0,00099	0,38407	0,064	0,0012	671,4	9,8	656	5,7	724	42	91
A_048.FIN2	273,9	296,5	0,34976	-1000	0,948	0,017	0,10714	0,00087	0,43751	0,06381	0,00098	676,5	8,4	656,1	5,1	727	34	90
A_049.FIN2	389,8	355	0,31811	790	0,919	0,021	0,1073	0,0013	0,51587	0,0619	0,0012	661	11	656,7	7,8	666	39	99
A_053.FIN2	202,4	283,7	0,47332	550	0,951	0,018	0,1102	0,0012	0,38142	0,0625	0,0011	677,2	9,3	673,6	6,9	674	38	100
A_054.FIN2	111,4	159	0,49102	170	0,993	0,022	0,1105	0,0012	0,377	0,0655	0,0014	698	11	675,3	6,9	766	45	88
A_055.FIN2	222	251	0,38559	560	1,055	0,023	0,1136	0,0012	0,59674	0,0676	0,0012	729	11	693,3	7,2	846	37	82
A_057.FIN2	690	1131	0,58986	2080	0,995	0,013	0,1141	0,0013	0,78028	0,06349	0,0006	700,4	6,8	696,4	8,4	719	20	97
A_058.FIN2	310	1390	1,39677	1410	1,034	0,019	0,1174	0,0014	0,56801	0,0636	0,00098	720	9,7	715,4	8	726	34	99
A_059.FIN2	263,3	223,9	0,23167	530	1,111	0,027	0,1176	0,0015	0,68149	0,0682	0,0012	756	13	716,5	8,5	860	38	83
A_062.FIN2	391,6	201,6	0,16062	1270	1,111	0,015	0,1232	0,0012	0,72351	0,06542	0,00067	757,4	7,1	748,9	7,1	786	21	95
A_063.FIN2	185,8	250	0,39559	850	1,166	0,023	0,1263	0,0017	0,57242	0,0664	0,0011	783	11	766,5	9,5	811	35	95
A_064.FIN2	129	458	0,93566	550	1,278	0,026	0,1309	0,0013	0,45878	0,0709	0,0015	834	12	793	7,3	937	43	85
A_065.FIN2	99,4	304	0,85513	328	1,284	0,029	0,1318	0,0015	0,41826	0,0709	0,0015	836	13	798,1	8,7	934	43	85
A_066.FIN2	421	528	0,36485	1190	1,195	0,018	0,1321	0,0014	0,60995	0,06569	0,00073	797,3	8,4	799,5	8,1	794	24	101
A_068.FIN2	317	1138	0,92114	840	1,458	0,022	0,144	0,002	0,77351	0,07305	0,00085	911,7	9,3	867	11	1009	24	86
A_069.FIN2	229,4	523	0,56495	700	1,448	0,024	0,1449	0,0017	0,48297	0,0723	0,001	909,7	9,3	872,2	9,6	984	29	89
A_074.FIN2	456,6	162,2	0,07249	1300	1,53	0,021	0,152	0,0015	0,57699	0,07331	0,00084	942,4	8,1	912,2	8,6	1017	23	90
A_076.FIN2	205,8	475	0,58163	490	1,633	0,026	0,1539	0,0016	0,47749	0,0773	0,0011	982	10	922,8	9,2	1129	29	82
A_077.FIN2	646,6	196,7	0,04251	1600	1,642	0,022	0,1546	0,0019	0,72037	0,07753	0,00078	985,5	8,6	926	11	1132	20	82
A_078.FIN2	478,5	946	0,45496	1890	1,567	0,02	0,1559	0,0017	0,73913	0,07297	0,00063	956,7	8	933,4	9,3	1009	17	93
A_079.FIN2	574,2	630,6	0,26942	1940	1,668	0,021	0,1599	0,0017	0,60385	0,07528	0,00079	995,5	8,1	956,2	9,4	1075	22	89
A_080.FIN2	226,4	429	0,40813	840	1,685	0,021	0,1644	0,0013	0,60873	0,07392	0,00077	1002,5	7,9	981	7	1035	20	95
A_081.FIN2	81	391	1,01728	290	1,86	0,036	0,1659	0,0016	0,1079	0,0809	0,0017	1065	13	989,2	8,9	1209	39	82
A_082.FIN2	128,4	258,7	0,45249	750	1,721	0,043	0,1712	0,0025	0,31043	0,0723	0,0016	1014	17	1018	14	982	45	104
A_083.FIN2	108,6	287	0,58748	320	1,805	0,066	0,1751	0,0055	0,9222	0,0742	0,0013	1044	26	1041	31	1035	35	101
A_085.FIN2	256,2	346	0,33294	780	1,81	0,039	0,1773	0,0026	0,51827	0,0747	0,0014	1048	14	1052	14	1053	38	100
A_086.FIN2	219	311,2	0,32192	2200	1,857	0,025	0,1774	0,0016	0,49343	0,07613	0,0009	1064,3	8,7	1052,7	8,9	1091	24	96
A_087.FIN2	328	619	0,39970	2500	1,84	0,029	0,1776	0,002	0,40327	0,0751	0,001	1059	10	1053	11	1071	29	98
A_089.FIN2	84,1	174,1	0,48823	304	1,905	0,05	0,1818	0,0025	0,22103	0,0762	0,0019	1080	17	1077	14	1102	50	98
A_090.FIN2	299,7	793	0,53720	1100	1,987	0,023	0,1838	0,0015	0,58535	0,07766	0,00068	1109,8	7,6	1087,3	8	1136	17	96
A_091.FIN2	205,2	686,8	0,67982	640	2,017	0,03	0,185	0,0019	0,47566	0,0787	0,0011	1120	10	1094	10	1158	27	94
A_093.FIN2	210,9	598	0,55287	1080	2,111	0,025	0,195	0,0018	0,41132	0,07821	0,00087	1151,3	8,1	1147,9	9,5	1147	22	100
A_094.FIN2	557,1	4450	1,29797	2300	3,438	0,081	0,2368	0,0045	0,92586	0,10451	0,00097	1508	19	1369	24	1703	17	80
A_095.FIN2	82,4	411,9	0,78762	460	3,067	0,049	0,2459	0,0021	0,56934	0,0904	0,0013	1422	12	1417	11	1423	28	100
A_096.FIN2	76,6	407,1	0,82833	300	3,771	0,065	0,2714	0,0028	0,27974	0,1011	0,0016	1583	14	1548	14	1640	30	94
A_097.FIN2	228	623	0,40307	1200	4,162	0,051	0,2936	0,0026	0,63695	0,10332	0,00094	1664,7	9,9	1659	13	1681	17	99
A_099.FIN2	208,1	927	0,63239	1000	4,159	0,056	0,294	0,0035	0,48674	0,1027	0,0014	1665	11	1661	18	1670	25	99
A_100.FIN2	301,1	513,2	0,14660	2400	13,56	0,16	0,5043	0,0059	0,78211	0,1957	0,0015	2718	11	2631	25	2790	12	94
A_101.FIN2	91,4	912	0,79978	1650	13,61	0,13	0,518	0,0043	0,7863	0,1905	0,0014	2720,9	8,8	2689	18	2744	12	98
A_102.FIN2	690	285	0,03290	7200	17,21	0,89	0,575	0,012	0,92837	0,2161	0,0067	2924	46	2922	50	2935	47	100
A_108.FIN2	224,7	2130	0,58611	2770	26,7	0,34	0,6573	0,0057	0,63546	0,2918	0,0029	3369	12	3255	22	3423	16	95

Table 7: Grain (n=70) distribution of sample Map2. The red box highlights the preferred ages used (<1500=Pb^{206}/U^{238}; ≥1500=Pb^{207}/U^{235}). Refer to the legend in Fig. 31.

4.3.1.2   Map3

Sample Map3 represents the midway point sandstone unit of the lEF, exposed at Maphutseng.

The sample consisted of fifty-eight (58) concordant grain analyses, of which 3.4% are metamorphic

in origin, the remaining 96.6% are magmatic oscillatory zoned (Table 8). The grain lengths varied

from 35.0-260.0 µm, with the majority of grains being 100.0-200.0 µm. Grain shots were all positioned at the grain rims for this sample, to allow for youngest depositional ages to be calculated. 67% of the concordant grains do not belong to any of the three (3) populations seen in this sample. The most abundant population occurs at the Cambrian (492.0-524.0 Ma), hosting 20.7% (n=12) of the total grains and more minor populations occur at the Early Neoproterozoic (541.0-548.0 Ma, n=4) and Mid-Neoproterozoic (731.0-738.0 Ma, n=3). The two metamorphic grain morphologies noted in the SEM images also displayed (n=2; 3.4%) a Th/U ratio <0.1. The youngest grain determination resulted in: 1) YSG= 206.8 ±2 Ma; 2) YDZ= 206.9 ±3.8 (-3.9) Ma; 3) TuffZirc (8)= 512.5 ±1.4 Ma; 4) YC2σ (3)= 492.6 ±7.9 Ma; 5) Weighted Average (8)= 513.8 ±4.2 Ma; 6) YPP= 220.0 Ma and; 7) YC1σ (3)= 492.6 ±6.1 Ma. The collective mean of the YSG, YDZ and YPP ages for Map3 result in an average youngest maximum depositional age of 211.3 Ma.

4.3.1.3   Q2

Sample Q2 were sampled from the Moyeni trackway hosting siltstone unit. A total of fifty-three (53) concordant grains were analysed, of which 7.5% (n=4) of the grains have complex, rounded metamorphic structures (Table 9). The grains' sizes range from 42.0-160.0 µm, the majority (60%) of which falls between 60.0-100.0 µm. Both rim (77.4%) and core (22.6%) analyses were done for this sample and only 43.4% of the overall 53 concordant grains do not belong to a population. There are six (6) main populations within this sample, however it would likely have been only three populations, had there been a larger quantity of concordant grains. The six populations include the: 1) Cambrian, 502.4-529.5 Ma at 20.8% abundance (n=11); 2) Neoproterozoic, 563.1-575.5 Ma at 9.4% abundance (n=5); 3) Neoproterozoic II, 599.3-604.0 Ma at 5.7% abundance (n=3); 4) Neoproterozoic III, 628.0-633.0 Ma at 7.5% abundance (n=4); 5) Neoproterozoic IV, 987.0-999.6 Ma at 7.5% abundance (n=4); and, 6) Mesoproterozoic, 1052.0-1057.0 Ma at 7.5% abundance (n=4). Only one (1) grain has a Th/U ratio <0.1, suggesting a poor proportion of overall metamorphic grain provenance. The youngest grain determination resulted in: 1) YSG= 502.4 ±6.2 Ma; 2) YDZ= 500.8 ±6.6 (-13) Ma; 3) TuffZirc (8)= 509.7 ±12.5 Ma; 4) YC2σ (3)= 505.4 ±8.2 Ma; 5) Weighted Average (8)=

510.9 ±6.2 Ma; 6) YPP= 500.0 Ma and; 7) YC1σ (3)= 505.4 ±6.3 Ma. The collective mean of all test ages was used for Q2 due to the distinct lack younger grains (<500 Ma) and overall concordance of the test ages, which resulted in an average youngest maximum depositional age of 504.9 Ma.

					RATIOS							AGES [Ma]						Conc.
Analysis	U [ppm]a	Pb [ppm]a	Th/Ua	206/204	$^{207}Pb/^{235}U^b$	2 σd	$^{206}Pb/^{238}U^b$	2 σd	rhoc	$^{207}Pb/^{206}Pb^e$	2 σd	$^{207}Pb/^{235}U$	2 σ	$^{206}Pb/^{238}U$	2 σ	$^{207}Pb/^{206}Pb$	2 σ	%
A_083.FIN2	362	260	0,82	-380	0,2287	0,0059	0,0326	0,0003	0,3835	0,0508	0,0012	209	5	206,8	2	223	50	93
A_082.FIN2	291	240	0,86	-150	0,2426	0,0087	0,0345	0,0004	0,1714	0,0519	0,0018	220	7	218,8	3	262	76	84
A_018.FIN2	532	337	0,73	1100	0,2508	0,0081	0,0350	0,0004	0,0509	0,0518	0,0017	227	7	221,4	2	260	72	85
A_079.FIN2	446	296	0,66	-1400	0,2655	0,0057	0,0374	0,0003	0,3257	0,0516	0,0010	239	5	236,7	2	263	44	90
A_048.FIN2	500	270	0,37	2500	0,3912	0,0089	0,0534	0,0005	0,3632	0,0537	0,0010	336	6	335,4	3	345	42	97
A_034.FIN2	329	625	1,00	50000	0,5960	0,0330	0,0761	0,0018	0,1363	0,0563	0,0034	474	21	473,0	11	450	130	105
A_015.FIN2	342	556	0,77	-500	0,6170	0,0140	0,0789	0,0010	0,5604	0,0575	0,0010	487	9	489,4	6	496	40	99
A_046.FIN2	78	247	1,59	-70	0,6180	0,0210	0,0793	0,0009	0,2824	0,0565	0,0019	485	13	491,9	6	435	70	113
A_030.FIN2	247	295	0,61	-1300	0,6330	0,0220	0,0798	0,0007	0,4127	0,0582	0,0027	496	13	494,7	4	469	68	105
A_069.FIN2	178	278	0,80	-280	0,6460	0,0220	0,0809	0,0019	0,2899	0,0576	0,0020	506	14	501,0	12	511	72	98
A_027.FIN2	300	491	0,76	900	0,6400	0,0130	0,0810	0,0007	0,3978	0,0578	0,0010	501	8	501,8	4	515	39	97
A_032.FIN2	243	348	0,65	400	0,6570	0,0160	0,0816	0,0010	0,4282	0,0592	0,0014	511	10	505,8	6	562	49	90
A_065.FIN2	293	379	0,59	-160	0,6610	0,0150	0,0826	0,0009	0,5239	0,0584	0,0012	514	9	511,6	6	530	45	97
A_024.FIN2	341	444	0,60	2300	0,6650	0,0180	0,0829	0,0010	0,4811	0,0583	0,0013	516	11	513,4	6	535	52	96
A_047.FIN2	176	308	0,83	340	0,6680	0,0160	0,0830	0,0008	0,1271	0,0583	0,0014	518	10	513,9	4	518	52	99
A_011.FIN2	280	255	0,46	-220	0,6670	0,0200	0,0830	0,0009	0,3238	0,0581	0,0017	518	12	513,9	6	515	64	100
A_053.FIN2	73	117	0,73	-370	0,6660	0,0250	0,0841	0,0014	0,2196	0,0581	0,0023	516	15	520,4	9	496	82	105
A_062.FIN2	79	138	0,82	-120	0,6890	0,0350	0,0845	0,0012	0,1649	0,0582	0,0031	529	21	523,1	7	480	110	109
A_087.FIN2	361	353	0,40	900	0,6790	0,0300	0,0847	0,0031	0,6474	0,0601	0,0020	526	18	524,0	18	599	73	87
A_044.FIN2	251	204	0,36	990	0,7020	0,0120	0,0870	0,0007	0,3106	0,0590	0,0009	539	7	537,4	4	553	36	97
A_050.FIN2	76	64	0,39	60	0,7180	0,0370	0,0876	0,0015	0,0388	0,0593	0,0033	546	22	540,9	9	530	120	102
A_057.FIN2	248	257	0,45	-1430	0,7150	0,0120	0,0878	0,0007	0,2901	0,0591	0,0010	547	7	542,7	4	556	35	98
A_086.FIN2	222	17	0,03	1030	0,7150	0,0150	0,0882	0,0006	0,2630	0,0588	0,0011	547	9	544,9	4	537	42	101
A_023.FIN2	373	14	0,02	120	0,7180	0,0110	0,0887	0,0007	0,4854	0,0593	0,0009	549	7	547,5	4	571	31	96
A_025.FIN2	263	138	0,23	-300	0,7320	0,0110	0,0898	0,0006	0,2531	0,0593	0,0009	557	7	554,5	4	565	34	98
A_055.FIN2	64	193	1,32	-190	0,7480	0,0220	0,0907	0,0010	0,0274	0,0598	0,0019	564	13	560,2	6	547	68	102
A_013.FIN2	522	469	0,39	400	0,7494	0,0091	0,0919	0,0007	0,5179	0,0597	0,0006	566	5	566,4	4	584	23	97
A_067.FIN2	173	87	0,21	330	0,7940	0,0430	0,0941	0,0023	0,2388	0,0605	0,0032	592	24	580,0	14	600	120	97
A_061.FIN2	175	663	1,67	-350	0,7870	0,0170	0,0954	0,0009	0,2730	0,0602	0,0013	590	10	587,5	5	594	45	99
A_081.FIN2	310	308	0,39	-3800	0,7970	0,0140	0,0958	0,0008	0,3005	0,0608	0,0011	594	8	589,9	5	630	36	94
A_016.FIN2	601	157	0,09	800	0,8510	0,0300	0,1011	0,0024	0,3543	0,0615	0,0021	625	17	621,0	14	651	74	95
A_006.FIN2	563	591	0,38	3200	0,9810	0,0170	0,1129	0,0011	0,4515	0,0628	0,0010	693	9	689,2	7	692	34	100
A_063.FIN2	348	612	0,56	-1200	1,0580	0,0210	0,1202	0,0021	0,5128	0,0654	0,0012	732	10	731,0	12	785	38	93
A_040.FIN2	331	408	0,45	400	1,0730	0,0280	0,1207	0,0014	0,3493	0,0642	0,0016	739	14	734,7	8	740	52	99
A_059.FIN2	503	424	0,26	600	1,1250	0,0130	0,1212	0,0008	0,4232	0,0673	0,0007	765	6	737,5	5	844	22	87
A_068.FIN2	110	213	0,67	-420	1,1600	0,0710	0,1275	0,0024	0,0191	0,0658	0,0044	778	33	774,0	14	760	130	102
A_051.FIN2	39	100	0,57	600	1,4090	0,0630	0,1464	0,0027	0,5456	0,0702	0,0027	882	27	880,0	15	876	79	100
A_042.FIN2	86	210	0,61	240	1,5780	0,0540	0,1541	0,0023	0,1561	0,0733	0,0024	959	21	924,0	13	1015	68	91
A_012.FIN2	221	495	0,69	-1500	1,5020	0,0460	0,1544	0,0036	0,2353	0,0699	0,0025	930	18	926,0	20	948	55	98
A_009.FIN2	444	1220	0,69	230	1,6890	0,0210	0,1585	0,0017	0,6864	0,0779	0,0008	1003	8	948,4	10	1139	19	83
A_084.FIN2	319	430	0,37	-5200	1,5610	0,0540	0,1588	0,0025	0,3195	0,0710	0,0024	954	22	950,0	14	952	71	100
A_019.FIN2	335	759	0,51	3900	1,6250	0,0300	0,1632	0,0018	0,5161	0,0738	0,0012	979	11	974,0	10	1029	32	95
A_076.FIN2	335	626	0,52	-3200	1,8310	0,0260	0,1640	0,0016	0,8083	0,0810	0,0007	1055	9	978,5	9	1217	18	80
A_077.FIN2	281	357	0,32	8200	1,6530	0,0700	0,1661	0,0055	0,6897	0,0756	0,0017	993	23	990,0	30	1076	47	92
A_052.FIN2	96	313	0,72	-1600	1,7360	0,0540	0,1706	0,0019	0,4783	0,0749	0,0021	1019	20	1016,0	10	1049	59	97
A_085.FIN2	67	135	0,48	100	1,7530	0,0360	0,1729	0,0014	0,2535	0,0734	0,0015	1026	13	1027,6	8	1001	42	103
A_054.FIN2	422	1706	0,94	-5300	1,7960	0,0310	0,1743	0,0022	0,4394	0,0745	0,0013	1043	11	1036,0	12	1049	36	99
A_041.FIN2	464	522	0,22	-100	1,8530	0,0240	0,1787	0,0018	0,5213	0,0758	0,0009	1063	8	1059,6	10	1088	22	97
A_035.FIN2	224	326	0,36	-530	1,8480	0,0320	0,1795	0,0017	0,4492	0,0743	0,0011	1061	11	1064,1	9	1041	31	102
A_021.FIN2	446	241	0,21	56000	2,0420	0,0190	0,1827	0,0013	0,5240	0,0813	0,0007	1130	6	1081,5	7	1225	16	88
A_043.FIN2	93	297	0,72	2200	1,9500	0,0610	0,1845	0,0026	0,1052	0,0760	0,0025	1096	21	1092,0	14	1078	67	101
A_064.FIN2	283	758	0,62	-700	2,0540	0,0700	0,1917	0,0043	0,2772	0,0769	0,0025	1133	24	1130,0	23	1116	69	101
A_017.FIN2	171	525	0,58	3000	2,1190	0,0440	0,1957	0,0024	0,3114	0,0806	0,0015	1157	13	1152,0	13	1213	39	95
A_028.FIN2	159	1010	1,30	-410	2,1260	0,0360	0,1959	0,0022	0,4959	0,0792	0,0011	1156	12	1153,0	12	1172	28	98
A_029.FIN2	811	1520	0,37	6800	2,6700	0,0220	0,2184	0,0015	0,6980	0,0885	0,0005	1319	6	1273,3	8	1393	12	91
A_058.FIN2	382	322	0,13	5000	3,9050	0,0470	0,2734	0,0025	0,8649	0,1036	0,0007	1613	10	1558,0	13	1688	12	92
A_007.FIN2	99	201	0,26	100	4,0800	0,1500	0,2913	0,0059	0,6290	0,1052	0,0030	1648	30	1648,0	30	1714	52	96
A_014.FIN2	223	1082	0,39	-2200	14,3300	0,1500	0,5379	0,0050	0,6303	0,1956	0,0016	2771	10	2774,0	21	2789	14	99
A_020.FIN2	347	4000	0,79	-1400	29,3400	0,1700	0,6840	0,0045	0,8007	0,3131	0,0013	3465	6	3359,0	17	3536	6	95

Table 8: Grain (=58) distribution of sample Map3. The red box highlights the preferred ages used (<1500=Pb^{206}/U^{238}; ≥1500=Pb^{207}/U^{235}). Refer to the legend in Fig. 31.

					RATIOS								AGES [Ma]						Conc.
																			Q2
Analysis	U [ppm]a	Pb [ppm]a	Th/Ua	206/204	207Pb/235Ub	2σd	206Pb/238Ub	2σd	rhoc	207Pb/206Pbe	2σd	207Pb/235U	2σ	206Pb/238U	2σ	207Pb/206Pb	2σ	%
A_113.FIN2	878	896	0,443052392	1240	0,583	0,024	0,0811	0,001	0,38282	0,0518	0,002	463	16	502,4	6,2	458	58	110
A_136.FIN2	541	139,4	0,121996303	8600	0,655	0,012	0,08162	0,00096	0,29951	0,0587	0,0011	510,9	7,1	505,7	5,7	559	37	90
A_146.FIN2	548	429,5	0,34689781	1250	0,6632	0,0097	0,08177	0,00072	0,51192	0,0587	0,0007	515,8	5,9	506,6	4,3	556	25	91
A_149.FIN2	248	318	0,592741935	280	0,65	0,014	0,08217	0,00089	0,22628	0,0578	0,0013	506,9	8,6	509	5,3	496	49	103
A_179.FIN2	261,8	206	0,383880825	1340	0,658	0,015	0,08238	0,00097	0,3285	0,0583	0,0012	514	9,4	510,3	5,7	544	46	94
A_110.FIN2	239	536	1,066945607	420	0,668	0,017	0,0833	0,0013	0,14666	0,0582	0,0016	519	10	515,9	7,6	532	57	97
A_163.FIN2	40,1	74,9	0,813965087	22	0,688	0,031	0,0844	0,0014	0,1007	0,06	0,0028	529	19	522,1	8,5	534	97	98
A_161.FIN2	195	311	0,717948718	110	0,68	0,016	0,08462	0,0009	0,28614	0,0591	0,0012	525,7	9,5	523,5	5,3	543	45	96
A_153.FIN2	172,8	309	0,745949074	320	0,69	0,013	0,0853	0,0008	0,31489	0,0589	0,0011	532,2	7,8	527,6	4,7	543	40	97
A_143.FIN2	295,1	325,5	0,475770925	3200	0,689	0,011	0,08547	0,0007	0,43616	0,0585	0,00087	531,9	7	528,6	4,2	547	32	97
A_165.FIN2	97,3	146	0,644398767	780	0,687	0,018	0,0856	0,0011	0,2982	0,0584	0,0015	529	11	529,5	6,3	512	55	103
A_119.FIN2	257,5	453	0,753398058	360	0,707	0,015	0,08713	0,00096	0,31917	0,0591	0,0012	542	8,8	538,5	5,7	551	46	98
A_133.FIN2	283,8	222,8	0,332628612	-120	0,711	0,013	0,08747	0,00088	0,29045	0,0593	0,0011	544,4	7,7	540,5	5,2	560	41	97
A_144.FIN2	437	832	0,8	430	0,7455	0,0099	0,0913	0,00086	0,47023	0,05923	0,00069	565	5,8	563,1	5,1	571	26	99
A_122.FIN2	392,2	371,2	0,399796022	1300	0,758	0,018	0,0923	0,0015	0,50342	0,0597	0,0012	572	10	569,1	8,7	591	42	96
A_129.FIN2	314	304	0,409872611	780	0,797	0,012	0,09259	0,00093	0,56434	0,06243	0,00082	594,2	6,8	570,7	5,5	688	28	83
A_118.FIN2	291,7	346	0,491943778	1700	0,76	0,02	0,0926	0,0012	0,46992	0,0597	0,0013	575	11	571	6,9	580	48	98
A_157.FIN2	633	1332	0,763033175	1170	0,712	0,025	0,09339	0,00094	0,48773	0,0552	0,0018	542	15	575,5	5,6	560	52	103
A_132.FIN2	1153	235,2	0,07745013	27000	0,793	0,011	0,09475	0,00098	0,73633	0,06091	0,0006	592,1	6,2	583,5	5,8	632	21	92
A_112.FIN2	524	199,5	0,125572519	1330	0,853	0,015	0,0975	0,0013	0,8138	0,06302	0,00066	624,7	8,3	599,3	7,7	704	23	85
A_117.FIN2	247,1	304,7	0,47592068	1730	0,806	0,017	0,0981	0,0011	0,54434	0,0594	0,0011	598,8	9,6	602,9	6,6	567	39	106
A_166.FIN2	187,4	110,1	0,221291355	660	0,812	0,016	0,09825	0,00093	0,22452	0,06005	0,00097	601,9	8,8	604	5,5	589	35	103
A_168.FIN2	173	130,2	0,271156069	880	0,917	0,038	0,1024	0,0027	0,89016	0,0644	0,0015	652	20	628	16	729	50	86
A_181.FIN2	727	542	0,279642366	1000	0,871	0,018	0,1027	0,0017	0,76944	0,06162	0,00077	635,3	9,7	629,9	9,9	660	28	95
A_114.FIN2	428	326,8	0,243457944	440	0,714	0,036	0,103	0,0011	0,48299	0,0501	0,0024	544	22	631,9	6,2	539	61	117
A_156.FIN2	1550	480	0,161935484	3350	0,88	0,021	0,1032	0,002	0,78994	0,06203	0,00094	639	12	633	11	666	33	95
A_171.FIN2	511	560	0,317221135	1340	1,03	0,039	0,1147	0,0019	0,52901	0,0652	0,0022	714	20	699	11	796	62	88
A_125.FIN2	546,5	288,8	0,163586459	3300	1,179	0,016	0,1261	0,0014	0,73804	0,06771	0,00064	790,4	7,6	766,1	8,3	857	20	89
A_115.FIN2	251	408	0,46374502	590	0,901	0,083	0,1267	0,0024	0,56077	0,0512	0,0046	621	55	768	14	718	77	107
A_167.FIN2	327,9	453	0,387008234	1020	1,094	0,045	0,1289	0,0017	0,31921	0,0617	0,0024	750	21	781,2	9,5	751	63	104
A_137.FIN2	239,2	414	0,405100334	0	1,222	0,057	0,1345	0,0017	0,45203	0,0656	0,0028	801	26	813	9,5	887	69	92
A_151.FIN2	53,9	128,3	0,590723562	320	1,343	0,035	0,1463	0,0017	0,38058	0,0671	0,0018	860	15	880,1	9,8	807	56	109
A_176.FIN2	657,8	657	0,113408331	920	1,472	0,048	0,1484	0,002	0,61532	0,0723	0,0019	914	20	892	11	972	54	92
A_148.FIN2	479,7	692,1	0,339170315	3100	1,602	0,02	0,1568	0,0016	0,74614	0,07439	0,00063	970,8	7,9	938,8	9	1048	17	90
A_109.FIN2	94,3	158,8	0,372216331	309	1,643	0,029	0,1585	0,0015	0,3569	0,075	0,0013	986	12	948,2	8,1	1058	34	90
A_170.FIN2	504,8	681	0,309429477	-9600	1,704	0,024	0,1655	0,002	0,55968	0,07503	0,00093	1009,1	8,9	987	11	1065	25	93
A_123.FIN2	294,1	358,9	0,281196872	690	1,716	0,024	0,1666	0,0018	0,72035	0,07442	0,00078	1012,8	8,9	993	10	1046	21	95
A_127.FIN2	215	186	0,200465116	1030	1,754	0,027	0,1668	0,0017	0,0044203	0,0763	0,0011	1027	10	994	9,3	1093	29	91
A_131.FIN2	224,6	613	0,593499555	1600	1,774	0,022	0,1678	0,0014	0,56493	0,07646	0,00076	1034,6	8,1	999,6	7,8	1104	20	91
A_126.FIN2	208,3	322	0,339414306	1540	1,866	0,037	0,1773	0,0023	0,61162	0,0767	0,0013	1067	13	1052	12	1105	33	95
A_142.FIN2	192	384	0,363541667	750	2,026	0,069	0,1775	0,0022	0,58938	0,0834	0,0023	1117	22	1053	12	1241	51	85
A_159.FIN2	157,4	197,9	0,258831004	-260	1,845	0,036	0,1778	0,0023	0,69024	0,0754	0,0011	1059	13	1054	13	1069	28	99
A_147.FIN2	363,3	453	0,252958987	400	1,941	0,043	0,1782	0,0026	0,35934	0,0795	0,0016	1094	14	1057	14	1176	38	90
A_150.FIN2	213,9	288,3	0,293595138	370	1,912	0,031	0,1809	0,002	0,48343	0,0772	0,0012	1084	11	1072	11	1118	30	96
A_164.FIN2	214,8	588	0,552607076	1500	1,886	0,031	0,1817	0,0024	0,56484	0,0757	0,0011	1075	11	1078	12	1081	28	100
A_120.FIN2	143,5	301,1	0,436933798	2500	1,937	0,034	0,1846	0,0019	0,52617	0,0761	0,0012	1092	12	1092	10	1088	31	100
A_160.FIN2	395,5	605	0,317572693	2300	2,012	0,033	0,1861	0,0024	0,64428	0,0788	0,001	1118	11	1100	13	1168	24	94
A_169.FIN2	231,9	931	0,80465718	6300	2,241	0,03	0,2026	0,0023	0,55809	0,08043	0,00091	1192,9	9,4	1189	12	1206	23	99
A_154.FIN2	154,5	801	0,842071197	1600	3,229	0,063	0,2414	0,0033	0,48492	0,0977	0,0017	1462	15	1394	17	1574	33	89
A_162.FIN2	662	3393	0,82326284	5700	3,063	0,045	0,2416	0,0035	0,89533	0,09215	0,00064	1421	11	1394	18	1468	13	95
A_152.FIN2	266,7	950	0,473940757	2600	3,929	0,055	0,2814	0,0036	0,62132	0,102	0,0012	1620,00	11,00	1598	18	1657	23	96
A_128.FIN2	186	707	0,539784946	580	3,978	0,04	0,2823	0,0022	0,72178	0,10192	0,00089	1628,10	8,10	1603	11	1655	16	97
A_158.FIN2	422	1373	0,454028436	3100	4,499	0,068	0,3081	0,0041	0,8193	0,10629	0,00085	1730,00	13,00	1731	20	1736	15	100
A_124.FIN2	271	1249	0,428413284	3500	11,091	0,096	0,4199	0,0036	0,78561	0,1914	0,0011	2530,20	7,90	2259	16	2752,5	9,4	82

Table 9: Grain (=53) distribution of sample Q2. The red box highlights the preferred ages used (<1500=Pb206/U238; ≥1500=Pb207/U235). Refer to the legend in Fig. 31.

4.3.1.4 Q6

Sample Q6 was extracted from the lowermost basal Clarens-uEF boundary. This sample comprises of a total of fifty-two (52) concordant grains, of which 5.8% had metamorphic complex internal structures and rounded external features (Table 10). The grain sizes range from 30.0-290.0 μm, with the vast majority (71.8%) of grains falling between 120.0-220.0 μm. Of the total concordant grain shots, 19.2% are located in the grain core and 80.8% on the grain rims. There are three (3) grain populations, the most abundant being the Cambrian-Neoproterozoic, ranging in age from 535.0 Ma to 558.4 Ma and hosting 11.5% (n=6) of the total grains. More minor populations include the Silurian

and Ordovician population (n=3) at 466.2-469.4 Ma and the older Mesoproterozoic population (n=3) at 1084.6-1096.0 Ma. The remaining fourty (40) concordant grains do not belong to any other populations (≥3 grains clustered together; Fig. 30). The Th/U ratio confirms that the three grains hosting complex and rounded structures are indeed metamorphic grains, with indicative Th/U ratios <0.1. The youngest grain determination resulted in: 1) YSG= 190.5 ±3.9 Ma; 2) YDZ= 191.0 ±3.9 (-9.3) Ma; 3) TuffZirc (8)= 542.0 ±16.5 Ma; 4) YC2σ (3)= 467.2 ±7.9 Ma; 5) Weighted Average (8)= 545.0 ±10 Ma; 6) YPP= 490.0 Ma and; 7) YC1σ (3)= 467.2 ±5.9 Ma. The collective mean of Q6 was based off of the YSG and YDZ ages only (other test ages influenced by the abundant Cambrian population), which resulted in an average youngest maximum depositional age of 190.8 Ma.

4.3.1.5   Q3

Sample Q3 represents the mid-lower section of the exposed uEF units of Quthing. The sample comprised of seventy-one (71) concordant analysed grains, of which 7.2% (n=7) of the grains have complex and rounded structures, often seen in metamorphic grains (Table 11). The grains range in length from 55.0-250.0 μm. 21.1% of the demarcated shots were of grain cores, and the remaining 78.9% were grain rim shots. Altogether, there are five (5) grain populations and the remaining 60.6% do not belong to any populations. The six populations include the: 1) Triassic population, 220.5-231.6 Ma spanning 5.6% (n=4) of the overall population; 2) The 503.6-528.6 Ma Cambrian population, spanning over 7.2% (n=7) of the overall grains; 3) Early Neoproterozoic population, 564.9-604.0 Ma, spanning 11.3% (n=8) of the total grains; 4) Late Neoproterozoic, 913.4-914.0 Ma, spanning over 4.2% (n=3) of the overall grains; 5) Mesoproterozoic,1050.4-1068.0 Ma, spanning over 11.3% (n=8) of the sample (Fig. 30). None of the grains in this sample have Th/U ratios <0.1, proving it is likely that no metamorphic grains are present within this sample, in contrast to what some metamorphic grain structures might infer. The youngest grain determination resulted in: 1) YSG= 220.5 ±2.2 Ma; 2) YDZ= 220.8 ±4.3 (-5.2) Ma; 3) TuffZirc (8) = 1054.6 ±10.6 Ma; 4) YC2σ (3)= 224.4 ±3.8 Ma; 5) Weighted Average (8)= 1059.0 ±3.4 Ma; 6) YPP= 200.0 Ma and; 7) YC1σ (3)= 224.4 ±2.9

Ma. The collective mean of Q3 included all of the test ages except for the least sensitive TuffZirc amd

Weighted Mean ages. This resulted in an average youngest maximum depositional age of 218.0 Ma.

					Q6														Conc.
					RATIOS									AGES [Ma]					
Analysis	U [ppm]a	Pb [ppm]a	Th/Ua	206/204	207Pb/235Ub	2σd	206Pb/238Ub	2σd	rhoc	207Pb/206Pbe	2σd	207Pb/235U	2σ	206Pb/238U	2σ	207Pb/206Pb	2σ	%
A_201.FIN2	106,1	77,5	0,923656927	22	0,213	0,018	0,02999	0,00062	0,076743	0,0519	0,0044	194	15	190,5	3,9	220	160	87
A_192.FIN2	253,3	232,7	1,127516779	81	0,2127	0,0063	0,03029	0,00031	0,16301	0,051	0,0015	195,2	5,3	192,3	1,9	224	62	86
A_250.FIN2	280	336	1,182142857	170	0,2899	0,0074	0,04046	0,00041	0,18287	0,052	0,0013	257,7	5,8	255,7	2,5	262	51	98
A_255.FIN2	808	650	0,603960396	1200	0,337	0,013	0,05209	0,00043	0,21859	0,0468	0,0018	292,9	9,8	327,3	2,6	404	51	81
A_231.FIN2	488	282,8	0,327459016	1730	0,5165	0,008	0,06641	0,00062	0,47301	0,05626	0,00078	422,2	5,4	414,5	3,7	453	32	92
A_257.FIN2	496,4	63,4	0,062046737	1320	0,5896	0,008	0,07501	0,00068	0,47926	0,05685	0,00066	470,6	5	466,2	4,1	485	26	96
A_244.FIN2	190	295	0,863157895	200	0,597	0,018	0,0752	0,001	0,42197	0,0576	0,0016	474	11	467,3	6,3	500	63	93
A_263.FIN2	429	676	0,842657343	1190	0,59	0,012	0,07554	0,00099	0,58458	0,0571	0,0012	470,4	7,4	469,4	6	479	46	98
A_260.FIN2	474	555	0,635232068	510	0,653	0,01	0,07856	0,00091	0,40612	0,0605	0,00093	510	6,4	487,5	5,4	613	33	80
A_222.FIN2	320,4	347,2	0,495318352	1810	0,634	0,011	0,0795	0,00079	0,28402	0,0578	0,001	497,9	6,8	493,1	4,7	507	38	97
A_225.FIN2	335,6	164,2	0,180274136	360	0,474	0,053	0,0802	0,0012	0,27487	0,0424	0,0046	374	39	497,4	7	577	95	86
A_227.FIN2	531,3	1817	1,613024657	560	0,681	0,01	0,08293	0,00075	0,3373	0,05921	0,00087	526,6	6,3	513,5	4,5	568	33	90
A_184.FIN2	85	108,8	0,576470588	134	0,689	0,021	0,0844	0,001	0,10661	0,0595	0,0018	529	13	522,1	6,2	539	67	97
A_183.FIN2	295,9	241,6	0,372423116	870	0,7	0,016	0,0865	0,0014	0,2494	0,0594	0,0015	538,4	9,6	535	8,4	567	57	94
A_248.FIN2	478	303	0,29665272	2800	0,725	0,012	0,08707	0,00091	0,44999	0,06038	0,00093	552,9	7,2	538,1	5,4	608	34	89
A_215.FIN2	196,6	273,3	0,598677518	120	0,711	0,023	0,0877	0,0014	0,34377	0,0589	0,0018	544	13	541,8	8,1	542	66	100
A_269.FIN2	148,3	261,5	0,797033041	480	0,709	0,02	0,0877	0,001	0,41713	0,0591	0,0015	544	12	542,1	6	545	54	99
A_239.FIN2	865	304	0,190751445	1720	0,752	0,026	0,0904	0,0017	0,582	0,0601	0,0018	566	16	558	10	641	51	87
A_268.FIN2	1002	51,1	0,012185629	2300	0,761	0,012	0,0905	0,00098	0,66966	0,06113	0,0009	574,2	6,8	558,4	5,8	638	31	88
A_262.FIN2	729	67,4	0,022496571	2600	0,824	0,015	0,09523	0,00092	0,445	0,06284	0,00096	609	8,3	586,3	5,4	692	33	85
A_196.FIN2	315,3	496,6	0,610212496	280	0,79	0,015	0,09542	0,00097	0,44661	0,0602	0,001	590,1	8,5	587,5	5,7	596	38	99
A_195.FIN2	798	619	0,313533835	1100	0,874	0,016	0,1014	0,0012	0,66292	0,06262	0,00083	636,8	8,5	622,5	6,8	689	28	90
A_217.FIN2	534	282	0,19082397	300	0,865	0,014	0,1019	0,0011	0,55426	0,0615	0,00082	632	7,4	625,6	6,6	649	29	96
A_204.FIN2	165,7	197,6	0,428485214	190	0,908	0,028	0,1046	0,0016	0,52191	0,0631	0,0016	654	15	641,5	9,1	703	55	91
A_190.FIN2	327,6	518	0,528388278	2100	0,938	0,019	0,1052	0,0014	0,47255	0,0649	0,0012	670,5	9,8	644,7	8	756	38	85
A_230.FIN2	413	1134	0,888619855	490	0,988	0,019	0,1096	0,0011	0,57044	0,0652	0,0011	698	9,1	670,3	6,5	769	35	87
A_189.FIN2	141,8	171,8	0,414880113	270	0,954	0,026	0,1104	0,0017	0,36346	0,0631	0,0019	678	13	675	10	680	63	99
A_237.FIN2	333	295,8	0,25015015	-7600	1,021	0,018	0,1118	0,0014	0,70189	0,0662	0,0012	713,5	9,1	683	8	810	38	84
A_220.FIN2	425	373	0,303529412	300	0,992	0,02	0,1133	0,0015	0,41288	0,0636	0,0012	699	10	691,7	8,9	719	40	96
A_236.FIN2	136,8	233,1	0,584064327	1800	0,993	0,02	0,1138	0,0011	0,31415	0,0631	0,0012	698	10	694,8	6,1	691	41	101
A_224.FIN2	559	894	0,492128801	1220	1,121	0,017	0,1178	0,0012	0,45713	0,06911	0,00097	762,2	8,2	717,5	7,2	893	30	80
A_197.FIN2	129,9	196,7	0,491147036	280	1,078	0,024	0,1197	0,0013	0,29571	0,0652	0,0014	741	12	728,6	7,5	758	48	96
A_214.FIN2	164,1	382	0,608775137	-1400	1,256	0,029	0,1318	0,0021	0,74382	0,0689	0,0011	823	13	798	12	881	33	91
A_188.FIN2	446	345	0,208520179	890	1,14	0,052	0,1335	0,0026	0,71093	0,0613	0,0022	760	26	807	15	745	58	108
A_259.FIN2	61,8	76,9	0,372653722	240	1,281	0,043	0,1389	0,0025	0,52155	0,067	0,002	832	19	838	14	807	65	104
A_249.FIN2	283,5	308,4	0,311111111	690	1,383	0,022	0,1403	0,0016	0,69528	0,07148	0,00084	880,7	9,5	845,9	8,8	965	24	88
A_211.FIN2	734	1356	0,576294278	1090	1,484	0,049	0,1481	0,0034	0,6994	0,0723	0,0016	918	20	889	19	981	50	91
A_252.FIN2	237,8	281,8	0,333894029	750	1,454	0,022	0,1484	0,0015	0,51375	0,07089	0,00094	909,6	9	891,8	8,4	944	27	94
A_186.FIN2	323	558	0,466873065	1510	1,518	0,019	0,1533	0,0013	0,37859	0,07195	0,00088	936,6	7,5	919,5	7,2	976	25	94
A_234.FIN2	301,3	258,4	0,224195154	1380	1,586	0,02	0,155	0,0014	0,47914	0,07378	0,0008	964,5	7,8	928,7	7,6	1032	22	90
A_223.FIN2	281,2	350	0,232147937	910	1,69	0,1	0,1554	0,0021	0,73105	0,0804	0,004	989	29	933	12	1140	66	82
A_264.FIN2	43,6	89,4	0,439678899	110	1,753	0,046	0,1656	0,0018	0,060537	0,0769	0,002	1022	17	987	10	1086	51	91
A_193.FIN2	193,4	443,6	0,53516029	210	1,669	0,023	0,1678	0,0014	0,36827	0,07236	0,00096	995,3	8,7	999,8	7,8	986	27	101
A_245.FIN2	876	1631	0,544178082	2590	1,861	0,032	0,1735	0,0016	0,67559	0,07764	0,00098	1067	11	1031,3	9	1134	25	91
A_200.FIN2	321	507	0,429283489	1010	1,888	0,043	0,1752	0,004	0,83864	0,0786	0,001	1073	15	1039	22	1152	26	90
A_199.FIN2	78,8	259	0,70177665	190	1,804	0,033	0,1754	0,0016	0,34792	0,0744	0,0014	1043	12	1041,6	8,9	1030	38	101
A_229.FIN2	385,1	647,5	0,364580628	-230	1,931	0,026	0,1801	0,0019	0,68304	0,07761	0,00086	1091,1	9	1067	10	1136	23	94
A_246.FIN2	490,8	1255	0,611858191	1200	1,903	0,028	0,1805	0,002	0,63837	0,07661	0,00083	1082,8	9,2	1070	11	1108	21	97
A_218.FIN2	418,1	1281	0,619229849	1720	1,996	0,02	0,1833	0,0015	0,56656	0,07887	0,00069	1113,2	6,8	1084,6	8,2	1166	17	93
A_194.FIN2	250	665	0,542	480	1,989	0,033	0,1838	0,0023	0,6339	0,0787	0,001	1110	11	1088	13	1164	25	93
A_221.FIN2	204,4	286	0,302837573	2200	1,947	0,031	0,1839	0,0022	0,2839	0,0767	0,0012	1096	11	1088	12	1113	34	98
A_256.FIN2	171,4	742	0,630105018	2100	4,203	0,046	0,2917	0,0029	0,57894	0,1046	0,0011	1673,1	8,9	1649	14	1703	19	97
A_266.FIN2	188	308,3	0,181117021	3300	5,107	0,055	0,3292	0,0031	0,55388	0,1128	0,001	1835,7	9	1834	15	1842	16	100

Table 10: Grain (=52) distribution of sample Q6. The red box highlights the preferred ages used (<1500=Pb^{206}/U^{238}; ≥1500=Pb^{207}/U^{235}). Refer to the legend in Fig. 31.

Analysis	U [ppm]a	Pb [ppm]a	Th/Ua	206/204	207Pb/235Ub	2σd	206Pb/238Ub	2σd	rhoc	207Pb/206Pbe	2σd	207Pb/235U	2σ	206Pb/238U	2σ	207Pb/206Pb	2σ	%
A_315.FIN2	343,8	172	0,526468877	470	0,2482	0,0059	0,0348	0,00035	0,27699	0,0516	0,0012	225,2	4,9	220,5	2,2	249	50	89
A_341.FIN2	164,7	83,8	0,501517911	85	0,258	0,012	0,03595	0,00052	0,0018916	0,0517	0,0025	231,8	9,7	227,6	3,3	253	98	90
A_385.FIN2	307,4	166,7	0,555627846	390	0,2539	0,0067	0,03595	0,0004	0,34342	0,0516	0,0014	229,2	5,4	227,6	2,5	248	56	92
A_340.FIN2	1223	662	0,590351594	-62000	0,258	0,0075	0,03659	0,00058	0,6492	0,0509	0,0014	232,8	6,1	231,6	3,6	228	59	102
A_322.FIN2	388	489	1,154639175	570	0,2968	0,0055	0,04148	0,00039	0,22029	0,0518	0,001	263,5	4,3	262	2,4	267	42	98
A_321.FIN2	129,5	284,2	1,068725869	480	0,631	0,02	0,07866	0,00096	0,26199	0,0577	0,0017	495	12	488	5,8	496	66	98
A_357.FIN2	368,9	515	0,686364869	1680	0,647	0,011	0,07927	0,00078	0,36026	0,05943	0,00097	506,8	6,8	491,7	4,6	570	35	86
A_332.FIN2	360	826	1,086111111	1380	0,544	0,051	0,08126	0,00088	0,27768	0,0478	0,0045	442	31	503,6	5,2	627	79	80
A_375.FIN2	151,3	287,6	0,892267019	140	0,65	0,015	0,08191	0,00073	0,16092	0,0582	0,0014	506,9	9,4	507,5	4,3	506	53	100
A_294.FIN2	395,4	533	0,529084471	680	0,477	0,049	0,0835	0,001	0,50436	0,0408	0,0041	381	36	516,7	6,1	517	89	100
A_316.FIN2	877	759	0,240935006	1020	0,64	0,023	0,0837	0,00091	0,42985	0,0552	0,0019	501	15	518,1	5,4	532	54	97
A_389.FIN2	122,9	152,8	0,602929211	440	0,671	0,025	0,0843	0,0013	0,18833	0,0581	0,0021	522	14	521,5	7,8	516	75	101
A_327.FIN2	75,4	152,8	0,889920424	270	0,694	0,023	0,08527	0,00096	0,044544	0,0589	0,0019	532	13	527,4	5,7	518	66	102
A_354.FIN2	209,9	415,6	0,848975703	670	0,679	0,012	0,08546	0,00073	0,28149	0,0577	0,001	524,7	7,5	528,6	4,4	496	39	107
A_311.FIN2	81,4	59,6	0,298034398	170	0,702	0,021	0,08678	0,00087	0,11713	0,0583	0,0017	536	12	536,4	5,1	495	62	108
A_367.FIN2	164,3	353	0,91965916	180	0,694	0,014	0,08683	0,00078	0,24976	0,0579	0,0011	534,4	8,7	536,7	4,6	503	41	107
A_317.FIN2	475,8	251	0,237704918	1090	0,644	0,03	0,0881	0,0014	0,41639	0,0526	0,0023	501	18	544	8,4	557	59	98
A_326.FIN2	466	1041	1,019313305	1700	0,703	0,025	0,0885	0,0011	0,42311	0,0571	0,0018	537	15	546,6	6,3	610	47	90
A_379.FIN2	199,9	217,3	0,456228114	640	0,751	0,015	0,0916	0,00097	0,352	0,06	0,0011	568,8	8,3	564,9	5,7	591	40	96
A_362.FIN2	132,3	134,6	0,405895692	250	0,754	0,019	0,0917	0,001	0,31197	0,0599	0,0014	569	11	565,3	5,9	582	52	97
A_388.FIN2	388	233,4	0,256185567	760	0,76	0,012	0,09243	0,00083	0,36251	0,06005	0,00094	573,2	7,2	569,8	4,9	593	34	96
A_348.FIN2	576	543,9	0,372048611	2300	0,795	0,012	0,09575	0,00096	0,51204	0,0602	0,00078	593,4	6,7	589,4	5,7	603	28	98
A_337.FIN2	369,1	386,9	0,408019507	-10000	0,802	0,016	0,0964	0,0011	0,68189	0,05993	0,00093	597	8,7	593,2	6,5	590	34	101
A_353.FIN2	137,9	280,1	0,762146483	290	0,852	0,022	0,0971	0,0012	0,19235	0,0638	0,0017	624	12	597,3	7,1	713	57	84
A_363.FIN2	110,6	57,5	0,196835443	20	0,814	0,021	0,098	0,0011	0,26199	0,0608	0,0016	605	12	602,7	6,5	600	56	100
A_304.FIN2	331	603	0,737160121	840	0,846	0,025	0,0982	0,0018	0,81575	0,0622	0,0011	620	14	604	11	670	39	90
A_320.FIN2	531	757	0,529943503	1100	0,835	0,013	0,0996	0,0011	0,66854	0,0606	0,00069	615,6	6,9	611,7	6,5	618	25	99
A_339.FIN2	151,4	65,9	0,166116248	1800	0,869	0,024	0,1016	0,0013	0,39553	0,0619	0,0016	633	13	623,5	7,6	646	58	97
A_393.FIN2	98,1	283	1,094801223	120	0,88	0,017	0,10165	0,00093	0,10104	0,0633	0,0013	640,2	9,3	624	5,5	693	46	90
A_303.FIN2	662	385,9	0,184592145	1100	0,824	0,026	0,1027	0,001	0,43307	0,058	0,0016	611	14	630,3	6	583	46	108
A_335.FIN2	510	300,4	0,215490196	600	0,826	0,032	0,10419	0,00094	0,43295	0,0569	0,0021	604	19	638,8	5,5	642	52	100
A_371.FIN2	471	144,6	0,112738854	720	0,894	0,011	0,1052	0,0011	0,44218	0,06194	0,0007	647,6	5,8	644,7	6,2	666	24	97
A_313.FIN2	69,7	173,6	0,909612626	450	0,934	0,028	0,1064	0,0014	0,10271	0,0636	0,002	666	15	651,7	8,2	686	69	95
A_360.FIN2	482	688	0,504149378	530	0,871	0,031	0,1084	0,0018	0,6555	0,0582	0,0018	634	17	664	10	648	47	102
A_314.FIN2	572	940	0,505244755	2500	1,009	0,03	0,1107	0,0024	0,86467	0,0657	0,0011	706	16	676	14	789	35	86
A_381.FIN2	211,2	339,5	0,562973485	810	1,022	0,02	0,1122	0,0014	0,44053	0,0664	0,0013	714	10	685,3	7,9	813	38	84
A_298.FIN2	229,2	346	0,496073298	460	1,003	0,021	0,1127	0,0015	0,55991	0,0646	0,0011	705	11	688,4	8,4	745	38	92
A_372.FIN2	101,3	133,4	0,426456071	320	0,982	0,023	0,1142	0,0013	0,28958	0,0631	0,0015	694	12	697,2	7,6	682	50	102
A_373.FIN2	189	198	0,362962963	470	1,062	0,027	0,1211	0,0022	0,59529	0,0642	0,0013	733	13	737	13	739	44	100
A_301.FIN2	435	873	0,590804598	1200	1,217	0,016	0,1246	0,001	0,15368	0,0701	0,00093	808,1	7,1	756,6	5,9	927	28	82
A_380.FIN2	320	346,1	0,331875	980	1,147	0,022	0,1281	0,0014	0,5999	0,06541	0,00098	774	10	776,7	8	778	32	100
A_378.FIN2	340,1	168,7	0,149661864	3200	1,216	0,027	0,1331	0,002	0,83178	0,06682	0,00097	809	13	805	11	827	30	97
A_344.FIN2	133,2	241,4	0,491741742	-1400	1,359	0,023	0,1407	0,0015	0,37126	0,0701	0,001	870,7	9,9	848,6	8,5	923	30	92
A_349.FIN2	220	600	0,600909091	630	1,492	0,024	0,1436	0,0012	0,13448	0,0749	0,0013	925	9,6	864,6	6,9	1055	35	82
A_307.FIN2	339	511	0,310914454	680	1,34	0,055	0,144	0,0023	0,54392	0,0669	0,0024	854	24	867	13	875	63	99
A_324.FIN2	213,1	297,7	0,296105115	740	1,249	0,079	0,1463	0,0017	0,46542	0,0616	0,0034	811	35	880	9,4	843	86	104
A_356.FIN2	208	154,6	0,163461538	760	1,406	0,076	0,1483	0,0027	0,39346	0,0677	0,0035	881	33	891	15	991	68	90
A_355.FIN2	284,1	334	0,199577614	670	1,339	0,059	0,1493	0,0021	0,29703	0,0648	0,0027	855	26	896	12	838	68	107
A_351.FIN2	403	1237	0,808933002	1610	1,482	0,037	0,1523	0,0017	0,48791	0,0703	0,0015	919	15	913,4	9,5	932	43	98
A_292.FIN2	660,8	1898	0,558414044	286	1,624	0,048	0,1524	0,0019	0,5114	0,0769	0,002	974	19	914	10	1119	49	82
A_334.FIN2	543	1502	0,747697974	1300	1,506	0,037	0,1524	0,0021	0,55678	0,0719	0,0015	931	16	914	11	960	43	95
A_350.FIN2	174	475	0,637931034	650	1,25	0,12	0,1554	0,0025	0,74159	0,0569	0,0057	854	45	931	14	890	87	105
A_310.FIN2	204,9	274	0,327476818	2400	1,574	0,032	0,156	0,0022	0,85489	0,07273	0,00098	956	12	934	12	995	27	94
A_370.FIN2	308,2	578	0,418559377	200	1,595	0,026	0,1585	0,0017	0,46886	0,0736	0,0011	967	10	948	9,4	1024	29	93
A_299.FIN2	128,6	263	0,522550544	260	1,665	0,043	0,1593	0,0029	0,68872	0,0754	0,0014	989	17	952	16	1065	37	89
A_386.FIN2	243	451	0,419753086	410	1,813	0,047	0,1757	0,0032	0,78216	0,0749	0,0011	1047	17	1043	18	1059	30	98
A_382.FIN2	368	517	0,317119565	200	1,829	0,023	0,177	0,0017	0,61671	0,07537	0,00074	1054,7	8,2	1050,4	9,1	1081	19	97
A_384.FIN2	337	588	0,390207715	1600	1,982	0,052	0,1772	0,0029	0,905	0,0811	0,0011	1102	18	1051	16	1213	29	87
A_394.FIN2	45,8	78,9	0,377947598	210	1,893	0,05	0,1774	0,0017	0,48687	0,0777	0,002	1072	18	1052,5	9,5	1110	52	95
A_302.FIN2	249	608	0,517269076	1770	1,905	0,024	0,1781	0,0015	0,47732	0,07725	0,00087	1081,5	8,5	1056,6	8,5	1121	23	94
A_296.FIN2	396	724	0,388383838	500	1,86	0,021	0,1786	0,0018	0,74294	0,07543	0,00063	1065,7	7,4	1058,9	9,6	1075	17	99
A_338.FIN2	364	308	0,181593407	12200	1,909	0,022	0,1797	0,0016	0,60821	0,07646	0,00072	1082,8	7,6	1065,1	8,8	1106	19	96
A_364.FIN2	125,9	439,5	0,769658459	360	1,85	0,039	0,1799	0,0019	0,28138	0,0751	0,0016	1065	14	1066	10	1062	43	100
A_305.FIN2	245,2	582	0,503262643	1240	1,905	0,023	0,1802	0,0019	0,57237	0,07642	0,00079	1081,4	8,1	1068	10	1100	21	97
A_390.FIN2	534,9	942	0,396709665	1700	1,902	0,025	0,1811	0,002	0,62975	0,07672	0,00082	1080,8	8,8	1073	11	1111	21	97
A_383.FIN2	236	510,6	0,476271186	820	1,874	0,025	0,1817	0,0019	0,50738	0,0756	0,00095	1072,1	9,2	1076	11	1078	25	100
A_361.FIN2	238	833	0,521848739	1140	2,95	0,14	0,2227	0,0067	0,79488	0,0962	0,0029	1384	36	1295	35	1543	54	84
A_391.FIN2	345,5	643	0,28683068	1100	2,87	0,1	0,2265	0,0047	0,67428	0,0923	0,0025	1368	28	1316	25	1470	48	90
A_300.FIN2	317	749	0,46214511	1170	2,921	0,082	0,2278	0,0038	0,80826	0,092	0,0017	1376	22	1322	20	1460	36	91
A_293.FIN2	100,5	690	0,951243781	620	4,11	0,11	0,2748	0,0058	0,89135	0,1078	0,0014	1643	23	1562	30	1753	24	89
A_345.FIN2	88,2	534	0,51814059	1500	11,87	0,2	0,4626	0,0071	0,87134	0,1851	0,0016	2594	16	2448	31	2696	14	91
A_358.FIN2	322,4	1454	0,381203474	5100	11,77	0,11	0,488	0,0045	0,69984	0,1754	0,0013	2584,9	8,7	2561	19	2608	12	98

Table 11: Grain (=71) distribution of sample Q3. The red box highlights the preferred ages used (<1500=Pb^{206}/U^{238}; ≥1500=Pb^{207}/U^{235}). Refer to the legend in Fig. 31.

88

Q4																		
				RATIOS								AGES [Ma]						Conc.
Analysis	U [ppm][a]	Pb [ppm][a]	Th/U[a]	206/204	^{207}Pb/^{235}U[b]	2 σ[d]	^{206}Pb/^{238}U[b]	2 σ[d]	rho[c]	^{207}Pb/^{206}Pb[e]	2 σ[d]	^{207}Pb/^{235}U	2 σ	^{206}Pb/^{238}U	2 σ	^{207}Pb/^{206}Pb	2 σ	%
A_079.FIN2	74	93,9	1,35	-41	0,262	0,018	0,03635	0,00069	0,009437	0,0525	0,0037	235	15	230,1	4,3	270	140	85
A_094.FIN2	952	583	0,637079832	-3100	0,2691	0,0061	0,03798	0,0005	0,43017	0,0521	0,0011	241,8	4,8	240,3	3,1	279	46	86
A_086.FIN2	123,9	191,8	1,594027441	-40	0,272	0,015	0,03869	0,00061	0,11104	0,0519	0,0029	243	12	244,7	3,8	250	110	98
A_066.FIN2	481	335	0,661122661	-790	0,277	0,0064	0,03884	0,00043	0,32694	0,0516	0,0011	247,9	5,1	245,6	2,6	260	47	94
A_018.FIN2	325,7	244,6	0,715689285	140	0,293	0,014	0,04088	0,00075	0,47944	0,0519	0,0021	261	11	258,3	4,7	267	90	97
A_032.FIN2	237,3	283	1,002949853	10	0,3064	0,0078	0,04262	0,00039	0,24886	0,0522	0,0013	270,6	6,1	269	2,4	278	53	97
A_108.FIN2	357	227	0,565826331	510	0,319	0,01	0,04369	0,00053	0,49738	0,0525	0,0016	279,9	7,9	275,6	3,2	284	63	97
A_053.FIN2	433,3	408,5	0,854373413	750	0,3172	0,0064	0,04375	0,00039	0,38573	0,05263	0,00099	279,3	5	276	2,4	301	42	92
A_076.FIN2	383	279	0,626631854	-240	0,319	0,018	0,044	0,0012	0,38229	0,0529	0,0028	280	14	277,6	7,6	310	110	90
A_046.FIN2	605	660	0,791735537	3000	0,3413	0,0073	0,04787	0,00046	0,19901	0,0515	0,001	297,8	5,5	301,4	2,8	259	47	116
A_051.FIN2	285	322	0,894736842	160	0,3421	0,0076	0,04817	0,00039	0,26254	0,0516	0,0011	298,7	5,9	303,3	2,4	258	47	118
A_016.FIN2	269,3	317	0,60527293	100	0,467	0,013	0,06139	0,00088	0,26775	0,0553	0,0017	388,3	9,3	384,1	5,3	400	66	96
A_060.FIN2	431	857	1,317865429	600	0,46	0,026	0,0621	0,0011	0,44416	0,0538	0,0027	384	18	388,1	6,9	350	110	111
A_068.FIN2	588	1792	1,724489796	-8900	0,586	0,023	0,0745	0,0018	0,12769	0,0576	0,0027	468	14	463	11	500	100	93
A_062.FIN2	214,8	114,7	0,304934823	-120	0,592	0,022	0,076	0,0014	0,23519	0,0566	0,0021	471	14	471,9	8,5	454	80	104
A_026.FIN2	246,7	382	0,774625051	-180	0,629	0,018	0,07605	0,00087	0,25165	0,0601	0,0017	494	11	472,5	5,2	583	63	81
A_080.FIN2	290	267	0,452068966	450	0,598	0,011	0,07647	0,00081	0,43963	0,05723	0,00094	474,7	7	474,9	4,8	483	37	98
A_010.FIN2	108,6	242	1,024861878	120	0,639	0,021	0,08032	0,00098	0,11119	0,0573	0,0019	500	13	498	5,9	468	72	106
A_022.FIN2	54,4	77,5	0,729779412	50	0,647	0,048	0,0808	0,0021	0,068099	0,0579	0,0049	504	29	501	13	480	190	104
A_111.FIN2	464,4	844	0,971576227	-900	0,661	0,028	0,0823	0,0033	0,20052	0,0578	0,003	515	17	510	19	510	110	100
A_006.FIN2	230	411	0,869565217	590	0,683	0,029	0,0844	0,0015	0,36904	0,0585	0,0023	527	18	522,5	8,7	525	89	100
A_109.FIN2	189,4	140,4	0,351636748	140	0,671	0,016	0,08468	0,00094	0,15225	0,0572	0,0015	520,6	9,7	523,9	5,6	479	57	109
A_082.FIN2	76,63	158,9	1,033537779	-20	0,683	0,032	0,0849	0,0017	0,075485	0,0592	0,003	526	19	525	10	530	110	99
A_093.FIN2	225,6	435	0,942375887	-360	0,675	0,017	0,085	0,0011	0,38508	0,0584	0,0014	523	10	525,6	6,4	531	52	99
A_017.FIN2	177,7	301,4	0,77771525	320	0,711	0,024	0,085	0,0012	0,21825	0,0605	0,0021	544	14	525,9	7	597	72	88
A_020.FIN2	146,7	237	0,764144513	-10	0,686	0,028	0,0851	0,0017	0,011526	0,0586	0,0026	529	17	526	10	530	100	99
A_019.FIN2	353,6	331,9	0,441176471	-70	0,687	0,018	0,0852	0,001	0,35256	0,0584	0,0014	530	11	527,3	6	531	53	99
A_012.FIN2	214	344	0,720093458	190	0,691	0,032	0,0854	0,002	0,35868	0,0585	0,0025	532	19	528	12	529	98	100
A_065.FIN2	280,1	311	0,524812567	610	0,684	0,03	0,0856	0,0019	0,29167	0,0584	0,0025	528	18	529	11	526	95	101
A_096.FIN2	259,6	355	0,615562404	-600	0,684	0,024	0,0855	0,0014	0,32887	0,0585	0,002	528	15	529	8,2	532	74	99
A_115.FIN2	274,4	180,1	0,305393586	-220	0,689	0,017	0,08562	0,00085	0,20763	0,0574	0,0014	531	10	529,5	5	491	54	108
A_074.FIN2	192,4	219,2	0,546777547	360	0,685	0,022	0,0859	0,0017	0,21106	0,0585	0,002	529	13	531	10	531	75	100
A_035.FIN2	1003	115,1	0,054735793	4300	0,7	0,024	0,0868	0,0023	0,38648	0,0589	0,002	538	14	537	14	558	73	96
A_049.FIN2	218,2	395	0,720439963	-580	0,719	0,016	0,0882	0,001	0,16336	0,0591	0,0013	548,6	9,7	545	6,1	550	50	99
A_101.FIN2	575	248	0,177913043	-270	0,729	0,038	0,0886	0,0037	0,90596	0,05912	0,00091	547	18	546	21	562	31	97
A_067.FIN2	221,5	23,5	0,042844244	340	0,727	0,02	0,0893	0,001	0,30177	0,0593	0,0016	553	12	551,5	6,2	553	59	100
A_013.FIN2	321,1	237	0,293366552	90	0,767	0,011	0,09408	0,00076	0,34309	0,05879	0,00083	577,2	6,5	579,5	4,5	546	31	106
A_095.FIN2	58,15	85,2	0,541702494	-30	0,769	0,054	0,0941	0,0026	0,23634	0,0598	0,0041	576	31	580	15	540	150	107
A_008.FIN2	318	111,9	0,136477987	720	0,822	0,018	0,0984	0,0015	0,44634	0,0604	0,0012	608	10	605,1	8,8	606	45	100
A_050.FIN2	469	770	0,667377399	1010	0,822	0,012	0,09902	0,00087	0,53672	0,06023	0,00074	608,1	6,8	608,6	5,1	606	26	100
A_075.FIN2	451	1003	0,864745011	-2000	0,841	0,015	0,0997	0,0011	0,39701	0,0616	0,001	618,9	8,3	612,6	6,3	653	37	94
A_059.FIN2	142,3	152,4	0,437104708	210	0,904	0,031	0,1021	0,0014	0,16959	0,0645	0,0022	652	16	626,5	8	734	73	85
A_041.FIN2	380	343	0,372368421	700	0,882	0,024	0,1023	0,0016	0,35118	0,0629	0,0016	641	13	627,7	9,2	696	56	90
A_103.FIN2	336,6	402	0,496732026	4000	0,93	0,03	0,108	0,0026	0,28215	0,0628	0,0022	667	16	661	15	691	77	96
A_047.FIN2	85,8	231,6	0,947552448	330	1,021	0,031	0,1094	0,0012	0,16129	0,0679	0,002	710	15	669	7,1	835	62	80
A_030.FIN2	241,2	326	0,497927032	1600	1,004	0,049	0,1156	0,0033	0,29589	0,0634	0,003	704	24	705	19	707	99	100
A_028.FIN2	185,2	167,2	0,287419006	200	1,053	0,043	0,1196	0,0025	0,096021	0,0642	0,0031	729	21	728	14	720	100	101
A_033.FIN2	183,2	95,3	0,163755459	-370	1,261	0,031	0,129	0,0019	0,50459	0,0716	0,0017	826	14	782	11	962	49	81
A_011.FIN2	350,4	530,3	0,412385845	220	1,278	0,02	0,1353	0,0012	0,58122	0,06794	0,00086	834,8	8,8	818	6,9	863	26	95
A_043.FIN2	123,7	55,5	0,102506063	550	1,4	0,024	0,1425	0,0012	0,3836	0,0712	0,0011	887	10	858,5	7	949	32	90
A_024.FIN2	129,6	380	0,68132716	-1400	1,499	0,074	0,1474	0,0019	0,83513	0,0735	0,0031	921	23	886	11	990	60	89
A_085.FIN2	344	280	0,208430233	-300	1,502	0,021	0,1542	0,0013	0,47501	0,0715	0,0009	930,1	8,6	924,3	7,2	965	25	96
A_009.FIN2	66,6	80,5	0,282582583	110	1,525	0,055	0,156	0,0025	0,12062	0,0708	0,0027	938	22	934	14	925	82	101
A_027.FIN2	252,9	399	0,375247133	-3000	1,506	0,036	0,156	0,0033	0,75095	0,0701	0,0014	931	14	934	18	930	40	100
A_044.FIN2	127,9	215	0,421422987	250	1,661	0,05	0,1626	0,0024	0,37156	0,0745	0,0021	992	19	971	13	1041	57	93
A_021.FIN2	697	867	0,27302726	2780	1,799	0,023	0,1647	0,0017	0,67247	0,07928	0,0008	1044,4	8,5	982,5	9,3	1176	20	84
A_014.FIN2	295,1	1092	0,739410369	1800	1,768	0,025	0,1699	0,0016	0,56666	0,07487	0,00087	1032,5	9,1	1011,3	9	1060	23	95
A_091.FIN2	150,3	210,8	0,358815702	-880	1,718	0,043	0,1703	0,0024	0,45848	0,0742	0,0016	1013	16	1014	13	1035	46	98
A_052.FIN2	137	965	1,591970803	1400	1,822	0,049	0,1711	0,0028	0,2696	0,0771	0,0022	1052	17	1018	15	1112	55	92
A_098.FIN2	380	317	0,214210526	-4500	1,753	0,041	0,1721	0,0025	0,60553	0,0746	0,0014	1027	15	1023	14	1054	37	97
A_045.FIN2	171,5	709	0,869387755	2000	1,746	0,051	0,1724	0,003	0,33381	0,0735	0,0021	1024	19	1025	17	1018	60	101
A_110.FIN2	192,2	350	0,415192508	-1400	1,785	0,059	0,1742	0,0042	0,1409	0,0735	0,0029	1039	22	1035	23	1019	78	102
A_054.FIN2	235,2	359,6	0,43537415	240	1,903	0,02	0,1785	0,0014	0,39242	0,07721	0,00083	1081,9	7	1058,5	7,6	1120	22	95
A_114.FIN2	276,9	1608	1,40122788	1500	1,917	0,047	0,183	0,0036	0,31717	0,0755	0,0021	1086	16	1083	19	1074	55	101
A_025.FIN2	222	1390	1,234234234	1000	2,075	0,043	0,1853	0,0028	0,81645	0,0812	0,001	1141	14	1095	15	1220	26	90
A_064.FIN2	154,7	409,9	0,548804137	-1600	2,047	0,033	0,1913	0,0018	0,2865	0,078	0,0013	1129	11	1128,2	9,9	1135	33	99
A_058.FIN2	245	535	0,47877551	500	2,186	0,066	0,2004	0,0034	0,58443	0,0795	0,0021	1175	21	1177	19	1178	52	100
A_112.FIN2	81,1	113,6	0,30702836	-90	2,213	0,082	0,2005	0,0029	0,019246	0,0792	0,0032	1182	26	1178	16	1156	81	102
A_031.FIN2	65,39	247	0,73895091	-610	2,41	0,14	0,212	0,0059	0,30752	0,0829	0,0046	1241	42	1239	31	1250	110	99
A_088.FIN2	155,5	1031	1,27073955	220	2,44	0,042	0,2144	0,0022	0,50288	0,0837	0,0012	1253	12	1252	11	1284	28	98
A_089.FIN2	217,4	710	0,685372585	-4700	2,61	0,052	0,2156	0,0031	0,70509	0,0891	0,0012	1302	14	1258	16	1403	26	90
A_061.FIN2	350,6	1480	0,634341129	-100	3,449	0,044	0,2427	0,0026	0,68469	0,1031	0,00097	1514	10	1400	13	1681	18	83
A_099.FIN2	60,3	367	0,991708126	-20	3,096	0,05	0,2487	0,0022	0,27146	0,0908	0,0014	1431	13	1432	11	1432	31	100
A_083.FIN2	111	326	0,497297297	-1300	3,41	0,19	0,2623	0,0089	0,79734	0,0953	0,0032	1499	42	1500	45	1524	63	98
A_087.FIN2	96,5	687	0,985492228	-350	4,105	0,052	0,2933	0,0027	0,46317	0,1029	0,0012	1654	10	1659	14	1673	21	99
A_078.FIN2	92,9	2440	3,390742734	-770	5,295	0,067	0,3312	0,0033	0,57646	0,1171	0,0012	1867	11	1843	16	1908	19	97
A_055.FIN2	108	712	0,730555556	40000	6,136	0,069	0,3657	0,0028	0,49022	0,1215	0,0012	1994,6	9,6	2009	13	1977	18	102
A_015.FIN2	200,4	983	0,420658683	1260	12,36	0,15	0,4826	0,0062	0,80203	0,1851	0,0015	2631	12	2537	27	2698	13	94
A_048.FIN2	128,1	1247	0,663544106	900	27,51	0,26	0,6506	0,0064	0,60242	0,3071	0,0026	3400,9	9,4	3230	25	3507	13	92

Table 12: Grain (=78) distribution of sample Q4. The red box highlights the preferred ages used (<1500=Pb^{206}/U^{238}; ≥1500=Pb^{207}/U^{235}). Refer to the legend in Fig. 31.

89

4.3.1.6   Q4

Sample Q4 represents the lower portion of the uEF lithologies exposed in Quthing. This sample comprises of seventy-eight (78) concordant grains of which 5.1% (=4) have metamorphic internal and external structures (Table 12). The concordant grains range in lengths from 36.0 to 265.0 µm, with the majority (60%) of grains being 100.0 ±20 µm. 29.5% of the total concordant grains belong to one of five (5) populations. The most abundant population occurs in the Cambrian, 522.5-529.5 Ma, comprising of 14.1% (n=11) of the total concordant population. Minor populations (n=3) include the Triassic (240.3-245.6 Ma), Permian (275.6-277.6 Ma), Silurian and Ordovician (471.9-474.9 Ma) and Mesoproterozoic (1011.3-1018.0 Ma). The concordant grain Th/U ratios (<1) shows that two of the four previously mentioned metamorphic grains have typical metamorphic signature grains. The increased number of metamorphic grain morphologies could be a likely result of core fragmenting of magmatic grains or the rarer instance of higher grade metamorphic grains with a Th/U>1. The youngest grain determination resulted in: 1) YSG= 230.1 ±4.3 Ma; 2) YDZ= 230.6 ±8.3 (-10) Ma; 3) TuffZirc (8) = 525.8 ±1.6 Ma; 4) YC2σ (3)= 276.0 ±4.8 Ma; 5) Weighted Average (8)= 525.4 ±2.6 Ma; 6) YPP= 280.0 Ma and; 7) YC1σ (3)= 276.0 ±3.6 Ma. The collective mean of the YSG, YDZ, YPP, YC2σ and YC1σ ages in Q4 resulted in an average youngest maximum depositional age of 258.5 Ma.

4.3.1.7   Map6

Sample Map6 represents the basal section of the Clarens Formation in Maphutseng. This sample comprises of eighty-nine (89) concordant grains, of which 100% (n=89) are magmatic, oscillatory zoned grains and fragments (Table 13). The grains range in lengths from 50.0 to 255.0 µm, with the majority (60%) of grains falling between 120.0-150.0 µm. This sample is dominated by various populations (9), where 39.3% of the total concordant grains do not belong to any population. The most abundant population is the Neoproterozoic, 545.2-555.0 Ma, which comprises of 12.4% (n=11) of the total concordant grains. More minor populations include the, Jurassic-Triassic at 198.0-204.7 Ma (n=4), Triassic-Permian at 252.2-266.3 Ma (n=9), Early Permian at 283.0-286.7 Ma (n=5), Silurian

and Ordovician at 470.7-479.2 Ma (n=3), Cambrian at 525.8-534.1 Ma (n=8), Early Neoproterozoic at 571.5-599.0 Ma (n=8), Mid-Neoproterozoic at 871.1-878.0 Ma (n=3) and Late Neoproterozoic at 994.0-1000.0 Ma (n=3). The lack of Thu/U<0.1 proves that there are no metamorphic grains within this sample. The youngest grain determination resulted in: 1) YSG= 198.0 ±2.6 Ma; 2) YDZ= 197.0 ±4.4 (-5.1) Ma; 3) TuffZirc (8) = 256.6 ±4.9 Ma; 4) YC2σ (3)= 199.7 ±3.8 Ma; 5) Weighted Average (8)= 526.9 ±3.1 Ma; 6) YPP= 200.0 Ma and; 7) YC1σ (3)= 199.7 ±2.7 Ma. The collective mean of the more abundant younger grain source input dominated Map6 (using YSG, YDZ, YPP, YC2σ and YC1σ ages) resulted in an average youngest maximum depositional age of 198.9 Ma.

4.3.1.8   Map5

Sample Map5 represents the midway point lithologies of the uEF of Maphutseng. This sample comprises of sixty-six (66) concordant grains, of which 1.5% (n=1) has a metamorphic morphology, confirmed by the single Th/U ratio <1 (Table 14). The grain sizes vary from 46.0 to 200.0 μm, with the majority (50.4%) of grains occurring 100.0 ±10 μm. The concordant grains make a total of two populations, excluding 65.2% of the total concordant grains. The most abundant population occurs in the Cambrian-Neoproterozoic, 529.8-565.5 Ma, comprising of 24.2% (n=16) of the total concordant grains. The Late Cambrian population, 480.4-493.9 Ma, comprises of a more minor 10.6% (n=7) of the overall population. The youngest grain determination resulted in: 1) YSG= 238.7 ±3.3 Ma; 2) YDZ= 238.8 ±7.4 (-7.5) Ma; 3) TuffZirc (8)= 487.7 ±6.5 Ma; 4) YC2σ (3)= 482.6 ±7.6 Ma; 5) Weighted Average (8)= 488.1 ±5.2 Ma; 6) YPP= 300.0 Ma and; 7) YC1σ (3)= 482.6 ±6.0 Ma. The collective mean of the YSG, YDZ and YPP ages in Map5 resulted in an average youngest maximum depositional age of 258.7 Ma.

					RATIOS								AGES [Ma]					Conc.
Analysis	U [ppm]a	Pb [ppm]a	Th/Ua	206/204	207Pb/235Ub	2 σd	206Pb/238Ub	2 σd	rhoc	207Pb/206Pbe	2 σd	207Pb/235U	2 σ	206Pb/238U	2 σ	207Pb/206Pb	2 σ	%
A_006.FIN2	203,5	222	1,292383292	-790	0,2196	0,0076	0,03115	0,00041	0,31825	0,051	0,0017	200,9	6,3	198	2,6	224	67	88
A_008.FIN2	183	223	1,349726776	-110	0,221	0,01	0,03153	0,00048	0,040923	0,0506	0,0024	202,1	8,5	200,1	3	216	98	93
A_009.FIN2	539	345	0,825602968	-1300	0,219	0,0074	0,03169	0,0004	0,31713	0,0501	0,0016	200,7	6,2	201,1	2,5	191	68	105
A_010.FIN2	328,2	230	0,804692261	-100	0,2289	0,0069	0,03227	0,00037	0,15602	0,0514	0,0015	208,8	5,7	204,7	2,3	243	63	84
A_013.FIN2	149,5	159	1,016722408	-900	0,273	0,017	0,03803	0,00071	0,024599	0,0522	0,0033	243	13	240,6	4,4	260	120	93
A_014.FIN2	93,6	115,6	1,176282051	-15	0,291	0,016	0,0399	0,00055	0,13187	0,053	0,0029	257	13	252,2	3,4	290	110	87
A_015.FIN2	523,7	406,4	0,746419706	380	0,2849	0,008	0,04031	0,00047	0,21537	0,0512	0,0014	254,1	6,3	254,7	2,9	237	59	107
A_016.FIN2	210,4	231,4	1,008079848	-100	0,2833	0,009	0,04035	0,00047	0,38023	0,0508	0,0015	252,6	7,1	255	2,9	229	63	111
A_017.FIN2	368	272,8	0,738586957	-1100	0,288	0,01	0,04046	0,00047	0,23043	0,0519	0,0019	257,6	8,4	255,7	2,9	260	75	98
A_020.FIN2	411	707	1,666666667	150	0,2925	0,0078	0,04075	0,00044	0,32901	0,0519	0,0013	260	6,1	257,4	2,7	270	54	95
A_021.FIN2	104,1	160,9	1,452449568	-60	0,296	0,015	0,04099	0,00056	0,063191	0,0529	0,0028	261	12	259	3,5	270	100	96
A_022.FIN2	1086	177,7	0,160865562	-2700	0,2938	0,0071	0,04138	0,00061	0,42019	0,0515	0,0011	261,3	5,5	261,4	3,8	253	50	103
A_023.FIN2	393,3	362	0,903381643	-170	0,299	0,011	0,04209	0,00069	0,2825	0,0516	0,0019	265,4	8,6	265,8	4,3	254	76	105
A_024.FIN2	313,1	194,2	0,555094219	10	0,3028	0,0074	0,04217	0,00039	0,12277	0,052	0,0013	268	5,7	266,3	2,4	275	53	97
A_025.FIN2	550	268	0,423636364	-290	0,3099	0,0059	0,04384	0,0004	0,048301	0,0514	0,0011	273,7	4,6	276,6	2,5	246	44	112
A_027.FIN2	781	533	0,614596671	-170	0,3335	0,0085	0,04489	0,00068	0,21949	0,0539	0,0014	291,9	6,5	283	4,2	352	59	80
A_028.FIN2	301,8	208,7	0,586149768	-10	0,329	0,011	0,04502	0,00063	0,33493	0,0527	0,0016	287,9	8,2	283,8	3,9	306	66	93
A_029.FIN2	549	960	1,555555556	1060	0,327	0,007	0,04512	0,00045	0,5451	0,0526	0,0011	286,9	5,4	284,5	2,8	297	47	96
A_030.FIN2	98,6	57,1	0,463488844	1110	0,331	0,011	0,04548	0,00058	0,018461	0,0532	0,002	290,2	9,1	286,6	3,6	300	76	96
A_031.FIN2	230,3	148,4	0,554059922	-290	0,325	0,014	0,04548	0,00071	0,53623	0,052	0,0021	285	10	286,7	4,4	268	86	107
A_033.FIN2	466,9	458,6	0,639751553	-1110	0,4246	0,0088	0,05693	0,00057	0,35518	0,0541	0,001	358,7	6,3	356,9	3,5	360	43	99
A_034.FIN2	363,7	562	0,888094583	-1500	0,4992	0,0092	0,06518	0,00062	0,36959	0,05556	0,00097	411,1	6,1	407	3,8	417	38	98
A_035.FIN2	107,2	253	1,296641791	90	0,516	0,014	0,06825	0,00073	0,046206	0,0548	0,0016	420,5	9,6	425,6	4,4	381	61	112
A_040.FIN2	187	186,8	0,548663102	5500	0,525	0,013	0,06841	0,00077	0,13761	0,0557	0,0014	427,1	8,7	426,5	4,6	420	56	102
A_041.FIN2	227,6	1343	3,09314587	-980	0,58	0,012	0,07327	0,00062	0,36176	0,0575	0,0012	464	7,5	455,8	3,7	491	45	93
A_042.FIN2	92,8	325,9	1,814655172	1460	0,576	0,019	0,07393	0,00084	0,36197	0,0568	0,0019	461	12	459,7	5	444	70	104
A_043.FIN2	141,6	548	2,127824859	170	0,594	0,026	0,0758	0,0012	0,18587	0,0569	0,0025	475	17	470,7	7	470	97	100
A_044.FIN2	289,9	557	0,92238703	-50	0,601	0,011	0,07648	0,00068	0,20903	0,0571	0,001	477	6,7	475,1	4,1	479	40	99
A_045.FIN2	296,6	67,6	0,10687795	-6900	0,602	0,011	0,07718	0,00068	0,339	0,0565	0,001	477,2	6,8	479,2	4,1	456	38	105
A_046.FIN2	123,9	137,1	0,596448749	80	0,617	0,037	0,0783	0,0015	0,041597	0,0565	0,0032	485	23	486	9,1	460	120	106
A_047.FIN2	65,7	149,4	1,095890411	-120	0,671	0,023	0,0801	0,001	0,13617	0,0608	0,0021	519	14	496,4	6,2	587	73	85
A_048.FIN2	82,4	125,4	0,705097087	-110	0,679	0,024	0,0842	0,0011	0,15803	0,0585	0,0021	523	15	521,3	6,7	508	77	103
A_049.FIN2	113,9	319,4	1,244073749	-490	0,691	0,03	0,085	0,0013	0,1288	0,059	0,0026	531	18	525,8	7,6	526	93	100
A_051.FIN2	101,8	162,2	0,68762279	290	0,677	0,022	0,0851	0,0011	0,25053	0,0582	0,002	525	14	526,2	6,8	502	73	105
A_052.FIN2	105,9	191	0,799811143	-2200	0,689	0,022	0,0852	0,001	0,020419	0,0584	0,002	530	14	526,9	6	514	75	103
A_053.FIN2	297,4	1004	1,442501681	560	0,718	0,018	0,08531	0,0009	0,47472	0,061	0,0013	548	10	527,6	5,3	618	46	85
A_054.FIN2	166,8	291	0,760191847	-220	0,686	0,016	0,08571	0,00087	0,19396	0,0581	0,0014	530	9,7	530,1	5,1	512	52	104
A_055.FIN2	320,8	222	0,286783042	160	0,686	0,011	0,08579	0,00083	0,39946	0,05799	0,00092	529,4	6,9	530,5	4,9	517	34	103
A_056.FIN2	171,9	216,3	0,580570099	-4600	0,689	0,02	0,0859	0,0011	0,14343	0,0584	0,0018	531	12	531	6,7	512	66	104
A_057.FIN2	205	330	0,770731707	-300	0,69	0,022	0,0864	0,0013	0,36637	0,058	0,0018	531	13	534,1	8	507	68	105
A_058.FIN2	308,2	195,1	0,285853342	-600	0,708	0,016	0,0883	0,0011	0,23247	0,0583	0,0013	543	9,3	545,2	6,7	527	50	103
A_059.FIN2	159,3	266	0,716258632	-100	0,727	0,02	0,0888	0,001	0,34893	0,0597	0,0016	553	12	548,4	6,2	568	58	97
A_061.FIN2	107,4	132,9	0,531657356	-8700	0,716	0,026	0,0889	0,0012	0,17842	0,0585	0,0021	545	16	548,6	6,9	512	81	107
A_063.FIN2	275,7	200,3	0,318462096	-290	0,744	0,017	0,08885	0,00096	0,26313	0,0608	0,0014	564	10	548,7	5,7	615	50	89
A_064.FIN2	137,1	105,5	0,33654267	-2300	0,723	0,02	0,0891	0,0011	0,12352	0,059	0,0017	550	12	550,1	6,2	535	62	103
A_065.FIN2	158,1	248,8	0,663504111	50	0,724	0,014	0,08924	0,0008	0,28474	0,0588	0,0011	551,7	8,3	551	4,7	536	42	103
A_066.FIN2	120,9	151	0,569065343	-400	0,727	0,029	0,0893	0,0018	0,46814	0,059	0,0021	552	17	551	11	531	78	104
A_067.FIN2	147,2	189	0,508831522	20	0,729	0,016	0,0894	0,00091	0,40236	0,0592	0,0012	554,3	9,1	551,9	5,4	551	43	100
A_068.FIN2	70,1	88,5	0,591298146	-50	0,726	0,046	0,0898	0,0017	0,10415	0,0582	0,0039	550	27	554	10	480	140	115
A_069.FIN2	138,2	144,8	0,448625181	50	0,73	0,015	0,08984	0,0008	0,31378	0,0588	0,0013	555	8,9	554,5	4,7	537		103
A_075.FIN2	256,6	222,7	0,37451286	-200	0,739	0,013	0,08991	0,00087	0,25718	0,0593	0,0011	560,7	7,8	555	5,2	576	39	96
A_076.FIN2	55,2	118,7	0,879710145	-1900	0,732	0,035	0,0899	0,0017	0,24878	0,0592	0,0028	553	20	555	9,9	540	100	103
A_077.FIN2	213,7	315,6	0,572297613	-210	0,798	0,014	0,09188	0,00082	0,33185	0,0628	0,0011	594,1	8	566,6	4,8	693	36	82
A_078.FIN2	202,9	236,9	0,471660917	-720	0,753	0,013	0,09242	0,00077	0,36346	0,05895	0,00094	569,3	7,4	569,8	4,5	555	35	103
A_079.FIN2	65,3	152,6	0,987748851	-180	0,756	0,033	0,0927	0,0016	0,10022	0,0593	0,0027	568	19	571,5	9,6	526	95	109
A_080.FIN2	53	50	0,39245283	-270	0,769	0,031	0,0929	0,0012	0,1202	0,0602	0,0024	574	18	572,6	6,9	545	85	105
A_081.FIN2	467	359,9	0,318415418	-2600	0,7604	0,0093	0,09386	0,00073	0,36051	0,05891	0,00071	573,6	5,4	578,3	4,3	554	26	104
A_082.FIN2	112,8	191,9	0,711879433	0	0,78	0,022	0,0955	0,0012	0,22552	0,0592	0,0017	584	13	587,6	6,8	545	62	108
A_083.FIN2	239,6	885	1,512103506	-710	0,837	0,019	0,0958	0,0012	0,19999	0,0635	0,0015	616	11	589,5	6,8	713	48	83
A_084.FIN2	364,7	250,4	0,284069098	-8100	0,797	0,017	0,0961	0,0014	0,65469	0,06003	0,00096	593,8	9,6	591,6	8,3	601	33	98
A_085.FIN2	33,01	74,1	0,908512572	-54	0,858	0,05	0,0971	0,0019	0,005269	0,0643	0,0038	621	27	597	11	670	130	89
A_086.FIN2	5,71	20,9	1,309982487	-11	0,89	0,13	0,0974	0,0039	0,063845	0,069	0,01	603	72	599	23	570	290	105
A_087.FIN2	57,4	149,7	0,926829268	-80	0,929	0,03	0,104	0,0015	0,21888	0,0648	0,0021	664	16	637,7	8,8	719	68	89
A_088.FIN2	357,9	981	0,935736239	140	0,963	0,012	0,11281	0,00085	0,37883	0,06197	0,00075	684,4	6,2	689	4,9	666	26	103
A_090.FIN2	301	380	0,453488372	620	1,02	0,031	0,1168	0,0017	0,15577	0,0635	0,0019	713	15	712,1	9,6	711	65	100
A_092.FIN2	121,9	219,9	0,582444627	-150	1,215	0,036	0,1335	0,002	0,15538	0,0662	0,002	806	16	807	11	806	62	100
A_093.FIN2	23,86	157,2	1,703688181	36	1,4	0,072	0,1429	0,0025	0,084133	0,0707	0,0036	877	30	861	14	870	110	99
A_094.FIN2	504	595	0,305753968	-70000	1,385	0,026	0,1438	0,0021	0,50012	0,0699	0,0012	882	11	866	12	920	35	94
A_095.FIN2	154,6	361,8	0,586675291	550	1,507	0,029	0,1447	0,0016	0,3099	0,0756	0,0015	933	12	871,1	8,8	1068	39	82
A_096.FIN2	215,9	581	0,649837888	970	1,501	0,024	0,1448	0,0016	0,4515	0,0751	0,0011	930	9,8	871,7	8,8	1067	30	82
A_097.FIN2	255,7	204,5	0,213570591	40	1,466	0,02	0,146	0,0013	0,52135	0,07273	0,00083	915,1	8,1	878	7,6	1001	24	88
A_098.FIN2	163,5	839	1,299082569	10600	1,426	0,035	0,1472	0,0022	0,46093	0,0703	0,0015	901	14	885	12	933	44	95
A_099.FIN2	494,1	1226	0,575996762	1160	1,584	0,024	0,1526	0,0018	0,49289	0,0752	0,0011	963,2	9,4	915,1	9,8	1070	28	86
A_101.FIN2	91,9	192,2	0,457018498	-1430	1,494	0,049	0,1546	0,0022	0,23293	0,0701	0,0023	924	20	926	12	903	68	103
A_102.FIN2	41,9	250	1,229116945	90	1,77	0,059	0,1668	0,0023	0,28101	0,0774	0,0026	1031	23	994	13	1102	66	90
A_108.FIN2	85,2	149,7	0,4342723	-480	1,753	0,042	0,1669	0,002	0,23253	0,0762	0,0018	1025	15	995	11	1080	49	92
A_109.FIN2	327	809	0,620795107	8500	1,684	0,043	0,1679	0,0024	0,4706	0,0728	0,0017	1001	16	1000	13	999	47	100
A_111.FIN2	162	454	0,595679012	-60	1,844	0,052	0,1706	0,0042	0,72217	0,0787	0,0015	1056	19	1014	23	1156	37	88
A_112.FIN2	486	456	0,214403292	-100	1,82	0,022	0,1726	0,0019	0,78472	0,07657	0,00057	1052,2	8,2	1026	10	1111	15	92
A_113.FIN2	78,7	186,3	0,579415502	-170	1,789	0,064	0,1751	0,0024	0,23118	0,0736	0,0024	1037	23	1040	13	1023	69	102
A_114.FIN2	164,7	235	0,315846995	-1600	1,912	0,03	0,1828	0,002	0,40045	0,076	0,0012	1084	11	1082	11	1089	31	99
A_116.FIN2	81,9	184	0,451159951	290	2,319	0,072	0,1988	0,0033	0,47423	0,0845	0,0023	1215	22	1168	18	1290	54	91
A_117.FIN2	425,5	869	0,406580494	-600	2,269	0,029	0,2005	0,002	0,456	0,08209	0,00099	1201,7	9,1	1178	10	1243	24	95
A_118.FIN2	273,3	598	0,429564581	540	2,219	0,031	0,2019	0,002	0,40471	0,0797	0,0011	1185,9	9,8	1187	11	1184	28	100
A_119.FIN2	183,3	398	0,343153301	-6300	2,76	0,041	0,2208	0,003	0,71616	0,09073	0,00098	1342	11	1285	16	1438	20	89
A_121.FIN2	231,6	938	0,679188256	-2700	3,158	0,053	0,2464	0,0026	0,41287	0,093	0,0013	1445	13	1420	13	1482	27	96
A_122.FIN2	223,3	967	0,665024631	-5200	3,142	0,04	0,2501	0,0024	0,55154	0,0908	0,001	1441,6	9,9	1439	12	1440	21	100
A_123.FIN2	103,4	463	0,564796905	-3400	5,212	0,071	0,3299	0,0036	0,58418	0,1147	0,0013	1852	12	1837	17	1872	20	98
A_125.FIN2	116	845	1,156896552	580	5,81	0,13	0,3361	0,0042	0,54104	0,126	0,0026	1944	20	1867	20	2034	36	92
A_126.FIN2	79,9	533	0,591989987	-600	12,77	0,21	0,4912	0,0077	0,74421	0,1887	0,0022	2664	17	2575	33	2733	18	94

Table 13: Grain (=89) distribution of sample Map6. The red box highlights the preferred ages used (<1500=Pb^{206}/U^{238}; ≥1500=Pb^{207}/U^{235}). Refer to the legend in Fig. 31.

Map5																		
				RATIOS									AGES [Ma]					Conc.
Analysis	U [ppm][a]	Pb [ppm][a]	Th/U[a]	206/204	^{207}Pb/^{235}U[b]	2 σ[d]	^{206}Pb/^{238}U[b]	2 σ[d]	rho[c]	^{207}Pb/^{206}Pb[e]	2 σ[d]	^{207}Pb/^{235}U	2 σ	^{206}Pb/^{238}U	2 σ	^{207}Pb/^{206}Pb	2 σ	%
A_303.FIN2	80,4	105,1	1,31840796	-139	0,266	0,012	0,03773	0,00052	0,076343	0,0514	0,0023	237,8	9,4	238,7	3,3	233	87	102
A_305.FIN2	371	264	0,67115903	-180	0,2929	0,0063	0,04098	0,00037	0,18163	0,052	0,0011	260,3	4,9	258,9	2,3	268	46	97
A_310.FIN2	245,2	222,1	0,771207178	-40	0,3286	0,0084	0,04429	0,00039	0,1756	0,0537	0,0013	287,6	6,4	279,4	2,4	339	54	82
A_312.FIN2	245,6	271,5	0,953175896	-580	0,332	0,0078	0,0452	0,00044	0,1256	0,0536	0,0013	290,3	6	285	2,7	329	53	87
A_313.FIN2	332	278,2	0,69246988	-10	0,3459	0,0075	0,04662	0,00039	0,20718	0,0538	0,0012	301,6	5,7	293,7	2,4	342	47	86
A_314.FIN2	188,3	155,8	0,651619756	-550	0,353	0,0098	0,04833	0,0005	0,27871	0,0529	0,0014	305,8	7,2	304,2	3,1	304	55	100
A_315.FIN2	339	209	0,338348083	1780	0,495	0,0094	0,06494	0,00056	0,23918	0,0553	0,001	407,5	6,4	405,5	3,4	410	42	99
A_316.FIN2	269	899	1,780669145	2100	0,58	0,012	0,0713	0,00058	0,23454	0,0588	0,0012	463	7,6	443,9	3,5	538	44	83
A_318.FIN2	355	553	0,814084507	-20	0,578	0,01	0,07355	0,00058	0,26676	0,05687	0,00097	462,1	6,6	457,5	3,5	472	38	97
A_319.FIN2	271	493	0,966420664	-580	0,589	0,01	0,07415	0,0006	0,13282	0,0577	0,001	469,3	6,5	461,1	3,6	499	39	92
A_320.FIN2	224	575	1,303571429	-120	0,592	0,011	0,07505	0,00065	0,41918	0,05717	0,00097	471,2	7	466,4	3,9	480	38	97
A_324.FIN2	146,9	309	0,891763104	-190	0,61	0,018	0,0774	0,001	0,14921	0,0573	0,0017	481	11	480,4	6	464	64	104
A_334.FIN2	122,2	133,4	0,546644845	3200	0,613	0,017	0,07761	0,00087	0,11451	0,0576	0,0016	484	10	481,8	5,2	477	58	101
A_340.FIN2	431	727	0,877030162	-720	0,6075	0,009	0,07797	0,00064	0,35313	0,05653	0,0008	481,3	5,7	483,9	3,8	460	32	105
A_346.FIN2	208	152,3	0,357692308	-890	0,621	0,016	0,07811	0,00075	0,31118	0,0577	0,0014	488,9	9,7	484,8	4,5	500	53	97
A_349.FIN2	250,6	140,1	0,266161213	-200	0,618	0,01	0,07899	0,00064	0,21667	0,05695	0,00095	487,7	6,4	490	3,8	472	37	104
A_350.FIN2	169	293	0,893491124	-160	0,629	0,018	0,0795	0,0011	0,58633	0,0574	0,0014	495	11	493,1	6,7	482	52	102
A_351.FIN2	187,4	278	0,706510139	-1120	0,654	0,014	0,07964	0,00069	0,20874	0,0596	0,0013	510,3	8,7	493,9	4,1	569	46	87
A_354.FIN2	64,9	116,5	0,796610169	-36	0,684	0,024	0,0811	0,0011	0,20845	0,0616	0,0021	526	15	502,6	6,8	599	74	84
A_355.FIN2	77,4	95,4	0,594315245	-21	0,696	0,022	0,0818	0,001	0,05611	0,062	0,002	533	13	506,9	6,1	618	71	82
A_356.FIN2	435,2	1018	1,082261029	20	0,6577	0,0097	0,08282	0,00061	0,32748	0,05771	0,00081	513,1	6,1	512,9	3,6	509	32	101
A_358.FIN2	212,6	183,8	0,372060207	-1450	0,687	0,013	0,08289	0,00075	0,25232	0,0602	0,0011	529,9	7,8	513,3	4,5	589	42	87
A_359.FIN2	135,9	163,5	0,550404709	-410	0,68	0,016	0,08568	0,00072	0,12028	0,0576	0,0014	524,9	9,9	529,8	4,3	488	53	109
A_360.FIN2	254,1	315,1	0,574970484	-10400	0,683	0,011	0,0857	0,00073	0,29774	0,05792	0,00095	527,5	6,9	530	4,3	509	37	104
A_361.FIN2	190,3	264	0,651077246	-480	0,685	0,013	0,08593	0,0007	0,26505	0,058	0,0011	529,3	7,7	531,4	4,1	514	41	103
A_362.FIN2	144,7	324,8	1,03593642	-80	0,694	0,016	0,08635	0,00077	0,051492	0,0583	0,0014	533,5	9,6	533,9	4,6	520	53	103
A_365.FIN2	212,3	266,7	0,506829958	-10	0,735	0,013	0,08652	0,00071	0,25294	0,0616	0,0011	559,3	7,7	534,8	4,2	643	39	83
A_367.FIN2	393	473	0,510941476	-400	0,7025	0,0096	0,08665	0,00067	0,38603	0,05885	0,00076	540,2	5,8	535,6	4	554	28	97
A_368.FIN2	148,2	307	0,9365722	-70	0,706	0,017	0,08677	0,00088	0,15041	0,0591	0,0014	540	10	536,3	5,2	536	53	100
A_369.FIN2	131,6	191	0,665653495	-380	0,725	0,018	0,08759	0,0009	0,2781	0,06	0,0015	551	10	541,2	5,4	575	54	94
A_371.FIN2	285,8	306	0,472358293	-610	0,734	0,012	0,08831	0,00074	0,49373	0,06012	0,00093	557,5	7,2	545,5	4,4	597	34	91
A_372.FIN2	262,4	197,8	0,30945122	-1070	0,732	0,013	0,08873	0,00078	0,35561	0,0601	0,0011	556,5	7,9	547,9	4,6	587	38	93
A_373.FIN2	184	42,4	0,081793478	-1720	0,751	0,015	0,08909	0,0012	0,29086	0,0612	0,0013	567	8,8	550,1	5,2	627	44	88
A_374.FIN2	81,8	125,3	0,652811736	-1230	0,738	0,019	0,0892	0,0012	0,21401	0,0603	0,0016	559	11	550,4	6,9	574	56	96
A_378.FIN2	255	413	0,694117647	-220	0,729	0,014	0,08926	0,00096	0,41567	0,0593	0,001	554,3	8,1	551	5,7	560	38	98
A_379.FIN2	113	215	0,82920354	-130	0,757	0,021	0,0908	0,0013	0,28312	0,0609	0,0017	569	12	560,3	7,6	595	58	94
A_381.FIN2	291	274,6	0,343642612	-120	0,794	0,015	0,0914	0,00077	0,16683	0,0629	0,0012	593,1	8,3	563,7	4,5	687	40	82
A_384.FIN2	110,7	509	1,973803071	-580	0,768	0,018	0,0917	0,00084	0,040738	0,061	0,0015	576	10	565,5	5	609	53	93
A_387.FIN2	254,5	313,8	0,525736739	-1800	0,786	0,014	0,09335	0,00086	0,22345	0,061	0,0011	587,5	8,1	575,3	5,1	629	39	91
A_388.FIN2	317,5	779	0,994330709	-1000	0,825	0,014	0,09757	0,00073	0,31272	0,06131	0,00099	609,5	7,8	600,1	4,3	637	35	94
A_389.FIN2	232,8	371,6	0,579037801	-210	0,891	0,015	0,1012	0,00092	0,21146	0,0639	0,0011	645,6	8,1	621,3	5,4	729	36	85
A_391.FIN2	415	1348	1,293975904	8100	0,853	0,011	0,10166	0,00081	0,33368	0,0612	0,00079	625,7	6,2	624	4,8	635	28	98
A_392.FIN2	141	629	1,673758865	180	0,893	0,018	0,1035	0,00095	0,17483	0,0628	0,0013	647,3	9,9	634,8	5,6	684	46	93
A_393.FIN2	46,57	169,9	1,381576122	-83	0,917	0,035	0,1048	0,0011	0,10771	0,064	0,0025	656	19	642,4	6,3	661	81	97
A_394.FIN2	389,3	442	0,259183149	-3400	1,11	0,021	0,1172	0,0017	0,77661	0,06862	0,00084	756	10	714,3	9,6	881	25	81
A_395.FIN2	477	470	0,312159329	150	1,171	0,014	0,12456	0,00098	0,49834	0,06828	0,00071	786	6,4	756,7	5,6	871	22	87
A_396.FIN2	310	427	0,319032258	-3000	1,487	0,023	0,1456	0,0013	0,22879	0,0739	0,0011	923,1	9,2	875,9	7,3	1032	31	85
A_397.FIN2	123	273,8	0,504065041	-80	1,582	0,029	0,1541	0,0017	0,44778	0,0747	0,0013	960	12	923,9	9,2	1048	34	88
A_398.FIN2	237,3	435	0,422671724	1390	1,602	0,023	0,155	0,0013	0,40372	0,07478	0,00098	969,5	8,9	928,6	7,3	1056	27	88
A_399.FIN2	124,19	174,6	0,329414607	-560	1,646	0,032	0,1575	0,0019	0,50257	0,0758	0,0013	986	12	942	11	1076	35	88
A_403.FIN2	380,2	1217	0,715938979	2400	1,665	0,022	0,1604	0,0016	0,69803	0,07517	0,00071	993,9	8,3	958,9	8,7	1068	19	90
A_404.FIN2	398	697,7	0,395477387	-7200	1,704	0,025	0,163	0,0019	0,76266	0,07582	0,0007	1008,1	9,3	973	10	1085	19	90
A_405.FIN2	406	340	0,199014778	-2900	1,687	0,02	0,165	0,0014	0,62666	0,07423	0,00069	1003,1	7,6	984,2	7,5	1047	19	94
A_406.FIN2	472	258	0,113347458	-3600	1,704	0,019	0,1665	0,0015	0,64492	0,07423	0,00065	1008,9	7,3	992,4	8,4	1045	17	95
A_407.FIN2	165,6	534	0,881642512	-1070	1,825	0,027	0,1708	0,0017	0,20396	0,0774	0,0013	1052,9	9,6	1016,3	9,1	1125	32	90
A_408.FIN2	204,5	1045	1,170660147	-1800	1,845	0,025	0,1709	0,0013	0,38751	0,0784	0,001	1059,9	9	1017,2	7,2	1148	26	89
A_409.FIN2	164,7	545	0,747419551	-50	1,8	0,025	0,1736	0,0013	0,38777	0,07513	0,00098	1043,6	9,2	1031,8	7,2	1065	26	97
A_413.FIN2	316	875	0,601265823	900	1,775	0,022	0,1739	0,0015	0,3344	0,07392	0,00094	1035,2	8,1	1033,6	8	1032	26	100
A_414.FIN2	383	1069	0,593994778	-2000	2,049	0,026	0,1756	0,0016	0,68859	0,08468	0,00077	1130,3	8,6	1042,7	8,8	1303	18	80
A_415.FIN2	356,6	650	0,421200224	-5000	1,836	0,019	0,1763	0,0013	0,51484	0,07557	0,0007	1057,3	6,9	1046,8	7,3	1081	18	97
A_416.FIN2	458	833	0,393449782	-6300	1,89	0,019	0,1804	0,0015	0,64617	0,07602	0,00061	1076,7	6,6	1068,7	8,1	1092	16	98
A_418.FIN2	580	1402	0,513793103	-20600	1,979	0,017	0,181	0,0014	0,52585	0,07945	0,00063	1107,5	5,8	1072,4	7,5	1182	16	91
A_420.FIN2	284,8	536,6	0,422752809	-1200	1,943	0,031	0,1833	0,0022	0,4769	0,077	0,0011	1095	11	1084	12	1115	30	97
A_422.FIN2	247,3	504	0,327537404	-3800	3,105	0,035	0,2444	0,0022	0,58545	0,09213	0,00078	1433,2	8,8	1409	11	1468	16	96
A_424.FIN2	301	1650	0,658139535	2400	6,052	0,061	0,332	0,0031	0,73687	0,13227	0,00095	1981,8	8,8	1847	15	2126	13	87
A_425.FIN2	135,8	1577	1,421207658	-22000	5,358	0,051	0,3373	0,0024	0,5021	0,11518	0,00095	1876,6	8,1	1873	12	1879	15	100
A_426.FIN2	66,7	1170	1,604197901	-1070	12,59	0,16	0,4903	0,005	0,60698	0,1862	0,0019	2647	12	2571	21	2705	17	95

Table 14: Grain (=66) distribution of sample Map5. The red box highlights the preferred ages used (<1500=Pb^{206}/U^{238}; ≥1500=Pb^{207}/U^{235}). Refer to the legend in Fig. 31.

93

4.3.1.9   Map4

Sample Map4 represents the contact between the uEF and lEF units in Maphutseng. The sample contains sixty-six (66) concordant grains, of which 7.6% (n=5) have metamorphic grain morphologies (Table 15). Grain sizes range from 60.0 to 295.0 µm, with a dominance (56.3%) in sizes between 150.0-200.0 µm. There are altogether seven (7) grain populations, hosting 34.8% of the total concordant grains. The remaining 65.2% do not belong to any grain populations. The populations include the: 1) Triassic, 212.6-217.7 Ma, hosting 4.5% of the overall grains (n=3); 2) Late Cambrian, 498.1-501.4 Ma, hosting 4.5% of the overall grains (n=3); 3) Early Cambrian, 523.0-528.2 Ma, hosting 6% of the overall grains (n=4); 4) Late Neoproterozoic, 550.8-559.4 Ma, hosting 6% of the overall grains (n=4); 5) Mid-Neoproterozoic, 679.1-683.0 Ma, hosting 4.5% of the overall grains (n=3); 6) Neo- to Mesoproterozoic, 1000.0-1005.0 Ma, hosting 4.5% of the overall grains (n=3); and, 6) Mesoproterozoic, 1040.3-1044.0 Ma, hosting 4.5% of the overall grains (n=3). The youngest grain determination resulted in: 1) YSG= 206.5 ±1.8 Ma; 2) YDZ= 206.5 ±3.9 (-4) Ma; 3) TuffZirc (8) = 1037.6 ±6.4 Ma; 4) YC2σ (3)= 499.4 ±7.6 Ma; 5) Weighted Average (8)= 1033.0 ±11 Ma; 6) YPP= 210.0 Ma and; 7) YC1σ (3)= 499.4 ±6.1 Ma. The collective mean of the YSG, YDZ and YPP ages in Map4 resulted in an average youngest maximum depositional age of 207.5 Ma.

4.3.1.10 Q5

Sample Q5 represents the midpoint of the upper section of uEF units in Quthing. This sample comprises of seventy-two (72) concordant grains, of which 5.6% (n=4) has metamorphic grain morphologies (Table 16). To further support the 5.6% presence of metamorphic grains, the Th/U ratio for all four grains all fall below 0.1 (<0.1). The grain sizes are limited to 32.0 to 204.0 µm, with the majority (63.2%) of grains concentrated between 120.0 ±20.0 µm. A total of five (5) populations are present in this sample, comprising of 30.6% of the total sample's grains. The most abundant population occurs in the Cambrian, 526.9-534.3 Ma, comprising of 12.5% (n=9) of the total grains. More minor populations include the, Triassic (203.6-209.9 Ma), Permian I (262.8-267.0 Ma), Permian II (274.0-276.4 Ma) and lastly the Early Neoproterozoic (993.0-998.2 Ma). The youngest grain

determination resulted in: 1) YSG= 203.6 ±2.2 Ma; 2) YDZ= 203.0 ±4.3 (-4.5) Ma; 3) TuffZirc (8) = 530.8 ±2.2 Ma; 4) YC2σ (3)= 265.0 ±4.5 Ma; 5) Weighted Average (8)= 530.4 ±1.8 Ma; 6) YPP= 200.0 Ma and; 7) YC1σ (3)= 265.0 ±3.4 Ma. The collective mean of the YSG, YDZ and YPP ages for Q5 resulted in an average youngest maximum depositional age of 202.2 Ma.

4.3.1.11 Map1

Sample Map1 was collected from the lowermost exposed unit of the lEF at Maphutseng. A total of fifty-nine (59) grains were concordant, of which 8.5% (n=5) has metamorphic external structures (Table 17). According to the Th/U ratios of the concordant grains, the selected five grains with metamorphic structures all have ratios <0.1 (Table 12). Grain sizes range from 20.0 to 210.0 μm, with the majority (66%) of grains being 100.0 ±20 μm. Core and rim spot analyses were dominated by rim (93.2%) selections, and very minor core selections (6.8%). Of the total concordant grain, 47.5% belong to various age-range populations. The most abundant population comprises of the Cambrian-Neoproterozoic at 27.1% (n=16) of the total concordant grains, falling within the 503.9-555.8 Ma age range. More minor populations include the Neoproterozoic I (625.0-632.1 Ma), Neoproterozoic II (712.0-717.3 Ma) and Neoproterozoic III (992.4-998.4 Ma). The youngest grain determination resulted in: 1) YSG= 216.7 ±1.4 Ma; 2) YDZ= 216.2 ±2.4 (-3) Ma; 3) TuffZirc (8) = 542.7 ±8.7 Ma; 4) YC2σ (3)= 506.0 ±7.0 Ma; 5) Weighted Average (8)= 537.2 ±5.3 Ma; 6) YPP= 225.0 Ma and; 7) YC1σ (3)= 506.0 ±6.0 Ma. The collective mean of the YSG, YDZ and YPP ages for Map1 resulted in an average youngest maximum depositional age of 219.3 Ma.

					RATIOS								AGES [Ma]					Conc.
Analysis	U [ppm]^a	Pb [ppm]^a	Th/U^a	206/204	^{207}Pb/^{235}U^b	2 σ^d	^{206}Pb/^{238}U^b	2 σ^d	rho^c	^{07}Pb/^{206}Pb	2 σ^d	^{207}Pb/^{235}U	2 σ	^{206}Pb/^{238}U	2 σ	^{207}Pb/^{206}Pb	2 σ	%
A_189.FIN2	542	394	0,817343	-160	0,2299	0,0046	0,03256	0,00028	0,2176	0,0513	0,0011	209,8	3,8	206,5	1,8	241	44	86
A_191.FIN2	567	292,8	0,576543	-610	0,2371	0,0044	0,03354	0,00028	0,12958	0,0512	0,001	215,7	3,7	212,6	1,7	238	43	89
A_192.FIN2	1162	665	0,69105	-1400	0,2386	0,0054	0,03354	0,00035	0,25724	0,0518	0,0011	217,8	4,2	212,7	2,2	265	46	80
A_193.FIN2	539	249,4	0,489425	160	0,2464	0,0047	0,03435	0,00026	0,30941	0,05192	0,00096	223,3	3,8	217,7	1,7	266	40	82
A_194.FIN2	305,5	206,8	0,66743	-690	0,2556	0,007	0,03603	0,0004	0,21415	0,0514	0,0014	231,3	5,5	228,2	2,5	244	58	94
A_197.FIN2	177,7	121,6	0,66179	40	0,265	0,0086	0,03695	0,00044	0,17824	0,0523	0,0017	237,9	6,9	233,9	2,7	269	68	87
A_199.FIN2	349	205,6	0,35702	-820	0,4889	0,0093	0,06339	0,00061	0,15122	0,0559	0,0011	403,5	6,4	396,2	3,7	433	46	92
A_200.FIN2	350,6	356	0,489732	-200	0,585	0,01	0,07444	0,00063	0,32083	0,0569	0,00093	466,9	6,4	462,8	3,8	472	36	98
A_201.FIN2	111,8	209	0,895349	-510	0,637	0,02	0,08025	0,00083	0,13924	0,0575	0,0018	499	13	498,1	5,1	473	68	105
A_202.FIN2	386	225,8	0,267358	260	0,639	0,011	0,08034	0,00074	0,35807	0,05763	0,00094	500,9	6,8	498,1	4,4	500	36	100
A_203.FIN2	364,4	404	0,525521	-1020	0,639	0,011	0,08088	0,0007	0,32152	0,05714	0,00093	500,8	6,7	501,4	4,2	484	37	104
A_204.FIN2	174,4	374,3	0,925459	-100	0,701	0,015	0,08453	0,00075	0,41306	0,0601	0,0012	538,9	9	523	4,4	589	46	89
A_210.FIN2	689	455,2	0,290131	-2700	0,6839	0,0088	0,08499	0,00067	0,47026	0,05822	0,00067	528,6	5,3	525,8	4	534	25	98
A_212.FIN2	555	82,8	0,062883	20	0,6874	0,0092	0,08519	0,00071	0,49075	0,05833	0,00065	531,3	5,4	527	4,2	537	24	98
A_214.FIN2	191,3	300,4	0,664924	680	0,692	0,016	0,0854	0,00094	0,21888	0,0587	0,0014	532,4	9,7	528,2	5,6	531	52	99
A_215.FIN2	74,4	109,6	0,607527	210	0,732	0,024	0,08922	0,00098	0,091415	0,0594	0,0019	554	14	550,8	5,8	534	70	103
A_216.FIN2	911	747	0,345554	-11000	0,7264	0,0073	0,08927	0,00068	0,56005	0,05891	0,00052	554	4,3	551,1	4	558	19	99
A_219.FIN2	127,3	546	1,838178	0	0,755	0,017	0,08963	0,00082	0,1424	0,0613	0,0014	572,1	9,8	553,3	4,9	624	51	89
A_220.FIN2	30,2	38,6	0,498675	-40	0,797	0,037	0,0907	0,0014	0,08891	0,0639	0,0031	586	21	559,4	8,5	660	100	85
A_223.FIN2	142,6	197,7	0,554488	-220	0,757	0,018	0,09193	0,0009	0,061031	0,0598	0,0015	571	10	566,8	5,3	565	54	100
A_225.FIN2	320,2	170,2	0,20534	-70	0,784	0,013	0,09215	0,00084	0,40697	0,06134	0,00094	587,6	7,3	568,2	5	644	33	88
A_226.FIN2	163,5	250,2	0,615902	-210	0,792	0,014	0,09544	0,0008	0,13541	0,0602	0,0011	590,7	8,2	587,5	4,7	585	42	100
A_228.FIN2	694	766	0,42219	-100	0,82	0,011	0,09701	0,00092	0,65001	0,06129	0,00063	607,1	6,3	596,8	5,4	645	22	93
A_229.FIN2	339	250,2	0,269322	-20	0,866	0,013	0,10112	0,00083	0,30839	0,06191	0,00089	632,2	7,1	620,9	4,9	665	31	93
A_230.FIN2	252,3	275,5	0,435593	20	0,865	0,014	0,1014	0,001	0,37578	0,06169	0,00095	632,5	7,6	622,7	5,8	652	34	96
A_231.FIN2	169	252,7	0,56568	1150	0,842	0,02	0,1026	0,0013	0,40974	0,0598	0,0013	621	11	629,2	7,9	579	47	109
A_233.FIN2	110,3	94,5	0,301904	-280	0,877	0,023	0,1033	0,001	0,36083	0,0611	0,0015	637	12	633,9	6	619	53	102
A_234.FIN2	222	250,2	0,399099	-70	0,872	0,015	0,10394	0,00099	0,42949	0,06066	0,00091	635,3	8,2	637,3	5,8	630	36	101
A_236.FIN2	129,3	168,4	0,458623	-470	0,896	0,024	0,1052	0,0012	0,31275	0,0615	0,0016	647	13	645	7,1	627	57	103
A_237.FIN2	459	754	0,593682	1400	0,906	0,011	0,10632	0,00082	0,42178	0,06176	0,00071	654,1	6	651,3	4,8	660	24	99
A_238.FIN2	743	128,1	0,06541	1900	0,993	0,025	0,1091	0,0018	0,92351	0,0656	0,0012	698	12	667	10	806	33	83
A_239.FIN2	93,5	137	0,497326	-370	1,014	0,029	0,1111	0,0016	0,34475	0,0659	0,0017	707	15	679,1	9,2	778	57	87
A_245.FIN2	411,3	649,3	0,521274	-690	0,95	0,012	0,11111	0,00089	0,51394	0,06196	0,00069	677,2	6,3	679,1	5,2	665	24	102
A_248.FIN2	313,7	662	0,721709	-680	0,981	0,015	0,1118	0,0012	0,46823	0,06359	0,00089	693,3	7,7	683	7	719	30	95
A_249.FIN2	233	206,4	0,284979	-360	1,007	0,019	0,1163	0,0013	0,48583	0,0628	0,001	706,6	9,5	708,9	7,7	688	35	103
A_250.FIN2	240,5	549	0,791268	-1300	1,153	0,026	0,1214	0,0012	0,42133	0,0687	0,0014	776	12	738,3	7	871	44	85
A_252.FIN2	176,9	400,3	0,685698	-1100	1,157	0,021	0,1236	0,0012	0,36236	0,068	0,0012	779	10	751,2	7,1	855	38	88
A_255.FIN2	258,8	651	0,757728	0	1,152	0,022	0,1254	0,0014	0,62011	0,06633	0,00094	776	10	761,2	7,9	804	30	95
A_257.FIN2	161,1	67	0,093731	-770	1,178	0,025	0,131	0,0017	0,60823	0,0653	0,0012	790	12	793,5	9,6	775	37	102
A_258.FIN2	254	936	0,755906	-780	1,432	0,03	0,1426	0,002	0,75094	0,0727	0,0012	900	12	859	11	1003	33	86
A_260.FIN2	185,5	127	0,145876	-390	1,368	0,022	0,1444	0,0014	0,58637	0,06836	0,00094	873,3	9,3	869,4	7,8	877	28	99
A_261.FIN2	231,4	321	0,286517	470	1,656	0,039	0,154	0,0016	0,32347	0,0776	0,0017	989	15	922,9	8,8	1125	43	82
A_266.FIN2	112	170	0,379464	-120	1,55	0,036	0,1549	0,0023	0,61931	0,0726	0,0013	949	15	928	13	984	37	94
A_267.FIN2	393	334,5	0,23028	300	1,591	0,02	0,1557	0,0017	0,55807	0,07413	0,00084	965,8	7,7	932,6	9,3	1040	23	90
A_268.FIN2	382	142,9	0,089267	-1600	1,626	0,02	0,1597	0,0013	0,59645	0,07357	0,00071	979,1	7,7	954,7	7	1026	20	93
A_270.FIN2	273	468	0,410989	-2000	1,683	0,023	0,1655	0,0015	0,60684	0,07367	0,0008	1000,7	8,7	986,9	8,4	1026	22	96
A_272.FIN2	653	881	0,312251	-4500	1,693	0,016	0,1668	0,0013	0,71805	0,0734	0,00048	1004,9	6	994,1	7,2	1024	13	97
A_273.FIN2	177,6	694	0,839527	130	1,886	0,03	0,1679	0,0024	0,38331	0,0817	0,0013	1074	10	1000	13	1226	32	82
A_276.FIN2	441	855	0,464853	-1800	1,703	0,021	0,1687	0,0017	0,62237	0,07299	0,00071	1008,5	8	1004,6	9,5	1011	20	99
A_277.FIN2	112	264,7	0,591964	140	1,862	0,037	0,1689	0,0029	0,50546	0,0804	0,0015	1064	13	1005	16	1188	37	85
A_278.FIN2	1181	216	0,043268	-400	1,787	0,026	0,171	0,0022	0,82845	0,0754	0,00066	1041,5	9,2	1018	12	1077	18	95
A_280.FIN2	235,6	152,1	0,143888	-720	1,789	0,022	0,1718	0,0014	0,41635	0,07533	0,0009	1041,5	8,1	1021,7	7,9	1077	24	95
A_281.FIN2	211,8	272,5	0,289896	-2800	1,796	0,024	0,1747	0,0015	0,56335	0,07444	0,00083	1042,1	9	1037,6	8,5	1048	23	99
A_282.FIN2	511	884	0,374951	-2500	1,837	0,018	0,1752	0,0013	0,60201	0,07593	0,00061	1057,9	6,4	1040,3	7,2	1090	16	95
A_285.FIN2	354	909	0,581921	-700	1,861	0,024	0,1754	0,0018	0,35308	0,0771	0,001	1066,5	8,7	1041,7	9,7	1119	26	93
A_286.FIN2	453	981	0,501104	-2700	1,811	0,035	0,1758	0,0021	0,80561	0,0746	0,001	1048	12	1044	11	1052	27	99
A_288.FIN2	388,6	580	0,256047	1190	2,025	0,024	0,1802	0,0017	0,59651	0,08136	0,00076	1123,3	8,3	1068	9	1230	19	87
A_289.FIN2	96,6	174,8	0,378882	-60	1,964	0,035	0,183	0,0018	0,1985	0,0781	0,0014	1102	12	1083,1	9,9	1140	36	95
A_290.FIN2	416	276	0,118269	2050	2,067	0,022	0,1893	0,0016	0,49815	0,07915	0,00075	1136,8	7,1	1117,5	8,7	1171	19	95
A_291.FIN2	85,6	329,6	0,717173	-180	2,321	0,067	0,1909	0,0039	0,81499	0,0875	0,0016	1210	21	1125	21	1365	35	82
A_292.FIN2	222,1	375,6	0,358397	280	2,094	0,041	0,1948	0,0035	0,76534	0,0779	0,001	1144	13	1147	19	1137	26	101
A_293.FIN2	450,8	1859	0,800577	-1800	2,239	0,022	0,2009	0,0016	0,62858	0,08068	0,00067	1193	6,9	1180	8,7	1213	16	97
A_294.FIN2	127,1	463	0,544453	-4200	3,517	0,048	0,2522	0,0024	0,71447	0,1006	0,0011	1528	11	1449	12	1634	21	89
A_295.FIN2	405	974	0,331605	-1300	4,126	0,032	0,2855	0,0022	0,68756	0,10445	0,00068	1658,5	6,3	1619	11	1702	12	95
A_297.FIN2	74,1	447	0,8583	-210	4,397	0,085	0,303	0,0037	0,34548	0,1051	0,002	1711	16	1705	18	1717	34	99
A_300.FIN2	76,7	535	0,873142	-230	4,854	0,067	0,3201	0,0033	0,42758	0,1101	0,0015	1795	12	1790	16	1801	24	99
A_302.FIN2	423	2800	0,562648	2600	16,1	0,15	0,4845	0,0046	0,86787	0,241	0,0011	2881,3	8,7	2545	20	3126,6	7,5	81

Table 15: Grain (=66) distribution of sample Map4. The red box highlights the preferred ages used (<1500=Pb^{206}/U^{238}; ≥1500=Pb^{207}/U^{235}). Refer to the legend in Fig. 31.

					RATIOS							AGES [Ma]						Conc.
Analysis	U [ppm]a	Pb [ppm]a	Th/Ua	206/204	207Pb/235Ub	2 σd	206Pb/238Ub	2 σd	rhoc	207Pb/206Pbe	2 σd	207Pb/235U	2 σ	206Pb/238U	2 σ	207Pb/206Pb	2 σ	%
A_118.FIN2	262,6	128,1	0,522848439	-270	0,2306	0,0066	0,03208	0,00035	0,18874	0,0516	0,0015	210,1	5,5	203,6	2,2	249	60	82
A_120.FIN2	238,3	238,8	1,10365086	290	0,2304	0,0097	0,03252	0,00044	0,14181	0,0513	0,0023	209,8	8	206,3	2,8	243	91	85
A_121.FIN2	390,7	986	2,562068083	430	0,236	0,011	0,0331	0,00055	0,096698	0,0518	0,0024	214,5	8,9	209,9	3,5	258	98	81
A_122.FIN2	243,5	460	1,605749487	-310	0,28	0,013	0,03898	0,0008	0,21502	0,0512	0,0024	250	10	246,5	5	239	98	103
A_123.FIN2	306	311	0,934640523	-80	0,2963	0,0072	0,04093	0,00037	0,17174	0,0524	0,0013	262,8	5,7	258,6	2,3	288	51	90
A_124.FIN2	498	412,5	0,714859438	440	0,2991	0,008	0,04162	0,0004	0,26205	0,052	0,0013	265,2	6,2	262,8	2,5	268	55	98
A_126.FIN2	702	322	0,415954416	-580	0,303	0,016	0,04229	0,00085	0,2178	0,0518	0,0027	268	12	267	5,3	260	110	103
A_127.FIN2	170,6	177,5	0,887456038	-430	0,304	0,0094	0,04229	0,00044	0,13634	0,0523	0,0016	268,4	7,3	267	2,7	284	65	94
A_129.FIN2	400	394	0,7725	510	0,308	0,019	0,04343	0,00088	0,010621	0,0518	0,0034	272	15	274	5,5	260	140	105
A_130.FIN2	259	224,8	0,721621622	-150	0,3212	0,0097	0,04368	0,00049	0,2153	0,0534	0,0016	281,9	7,4	275,6	3	322	63	86
A_131.FIN2	232,6	135,7	0,490541702	-320	0,3158	0,0084	0,04368	0,00044	0,25804	0,0521	0,0014	277,7	6,4	275,6	2,7	267	54	103
A_135.FIN2	274,6	223,5	0,724326293	120	0,319	0,01	0,04382	0,00059	0,097963	0,0521	0,0017	280,8	7,6	276,4	3,6	271	70	102
A_137.FIN2	231,2	129	0,511245675	-300	0,32	0,04	0,0447	0,0021	0,068668	0,0514	0,0069	281	31	282	13	230	280	123
A_142.FIN2	465,7	406,5	0,565600172	-430	0,3448	0,0061	0,04763	0,00052	0,66001	0,05219	0,00078	300,4	4,5	300,4	3,3	287	34	105
A_143.FIN2	115,7	170,1	0,780466724	-90	0,583	0,022	0,0746	0,001	0,16178	0,0567	0,0022	464	14	464	6,1	445	82	104
A_144.FIN2	370,6	703	0,902320561	340	0,5981	0,0091	0,07636	0,00056	0,1928	0,05699	0,0009	475,3	5,8	474,3	3,3	475	35	100
A_145.FIN2	197	371	0,874111675	-400	0,61	0,015	0,0781	0,00086	0,22073	0,0566	0,0014	482,2	9,7	484,7	5,1	450	52	108
A_146.FIN2	94,1	157,4	0,754516472	-390	0,688	0,021	0,08518	0,00099	0,14519	0,0587	0,0018	530	12	526,9	5,9	521	64	101
A_147.FIN2	155,1	246	0,783365571	-100	0,694	0,028	0,0854	0,0024	0,41696	0,0581	0,0021	535	17	528	14	522	80	101
A_150.FIN2	312,7	237,7	0,292292933	-60	0,764	0,012	0,08546	0,00076	0,39119	0,05921	0,00086	575,6	6,8	528,6	4,5	563	32	94
A_151.FIN2	175,8	371,2	0,893060296	-190	0,694	0,013	0,08567	0,00075	0,19327	0,0588	0,0011	534	8	529,8	4,5	542	43	98
A_154.FIN2	181,8	517	1,193069307	410	0,69	0,015	0,08571	0,00085	0,27642	0,0588	0,0012	531,7	9	530,1	5	540	46	98
A_155.FIN2	275	538	0,825454545	30	0,689	0,014	0,08594	0,00088	0,31136	0,0585	0,0012	531	8,4	531,4	5,3	535	42	99
A_156.FIN2	137,7	319	1,021060276	-170	0,692	0,016	0,08618	0,00086	0,10111	0,0584	0,0014	532,4	9,4	532,8	5,1	517	53	103
A_157.FIN2	382	169,8	0,184031414	560	0,698	0,012	0,08619	0,00078	0,2829	0,05877	0,00096	536,8	7	532,9	4,7	551	35	97
A_158.FIN2	292	241	0,361643836	-120	0,697	0,016	0,0864	0,0011	0,29846	0,0586	0,0014	536,1	9,8	534,3	6,7	534	50	100
A_160.FIN2	224,6	652	1,211932324	700	0,713	0,023	0,0877	0,0019	0,22134	0,0595	0,0021	546	14	542	11	574	78	94
A_161.FIN2	980	192	0,054591837	-60000	0,714	0,031	0,0882	0,0029	0,68302	0,0587	0,0018	547	18	545	17	554	67	98
A_164.FIN2	190,5	94,4	0,194225722	-260	0,737	0,015	0,08986	0,00085	0,18175	0,0596	0,0012	560,2	8,4	554,7	5	571	45	97
A_165.FIN2	120,5	113,6	0,414522822	-90	0,789	0,029	0,0918	0,0017	0,71029	0,062	0,0017	585	16	565,6	9,9	628	60	90
A_166.FIN2	212,2	142,5	0,280867107	50	0,767	0,017	0,09406	0,00087	0,31797	0,0592	0,0012	576,3	9,5	579,4	5,1	548	45	106
A_168.FIN2	126,8	104,5	0,349053628	-300	0,784	0,023	0,0954	0,001	0,2291	0,0597	0,0017	585	13	587,2	6	560	62	105
A_169.FIN2	188,5	441	0,858885942	-20	0,862	0,023	0,09706	0,00087	0,3705	0,0647	0,0016	630	12	597	5,1	745	53	80
A_170.FIN2	533,3	40,9	0,025745359	-500	0,832	0,014	0,09939	0,00096	0,55739	0,05978	0,00084	614	7,8	610,8	5,6	589	31	104
A_128.FIN2	568	101	0,070985915	200	0,821	0,03	0,0994	0,0036	0,19806	0,0589	0,0018	609	17	611	21	561	66	109
A_130.FIN2	191,7	25,5	0,028064684	-200	0,852	0,046	0,101	0,0023	0,31932	0,0611	0,0032	625	25	620	14	630	120	98
A_132.FIN2	94,7	56,5	0,214783527	-20	0,905	0,041	0,1022	0,0032	0,8486	0,0643	0,0017	648	22	626	18	711	59	88
A_133.FIN2	113,81	148,5	0,508742641	-1600	0,857	0,03	0,1023	0,0021	0,057206	0,0607	0,0024	627	16	627	12	600	84	105
A_134.FIN2	111,2	131,3	0,431654676	430	0,876	0,025	0,1043	0,0013	0,25999	0,061	0,0017	637	13	639,3	7,7	613	59	104
A_136.FIN2	246,2	623	0,879366369	-3600	0,998	0,026	0,1149	0,0016	0,18503	0,0631	0,0017	701	13	701,1	9	693	58	101
A_137.FIN2	1135	1520	0,451982379	-2100	1,06	0,019	0,1155	0,0017	0,63939	0,06713	0,00094	733,3	9,2	704	10	839	30	84
A_143.FIN2	607	282	0,119769357	3000	1,567	0,032	0,1507	0,0025	0,67174	0,0742	0,0011	957	13	905	14	1044	31	87
A_144.FIN2	464	427	0,212284483	3600	1,625	0,028	0,1641	0,0022	0,6789	0,07259	0,00094	979	11	979	12	999	27	98
A_145.FIN2	127,3	426	0,747839749	680	1,652	0,036	0,1655	0,0019	0,29753	0,0712	0,0016	988	14	987	11	949	45	104
A_147.FIN2	219,5	227,1	0,233667426	-500	1,792	0,04	0,1665	0,0022	0,37651	0,0735	0,0015	1041	14	993	12	1022	41	97
A_149.FIN2	330	584	0,395757576	600	1,717	0,028	0,1672	0,0018	0,56139	0,0745	0,001	1013	11	996	10	1048	28	95
A_150.FIN2	83,7	163,6	0,398088411	-150	1,78	0,037	0,1675	0,0015	0,25474	0,0772	0,0016	1035	13	998,2	8,3	1107	41	90
A_151.FIN2	97,4	282	0,679671458	-210	1,69	0,032	0,1687	0,0017	0,44129	0,0729	0,0014	1002	12	1004,4	9,4	995	38	101
A_152.FIN2	242,1	324	0,311028501	-3300	1,695	0,023	0,169	0,0014	0,47812	0,07279	0,00087	1005,2	8,6	1006,2	7,8	1001	25	101
A_153.FIN2	358,1	463	0,288187657	1700	2,001	0,064	0,1726	0,0044	0,30851	0,0726	0,0025	1115	22	1026	24	997	70	103
A_156.FIN2	77,1	146,1	0,473929961	-400	1,932	0,046	0,173	0,0019	0,52016	0,0814	0,0016	1087	16	1028	10	1216	40	85
A_157.FIN2	63,7	145,1	0,491365777	-30	1,789	0,041	0,1741	0,0018	0,33798	0,0745	0,0016	1037	15	1034,4	9,7	1031	45	100
A_159.FIN2	58,1	121,3	0,449225473	140	1,805	0,042	0,1753	0,0019	0,23958	0,0749	0,0017	1045	15	1042	11	1038	47	100
A_160.FIN2	112,2	434	0,780748663	-500	1,811	0,041	0,1765	0,0019	0,37663	0,0745	0,0016	1047	15	1047	11	1038	44	101
A_163.FIN2	75,3	385	1,057104914	-610	1,85	0,059	0,1793	0,0032	0,20378	0,0725	0,0023	1062	21	1063	17	988	65	108
A_164.FIN2	178,6	467	0,524636058	-160	1,887	0,027	0,1818	0,0014	0,57739	0,0755	0,001	1074,4	9,5	1076,4	7,7	1072	27	100
A_165.FIN2	118,2	215,1	0,366328257	-250	2,047	0,033	0,1821	0,0016	0,28636	0,0755	0,0012	1129	11	1078,1	8,5	1072	33	101
A_167.FIN2	171,7	251	0,291788002	-2500	1,95	0,024	0,1847	0,0015	0,43115	0,07663	0,00094	1096,9	8,4	1092,4	8,2	1103	24	99
A_169.FIN2	534	696	0,265730337	-500	2,065	0,024	0,192	0,0018	0,5819	0,07799	0,00076	1136,1	8	1132,2	9,5	1143	19	99
A_170.FIN2	171,6	492,1	0,520979021	-1000	2,258	0,044	0,1973	0,0022	0,52184	0,0807	0,0013	1197	14	1161	12	1206	33	96
A_171.FIN2	220,3	835	0,685428961	4300	2,173	0,086	0,1984	0,0042	0,039042	0,0787	0,0035	1172	27	1167	23	1160	88	101
A_176.FIN2	63,3	97	0,283728278	280	2,173	0,052	0,1997	0,0023	0,4279	0,0773	0,0018	1169	16	1173	12	1116	49	105
A_178.FIN2	137,5	260	0,354181818	-670	2,182	0,032	0,1997	0,0017	0,45352	0,0777	0,001	1173	10	1173,5	9,4	1128	27	104
A_179.FIN2	242,3	357	0,274865869	-900	2,223	0,042	0,2021	0,003	0,43758	0,0799	0,0015	1187	13	1186	16	1196	34	99
A_180.FIN2	76,1	351	0,812089356	60	2,348	0,044	0,2096	0,002	0,40765	0,0813	0,0014	1225	13	1226	11	1220	35	100
A_181.FIN2	72	267	0,515277778	530	3,056	0,082	0,2107	0,0021	0,12481	0,0921	0,0029	1420	21	1232	11	1441	58	85
A_182.FIN2	263	1412	0,8121673	60000	3,282	0,034	0,2568	0,002	0,528	0,09251	0,00084	1476,4	8,2	1473	10	1474	17	100
A_183.FIN2	349	484	0,157593123	100	5,855	0,068	0,3473	0,0037	0,77925	0,12245	0,00079	1952	10	1920	18	1990	11	96
A_184.FIN2	253,8	968	0,428684003	2800	6,191	0,053	0,3504	0,0025	0,60869	0,12824	0,00092	2001,9	7,5	1936	12	2072	13	93
A_185.FIN2	380	4020	1,068421053	-1800	6,572	0,07	0,3746	0,0035	0,7852	0,1252	0,00083	2054,4	9,5	2050	17	2030	12	101
A_186.FIN2	241,4	1090	0,430820215	300	7,759	0,086	0,3927	0,0036	0,79468	0,14399	0,00094	2202	10	2134	17	2274	11	94
A_187.FIN2	545	3589	0,63853211	3200	9,233	0,064	0,4121	0,0029	0,7725	0,16251	0,00077	2360,5	6,3	2224	13	2480,9	8	90
A_188.FIN2	219	2556	0,932420091	5400	12,71	0,16	0,4397	0,0055	0,8433	0,1865	0,0013	2657	12	2348	25	2710	11	87

Table 16: Grain (=72) distribution of sample Q5. The red box highlights the preferred ages used (<1500=Pb^{206}/U^{238}; ≥1500=Pb^{207}/U^{235}). Refer to the legend in Fig. 31.

4.3.1.12 Q1

Sample Q1 was collected from the lowermost uEF exposures at Quthing. This sample comprises of seventy-three (73) concordant grains, of which 5.5% (n=4) have metamorphic structures (Table 18). These same four metamorphic structured grains have Th/U ratios <0.1, confirming that these are indeed metamorphosed grains. This sample's analysis is dominated by rim grain analyses (90.4%). A minor number (32.9%) of grains belong to five (5) populations found throughout the concordant grain distributions. These populations include the most abundant, Cambrian based population (505.3-519.2 Ma) hosting 12.3% of the total population and more minor populations of the, Cambrian-Neoproterozoic (537.1-541.5 Ma), Late Neoproterozoic (572.2-579.7 Ma), Mid-Neoproterozoic (642.3-648.5 Ma) and Mesoproterozoic (1076.4-1080.4 Ma). The youngest grain determination resulted in: 1) YSG= 197.8 ±1.4 Ma; 2) YDZ= 197.8 ±3.1 (-3.2) Ma; 3) TuffZirc (8) = 515.1 ±3.8 Ma; 4) YC2σ (3)= 507.4 ±7.3 Ma; 5) Weighted Average (8)= 515.2 ±3.4 Ma; 6) YPP= 500.0 Ma and; 7) YC1σ (3)= 507.4 ±6.0 Ma. The collective mean of the YSG and YDZ ages for Q1 resulted in an average youngest maximum depositional age of 197.8 Ma.

Map1																		
				RATIOS									**AGES [Ma]**					**Conc.**
Analysis	U [ppm][a]	Pb [ppm][a]	Th/U[a]	206/204	207Pb/235U[b]	2 σ[d]	206Pb/238U[b]	2 σ[d]	rho[c]	207Pb/206Pb[e]	2 σ[d]	207Pb/235U	2 σ	206Pb/238U	2 σ	207Pb/206Pb	2 σ	%
A_006.FIN2	393,1	181,6	0,484863902	-100	0,2427	0,0045	0,03418	0,00023	0,1705	0,05105	0,00093	220,3	3,7	216,7	1,4	240	41	90
A_008.FIN2	823	227,1	0,291980559	640	0,2432	0,0038	0,03422	0,00024	0,030425	0,05118	0,00086	220,9	3,1	216,9	1,5	245	38	89
A_116.FIN2	304	153	0,542763158	-70	0,249	0,0069	0,03554	0,00036	0,22544	0,0511	0,0014	225,3	5,6	225,1	2,3	237	60	95
A_117.FIN2	304,2	90,4	0,189940828	-1320	0,453	0,011	0,05815	0,00042	0,40388	0,0563	0,0012	379,4	7,6	364,3	2,6	445	48	82
A_114.FIN2	285,4	144,4	0,287316048	-150	0,4737	0,0087	0,0609	0,00046	0,076998	0,05604	0,00098	393,1	6	381,1	2,8	437	39	87
A_012.FIN2	268	223	0,312686567	670	0,454	0,037	0,07841	0,00086	0,46826	0,0413	0,0034	371	26	486,5	5,2	608	74	80
A_013.FIN2	320	263,3	0,3446875	620	0,505	0,04	0,08131	0,00083	0,44021	0,0453	0,0033	406	28	503,9	5	540	73	93
A_015.FIN2	165	318,7	0,870909091	320	0,635	0,012	0,08172	0,00061	0,29284	0,0564	0,00097	498,7	7,3	506,3	3,6	449	37	113
A_017.FIN2	264,2	328,3	0,569265708	-280	0,6435	0,0098	0,08176	0,00053	0,047323	0,05729	0,00095	504,6	6,2	506,6	3,2	488	36	104
A_018.FIN2	224,4	339,6	0,684937611	-1010	0,672	0,011	0,0825	0,00061	0,47638	0,05854	0,00088	522	6,7	511	3,6	534	33	96
A_019.FIN2	291	344	0,515120275	-50	0,6717	0,0093	0,08348	0,00049	0,10481	0,05827	0,00085	521,6	5,8	516,8	2,9	529	32	98
A_021.FIN2	380	34,8	0,036578947	700	0,612	0,024	0,08351	0,00054	0,31872	0,0525	0,002	481	15	517	3,2	532	53	97
A_023.FIN2	246,2	344,2	0,612103981	-560	0,692	0,016	0,08407	0,0008	0,50939	0,0591	0,0012	533,3	9,7	520,3	4,8	563	47	92
A_088.FIN2	202	212	0,455445545	270	0,685	0,01	0,08579	0,00055	0,2628	0,05742	0,0009	528,9	6,3	530,6	3,3	491	35	108
A_089.FIN2	264,8	64,9	0,110234139	-400	0,694	0,013	0,08595	0,00067	0,20844	0,058	0,0011	534,5	7,9	531,5	4	518	43	103
A_026.FIN2	534	82,7	0,061853933	1800	0,7106	0,0078	0,08685	0,00054	0,25873	0,05911	0,00066	544,8	4,6	537,3	3,1	565	24	95
A_028.FIN2	115	113	0,431304348	170	0,685	0,016	0,08709	0,00072	0,14262	0,0572	0,0013	527,8	9,5	538,2	4,3	480	51	112
A_029.FIN2	369	551	0,644715447	460	0,708	0,01	0,08784	0,00064	0,23902	0,05837	0,00084	542,7	6	542,7	3,8	533	32	102
A_067.FIN2	139,8	111,9	0,365522175	-160	0,711	0,02	0,08794	0,00083	0,22145	0,0588	0,0016	544	12	543,3	4,9	538	61	101
A_068.FIN2	617	976	0,409562399	472	0,662	0,039	0,0888	0,0011	0,41239	0,0534	0,0029	509	24	548,5	6,5	618	79	89
A_035.FIN2	79	16,7	0,084936709	-20	0,756	0,025	0,08931	0,00098	0,10507	0,0611	0,0021	569	15	551,4	5,8	610	75	90
A_041.FIN2	134,6	165,1	0,495542348	400	0,737	0,02	0,09005	0,00078	0,042493	0,0593	0,0016	559	11	555,8	4,6	551	60	101
A_042.FIN2	1094	456	0,081444241	1095	0,743	0,017	0,0918	0,001	0,44407	0,0584	0,0012	562,6	9,8	566,1	5,9	551	41	103
A_043.FIN2	283	341	0,427561837	990	0,688	0,033	0,09263	0,00078	0,42172	0,0532	0,0024	523	20	571	4,6	632	58	90
A_044.FIN2	109,3	106,2	0,378774016	-700	0,778	0,019	0,094	0,0011	0,32129	0,0602	0,0015	582	11	579,1	6,2	609	50	95
A_045.FIN2	636	378	0,201415094	-2200	0,806	0,016	0,0945	0,0013	0,83131	0,06159	0,00073	599,1	9,3	582,2	7,9	654	25	89
A_046.FIN2	652	466,9	0,282208589	3090	0,81	0,011	0,09786	0,00096	0,5911	0,06011	0,00064	602	5,9	601,8	5,6	607	22	99
A_048.FIN2	102,6	379,7	1,402534113	-480	0,803	0,02	0,09791	0,00085	0,083621	0,0593	0,0015	598	11	602,1	5	550	56	109
A_014.FIN2	123,4	133,1	0,40356564	240	0,864	0,021	0,10251	0,00097	0,35558	0,0613	0,0013	631	11	629	5,7	632	47	100
A_051.FIN2	394	649	0,613451777	1300	0,892	0,016	0,10266	0,00078	0,43102	0,0628	0,001	647,4	8,8	629,9	4,5	695	35	91
A_031.FIN2	306,3	150,7	0,18805093	1650	0,826	0,04	0,10303	0,00087	0,40757	0,0576	0,0026	612	23	632,1	5,1	663	67	95
A_053.FIN2	145,4	147,7	0,366574966	321	0,881	0,014	0,10484	0,00071	0,097982	0,0615	0,001	640,4	7,7	642,6	4,1	646	35	99
A_062.FIN2	525	676	0,301333333	1310	0,858	0,029	0,1059	0,0013	0,6904	0,0584	0,0016	625	16	648,9	7,4	632	47	103
A_056.FIN2	552	733	0,393115942	2040	1,062	0,012	0,11679	0,0009	0,58682	0,06621	0,00063	734,1	6,1	712	5,2	808	20	88
A_065.FIN2	237	295	0,38185654	250	0,78	0,25	0,1178	0,0022	0,34477	0,044	0,016	678	26	717	12	743	65	97
A_058.FIN2	95,1	89	0,259516299	-40	1,126	0,023	0,1177	0,0012	0,30454	0,0694	0,0014	764	11	717,3	6,8	894	42	80
A_059.FIN2	398,4	512,3	0,424949799	1210	1,044	0,038	0,1183	0,0018	0,63483	0,0638	0,0019	723	19	720	11	764	52	94
A_063.FIN2	127,2	43,4	0,041037736	260	0,89	0,073	0,1198	0,0016	0,48473	0,0527	0,0042	610	45	729	9	844	85	86
A_034.FIN2	145	195,6	0,242068966	470	1,036	0,095	0,1242	0,0031	0,56098	0,0596	0,0048	696	52	754	18	936	91	81
A_040.FIN2	498	1606	0,86746988	1540	1,188	0,024	0,12421	0,00081	0,54068	0,0701	0,0012	796	11	754,6	4,6	918	34	82
A_024.FIN2	107,2	570	0,508395522	210	0,98	0,15	0,1327	0,0022	0,65346	0,0484	0,0089	675	75	803	13	1000	110	80
A_025.FIN2	226,6	390,1	0,356575463	641	1,148	0,068	0,1418	0,0017	0,55901	0,0575	0,0033	774	30	855,6	9,2	795	64	108
A_027.FIN2	589,8	1593	0,686673449	2000	1,477	0,022	0,1442	0,0015	0,73812	0,07377	0,00075	920,1	8,9	868,1	8,7	1032	20	84
A_069.FIN2	132,2	155	0,233736762	510	1,555	0,025	0,151	0,0022	0,067693	0,075	0,0014	950	10	906	12	1048	37	86
A_076.FIN2	189,7	506,1	0,597785978	850	1,557	0,018	0,1519	0,00098	0,31638	0,07398	0,00083	952	7	911,5	5,5	1033	23	88
A_078.FIN2	568	1710	0,737676056	600	1,609	0,018	0,1577	0,0013	0,64784	0,07342	0,00057	973,7	6,6	943,6	7,4	1029	16	92
A_080.FIN2	55,6	135,8	0,428417266	-400	1,666	0,033	0,1665	0,0017	0,26469	0,0722	0,0014	993	13	992,4	9,3	971	41	102
A_082.FIN2	217	338	0,184331797	680	1,437	0,086	0,1673	0,0013	0,54426	0,0618	0,0036	883	41	996,9	7,2	829	76	120
A_083.FIN2	195,3	365,2	0,420378904	1160	1,707	0,026	0,1675	0,0015	0,45572	0,07349	0,00098	1009,8	9,9	998,4	8,3	1021	27	98
A_084.FIN2	107,7	382,6	0,779015785	-410	1,782	0,031	0,1717	0,0016	0,33686	0,0756	0,0013	1037	11	1021,2	9,1	1074	34	95
A_092.FIN2	45,7	150	0,711159737	-30	1,863	0,034	0,1757	0,0014	0,13289	0,0764	0,0014	1066	12	1043	7,8	1093	38	95
A_093.FIN2	71,4	149,3	0,471148459	-200	1,798	0,032	0,1759	0,0013	0,1139	0,0745	0,0014	1042	12	1044,6	6,9	1048	36	100
A_094.FIN2	494,9	486	0,210143463	2700	2,133	0,092	0,1775	0,0048	0,94735	0,0857	0,0017	1145	30	1052	26	1316	40	80
A_095.FIN2	155,6	297	0,395886889	500	1,874	0,023	0,1779	0,001	0,46292	0,07614	0,00085	1070,7	8,2	1055,3	5,5	1094	23	96
A_096.FIN2	387	1296	0,645994832	1200	2,312	0,032	0,1924	0,0022	0,19748	0,08649	0,00085	1213,7	9,9	1134	12	1350	20	84
A_097.FIN2	124,3	151,5	0,236122285	-150	2,156	0,032	0,198	0,0013	0,1885	0,0784	0,0011	1165	10	1164,7	7	1150	28	101
A_098.FIN2	208,9	1342	0,923408329	-3400	3,769	0,058	0,267	0,0029	0,59331	0,1018	0,0013	1585	12	1525	15	1653	24	92
A_099.FIN2	138,6	416,2	0,435064935	-1100	3,776	0,07	0,2717	0,004	0,86773	0,10004	0,00095	1583	15	1548	20	1621	18	95
A_100.FIN2	158,3	972	0,547694251	-2800	10,97	0,17	0,4661	0,0055	0,90538	0,1693	0,0012	2517	15	2465	24	2549	12	97
A_112.FIN2	222	1892	0,622522523	1500	19,9	0,37	0,6137	0,0096	0,93351	0,2341	0,0016	3082	19	3082	38	3079	11	100

Table 17: Grain (=59) distribution of sample Map1. The red box highlights the preferred ages used (<1500=Pb206/U238; ≥1500=Pb207/U235). Refer to the legend in Fig. 31.

					RATIOS								AGES [Ma]					Conc.
Analysis	U [ppm]a	Pb [ppm]a	Th/Ua	206/204	207Pb/235Ub	2 σd	206Pb/238Ub	2 σd	rhoc	207Pb/206Pbe	2 σd	207Pb/235U	2 σ	206Pb/238U	2 σ	207Pb/206Pb	2 σ	%
A_370.FIN2	414	334,5	0,956038647	-4900	0,2155	0,0044	0,03115	0,00022	0,18729	0,0502	0,001	197,9	3,7	197,8	1,4	193	43	102
A_345.FIN2	209	191,9	0,776076555	-410	0,3022	0,007	0,04213	0,00032	0,024738	0,052	0,0013	267,4	5,5	266	2	266	51	100
A_357.FIN2	180,2	116,1	0,593784684	0	0,301	0,01	0,04235	0,00046	0,041129	0,0519	0,0019	266,6	7,9	267,4	2,9	258	75	104
A_371.FIN2	126,3	220,5	0,819477435	-350	0,653	0,015	0,08155	0,00065	0,075192	0,058	0,0014	508,5	9,3	505,3	3,9	500	52	101
A_383.FIN2	342	449	0,569883041	400	0,605	0,029	0,082	0,00064	0,51683	0,0533	0,0023	476	18	508	3,8	633	62	80
A_380.FIN2	350	357	0,444285714	-800	0,677	0,012	0,08222	0,00075	0,040364	0,05907	0,00091	524	7,1	509,3	4,4	566	30	90
A_368.FIN2	1353	369	0,121433851	140000	0,6656	0,0057	0,08312	0,00043	0,4108	0,05791	0,00047	517,8	3,5	514,7	2,6	523	18	98
A_414.FIN2	101	92,2	0,426534653	130	0,668	0,018	0,08324	0,00073	0,19743	0,0582	0,0015	517	11	515,4	4,4	504	56	102
A_341.FIN2	95	138,6	0,634736842	-180	0,661	0,014	0,0832	0,00066	0,15671	0,0575	0,0012	514,9	8,8	515,6	4	497	48	104
A_367.FIN2	350,9	472,4	0,619549729	17000	0,6672	0,0094	0,08382	0,00052	0,40591	0,05759	0,00074	518,5	5,7	518,8	3,1	507	29	102
A_392.FIN2	512	453	0,395117188	3400	0,63	0,028	0,08387	0,00068	0,47481	0,0547	0,0021	496	17	519,1	4,1	570	56	91
A_366.FIN2	146,2	169,8	0,538303694	7300	0,663	0,015	0,08389	0,00069	0,16707	0,057	0,0012	516,6	8,9	519,2	4,1	487	48	107
A_422.FIN2	144,3	284	0,857241857	870	0,726	0,019	0,08511	0,00085	0,49892	0,0618	0,0014	551	11	526,5	5	636	49	83
A_430.FIN2	140,9	134,7	0,446415898	550	0,703	0,018	0,08544	0,00082	0,35439	0,0595	0,0014	539	11	528,5	4,8	567	54	93
A_389.FIN2	80,5	130,3	0,750310559	570	0,681	0,022	0,08574	0,00075	0,07251	0,0578	0,002	527	14	530,2	4,4	482	71	110
A_442.FIN2	179	235	0,575418994	21000	0,707	0,019	0,0869	0,0008	0,44783	0,0592	0,0015	542	11	537,1	4,7	573	54	94
A_354.FIN2	54,9	61	0,469398907	-390	0,715	0,027	0,08694	0,00095	0,044854	0,0595	0,0023	544	16	537,3	5,6	535	83	100
A_355.FIN2	316,2	1007	1,319101834	-8300	0,705	0,01	0,08763	0,00058	0,10114	0,05819	0,0009	541	6,2	541,5	3,4	524	35	103
A_375.FIN2	101,7	122	0,456243854	-820	0,738	0,022	0,08879	0,00076	0,019125	0,0597	0,0018	559	12	548,3	4,5	575	66	95
A_378.FIN2	356,3	119	0,137468425	-300	0,739	0,01	0,08959	0,00072	0,33313	0,05974	0,00082	561,1	6	553,1	4,2	586	30	94
A_417.FIN2	76	180,1	0,932894737	1730	0,774	0,031	0,08982	0,00094	0,43724	0,0629	0,0024	574	16	554,4	5,5	655	77	85
A_418.FIN2	611	665	0,349427169	990	0,735	0,024	0,09116	0,00097	0,51812	0,0581	0,0017	555	14	563,5	5,7	639	49	88
A_379.FIN2	396	245,1	0,205555556	1170	0,717	0,03	0,09175	0,00072	0,33965	0,0563	0,0023	542	19	565,8	4,2	681	56	83
A_441.FIN2	580,9	2566	1,779996557	1130	0,7908	0,0098	0,09283	0,00054	0,22208	0,06195	0,00078	591,2	5,6	572,2	3,2	666	27	86
A_402.FIN2	199	494	0,991457286	1110	0,763	0,015	0,094	0,00075	0,37486	0,0587	0,0011	574,4	8,6	579,1	4,4	540	40	107
A_349.FIN2	339,1	160,9	0,182836921	-230	0,81	0,014	0,09411	0,0007	0,63354	0,06225	0,00091	602,1	7,9	579,7	4,1	671	31	86
A_350.FIN2	179,7	1584	3,494713411	-370	0,811	0,015	0,09463	0,0007	0,41713	0,0624	0,0011	602,6	8,4	582,8	4,1	667	39	87
A_405.FIN2	227,1	320,8	0,538969617	4700	0,808	0,011	0,09492	0,00058	0,091069	0,06183	0,00092	601,2	6,4	584,5	3,4	655	32	89
A_360.FIN2	114,9	128,9	0,469103568	26000	0,839	0,021	0,09767	0,00092	0,28829	0,0622	0,0015	616	11	600,7	5,4	650	51	92
A_386.FIN2	544,8	418	0,207415565	-15000	0,821	0,029	0,0983	0,0016	0,51887	0,0605	0,0018	607	16	604,4	9,4	660	55	92
A_433.FIN2	357	37,9	0,030028011	1400	0,896	0,012	0,10477	0,00082	0,50687	0,06218	0,00075	648,7	6,7	642,3	4,8	672	26	96
A_340.FIN2	179,1	233,8	0,419877164	-20	0,96	0,02	0,10497	0,00074	0,42628	0,0661	0,0013	682	10	643,4	4,3	799	42	81
A_399.FIN2	309	93,6	0,103559871	180	0,904	0,014	0,1052	0,0011	0,3272	0,06233	0,00082	652,3	7,7	644,9	6,1	673	29	96
A_364.FIN2	144,1	141,2	0,358778626	8500	0,892	0,016	0,10531	0,00066	0,062249	0,0614	0,0012	645,8	8,7	645,4	3,8	629	41	103
A_351.FIN2	380	65,8	0,033131579	-1400	0,964	0,017	0,1057	0,0011	0,57565	0,06579	0,00093	684,3	8,5	647,8	6,1	790	30	82
A_436.FIN2	620,9	250	0,133515864	1430	0,942	0,01	0,1059	0,001	0,68685	0,06477	0,00059	673,2	5,4	648,5	5,9	762	19	85
A_381.FIN2	729	1100	0,358847737	860	0,988	0,043	0,1103	0,0024	0,57874	0,0651	0,0025	696	23	674	14	781	75	86
A_429.FIN2	269,1	176,9	0,226681531	4200	0,949	0,016	0,11043	0,00068	0,057929	0,0624	0,0011	677	8,2	675,2	4	684	36	99
A_408.FIN2	456	282,9	0,171929825	1700	0,936	0,054	0,1132	0,0013	0,4416	0,0594	0,0032	651	30	690,9	7,3	813	67	85
A_390.FIN2	241,4	87,4	0,044241922	8300	1,02	0,062	0,1182	0,0018	0,57095	0,0628	0,0032	707	31	720	10	811	84	89
A_384.FIN2	104,2	205,1	0,648464491	-5900	1,07	0,022	0,1183	0,0013	0,50457	0,0655	0,0012	736	11	720,5	7,5	778	37	93
A_397.FIN2	437,7	893	0,513593786	830	1,171	0,037	0,121	0,0011	0,59198	0,0696	0,002	781	18	736,5	6,1	904	55	81
A_385.FIN2	176,9	199	0,356133409	-12900	1,135	0,019	0,1246	0,0011	0,49029	0,06596	0,00095	768,1	8,9	756,8	6,3	795	30	95
A_356.FIN2	233,7	364,7	0,475823706	-15200	1,127	0,016	0,12535	0,00087	0,29949	0,06527	0,00093	765,4	7,7	761,2	5	773	30	98
A_403.FIN2	525	2340	1,39047619	1340	1,147	0,031	0,12697	0,00094	0,51462	0,065	0,0016	774	16	770,5	5,4	784	47	98
A_406.FIN2	625	690	0,33408	3000	1,221	0,025	0,1303	0,0013	0,59353	0,0678	0,0011	807	11	789,3	7,4	848	35	93
A_395.FIN2	603	606	0,232338308	3600	1,352	0,031	0,1338	0,0026	0,899	0,07303	0,0007	865	13	809	15	1013	20	80
A_382.FIN2	539	891	0,474953618	1700	1,357	0,034	0,1354	0,0017	0,78698	0,0721	0,0011	868	14	818,3	9,9	988	33	83
A_413.FIN2	256,5	497	0,587524366	490	1,287	0,021	0,136	0,0012	0,39816	0,0688	0,0011	839	9,3	821,7	7,1	885	32	93
A_358.FIN2	349,8	688	0,468839337	-3300	1,432	0,041	0,1396	0,0021	0,54715	0,0741	0,0018	897	17	842	12	1035	49	81
A_363.FIN2	467,2	768	0,271832192	729	1,35	0,039	0,14086	0,00088	0,37052	0,0692	0,0019	867	16	849,4	5	910	51	93
A_353.FIN2	179,1	339	0,614182021	-5700	1,466	0,029	0,1445	0,0023	0,52405	0,0734	0,0013	915	12	870	13	1018	36	85
A_420.FIN2	242,7	438	0,498145859	620	1,431	0,06	0,1466	0,0021	0,43702	0,0705	0,0027	895	25	882	12	977	67	90
A_396.FIN2	108,7	261	0,640294388	2800	1,576	0,027	0,1516	0,0011	0,33173	0,0753	0,0012	959	11	909,8	6,4	1064	33	86
A_427.FIN2	654	577	0,172629969	5200	1,594	0,034	0,15385	0,00076	0,42495	0,0755	0,0016	967	13	922,5	4,2	1072	37	86
A_369.FIN2	255	518	0,481568627	-35000	1,588	0,02	0,1593	0,0012	0,44583	0,07208	0,00081	964,4	7,7	952,6	6,6	982	23	97
A_347.FIN2	101,5	93,4	0,368472906	-800	1,786	0,025	0,1638	0,0019	0,44155	0,0792	0,0011	1039,4	8,9	977	11	1164	28	84
A_404.FIN2	164,4	161,2	0,229318735	3200	1,662	0,029	0,1663	0,0013	0,17366	0,0723	0,0013	994	11	991,4	7,4	998	39	99
A_400.FIN2	205,9	257,5	0,28542982	5000	1,716	0,02	0,16748	0,0009	0,21606	0,07404	0,00085	1013,4	7,3	998,1	5	1041	23	96
A_431.FIN2	87,5	221,2	0,565714286	1060	1,769	0,027	0,1723	0,0012	0	0,0749	0,0013	1033	10	1024,6	6,4	1049	34	98
A_394.FIN2	521	195,9	0,085796545	1000	1,78	0,014	0,17264	0,00088	0,37987	0,07471	0,00058	1037,5	5	1026,6	4,8	1057	16	97
A_361.FIN2	305,7	474	0,417075564	15000	1,868	0,026	0,1744	0,0013	0,42133	0,0774	0,001	1069,1	9,1	1036,5	7	1128	26	92
A_362.FIN2	52,93	441,7	1,809937654	8200	1,822	0,038	0,176	0,0017	0,1896	0,0749	0,0016	1049	14	1044,8	9,1	1047	43	100
A_388.FIN2	42,18	121,4	0,620673305	1600	1,935	0,047	0,1818	0,0016	0,073088	0,0772	0,0019	1088	16	1076,4	8,6	1095	52	98
A_372.FIN2	264,4	473	0,38086233	-9700	1,894	0,019	0,1818	0,00095	0,31715	0,07537	0,00072	1078,2	6,5	1076,7	5,2	1073	19	100
A_443.FIN2	295	1005	0,771525424	-11300	1,865	0,028	0,1825	0,0015	0,49059	0,07417	0,0009	1067,8	9,7	1080,4	8,3	1042	25	104
A_407.FIN2	259,3	831	0,629772464	13000	2,168	0,021	0,1992	0,0012	0,41094	0,079	0,00074	1170	6,8	1171,1	6,6	1167	19	100
A_393.FIN2	254,1	969	0,628886265	3500	4,081	0,034	0,277	0,002	0,66295	0,10673	0,0007	1649,5	6,8	1576	10	1742	12	90
A_419.FIN2	543	550	0,138305709	31000	4,273	0,025	0,2955	0,0014	0,59424	0,10509	0,00054	1687,6	4,9	1668,8	6,9	1714,5	9,4	97
A_435.FIN2	204,8	671	0,384765625	1000	4,826	0,038	0,3145	0,0017	0,79735	0,11119	0,00075	1789,6	7	1762,5	8,3	1817	12	97
A_365.FIN2	213,1	1224	0,61520413	50000	8,873	0,096	0,4049	0,0038	0,83414	0,15836	0,00096	2323	10	2191	18	2437	10	90
A_432.FIN2	516	6431	1,246124031	19300	9,581	0,075	0,4252	0,003	0,91667	0,16355	0,0006	2394,1	7,2	2283	14	2492,1	6,2	92
A_415.FIN2	92,2	762	0,637744035	1200	16,87	0,15	0,566	0,0037	0,64171	0,2162	0,0015	2926,9	9	2890	15	2951	12	98
A_359.FIN2	72,7	74	0,067400275	-36000	20,87	0,41	0,5981	0,0055	0,60043	0,252	0,0041	3124	20	3021	22	3186	26	95

Table 18: Grain (=73) distribution of sample Q1. The red box highlights the preferred ages used (<1500=Pb^{206}/U^{238}; ≥1500=Pb^{207}/U^{235}). Refer to the legend in Fig. 31.

100

4.3.1.13 Q7

Sample Q7 was collected from the uppermost Clarens units, specifically at the contact between the Clarens and overlying Drakensberg basalt units. Fifty-one (51) concordant grains were analysed, of which all grains have magmatic structures and Th/U ratios >0.1, confirming that the concordant grain sources were magmatic in origin (Table 19). The grain sizes range from 26.0-275.0 µm. Grain analyses included both core (11.8%) and rim (88.2%) selections. Grain populations comprises of 29.4% of the total sample grains, including the: 1) Permian at 11.8% (n=6); 2) Cambrian I at 5.9% (n=3); 3) Cambrian II at 5.9% (n=3); and 4) Neoproterozoic at 5.9% (n=3). The youngest grain determination resulted in: 1) YSG= 186.7 ±1.6 Ma; 2) YDZ= 186.5 ±3.8 (-3.4) Ma; 3) TuffZirc (8) = 236.6 ±2.4 Ma; 4) YC2σ (3)= 261.9 ±3.8 Ma; 5) Weighted Average (8)= 262.0 ±3.0 Ma; 6) YPP= 260.0 Ma and; 7) YC1σ (3)= 261.9 ±3.1 Ma. The collective mean of the YSG and YDZ ages for Q7 resulted in an average youngest maximum depositional age of 186.6 Ma.

4.3.1.14 Mas1

Sample Mas1 was collected from the basal Clarens-uEF contact at the tridactyl trackway hosting Masitise cave house. This sample comprises of sixty (60) concordant grains, of which 100% (n=60) have igneous structures and Th/U ratios >0.1 (Table 20). Grain sizes range from 30.0-210.0 µm, with the majority (96%) of grains being 180.0 ±20 µm. Grain analysis included both grain rim (90%) and core (10%) shots. Of the total 60 concordant grains, only 23.3% belong to any of the three (3) sample populations. These populations include the youngest Triassic population between 247.3-251.5 Ma (5%), Early Cambrian population between 505.8-507.9 Ma (5%) and lastly, the most abundant Cambrian population between 512.9-528.6 Ma, hosting 13.3% of the total grains (n=8). The youngest grain determination resulted in: 1) YSG= 196.4 ±2.1 Ma; 2) YDZ= 196.3 ±4.8 (-4.6) Ma; 3) TuffZirc (8) = 515.7 ±4.5 Ma; 4) YC2σ (3)= 249.0 ±3.8 Ma; 5) Weighted Average (8)= 511.4 ±3.8 Ma; 6) YPP= 250.0 Ma and, 7) YC1σ (3)= 249.0 ±3.0 Ma. The collective mean of the YSG and YDZ ages for Mas1 resulted in an average youngest maximum depositional age of 196.5 Ma.

					RATIOS								AGES [Ma]						Conc.
Analysis	U [ppm][a]	Pb [ppm][a]	Th/U[a]	206/204	$^{207}Pb/^{235}U^b$	2 σ[d]	$^{206}Pb/^{238}U^b$	2 σ[d]	rho[c]	$^{207}Pb/^{206}Pb^e$	2 σ[d]	$^{207}Pb/^{235}U$	2 σ	$^{206}Pb/^{238}U$	2 σ	$^{207}Pb/^{206}Pb$	2 σ	%
A_214.FIN2	196	238	1,454081633	-260	0,2056	0,0061	0,02939	0,00026	0,028989	0,0512	0,0015	189,2	5,1	186,7	1,6	227	61	82
A_145.FIN2	142,8	105,8	0,775210084	-140	0,247	0,011	0,03504	0,00041	0,044282	0,0511	0,0024	223,2	9,1	222	2,5	216	94	103
A_162.FIN2	272,9	319	1,062660315	290	0,2933	0,0061	0,04093	0,00029	0,063881	0,0522	0,0011	261,3	4,9	258,6	1,8	282	48	92
A_211.FIN2	330,2	203,6	0,560569352	-410	0,299	0,0058	0,04123	0,00028	0,054663	0,0527	0,0011	265,2	4,6	260,5	1,7	306	45	85
A_132.FIN2	129,8	233	1,502311248	-30	0,2982	0,0082	0,04174	0,00049	0,19391	0,0517	0,0015	264,2	6,5	263,6	3	253	58	104
A_134.FIN2	137,2	75,2	0,481049563	120	0,299	0,011	0,04174	0,00041	0,043608	0,0518	0,002	266,9	8,6	263,6	2,5	260	80	101
A_118.FIN2	242,7	332	1,173465183	234	0,3029	0,0064	0,04195	0,00031	0,10518	0,0522	0,0011	268,3	5	264,9	1,9	278	47	95
A_222.FIN2	107,8	281	2,17903525	-210	0,307	0,011	0,04213	0,00049	0,089065	0,0534	0,002	270,6	8,8	266	3	306	78	87
A_163.FIN2	214	189,8	0,750934579	-150	0,334	0,011	0,0458	0,00051	0,020775	0,0529	0,0019	291,8	8,7	288,6	3,2	299	76	97
A_166.FIN2	336,1	391	0,94019637	-630	0,3439	0,0066	0,04612	0,00036	0,36034	0,05408	0,00097	299,7	5	290,6	2,2	359	40	81
A_128.FIN2	739	916	0,51691475	592	0,46	0,22	0,0623	0,0014	0,98644	0,069	0,02	360	12	389,1	8,2	485	50	80
A_203.FIN2	590	423	0,342542373	620	0,481	0,023	0,07229	0,00051	0,50874	0,0479	0,0022	393	16	449,9	3,1	436	53	103
A_180.FIN2	211	405	0,993364929	-1460	0,578	0,012	0,07376	0,0005	0,15493	0,0568	0,0011	462	7,4	458,8	3	465	44	99
A_193.FIN2	166	251,9	0,76686747	50	0,585	0,011	0,07479	0,00054	0,056579	0,0567	0,0011	468,2	6,6	464,9	3,2	468	44	99
A_170.FIN2	250,9	275,3	0,564368274	-900	0,596	0,013	0,07483	0,00062	0,19079	0,0577	0,0013	473,6	8,2	465,2	3,7	501	48	93
A_195.FIN2	96,3	109,5	0,521287643	-80	0,62	0,018	0,07727	0,0006	0,31962	0,0584	0,0016	488	11	479,8	3,6	511	58	94
A_152.FIN2	732	970	0,31010929	670	0,625	0,025	0,0813	0,0014	0,54398	0,0558	0,0021	488	16	503,5	8,7	592	59	85
A_144.FIN2	245,6	463,7	0,899429967	-150	0,664	0,016	0,08244	0,00064	0,45277	0,0584	0,0013	516,2	9,9	510,7	3,8	530	48	96
A_161.FIN2	456,4	270,5	0,271910605	-1500	0,6713	0,0098	0,08301	0,00063	0,2376	0,05871	0,00075	521,1	6	514	3,8	550	28	93
A_205.FIN2	281,7	479,9	0,816116436	-670	0,662	0,012	0,08318	0,00068	0,17635	0,0579	0,0011	516	7,3	515,1	4,1	512	40	101
A_212.FIN2	483,1	699	0,661974746	-1400	0,6803	0,0088	0,08384	0,00052	0,23134	0,05897	0,00079	526,5	5,3	519	3,1	558	29	93
A_192.FIN2	134,9	159,7	0,512305411	-720	0,71	0,015	0,0849	0,0006	0,036309	0,0605	0,0013	543,2	8,7	525,3	3,5	598	48	88
A_183.FIN2	113	270	1,115044248	10	0,699	0,02	0,08688	0,00083	0,10897	0,0587	0,0016	537	11	537	4,9	520	59	103
A_218.FIN2	309	333,3	0,464401294	-180	0,706	0,015	0,08708	0,00061	0,30254	0,0588	0,0012	541,4	8,7	538,2	3,6	545	44	99
A_121.FIN2	230,7	66,9	0,116601647	970	0,71	0,012	0,08736	0,00063	0,18922	0,0586	0,001	543,7	6,9	539,9	3,7	536	37	101
A_153.FIN2	236	183	0,314830508	510	0,723	0,01	0,08886	0,00066	0,4494	0,0588	0,00079	551,8	6	548,7	3,9	547	30	100
A_143.FIN2	120,2	188	0,668885191	50	0,728	0,025	0,0889	0,00089	0,14746	0,0592	0,0021	553	15	549	5,3	544	76	101
A_199.FIN2	312,6	267,8	0,356046065	-540	0,727	0,013	0,08935	0,00072	0,18626	0,0592	0,0011	553,9	7,3	551,7	4,3	560	40	99
A_186.FIN2	633,4	433,6	0,273918535	-9300	0,8028	0,0089	0,09397	0,00062	0,39375	0,06199	0,00066	598	5	578,9	3,7	668	23	87
A_142.FIN2	96,8	70,5	0,301652893	10	0,817	0,024	0,095	0,0011	0,58217	0,0622	0,0015	604	13	585,1	6,3	647	52	90
A_119.FIN2	129,5	139,5	0,372972973	330	0,858	0,016	0,10119	0,00078	0,37488	0,0611	0,0011	627,6	8,5	621,3	4,6	623	39	100
A_226.FIN2	300	556	0,324666667	870	0,833	0,045	0,1014	0,0017	0,52116	0,0595	0,0027	622	24	622,4	9,9	746	67	83
A_204.FIN2	311,3	604	0,706071314	10	0,866	0,01	0,10282	0,00056	0,28328	0,06105	0,00074	632,6	5,7	630,9	3,3	631	26	100
A_131.FIN2	172,1	436	0,696687972	140	1,239	0,016	0,12891	0,00084	0,35727	0,06923	0,00082	817,4	7,4	781,6	4,8	906	25	86
A_133.FIN2	146,5	120,2	0,193720137	40	1,313	0,025	0,1362	0,0018	0,73101	0,06952	0,00091	849	11	823	10	904	27	91
A_220.FIN2	336	313	0,174702381	-1200	1,336	0,027	0,1386	0,002	0,89687	0,06995	0,00073	859	11	836	11	920	22	91
A_130.FIN2	209	394	0,443062201	880	1,37	0,084	0,1395	0,0024	0,1992	0,0712	0,0035	870	34	841	14	1026	73	82
A_156.FIN2	453	1550	0,686534216	401	1,45	0,77	0,144	0,017	0,43555	0,0678	0,0066	925	41	860	110	948	95	91
A_200.FIN2	191,2	316,4	0,413179916	160	1,677	0,021	0,1587	0,001	0,4416	0,07681	0,0009	998,3	8	949,3	5,8	1114	24	85
A_146.FIN2	159,3	185,9	0,288135593	650	1,592	0,023	0,1596	0,0014	0,68925	0,07211	0,00084	965,5	9,1	954,5	7,7	982	24	97
A_184.FIN2	160,1	241,4	0,36039975	790	1,617	0,024	0,1598	0,001	0,51226	0,0737	0,001	977,4	9,3	955,7	5,6	1026	27	93
A_151.FIN2	457	691	0,350547046	1100	1,69	0,015	0,1603	0,001	0,41955	0,07642	0,00067	1004,7	5,6	958,6	5,8	1102	18	87
A_167.FIN2	332,9	685	0,488434965	2400	1,692	0,018	0,1682	0,0011	0,34278	0,07299	0,00079	1005,8	7	1001,9	6,3	1010	22	99
A_181.FIN2	310	1290	1	-1500	1,928	0,026	0,1819	0,0017	0,39733	0,077	0,001	1090,4	9,1	1077,5	9,4	1123	28	96
A_182.FIN2	227	852	0,815859031	-2000	2,092	0,029	0,1871	0,0013	0,37943	0,0809	0,001	1145,2	9,5	1105,8	7,3	1213	25	91
A_129.FIN2	156	366	0,467948718	770	2,066	0,024	0,1905	0,0012	0,53546	0,07835	0,00091	1136	8,1	1123,7	6,4	1150	23	98
A_198.FIN2	219,1	664	0,654495664	-1000	2,15	0,036	0,1968	0,002	0,75569	0,0793	0,0013	1164	12	1158	11	1173	32	99
A_201.FIN2	320,9	1909	1,060766594	1100	2,811	0,02	0,2264	0,0013	0,5592	0,09011	0,00059	1357,7	5,4	1315,4	6,8	1425	13	92
A_189.FIN2	283	752	0,398233216	2520	3,828	0,048	0,2661	0,0028	0,86448	0,10437	0,00066	1596,6	9,9	1521	14	1701	12	89
A_160.FIN2	11,85	565	4,008438819	130	7,46	0,72	0,3527	0,0085	0,40726	0,147	0,013	2147	90	1942	40	2360	120	82
A_149.FIN2	117,4	524,5	0,455706985	70	7,378	0,094	0,3669	0,003	0,46663	0,1453	0,0013	2156	11	2014	14	2288	16	88

Table 19: Grain (=51) distribution of sample Q7. The red box highlights the preferred ages used (<1500=Pb^{206}/U^{238}; ≥1500=Pb^{207}/U^{235}). Refer to the legend in Fig. 31.

Analysis	U [ppm][a]	Pb [ppm][a]	Th/U[a]	206/204	RATIOS 207Pb/235U[b]	2σ[d]	206Pb/238U[b]	2σ[d]	rho[c]	207Pb/206Pb[e]	2σ[d]	AGES [Ma] 207Pb/235U	2σ	206Pb/238U	2σ	207Pb/206Pb	2σ	Conc. %
A_337.FIN2	130,3	93,5	0,855717575	19	0,2161	0,0077	0,03093	0,00033	0,055223	0,0507	0,0019	197,9	6,4	196,4	2,1	212	74	93
A_335.FIN2	97,4	138,2	1,602669405	-88	0,232	0,011	0,03277	0,0004	0,051162	0,0516	0,0025	210,6	9	207,8	2,5	232	95	90
A_314.FIN2	371	388	1,134770889	-1140	0,2455	0,0052	0,0345	0,00023	0,25355	0,0514	0,0011	222,5	4,2	218,7	1,4	244	44	90
A_259.FIN2	249	430	1,710843373	-380	0,2739	0,0082	0,03911	0,00036	0,079451	0,0506	0,0015	245,6	6,4	247,3	2,2	223	62	111
A_315.FIN2	150,3	183	1,151696607	36	0,284	0,0085	0,03944	0,00035	0,054901	0,0524	0,0017	252,8	6,7	249,3	2,1	271	64	92
A_257.FIN2	192,5	475	2,332467532	-1680	0,2817	0,0096	0,03979	0,00045	0,30943	0,0511	0,0019	251,3	7,6	251,5	2,8	230	75	109
A_279.FIN2	308	453	1,444805195	-360	0,29	0,017	0,0413	0,0018	0,52324	0,0532	0,0016	259	11	260	11	308	61	84
A_262.FIN2	125,8	79,8	0,544515103	-880	0,2986	0,0098	0,04137	0,00045	0,2294	0,0528	0,0017	264,8	7,8	261,3	2,8	292	67	89
A_278.FIN2	96	143,5	1,319791667	-70	0,319	0,014	0,04396	0,00046	0,12997	0,0526	0,0022	281	11	277,3	2,8	284	87	98
A_301.FIN2	147,8	191	1,01014885	-170	0,341	0,01	0,0476	0,00045	0,1727	0,052	0,0016	297,6	8	299,8	2,8	272	64	110
A_336.FIN2	306	258,9	0,549346405	30	0,417	0,007	0,05527	0,00031	0,3062	0,05459	0,00084	353,4	5	346,8	1,9	380	34	91
A_236.FIN2	40,52	59,1	0,693237907	-20	0,632	0,039	0,0756	0,0015	0,079448	0,06	0,0036	492	24	469,5	9,1	550	130	85
A_299.FIN2	309	603	0,925566343	0	0,669	0,012	0,08163	0,00059	0,20782	0,0596	0,0011	519,1	7,4	505,8	3,5	573	41	88
A_333.FIN2	144,9	155,6	0,487922705	-80	0,654	0,013	0,08166	0,00059	0,30064	0,0576	0,0011	509,3	7,8	506	3,5	490	43	103
A_249.FIN2	427	386,2	0,390163934	-1900	0,6672	0,0074	0,08197	0,00043	0,1582	0,05901	0,00067	518,5	4,5	507,9	2,6	558	25	91
A_325.FIN2	544,4	412	0,36002939	-15600	0,678	0,012	0,08282	0,00056	0,31243	0,0592	0,001	524,8	7,5	512,9	3,4	564	39	91
A_312.FIN2	507	540	0,50295858	-5600	0,673	0,011	0,08305	0,00059	0,49609	0,05874	0,00097	522,1	6,6	514,3	3,5	548	36	94
A_276.FIN2	204,1	214	0,472807447	-7600	0,685	0,018	0,08322	0,00075	0,5448	0,0595	0,0014	528	11	515,3	4,5	568	50	91
A_258.FIN2	312,1	518,3	0,727010574	-2000	0,6823	0,0099	0,08335	0,00056	0,60245	0,05921	0,00079	527,5	6	516,1	3,3	568	30	91
A_230.FIN2	132,6	218,9	0,697586727	240	0,679	0,015	0,08344	0,00057	0,18634	0,0591	0,0013	524,3	8,9	516,6	3,4	549	49	94
A_287.FIN2	152,1	310,9	0,925706772	-840	0,681	0,013	0,08404	0,00057	0,11285	0,0587	0,0012	526,8	8,2	520,2	3,4	536	45	97
A_260.FIN2	227	361,6	0,629955947	-600	0,622	0,081	0,0849	0,0012	0,94779	0,0501	0,0046	443	26	525,1	6,8	639	78	82
A_298.FIN2	261	81,5	0,138697318	-2700	0,693	0,012	0,08547	0,00063	0,22376	0,0589	0,001	533,5	7,2	528,6	3,7	545	39	97
A_302.FIN2	299,7	324	0,489155822	-2800	0,704	0,012	0,08586	0,00062	0,30414	0,0593	0,001	540,5	7,2	531	3,7	565	37	94
A_229.FIN2	166,6	469,7	1,1242497	620	0,711	0,012	0,08753	0,0007	0,24311	0,059	0,001	543,9	7,4	540,8	4,1	545	38	99
A_250.FIN2	231,6	150,2	0,263816926	-1440	0,713	0,012	0,08876	0,00062	0,1457	0,05823	0,00099	545,8	7,1	548,2	3,6	523	38	105
A_283.FIN2	550	875	0,526909091	1090	0,693	0,043	0,089	0,0024	0,55929	0,0562	0,0027	532	25	549	14	634	72	87
A_272.FIN2	194,7	203	0,45146379	-3000	0,768	0,013	0,09013	0,00063	0,11431	0,0619	0,0011	577,6	7,3	556,3	3,7	649	38	86
A_291.FIN2	193,2	453,3	1,02484472	-370	0,792	0,018	0,0941	0,0011	0,68278	0,0612	0,0011	591	10	579,6	6,7	633	39	92
A_265.FIN2	64,7	101,8	0,593508501	-1400	0,771	0,021	0,09489	0,00089	0,084067	0,059	0,0018	577	12	584,3	5,2	521	64	112
A_256.FIN2	162,5	235	0,574769231	270	0,81	0,023	0,09531	0,00087	0,014038	0,0616	0,0018	600	13	586,8	5,1	631	65	93
A_322.FIN2	85,4	257,6	1,25058548	-1300	0,802	0,028	0,09613	0,00095	0,27262	0,0604	0,0023	596	16	591,7	5,6	579	82	102
A_323.FIN2	132,1	151,2	0,415594247	-2500	0,922	0,019	0,10123	0,00077	0,24259	0,0656	0,0015	662,2	9,6	621,5	4,5	772	48	81
A_255.FIN2	258,7	313	0,198299188	810	1,018	0,045	0,1134	0,002	0,42684	0,0651	0,0024	704	24	692	11	854	62	81
A_293.FIN2	521	424	0,234932821	-6900	1,11	0,035	0,11996	0,00082	0,40806	0,0669	0,002	755	17	730,3	4,7	814	63	90
A_286.FIN2	210	284	0,405238095	220	1,202	0,028	0,123	0,002	0,38256	0,0711	0,0015	799	13	748	11	940	43	80
A_334.FIN2	388,1	1309	0,968564803	300	1,199	0,035	0,1266	0,0013	0,5832	0,0683	0,0017	798	16	768,2	7,3	877	50	88
A_310.FIN2	217,2	353	0,370626151	700	1,178	0,054	0,1303	0,0024	0,53883	0,0657	0,0025	787	24	789	14	875	64	90
A_289.FIN2	220,1	713	0,819627442	-410	1,277	0,049	0,13625	0,00098	0,4687	0,0679	0,0024	824	24	823,3	5,6	950	57	87
A_247.FIN2	368	284,9	0,176358696	1070	1,404	0,013	0,13801	0,00081	0,43626	0,07371	0,00067	889,8	5,4	833,3	4,6	1030	18	81
A_228.FIN2	459,4	167,5	0,112581628	1200	1,438	0,016	0,14317	0,00097	0,2566	0,07283	0,00084	904,5	6,8	862,5	5,5	1005	24	86
A_297.FIN2	230	424	0,48	-660	1,429	0,023	0,1471	0,0013	0,62771	0,07034	0,00089	899,4	9,7	884,3	7,6	934	26	95
A_290.FIN2	429	2170	1,111888112	940	1,522	0,057	0,1539	0,0017	0,48628	0,0714	0,0024	936	23	922,8	9,8	951	74	97
A_254.FIN2	468	1019	0,495512821	1700	1,62	0,019	0,1589	0,0012	0,65486	0,07372	0,00065	977,2	7,2	950,5	6,6	1030	18	92
A_244.FIN2	166,3	252	0,346361996	-280	1,583	0,028	0,1589	0,0019	0,65635	0,0721	0,00093	962	11	951	11	981	26	97
A_327.FIN2	208	616	0,645673077	-2200	1,717	0,036	0,1644	0,0029	0,70928	0,07546	0,00084	1010	14	980	16	1073	23	91
A_246.FIN2	81,8	318	0,844743276	200	1,775	0,038	0,1653	0,0017	0,31507	0,078	0,0017	1032	14	985,7	9,3	1119	43	88
A_332.FIN2	210	480	0,55952381	-10	1,739	0,023	0,1664	0,0013	0,50824	0,07536	0,00081	1023,7	8	992	7,3	1078	20	92
A_251.FIN2	104,6	213,1	0,443594646	-1710	1,767	0,023	0,1722	0,0011	0,21252	0,07427	0,00096	1031,7	8,4	1023,9	6	1039	26	99
A_326.FIN2	158,9	486,5	0,664568911	750	1,839	0,026	0,1761	0,0016	0,49996	0,0757	0,001	1058,1	9,3	1045,6	8,9	1082	28	97
A_237.FIN2	131,5	575,6	0,895057034	360	1,837	0,026	0,1771	0,0013	0,23399	0,0752	0,0011	1057,2	9,2	1050,8	7,1	1064	28	99
A_270.FIN2	338	565,7	0,350295858	-34000	1,949	0,021	0,1789	0,0014	0,49361	0,07885	0,00077	1097,4	7,1	1061	7,7	1165	19	91
A_300.FIN2	269	483	0,405204461	-1800	1,918	0,03	0,1808	0,002	0,57012	0,0769	0,001	1086	10	1071	11	1112	26	96
A_285.FIN2	129,4	639	0,878670788	-500	1,801	0,094	0,1858	0,0014	0,80788	0,0696	0,0035	1033	31	1100	7,9	1003	68	110
A_296.FIN2	179,3	281,7	0,299665365	-1800	2,065	0,028	0,1876	0,0011	0,27667	0,0799	0,0011	1135,8	9	1108,4	5,9	1186	26	93
A_294.FIN2	352	321	0,181534091	500	2,333	0,036	0,1929	0,0018	0,58379	0,0877	0,0012	1221	11	1137	9,6	1369	26	83
A_273.FIN2	305,6	1434	0,585078534	-33000	5,009	0,037	0,3178	0,0018	0,75647	0,11419	0,0007	1820,1	6,2	1778,7	8,8	1865	11	95
A_234.FIN2	48,3	221	0,540372671	130	5,839	0,083	0,336	0,0031	0,50874	0,126	0,0015	1949	12	1867	15	2036	22	92
A_271.FIN2	286,5	1295	0,507155323	-60000	8,779	0,07	0,3836	0,0034	0,65479	0,1657	0,0012	2314,5	7,3	2092	16	2513	12	83
A_261.FIN2	213,2	1388	0,580206379	900	10,07	0,18	0,4066	0,0067	0,92756	0,1793	0,0012	2437	17	2197	31	2645	11	83
A_328.FIN2	57,3	351,9	0,512565445	50	12,3	0,12	0,4816	0,0032	0,62085	0,185	0,0014	2626,7	9,4	2534	14	2695	12	94

Table 20: Grain (=60) distribution of sample Mas1. The red box highlights the preferred ages used (<1500=Pb^{206}/U^{238}; ≥1500=Pb^{207}/U^{235}). Refer to the legend in Fig. 31.

103

4.3.2   Detrital zircon populations

Populations exhibited throughout the lEF, uEF and Clarens Formation all show similar population clusterings. Populations comprise of ≥3 grains of similar age, with age clusters easily evident in graphical peaks. Three major populations (Jurassic-Permian, Cambrian-Neoproterozoic and Neo- to Mesoproterozoic) are present throughout all samples, and although some variances in youngest constraining ages and additional minor populations do occur, the overall graphical clusterings remain the same (Fig. 32).
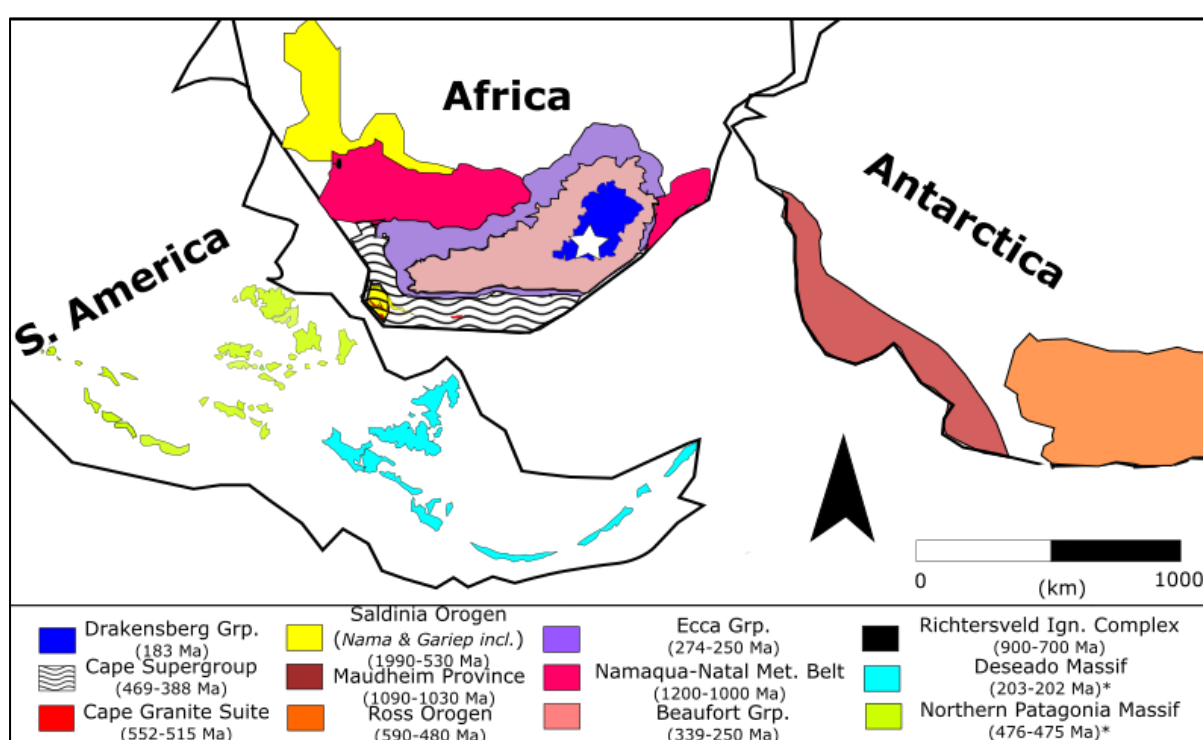
Fig. 32: A Mesozoic, Early Jurassic, snapshot of the southern Gondwana georgraphy. All plausible sources for the upper Stormberg detrital zircon grain ages have been highlighted, spread over three distinct grain populations hosted within this study's three main localities. The map was compiled using Borg et al. (1990); Cole (1992); Frimmel et al. (2001); Eglington (2006); Pankhurst et al. (2014), Pierce et al. (2014) and McKay et al. (2015). * denotes specific age ranges of relevance to this study.

The youngest population of grains throughout the three formations falls between 186.7-288.6 Ma (Fig. 33; 34). A total count of one-hundred and thirteen (n=113) grains belong to this Jurassic-Permian age range. The minority of grains concentrated within the Jurassic (n=10) occur consistently throughout the uEF and Clarens samples; however, they suggest a general lack of Early Jurassic sources. The grain morphologies supplying this youngest population range from elongate, acicular and fragmentary Triassic and Permian grains, to pristine, elongate Jurassic grains (Fig. 33). It can be

noted that all grains in this population have oscillatory zoning and Th/U ratios >0.1, confirming that the detrital grain sources are strictly magmatic (Fig. 33). The Th/U ratios are predominantly moderate to high, with the majority of grains being >0.8. Magmatic sources for the Late Triassic-Early Jurassic grains were likely transported (ash) from the South American Patagonian Magmatic Provinces (Fig. 33). Upper Triassic to Lower Jurassic calc-alkaline granitoids of the North Patagonian Massif are the most likely sources of grains aged between 290-186 Ma, some of the likely other sources include: the Triassic-Jurassic Treneta Plutonic and Volcanic Province (290-172 Ma; Pankhurst et al., 2006) and the Permian central Yaminué Complex (250 Ma; Pankhurst et al., 2014). The southern Patagonian, Deseado Massif hosts two Late Triassic-Early Jurassic complexes, namely La Calandria (203 Ma) and Bajo de La Leona (202 Ma; Pankhurst et al., 1993). The dating of the abundance of tuffaceous beds within the Beaufort and Ecca Groups of the Karoo stratigraphy determined the volcanic Choiyoi and Puesto Viejo igneous suites as likely synchronous ash-fall sources for the Permo-Triassic Karoo beds (including some reworked ash grains) (Valencio et al., 1975; Kay et al., 1989; Cole, 1992; Rocha-Campos et al., 2011; Rubidge et al., 2013; Ottone et al., 2014; McKay et al., 2015; Walters, 2017[Unpublished]). The higher proportion of Earlier Triassic-Late Permian grains within the youngest population presents the plausible recycling model of the proximal older material of the Ecca and Beaufort groups into the Stormberg Group elements (Walters, 2017[Unpublished]; Viglietti et al., 2018) (Fig. 6; 33).
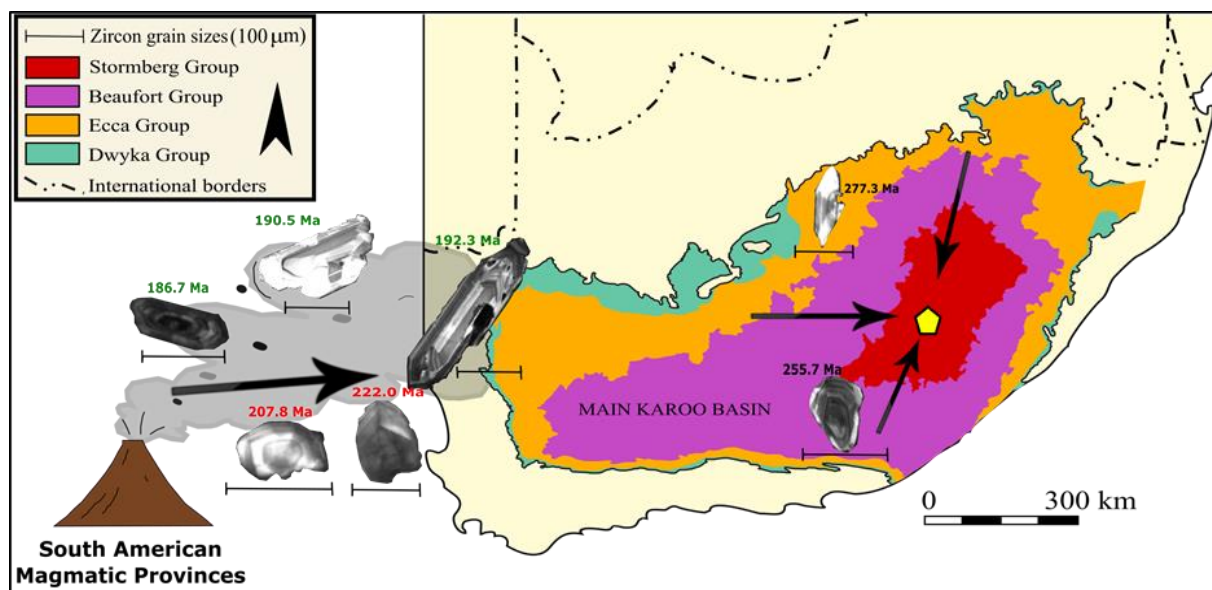
Fig. 33: Illustration of the likely sources for the youngest grain clusters (Jurassic-Permian), including the Jurassic and Triassic South American Magmatic Provinces and older Triassic-Permian Karoo Groups (Ecca and Beaufort). Grain images included to illustrate the oscillatory zoning and morphological characteristics of the youngest population grains. Note: Permian (black), Triassic (red) and Jurassic (green) grains were selected to represent the youngest population as a whole.

The largest cluster belongs to the Cambrian-Neoproterozoic grains of all samples, with ages ranging from 496.4 Ma to 799.5 Ma (Fig. 34). A total of four-hundred and fifty-eight (n=458 Ma) grains form part of this massive population. The grains comprise of rounded to sub-rounded external morphologies (often fragmented), predominantly oscillatory zoned internal structures and more minor complex internal structures. The Th/U ratios show that fourteen of the total population grains have ratios <0.1, indicative of a small metamorphic source input. The abundance of Cambrian grains was likely the result of a substantial influence of the coeval Cambrian Cape Granite Suite, ranging in age from 552.0 Ma to 515.0 Ma (Da Silva et al., 2000; Scheepers and Armstrong, 2002). The tectonic extension derived Cape Granite Suite (CGS) is relatively proximal to the southern part of the Karoo Basin and stratigraphically hosted directly below the Cape Supergroup (Belcher and Kisters, 2003). Another major source of Cambrian-Neoproterozoic grains includes the southern African (750-550 Ma) Saldania and Gariep Belts; which, in conjunction with other orogenic belts, form part of the Neoproterozoic juvenile Pan-African crustal system (Rozendaal et al., 1999; Gresse et al., 2006; Andersen et al., 2018). A recent study by Andersen et al. (2018) highlighted the recycled nature of the Saldania and Gariep Belts sediments; which, in addition to the Neoproterozoic (<750 Ma)

population, host Early Neoproterozoic-Late Mesoproterozoic (950-1300 Ma) and Palaeoproterozoic (1775-1990 Ma) provenance clusters similar to those seen in this study. Further confirming the assimilation of these recycled sediments within the Elliot and Clarens deposits. The Pan-African Saldania and Gariep Belt volcanics and recycled sediments, alongside the aforementioned CGS granitoid Neoproterozoic-Cambrian age cluster peaks are similarly abundant within the Cape Supergroup and older Karoo groups (Fourie et al., 2011; Craddock and Thomas, 2011; Vorster, 2013 [Unpublished]; Blewett and Phillips, 2016; Walters, 2017[Unpublished]; Viglietti et al., 2018). This abundant cluster similarity indicates a plausible high-input source of reworked, mixed and redistributed Cape Supergroup and older Karoo sediments in the Stormberg Group. This interpretation concurs with previous palaeodrainage based Stormberg provenance interpretations (Catuneanu et al., 1998; Bordy et al., 2004b). Further plausible southern Gondwana sources include: the Sierra de la Ventana Fold Belt of Patagonia, with similar Neoproterozoic orogeny followed by rifting derived Cambrian intrusives (Rapela et al., 2003); reworked material from the proximal Pan-African, 530-560 Ma, Nama Group sediments (Gresse et al., 1996; Andersen et al., 2018); other more distal Patagonian/southern African orogens including the Dom Feliciano and Damara Belts. Plausible sources younger than 500 Ma are less abundant, however the Cambrian-Ordovician Ross Orogeny of Antarctica correlatively displays similar timings of its magmatic and structural events to the Saldania Orogeny, thus offering a likely younger, proximal input source (Rozendaal et al., 1999; Foden et al., 2006).

The second most abundant age cluster falls within the Early Neoproterozoic-Mesoproterozoic, comprising of ages ranging from 911.5 Ma to 1178.0 Ma (Fig. 34). Grain morphologies range from fragmentary with oscillatory internal structures (magmatic) to rounded, highly luminescent grains with complex internal structures (metamorphic). Th/U ratios show a minor amount of grains below 0.1, with the majority of grains being between 0.2 and 0.8. The most probable source of Mesoproterozoic (1.0-1.2 Ga) grains is the Late Mesoproterozoic Namaqua-Natal Metamorphic Province (Thomas et al., 1994; Eglington, 2006). The position of the Namaqua-Natal Metamorphic

Belt lies proximal to the Stormberg sediments, forming the majority of the basement in Lesotho itself. Adjacent and related juvenile orogenic belts with a plausible population influence includes the Grenville-aged Mid- to Late Proterozoic Maudheim Province (1030.0-1090.0 Ma) of Dronning Maud Land and to a lesser extent, the Rayner Province (900.0-990.0 Ma), Antarctica (Groenewald et al., 1991; Pierce et al., 2014). The only Late Neoproterozoic (700-900 Ma) southern African source is the Richterveld Igneous Complex, geographically positioned between Namibia and South Africa and predating the juvenile Pan-African metamorphic belts by 250 million years (Frimmel et al., 2001). The dominant clustering of Namaqua-Natal Province sourced Mesoproterozoic grains is again shared with the Cape Supergroup Proterozoic detrital populations (Cole, 1992; Fourie, et al., 2011; Blewett and Phillips, 2016). This uniformity in grain clustering, similar to the previous Cambrian-Neoproterozoic clustering, highlights a probable recycling and/or reworked grain deposition of the Cape Supergroup in the Stormberg units. This reworked nature is further confirmed through the rounded and fragmentary nature of the Neo- and Mesoproterozoic grains (Fourie et al., 2011; Vorster, 2013).

More minor populations that occur throughout the collective detrital grains, include: a very minor amount of Kaapval Craton derived Archean grains between 2571.0 Ma and 2575.0 Ma; Palaeoproterozoic grains at 1867.0 Ma; Early Mesoproterozoic grains between 1439.0 Ma and 1668.8 Ma; Early Neoproterozoic grains from 803.0 Ma to 909.8 Ma, and; Ordovician grains from 455.8 Ma to 494.7 Ma. The Early Neoproterozoic grain cluster is likely sourced by Kalahari Craton rifting volcano-sedimentary sequences, including the Richterveld Igneous Complex, aged between 833.0 Ma and 771.0 Ma (Frimmel et al., 2001). The Ordovician grains pertain to a likely combination of Patagonian Magmatic Province sources, namely the 475.0 Ma early granitoid intrusions of Pichi Mahuida, the 475.0 Ma and 476.0 Ma Arroyo Salado granites, the 476.0 Ma Sierra Grande granite, and most importantly, the Ordovician Famatinian magmatic arc (Pankhurst et al., 1998; Pankhurst et al., 2000; Pankhurst et al., 2006). The very minor clusters of Palaeoproterozoic (and some Early Mesoproterozoic grains) could be linked to the preexisitng Kheis terrane, Richtersveld sub-province

and Bushmanland sub-province protolith lavas and granitoids (Thomas et al., 1994; Reid, 1997; Eglington, 2006). However, these Palaeoproterozoic and Mesoproterozoic populations are more likely inhereted from the Nama Group and Gariep and Saldania Belts sediments. The Archean and Early Palaeoproterozoic aged grains (3.5-2.0 Ga), although not forming significant population clusters, do occur consistently throughout all of the samples. This implies a constant source input from the proximal Archean Kaapval Craton, Zimbabwean Craton and Limpopo Orogenic Belt, most probably through reworked material (de Wit, et al., 1992; Krönera et al., 1999; Oberthür et al., 2002).
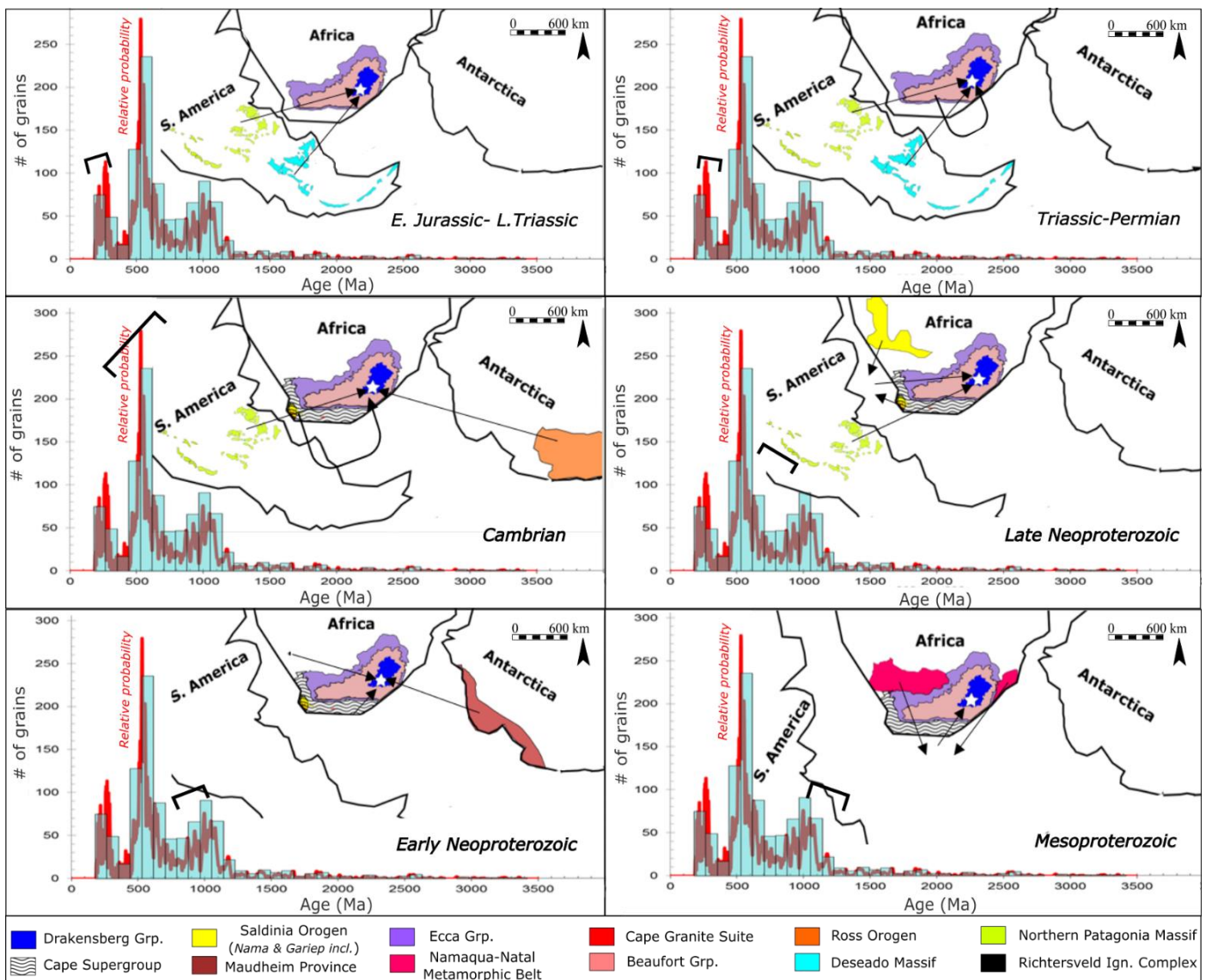
Fig. 34: Geographic map illustrating the probability-density of various grains and the associated possible source terranes for the major population grain clusterings.

4.3.3   K-S Test

The Kolmogorov-Smirnov (K-S) test allows for the relative insight on whether two distributions are comparatively drawn from the same population, referred to as the null hypothesis (Gehrels, 2000; Amidon et al., 2005a, b). In essence, this test seeks to comparatively provide the probability of same source grains of various age trends. All of the samples spread throughout the lEF, uEF and Clarens formations of this study were included. The comparative probabilities (P-test) higher than 0.05 presents proof of a similar source model (Table 21).

The sample trends displayed in the cumulative probability plots of Fig (35) display overall genetically similar source populations, with some minor input variations occurring between the younger (Jurassic-Permian and Cambrian-Neoproterozoic) populations. From Table (21), it is clear that the majority of grains passed the K-S Test, with samples such as Map3, Q4 and Mas1 being strongly compatible with all other samples. Samples Map6, Map5 and Q7 on the other hand do not share sources with any of the other samples aside from Map3, Q4 and Mas1, making them 'failed' test samples. The Map4 and Map2 sample combination pass the K-S test perfectly (P=1.0), confirming a definite shared source for these two lEF (one being the trackway the other the lEF-uEF contact) samples. The remaining sample combinations all have varying P-values, ranging between extremely strong (1.0) to the weak (0.05). Sample combinations with P<0.05 are the result of the presence of the three failed test samples.

It is interesting to note, however; when combined, these three failed samples have moderate to strong P-values (0.277-0.920), suggesting predominant genetic links amongst the sources of the three samples pertaining from the Maphutseng uEF and uEF-Clarens contact and Moyeni uppermost Clarens units (Table 22; Fig. 36). The failed test probability plots, Map6, Map5 and Q7 (Fig. 36), share a unique, abundant source input during the Ediacaran (Late Neoproterozoic) and similar probability trends further indicate a shared source dominance from the Late Neoproterozoic (>560.4 Ma) onwards. A variance in the younger population trends between Map5 (uEF) and the other two

samples indicate different source influences between the uEF and Clarens Formation (Map6 and Q7) deposits. Alternately, the near identical probability trends throughout Map6 and Q7 suggest strongly similar depositional sources within these Clarens units.

4.3.3.1   lower Elliot Formation

The overall closely correlated trends of the lEF samples points toward a cogenetic source relationship between the lEF units. The younger populations, ranging from the Triassic-Permian to the Ordovician-Silurian display near-perfect shared source inputs, which can be linked to the greater consistency noted in the Triassic (Norian) youngest maximum single grain ages associated with these samples (Table 23; Fig. 37). Population source inputs over the Cambrian display a slight divergence in source inputs, including: Map1 (lowest lEF sample), which hosts an increase in variable source inputs during the Cambrian-Neoproterozoic, and; Map2, which shows a distinct lack of Late Mesoproterozoic source inputs, when compared to the other sample trends. The older population sources (>1600 Ma), as is the case with the uEF and Clarens Formation, tends to have close cogenetic source correlations.

4.3.3.2   upper Elliot Formation

The uEF samples display a similar overall trend in population sources, however the younger (<500 Ma) population sources and input densities vary greatly. The Jurassic-Permian population sources, in particular, show a large spread of sources, or lack thereof; as is the case for sample Q2. This strong diversity of younger grain inputs aid in explaining the greater diversity of youngest single grain maximum ages predominant throughout the uEF samples (Table 23; Fig. 37). The sample trends correlate more closely from the Cambrian onwards, boasting more cogenetic source inputs, aside from minor input variations from the previously discussed ('failed' test) sample Map5.
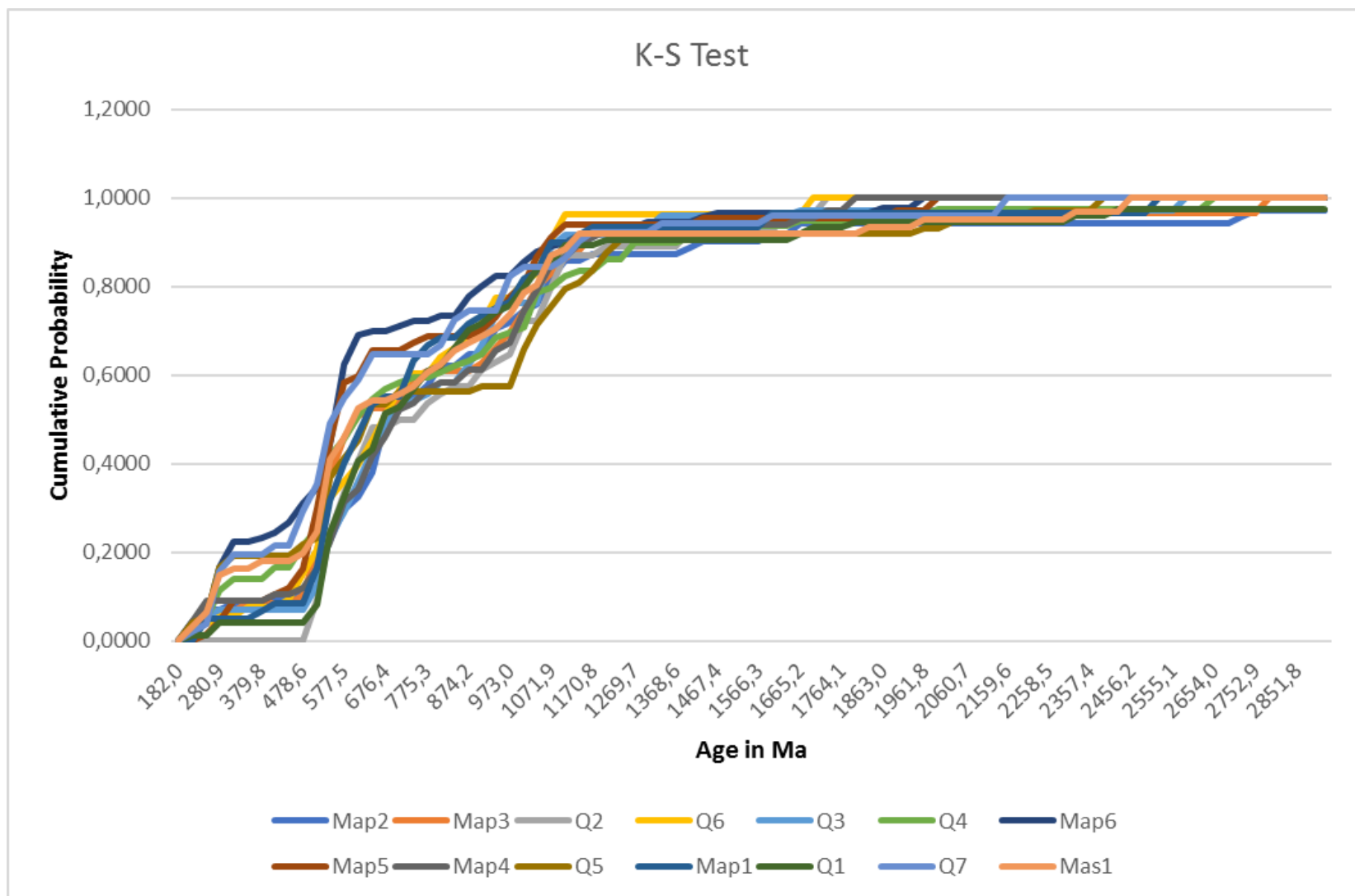
Fig. 35: K-S test P values plotted against U/Pb detrital zircon ages (Ma) for all the samples analysed in this study. All samples noticeably follow similar trends, with some slight source variances throughout.

	Map2	Map3	Q2	Q6	Q3	Q4	Map6	Map5	Map4	Q5	Map1	Q1	Q7	Mas1
K-S P-values using error in the CDF														
Map2		0,205	0,726	0,904	0,964	0,115	0,000	0,007	1,000	0,338	0,447	0,953	0,014	0,120
Map3	0,205		0,279	0,876	0,201	0,744	0,053	0,637	0,296	0,543	0,802	0,534	0,156	0,905
Q2	0,726	0,279		0,266	0,807	0,085	0,001	0,013	0,806	0,069	0,461	0,636	0,010	0,125
Q6	0,904	0,876	0,266		0,919	0,538	0,007	0,135	0,787	0,177	0,976	0,521	0,243	0,702
Q3	0,964	0,201	0,807	0,919		0,092	0,000	0,007	0,915	0,159	0,561	0,900	0,010	0,117
Q4	0,115	0,744	0,085	0,538	0,092		0,075	0,596	0,070	0,718	0,446	0,128	0,611	0,973
Map6	0,000	0,053	0,001	0,007	0,000	0,075		0,277	0,000	0,015	0,037	0,002	0,920	0,286
Map5	0,007	0,637	0,013	0,135	0,007	0,596	0,277		0,017	0,152	0,319	0,030	0,684	0,791
Map4	1,000	0,296	0,806	0,787	0,915	0,070	0,000	0,017		0,376	0,573	0,686	0,016	0,139
Q5	0,338	0,543	0,069	0,177	0,159	0,718	0,015	0,152	0,376		0,176	0,160	0,051	0,334
Map1	0,447	0,802	0,461	0,976	0,561	0,446	0,037	0,319	0,573	0,176		0,857	0,120	0,617
Q1	0,953	0,534	0,636	0,521	0,900	0,128	0,002	0,030	0,686	0,160	0,857		0,025	0,231
Q7	0,014	0,156	0,010	0,243	0,010	0,611	0,920	0,684	0,016	0,051	0,120	0,025		0,827
Mas1	0,120	0,905	0,125	0,702	0,117	0,973	0,286	0,791	0,139	0,334	0,617	0,231	0,827	

Table 21: P values produced by the K-S test. Note the varying number of blank cells per sample, illustrating that although all samples have genetic similarities, samples Map6, Map5 and Q7 to a lesser degree.

	Map6	Map5	Q7
K-S P-values using error in the CDF			
Map6		0,265	0,906
Map5	0,265		0,721
Q7	0,906	0,721	

Table 22: Comparative P values for the three failed test (K-S Test II) samples from the overall group test. These three samples display a positive genetic relationship.
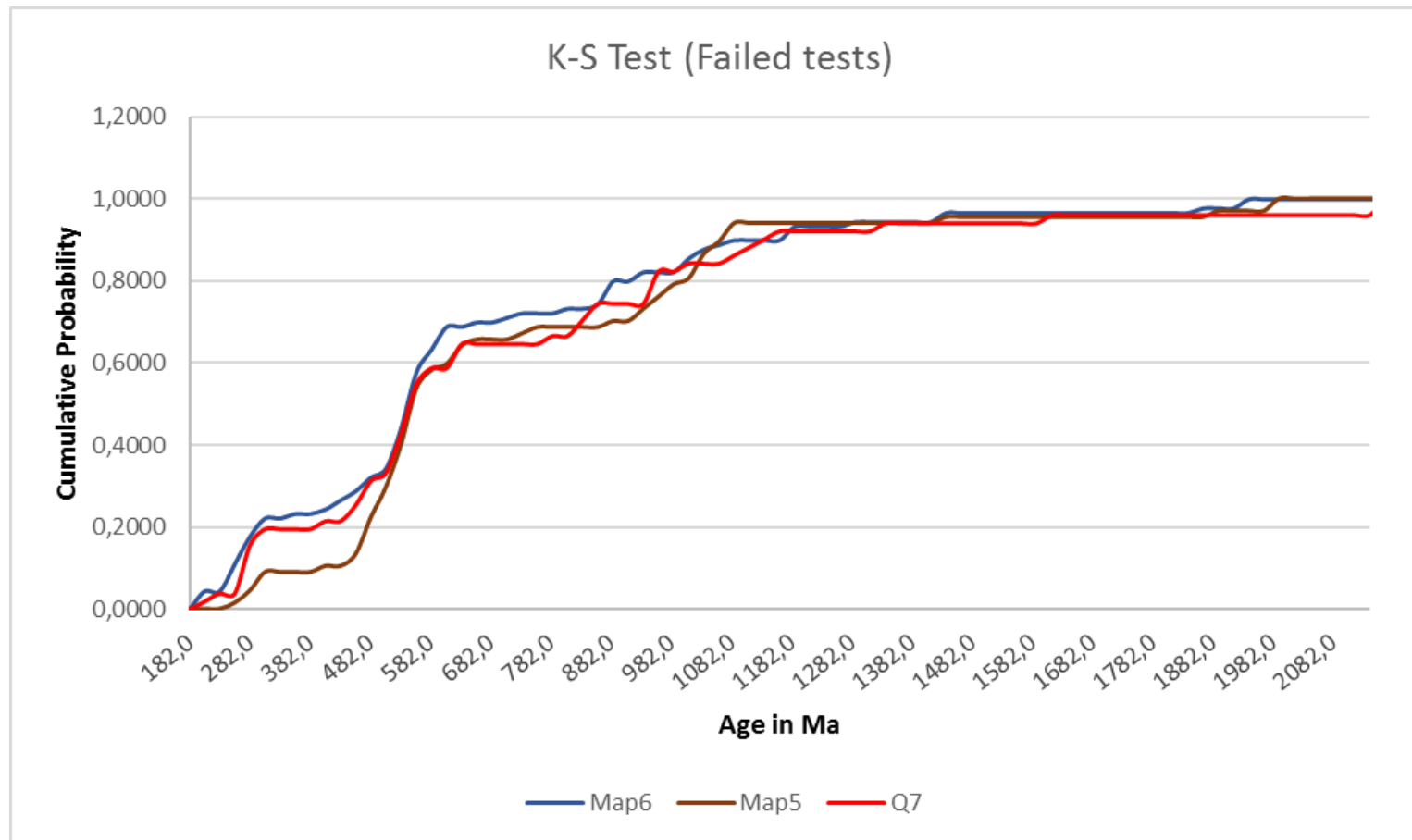
Fig. 36: K-S test P values plotted against U/Pb detrital zircon ages (Ma) for the three 'failed' samples from the original plots. These samples illustrate definite source similarities from 560,4 Ma onward and variation between Map5 and the other two samples between the Jurassic-Cambrian.

114
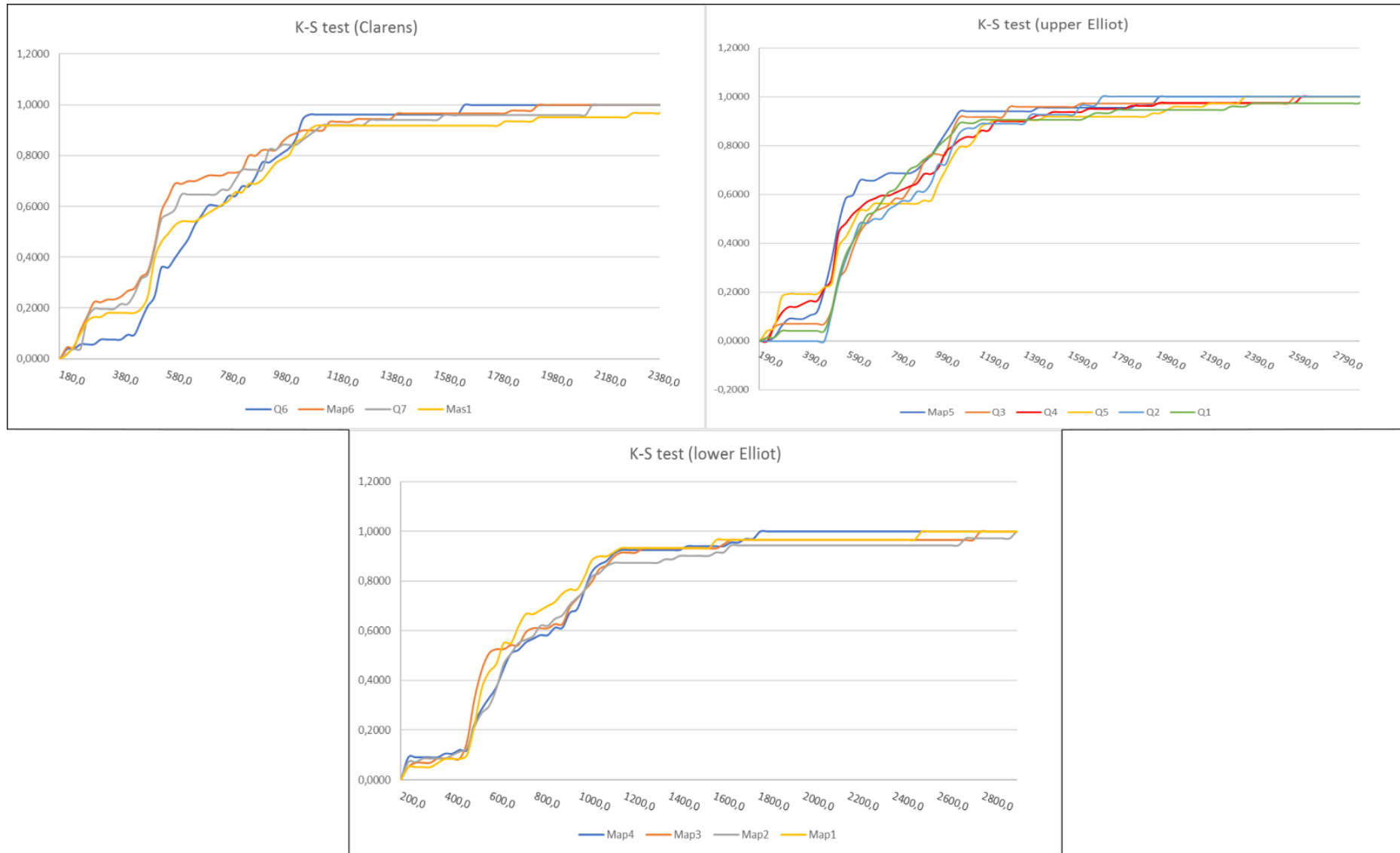
Fig. 37: Compilation of probability plots for all samples, divided into the Clarens (basal and uppermost), uEF and lEF (including the lEF-uEF contact to lEF samples) stratigraphic units.

4.3.3.3   Clarens Formation

Basal to uppermost Clarens sample probability trends all display variant younger (<500 Ma) and Cambrian-Neoproterozoic grain trends, illustrating a diverse array of sources. However, similarities in the Jurassic-Late Triassic plot sections conversely point toward a consistent, similar Jurassic-Late Triassic source input throughout the study areas. Samples Map6 and Q7 ('failed' test), as previously stated, share close cogenetic source inputs, whereas Sample Q6 hosts more discrete population sources. Overall, the Clarens samples display a more diverse source input history and a greater abundance of Jurassic source inputs.

Ultimately, these trends point toward consistent shared input sources of younger Jurassic-Triassic grains in samples associated with the lEF and Clarens Formation, whereas uEF sample variances suggest general inconsistencies in younger grain population depositional inputs.

4.3.4   Youngest maximum detrital zircon U-Pb age

Of the total fourteen (14) samples analysed: 1) two was from the lEF (Maphutseng); 2) one from the base of the lEF-uEF contact (Maphutseng); 3) five samples throughout the uEF, with intense sampling at Moyeni (4) and Maphutseng (1); 4) two from the uEF-Clarens contacts in Moyeni and Maphutseng; 5) one from the top of the Clarens (contact with Drakensberg basalts; Moyeni), and; 6) three samples from each footprint site in Moyeni (uEF), Masitise (uEF-Clarens) and Maphutseng (lEF). The age of sediment emplacement can be more accurately estimated by use of the average youngest detrital zircon ages calculated in Section 4.3.1 and derived from the collective mean of the youngest age determining methods (Table 23; 24). The abundant clustering of Cambrian-Neoproterozoic grains (major source input) and limited numbers of Triassic-Jurassic grains (limited source input) resulted in the less sensitive methods, especially TuffZirc (+8) and Weighted Mean (+8), yielding significantly older ages and collectively increasing the average youngest grain ages (Table 24, red markers). More sensitive tests, including (but not confined to) the YSG, YDZ and YPP were resultantly used to calculate the average youngest depositional ages for each sample, such that

the average ages were more representative of the less abundant younger grain populations (Table 23; 24, black circles).

Conversely, the source input of the youngest subset of detrital grains (Triassic and Jurassic), although minimal, is present within each sample (except Q2), illustrating a constant input. Collectively, the youngest single grain ages display a consistent younging up trend throughout the stratigraphy, ranging from Late Triassic basal Elliot units to the youngest Early Jurassic upper Clarens (Table 25; Fig. 38). This consistency allows for the consideration of the youngest maximum depositional single grain ages (Table 23; 25) as primary representative youngest deposition age constraints, with the more fluctuant average maximum youngest ages (Table 24) acting as supplementary absolute maximum constraints. Due to the detrital character of the samples, these youngest maximum ages do not reflect the true age of deposition; however, they provide the maximum youngest age of deposition and an insight into detrital source input dynamics.

4.3.4.1   lower Elliot Formation

The two lEF samples, Map3 and Map1, represent the mid-lEF lithologies and the underlying lowermost lEF lithologies, respectively. This excludes the lEF Maphutseng trackway site sample Map2, which is described under 'Footprint Sites'. The oldest youngest single grain age of the lEF belongs to Map1 (~70 m below the lEF-uEF contact) at an age of 216.7 Ma, with the overlying Map3 (~30 m below the lEF-uEF contact) at 206.8 Ma (Table 23; 25). The average youngest depositional ages of Map1 and Map3 are 219.3 Ma and 211.3 Ma, respectively (Table 23; 24). Collectively, the lEF (including Map2) hosts a Late Triassic Norian average maximum age of 213.1 Ma. The youngest maximum single grain and average youngest depositional ages dated in this study fall well within the Triassic (Norian) and illustrate a younging up trend. The ~10 Ma gap between the YSG ages of Map1 and Map3 are the result of different youngest source inputs.

4.3.4.2   lower Elliot-upper Elliot contact

The lEF-uEF contact is represented by Map4, extracted from the uppermost surface of the lEF-uEF regionally traceable marker layer. The youngest single grain age is 206.5 Ma, which is slightly younger than the underlying (~30.0 m below) mid-lEF sample (206.8 Ma) (Table 23; 25), displaying a consistent decrease in younger source input ages. The average maximum youngest age is 207.5 Ma (Table 23; 24).

4.3.4.3   upper Elliot Formation

The uEF is represented by five samples from both Moyeni (Quthing) and Maphutseng, namely (from stratigraphically youngest to oldest): Q5, Q4 (mid-uEF in Moyeni), Map5 (mid-uEF in Maphutseng), Q3 and the lowermost Q1 (~17 m above the uEF-lEF contact). The youngest single grain ages, within this order are: Q5 at 203.6 Ma, Q4 at 230.1 Ma, Map5 at 238.7, Q3 at 220.5 Ma and lastly, Q1 at 197.8 Ma (Table 23; 25). These trends show a unique deviation of the single grain ages, whereby the oldest sample, stratigraphically (Q1), has the youngest single grain age overall, which represents the single maximum youngest age of the uEF is 197.8 Ma. Q1 is also the only sample with an Early Jurassic input source, with the other samples displaying a distinct lack of grain input from Jurassic sources into the uEF lithologies. This could be linked to the increase in loessic and reworked deposits, as well as the decline in channelised fluvial deposits seen more frequently throughout the uEF. Although statistically biased, the presence of this single Jurassic grain at the basal uEF represents a probable minor, but true youngest source for the uEF. The average youngest maximum ages from stratigraphically youngest to oldest samples include: Q5 at 202.2 Ma, Q4 at 258.5 Ma, Map5 at 258.7 Ma, Q3 at 218.0 Ma and lastly, Q1 at 197.8 Ma (Table 23; 24). The average maximum depositional age of the uEF units (including trackway site Q2) is 273.4 Ma. This age is relatively high as a result of the aforementioned general lack of younger grain inputs into the uEF.

		Map2	Map3	Q2	Q6	Q3	Q4	Map6	Map5	Map4	Q5	Map1	Q1	Q7	Mas1
YSG	Age (Ma)	208.1 ±2.6	206.8 ±2	502.4 ±6.2	190.5 ±3.9	220.5 ±2.2	230.1 ±4.3	198.0 ±2.6	238.7 ±3.3	206.5 ±1.8	203.6 ±2.2	216.7 ±1.4	197.8 ±1.4	186.7 ±1.6	196.4 ±2.1
YDZ	Age (Ma)	208.3	206.9	500.8	191.0	220.8	230.6	197.0	238.8	206.5	203.0	216.2	197.8	186.5	196.3
	Range	±5.3/-6.1	±3.8/-3.9	±6.6/-13	±3.9/-9.3	±4.3/-5.2	±8.3/-10	±4.4/-5.1	±7.4/-7.5	±3.9/-4	±4.3/-4.5	±2.4/-3	±3.1/-3.2	±3.8/-3.4	±4.8/-4.6
	Confidence	95%	95%	95%	95%	95%	95%	95%	95%	95%	95%	95%	95%	95%	95%
YPP	Age (Ma)	210.0	220.0	500.0	490.0	200.0	280.0	200.0	300.0	210.0	200.0	225.0	500.0	260.0	250.0
TuffZirc (+8)	Age	655.2	512.5	509.7	542.0	1054.6	525.8	256.6	487.7	1037.6	530.8	542.7	515.1	236.6	515.7
	Range	±1.5/-7.7	±1.4/-10.7	±12.5/-4.0	±16.5/-9.3	±10.6/-4.1	±1.6/-1.9	±4.9/-1.9	±6.5/-5.6	±6.4/-32.6	±2.2/-2.2	±8.7/-11.2	±3.8/-7.1	±2.4/-5.0	±4.5/-2.8
	Confidence	93%	93%	93%	93%	93%	93%	93%	93%	98.4%	93%	98.4%	93%	96.9%	93%
	Total Coherent grains	8 of 8	8 of 8	8 of 8	8 of 8	8 of 8	8 of 8	8 of 8	8 of 8	7 of 8	8 of 8	7 of 8	8 of 8	6 of 8	8 of 8
Weighted Average (+8)	Age (Ma)	656.0 ±6.1 [0.9%]	513.8 ±4.2 [0.8%]	510.9 ±6.2 [1.2%]	545.0 ±10 [1.9%]	1059.0 ±3.4 [0.4%]	525.4 ±2.6 [0.5%]	256.9 ±3.1 [1.2%]	488.1 ±5.2 [1.1%]	1033.0 ±11 [1.1%]	530.4 ±1.8 [0.3%]	537.2 ±5.3 [1.0%]	515.2 ±3.4 [0.7%]	262.0 ±3.0 [1.2%]	511.4 ±3.8 [0.7%]
	Confidence	95%	95%	95%	95%	95%	95%	95%	95%	95%	95%	95%	95%	95%	95%
	Rejected	0	0	0	0	0	0	0	0	0	0	0	0	0	0
	MSWD	5.7	2.7	6.7	8.4	2.0	0.2	5.2	7.0	6.5	0.6	8.5	4.9	7.3	7.3
	Probability	0.0	0.1	0.0	0.0	0.1	1.0	0.0	0.0	0.0	0.7	0.0	0.0	0.0	0.0
YC1σ (+3)	Age (Ma)	524.1 ±6.7 [1.3%]	492.6 ±6.1 [1.2%]	505.4 ±6.3 [1.2%]	467.2 ±5.9 [1.3%]	224.4 ±2.9 [1.3%]	276.0 ±3.6 [1.3%]	199.7 ±2.7 [1.4%]	482.6 ±6.0 [1.2%]	499.4 ±6.1 [1.2%]	265.0 ±3.4 [1.2%]	506.0 ±6.0 [1.2%]	507.4 ±6.0 [1.4%]	261.9 ±3.1 [1.2%]	249.0 ±3.0 [1.2%]
	Systematic Error	1.1	1.1	1.1	1.1	1.1	1.1	1.1	1.1	1.1	1.1	1.1	1.1	1.1	1.1
	MSWD	1.1	1.4	0.6	0.3	11.4	0.1	1.5	0.5	0.8	2.9	0.4	1.0	2.9	2.8
YC2σ (+3)	Age (Ma)	524.1 ±8.8 [1.7%]	492.6 ±7.9 [1.6%]	505.4 ±8.2 [1.6%]	467.2 ±7.9 [1,7%]	224.4 ±3.8 [1.7%]	276.0 ±4.8 [1.7]	199.7 ±3.8 [1.9%]	482.6 ±7.6 [1.6%]	499.4 ±7.6 [1.5%]	265.0 ±4.5 [1.6%]	506.0 ±7.0 [1.4%]	507.4 ±7.3 [1.4%]	261.9 ±3.8 [1.4%]	249.0 ±3.8 [1.5%]
	Systematic Error	1.1	1.1	1.1	1.1	1.1	1.1	1.1	1.1	1.1	1.1	1.1	1.1	1.1	1.1
	MSWD	0.3	0.3	0.1	0.1	2.9	0.02	0.4	0.1	0.2	0.7	0.1	0.3	0.7	0.7
Average youngest depositional age (Ma)		208.8	211.2	504.9	190.8	218.0	258.5	198.9	258.7	207.5	202.2	219.3	197.8	186.7	196.5

Table 23: A summary of all the youngest detrital ages derived from the seven methodologies and the resultant average youngest depositional ages for all 14 samples. Note: shaded (blue) ages indicate the ages used to calculate the average youngest depositional age for each sample.
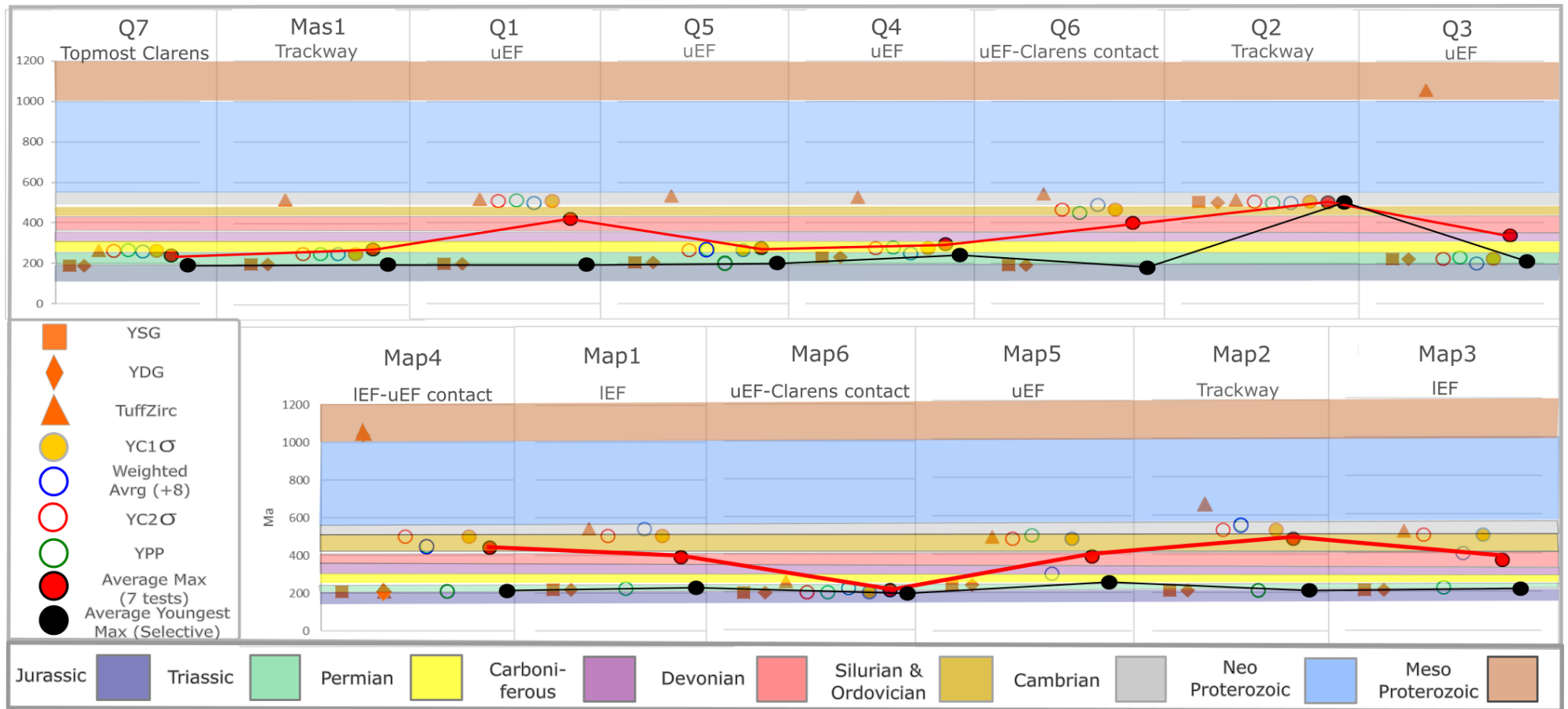
Table 24: A graphical representation of the 14 samples analysed in this study. The seven main methodologies, their collective mean ages (red markers) and the average maximum youngest ages based on the selection of sensitive test ages (black markers) are plotted, with the average trends represented by the red and black lines.
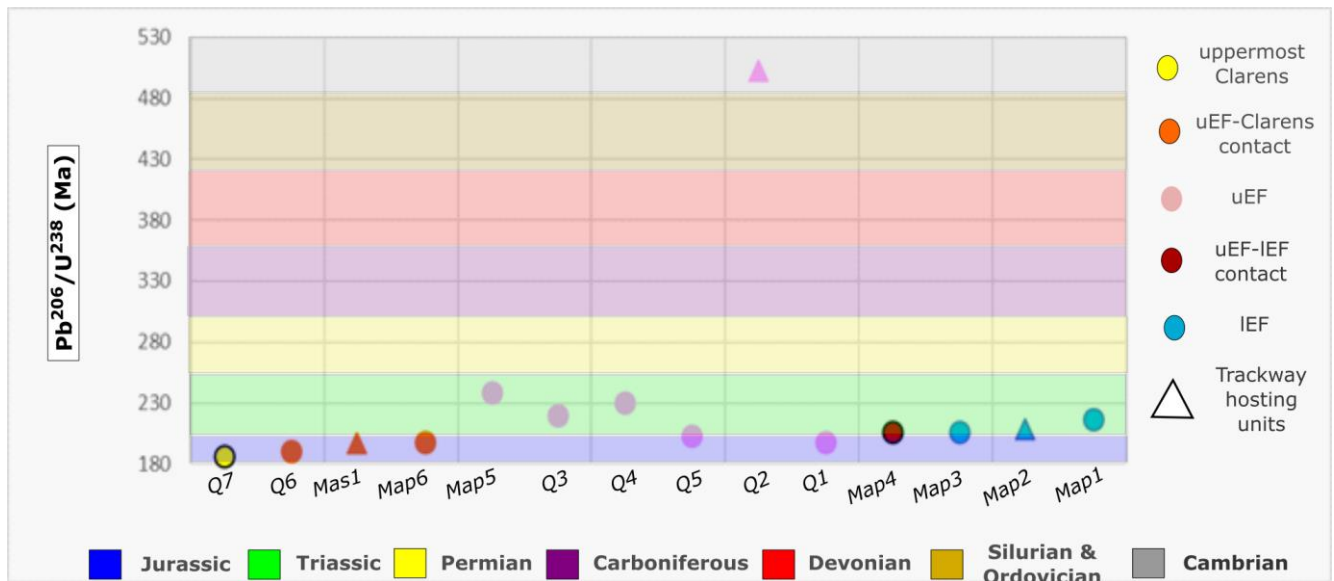
Table 25: The distribution of the youngest maximum single grain ages for each sample. Although some variants occur, the general younging up trend displays an increase in single grain ages with lowering stratigraphic sample positions (left to right: uppermost Clarens to lowest lEF exposure). Note: the relative stratigraphic position of each sample is annotated by the data point colour and samples that are directly associated with trackway-bearing surfaces are represented as triangles.

4.3.4.4   upper Elliot-Clarens contact

The uEF-Clarens contact comprises of two (2) samples from Maphutseng and Moyeni (Quthing). Another sample (Mas1) was taken at the uEF-Clarens contact at Masitise and discussed under 'Footprint Sites'. The youngest single grain ages include the Early Jurassic Q6 at 190.5 Ma and Map6 at 198.0 Ma (Table 23; 25). The average youngest depositional age of Q6 is 190.8 Ma and 198.9 Ma for Map6 (Table 23). It should be noted that Map6 hosts a comparatively robust younger grain population, pointing toward an uncharacteristic abundance of younger Jurassic and Triassic source inputs into the Maphutseng uEF-Clarens contact deposits (Table 24; Fig. 25). The average maximum depositional age for the uEF-Clarens contact (including Mas1) is constrained to a 194.5 Ma Early Jurassic (Sinemurian) age.

4.3.4.5   Top of Clarens

The top of the Clarens Formation beds exposed in Quthing, is represented by one sample, namely: Q7. Q7 has a youngest maximum single grain age of 186.7 Ma and an average maximum youngest depositional age of 186.7 Ma (Table 23; 24; 25). This Early Jurassic youngest maximum depositional age (186.7 Ma) falls well within the stratigraphic constraint of the Pliensbachian.

4.3.4.6   Footprint sites

Remaining within the focus of this study, direct temporal analysis of well-known trackway sites provides a more direct temporal association with these marker units. A total of three (3) trackway-bearing units were directly analysed, including the lower Moyeni footprint site (Q2), the Masitise Cave House trackway (Mas1) and the Maphutseng trackway platform (Map2). The lower Moyeni trackway, positioned within the uEF, stratigraphically lies <1 m above the previously mentioned Q1 (197.8 Ma). The Masitise Cave House trackway occurs on the uEF-Clarens Formation boundary and the Maphutseng trackway is set within the upper segment of the lEF, <20 m below the lEF-uEF contact as established by Bordy et al. (2015). Youngest maximum single grain ages range from 208.1 Ma for sample Map2, 502.4 Ma for Q2 and 196.4 Ma for Mas1 (Table 25). The youngest single grain ages of both the Maphutseng (208.1 Ma) and Masitise Cave House (196.4 Ma) trackways follow the younging up trend relative to their respective stratigraphic positions fairly consistently (Table 25). The average youngest maximum depositional ages include: 208.8 Ma for Map2, 504.9 Ma for Q2 and 196.5 Ma for Mas1. The lower Moyeni trackway sample presents a good average group clustering as seen in Table (24), however, through the complete lack of younger (Early Jurassic) single grains it is evident that a negligible amount of younger grain inputs belonging to Jurassic-Triassic populations were deposited in this stratigraphic unit.
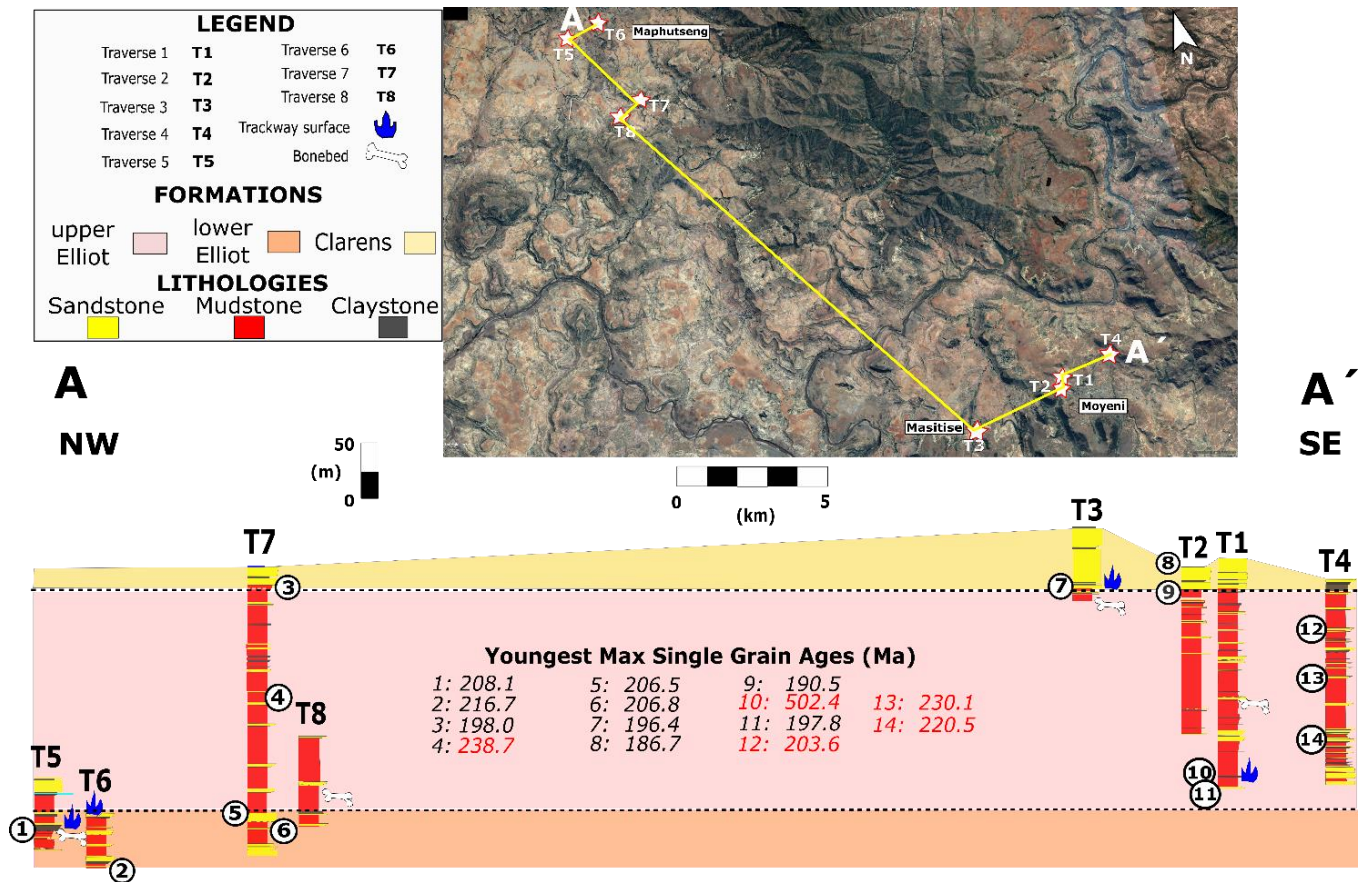
Fig. 38: Stratigraphic compilation (A to A') of all 8 Traverses. The indicative youngest single grain ages (Ma) of each of the fourteen (14) radiometrically dated samples are marked and numbered relative to their stratigraphic positions. All single grain ages imply plausible maximum depositional ages throughout the regional stratigraphy, however red highlighted ages belong to the previously ascertained younger-grain poor uEF units. Black numbered ages present the consistent and relatively robust single grain ages used in the regional temporal framework.

123

5   DISCUSSION

5.1   Palaeoenvironmental evolution

The Elliot and Clarens formations have received significant attention with regard to their unique fossil vertebrate heritage, which allows the global correlation of these Upper Triassic to Lower Jurassic units (e.g., Ellenberger, 1970; Olsen and Galton, 1984; Kitching and Raath, 1984; Lucas and Hancox, 2001; Knoll, 2004; Yates, 2005; Knoll, 2005; Irmis, 2011; McPhee et al., 2017). While the unique biostratigraphic record of the Elliot and Clarens formations has been placed into a firm lithostratigraphic framework (e.g., Botha, 1968; Beukes, 1970; Le Roux, 1974; Johnson, 1976; Eriksson 1983; 1986; Smith et al., 1993; Johnson et al., 1996; Smith and Kitching, 1997; Bordy et al., 2004a, b, c, d; Bordy et al., 2005; Holzförster, 2007; Smith et al., 2009; Bordy and Eriksson, 2015; Sciscio et al., 2017a), its global stratigraphic correlation requires further refinement. This prompted the more recent magnetostratigraphic investigation by Sciscio et al. (2017a), which successfully matched the units to global counterparts, but lacked the desired temporal precision. This ultimately motivated this project, which aimed to provide a maximum depositional temporal framework for the Elliot and Clarens Formations at 3 sites in the SW part of Lesotho.

The multidisciplinary approach utilised within this study included in-depth facies, architectural element (geometry, proportions and spatial distribution of assemblages) and lithostratigraphic analyses at the three study sites, in addition to radiometric isotope (U/Pb) detrital zircon dating. The facies and architectural element analyses of this study confirm the widely accepted progressive aridification trend associated with the Stormberg Group (Eriksson, 1981; Eriksson, 1985; Eriksson, 1986; Smith et al., 1993; Bordy et al., 2004a, c; Holzförster, 2007; Bordy and Eriksson, 2015). However, sedimentological variations regarding unique marker units are prevalent throughout the localised stratigraphy, ultimately providing a clearer and more refined local palaeoenvironmental reconstruction. The stratigraphic consistency of the Early Jurassic-Late Triassic detrital zircons make

124

them ideal primary constraints for the youngest maximum depositional age interpretations (Fig. 38).

These youngest single grain ages offer a baseline chronostratigraphic framework for the Elliot and

Clarens formations, which falls well within the radiometrically and biostratigraphically constrained

ages of the capping Drakensberg Basalts (183 ±1 Ma; Duncan et al., 1997) and basal lEF Norian

faunal assemblages (Kitching and Raath, 1984; Lucas and Hancox, 2001; Knoll, 2004) (Fig. 38). These

age constraints, in conjunction with the correlated stratigraphy for this study, provide a crucial

timeline, which consequently aids in the further refinement of the TJB and ETE stratigraphic

positions in southern Africa (Fig. 39).
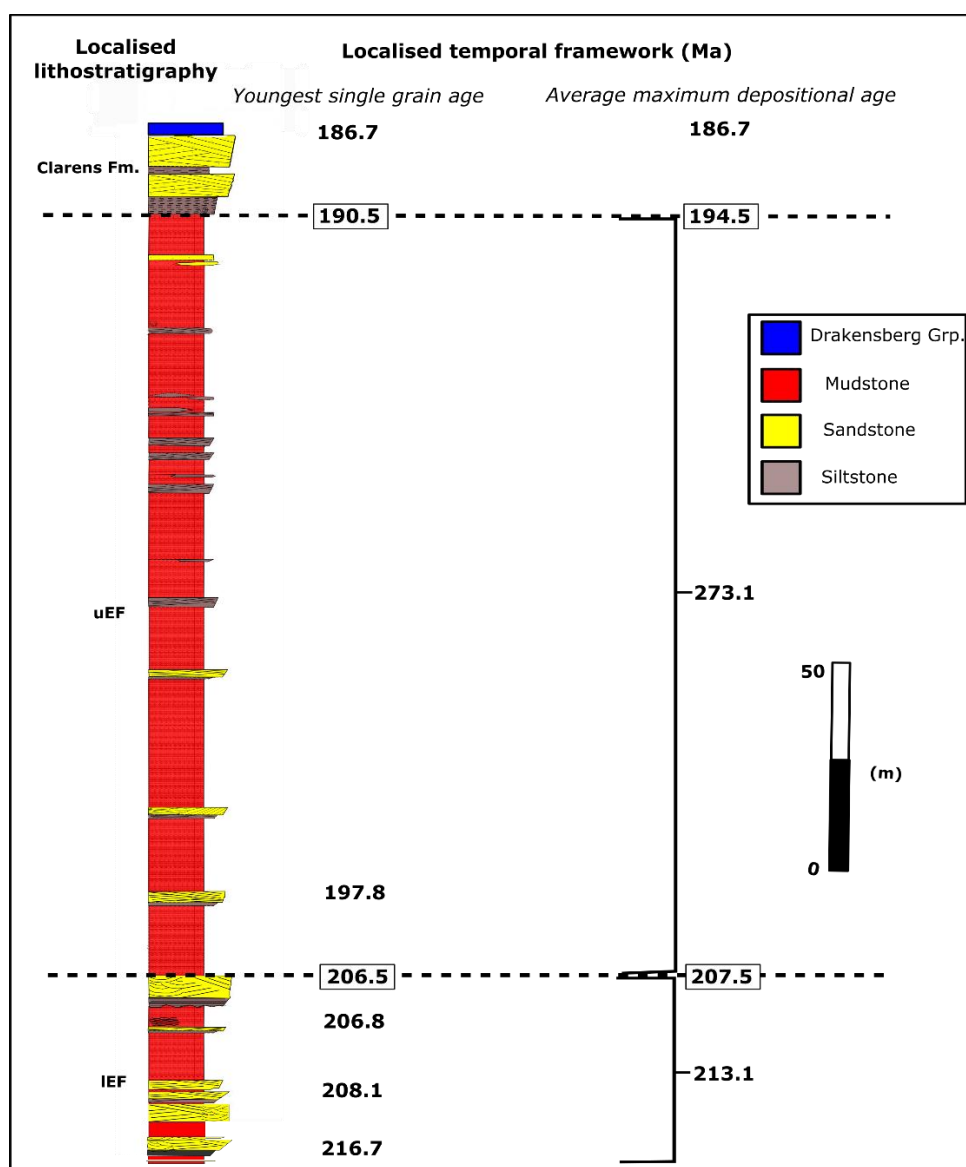
Fig. 39: Chronostratigraphic framework of the three study areas. In this study the youngest single grain ages act as the primary absolute age constraints, supplemented with the average maximum depositional ages of each stratigraphic unit.

The fourteen radiometrically dated samples (Fig. 38) additionally provide the first insight into detrital zircon provenance variations seen throughout the localised stratigraphy. Previous basinal provenance works by Botha (1968), Beukes (1970), Visser (1984), Johnson (1991), Cole (1992), Catuneanu et al. (1998) and Bordy et al. (2004b) were primarily based on palaeocurrent datasets and petrographic results, which show changing sediment supply patterns. These datasets pinpointed sediment sources predominantly in the south, south-east and west. Specific emphasis was placed on the reworking of the lower Karoo strata and Cape Supergroup (Johnson, 1991; Cole, 1992; Catuneanu et al., 1998; Bordy et al., 2004b). Sandstone petrographic studies implied a differential, tectonically driven provenance model, dominated by a recycled orogenic source in the south and south-west (Cape Fold Belt). Some petrographic variations in the uEF, initially interpreted as a direct result of increased aridity (e.g., Visser and Botha, 1980; Eriksson et al., 1994), in conjunction with palaeocurrent data was implied by Bordy et al. (2004b) to originate from a 'intra-basinal palaeohigh' west of the basin. Palaeocurrents from large-scale cross-bedded sandstones in the Clarens Formation very consistently show a main current direction from west to east (Beukes, 1970; Visser, 1984; Eriksson, 1986; Holzförster, 2007). Catuneanu et al. (1998) suggested a widely accepted basinal tectonic-driven provenance model, whereby Stormberg Group deposition from the Late Triassic onward was confined to a single source, the Cape Fold Belt. This single source constituted of pre-Stormberg strata and Cape Supergroup units actively supplying sediments driven by the final orogenic unloading in the Karoo foreland basin system. Tankard et al. (2009) pointed toward a transtensional Stormberg basinal setting, confined by subsidence of the Natal basement in the east and contemporaneous uplift of the Namaqua basement in the south and north-west. This resulted in the erosion of the older Beaufort Group. As reasoning stands, the overall Elliot and Clarens sequences define a generally coarsening upward trend, synonymous with an orogenic unloading dominance (Catuneanu et al., 1998); however, grain cluster signatures and provenance indicators found within this study offer a more diverse provenance model.

Interestingly, all of the samples in this study generally share identical grain population clusters. However, some younger grain source variances occur between the stratigraphic units, especially the uEF as displayed in the grain population distributions and K-S test results (<300 Ma) (Fig. 34; 37). The overall genetic similarity amongst the samples, in accordance with dominantly positive K-S test results, attest to similar 'major' input sources of sedimentation throughout the Elliot and Clarens formations (Fig. 35). Comparatively, geochronological radiometric age clusters derived from all 14 samples in this study and Devonian-Ordovician Cape Supergroup grain distributions similarly indicate major peak clusters at the Cambrian-Neoproterozoic and Neoproterozoic-Mesoproterozoic populations (Fourie et al., 2011). This strong likeness in peak grain ages, alongside the weathered, rounded to fragmentary nature of zircon grains confirm a major reworked source (pre-Stormberg and Cape Supergroup). However, some cluster variations and more euhedral, magmatic, grain morphologies indicate more direct source inputs (e.g., Patagonia and Antarctica terranes). The very minor inputs of Jurassic grains range from poor source inputs (or general lack thereof) in the uEF, to the more consistent, shared source inputs in the Clarens Formation, which are linked to direct source inputs from magmatic Patagonian sources (Pankhurst et al., 1993; Pankhurst et al., 2006; Pankhurst et al., 2014; Riley et al., 2016). Higher concentrations of Triassic-Permian grains (especially within the lEF) are correlated to direct Patagonian source inputs and more constant recycled source inputs from the proximal Triassic-Carboniferous older Karoo Supergroup strata (Turner, 1999; Werner, 2006; Fildani et al., 2009; Rubidge et al., 2013; McKay et al., 2015).

One might argue the distinct shared Cape Supergroup population clusters were inherited solely from older Karoo sediments; however, comparisons with recent detrital zircon focused studies of the Dwyka Group (Craddock and Thomas, 2011), Ecca Group (Walters, 2017 [Unpublished]) and Beaufort Group (Viglietti et al., 2018) suggest varying influences on the provenance history. Comparatively, the Dwyka units display a variety of major Proterozoic sources (Craddock and Thomas, 2011). In particular, the major peaks of the Western- and Southern Cape units are similar to those of this study. The Ecca and Beaufort groups share three similar major population peaks with

127

those seen in this study; however, the relative major source concentration ratios vary greatly. The Ecca and Beaufort Group populations are dominated by a major youngest Carboniferous-Triassic peak and more minor Cambrian-Neoproterozoic and Mesoproterozoic peaks. These shared population clusters indicate a definite recycled older Karoo Supergroup influence on the upper Karoo sediment supply, especially regarding Carboniferous-Permian and minor Triassic populations sources. Similarities in older population densities between the older Karoo units and upper Karoo sediments from this study implies little change with regard to major recycled source areas. The Cape Supergroup, as previously established, thus presents an irrefutable source influence, alongside additional direct 'source to sink' magmatic and metamorphic sources (including Namaqua-Natal Metamorphic Belt and Saldania Orogeny).

This diverse, recycled and mixed source dominant input model proposes a more dynamic tectonic influence than the current first-order orogenic unloading model. Comparative petrographic and geochemical analyses were not utilized in this study; however, might in future further aid the resolution of the probable upper Stormberg depositional sources and offer a greater understanding of the associated tectonic basin-fill.

5.1.1   lower Elliot Formation

The lEF beds form the basal beds of the Maphutseng traverses from this study and are characterized by their thick multi-storey meandering fluvial and associated overbank facies deposits. FA 2 fluvial units are the pervasively dominant units throughout the lEF, with main channel (CH) body morphologies ranging from narrow fixed shallow ribbons, to broad unconfined sheets, to complex, relatively laterally continuous, thick multi-storey mobile channels (CH). These thick, stacked channel units, are associated with: asymmetrical, deeply incised basal scour hollows (HO); extensive, interconnecting channel wings (CW); and, lateral accretions (LA) associated with channel meandering (Fig. 40). As proposed by Bordy et al. (2004a), these thick, relatively continuous channel fill bodies can be described as perennial in nature. Point and scroll bars are common and host a

128

variety of Triassic trackways. Load cast bearing, massively bedded units of sandy bedforms (SB), limited to the lEF, act as verification of the variability in the fluvial dynamics, illustrating periods of increased energy deposition. Intercalated successions of pedogenically altered overbank deposits, including crevasse splays and levees (FA 3) and floodplain fines (FA 1), indicate intermittent periods of extensive flooding and subsequent energy waning. Rarer instances of backswamp-type LC water bodies (FA 5) are found within the floodplain fines. Collectively, these architectural elements and facies associations provide proof of a dynamic, mobile fluvial dominated local depositional setting with periods of increased and waning flow energy (Fig. 40). This interpretation of the lEF palaeoenvironmental meandering fluvial setting with intermittent floodplain fines agrees with previous basin-wide interpretations of the lEF (Stockley, 1947; Botha, 1968; Le Roux, 1974 [Unpublished]; Eriksson, 1983 [Unpublished]; Smith et al., 1993; Johnson et al., 1996; Johnson et al., 1997; Smith and Kitching, 1997; Bordy et al., 2004a, b, c, d).

The lEF displays a general upward coarsening trend of the lEF units at Maphutseng. This coarsening abruptly stops at the top of the thick, laterally continuous marker unit, which denotes the lEF-uEF contact. The youngest maximum (single grain) age (Fig. 38) attained from the lowermost lEF unit of Maphutseng interestingly shows an age of 216.7 Ma. It should be noted that this lowermost lEF exposure is not the oldest lEF unit, but rather representative of a middle lEF unit. Nonetheless, its single zircon youngest maximum age of 216.7 Ma, sets these lEF exposures well within the Late Triassic Norian. This age coincides well with the biostratigraphically defined lEF temporal framework set by Lucas and Hancox (2001) and Knoll (2004); however, is comparatively older than the ~213 Ma basal lEF age constraint provided by Sciscio et al. (2017a). The aforementioned slightly older source dominant nature of this unit (Map1) and detrital nature of the maximum youngest single grain age; however, does not completely disprove the eligibility of Sciscio's basal lEF age constraint. Subsequent overlying lEF samples show a consistent younging up trend of youngest maximum ages up to the lEF-uEF contact, which was dated at 206.5 Ma (Fig. 39;

129

40). This infers that the Upper Triassic lEF at Maphutseng spans from the Norian to Rhaetian (216.7-206.8 Ma).

Local palaeocurrent indicators show a generally north-east (NE) flowing fluvial environment; however, the basal units of the lEF at Maphutseng show some variance with SE and SW indicated flows. This variance is likely the result of secondary channels diverging and meandering channel palaeocurrent variation. Palaeocurrent directions in the regional work of Bordy et al. (2004b) show a very strong prevalence in north directed flows in the lEF, with only 40 measurements out of 370 (~10%) indicative of currents directed from NE to SW. Therefore, the current study of the uEF at Maphutseng mimics the regional palaeocurrent distribution pattern of the lEF well. This similarity in the drainage patters, together with the results on the type and location of source areas (e.g., reworking of pre-Stormberg strata), provides further, albeit highly localized, evidence for the overfilled phase basinal model for the Stormberg Group, suggested by Catuneanu et al. (1998) and further refined by Bordy et al. (2004b; 2005). As indicated in Fig. (4), the higher energy, meandering fluvial system of the lEF at Maphutseng, in conjunction with the general coarsening upward grain size trend in the lEF, can possibly point toward an increasingly higher palaeoslope at this study site.
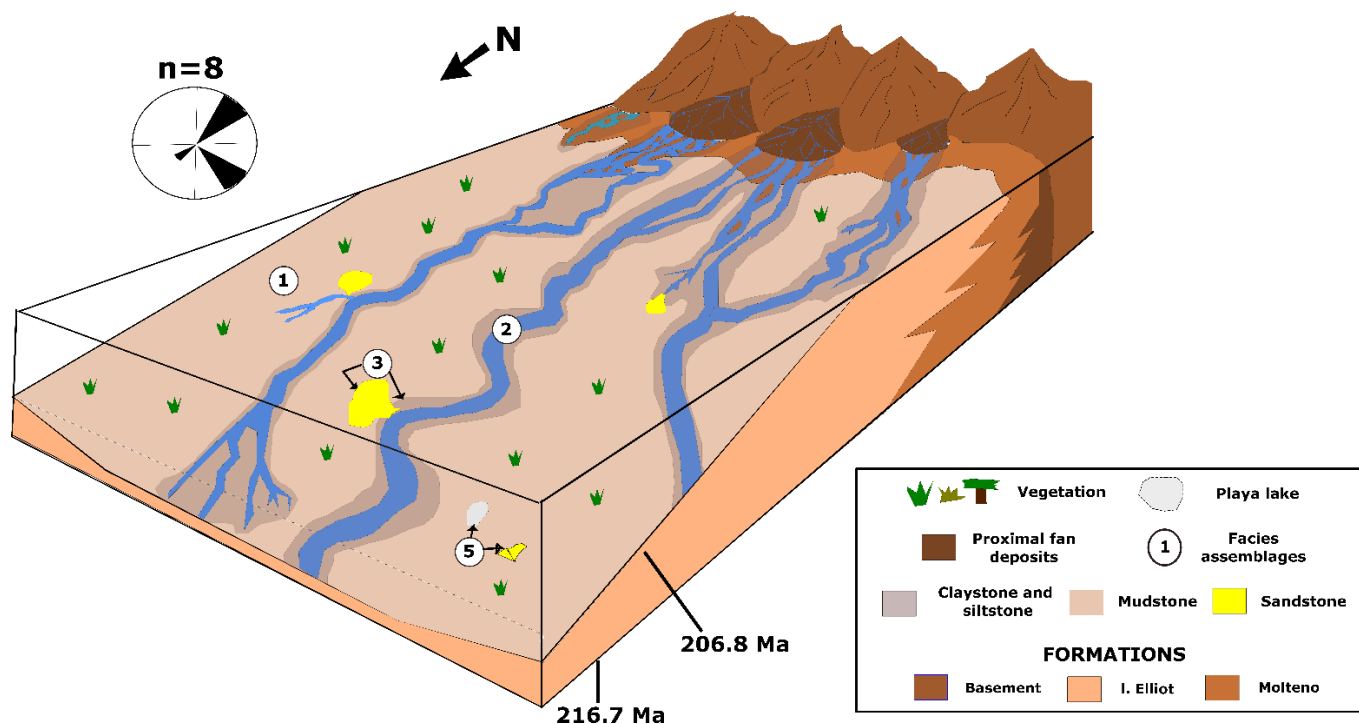
Fig. 40: Schematic model illustrating a local palaeoenvironmental reconstruction of the FA 2 fluvial dominated deposition in the lEF. Interbedded units of overbank material FA3 and FA 5 occur throughout the well-vegetated FA 1 floodplain fines. Fluvial channels are dominantly perennial meandering systems with commonly associated secondary channels. Note: lEF palaeocurrent readings included in the attached rose-diagram as well as the youngest single grain depositional temporal constraints. Illustration not to scale.

5.1.2   upper Elliot Formation

In contrast to the underlying lEF, the uEF alters from predominantly meandering channels-dominated fluvial successions to a flash flood dominated depositional regime, characterized by pedogenically altered, massively bedded mudstone-rich successions. The deposition of thick units of floodplain fines (FA 1), which often host pedogenic nodules, calcareous rhizoliths, desiccation cracks, soil peds and calcareous infill/surfaces, was punctuated by extended periods of drying, resulting in the oxidative processes (rubification) linked to the familiar continental 'red bed' successions. The combination of pervasive pedogenic alteration, extended periods of drying and aeolian input (loess) are strong indications of depositional hiatus periods. These loessic sediments in FA 1 deposits become more prevalent in the upper part of the uEF stratigraphy. An upward increasing dominance of interbedded poorly-channelised fluvial sandstone bodies (FA 2/5), comprising of thin, single ribbon-type channel (CH) bodies with a sheet-type architecture typify the uEF at all 3 study sites. Conversely, thick, channelised, multi-storey tabular CH and laterally accreted (LA) FA 2 sandstone

bodies are concentrated, and largely limited, to the basal uEF of Quthing (Fig. 41). The more common, intermittent, individual sheet sandstones (FA 2/5) can comparatively be classified as products of sheetfloods, which were predominantly ephemeral by nature (Turner, 1981; Stear, 1983; Sneh, 1983; Tunbridge, 1984; Stear, 1985; Kelly and Olsen, 1993; Miall, 1996; Hampton and Horton, 2007; Bordy et al., 2004a).

Previous works focusing on tectonic controls on alluvial architecture suggest a dominance in floodplain deposits (FA 1) and individual unconstrained ephemeral sheetfloods (FA 2/5) are directly proportional to increased tectonic subsidence rates, connotated to a resultant increase in accommodation space (Allen, 1978; Bridge and Leeder, 1979; Hampton and Horton, 2007). The intense pedogenic alteration noted throughout the uEF, alternatively concurs with the suggested diminished basin-wide orogenic unloading associated with decreased subsidence noted by Bordy et al. (2004b) throughout the uEF deposition. The localised nature of this study; however, does not allow for any definite interpretations in this regard and further regional study is required.

Aside from the dominant FA 1 pedogenically altered floodplain fines and alluvial architectural variations within the uEF, additional calcretized FA 3 crevasse splay (CS) siltstone lenses occur abundantly throughout the thick FA 1 successions. An increase in intermittent ephemeral fluvial bodies is accompanied by increased occurrences of FA 5 ephemeral lake (LC) and laminated sandsheets (LS). The internal structures of the laminated sandsheets range from: massive and planar cross-bedded as a result of rapid flashflood events; to clay-rich, pedogenically altered, ripple cross-laminated aeolian loessic material deposits. These pervasively more aeolian units, including instances of aeolian dune (FA 4) beds, become more common toward the uppermost uEF (Fig. 41). The uEF section of Maphutseng (Traverse 5) also hosts a pedogenic glaebule conglomerate (FA 6) similar to the marker bed, which Bordy et al. (2004a) termed the 'hallmark' of the uEF. The floodplain denudation model in this study, although localised, additionally provides proof of flashflood related gullying (and arroyos) in the ancient uEF FA 1 loessic-rich units. This flashflood

driven gullying is a likely consequence of periods of increased erosion, which modern-day analogues have shown not to be limited to individual factors (Rydgren, 1988; Bull, 1997; Grab and Deschamps, 2004). In addition to tectonics, increased climatic aridity may well also play a role, with increased unconfined clay-rich palaeosols providing ample opportunity for significant denudation, comparatively similar to what is seen in the majority of modern day Lesotho (Van Zijl, 2010 [Unpublished]).

The increasingly arid deposits within the uEF was largely determined by the relative palaeogeographic and palaeolatitudinal positioning of southern Africa and semi-arid palaeosol indicators within the calcretized floodplain fines (Botha, 1968; Le Roux, 1974; Eriksson, 1983; Smith and Kitching, 1997; Bordy et al., 2004a, b, c, d; Smith et al., 2009). The uEF facies in this study displayed a definite palaeoclimatic shift from the perennial rivers reconstructed in the lEF to the episodic fluvial and lake sedimentation indicative of semi-arid to arid conditions in the of the uppermost uEF. This climatic shift also implies variations in discharge, sediment yield and seasonality; highlighted by the general waning of the fluvial environment, increasingly episodic sedimentation and prolonged 'drier' seasonal periods when calcretization of soils dominated (FA 1). The palaeoclimatic shift is further evidenced by the increased predominance of: surface desiccation cracks; rubification; calretized rhizoliths; ephemeral sheet-flows; playa-lakes (LC); loessic LS beds, and; rarer aeolian dune beds (FA 4). In-depth palaeosol classifications were not attempted in this study; however, may in future offer a more detailed view on palaeoprecipitation trends and sedimentation seasonality (Cecil and Dulong, 2003).

The FA 1 dominated overall fining up trend seen throughout the localised uEF exposures of this study occurs due to a combination of palaeoclimatic and tectonic allogenic controls (Miall, 1991; Catuneanu et al., 2011). The general fining upward trend of the local uEF differs from the systematic regional study of Bordy et al., (2004a, b, c; 2005), whereby grain size change within the uEF was not detected. This fining upward trend at the uEF study sites of this investigation, can be attributed to a

local palaeoslope variation of the accepted basinal tectonic and climatic models based on regional and more robust datasets (e.g., Bordy et al., 2004a, b, c, 2005; Catuneanu et al., 1998; 2009; 2011). Palaeoslope is generally considered inversely proportional to discharge and positively proportional to grain size, thus the gradual upward fining can be roughly equilibrated to the overall decrease of the palaeoslope angle (Hickson et al., 2005). The concept of a greater tectonic and lesser climatic influence on the deposition of the Elliot Formation, although previously discussed in Catuneanu et al. (1998), Turner (1999) and Bordy et al. (2004a, b, c; 2005), remains relatively unclear, while sequence stratigraphic tectonic interpretations of continental deposits remain complex (Allen, 1978; Bridge and Leeder, 1979; Schumm, 1985; Hampton and Horton, 2007; Catuneanu et al., 2009).

Palaeocurrent indicators, although limited, show a bivariate trend in dominant flow directions; with SE trending (n=8) flows in Maphutseng and NE trending (n=6) flows in Quthing (Moyeni). Previous studies documented regional palaeocurrent direction from south to north in the lEF and uEF, with an additional west to east in the uEF (see Bordy et al. 2004b for a discussion and review). Consequently, the NW-SE palaeoflows of the Maphutseng uEF point toward an additional sediment input from the north, which may include older Karoo strata as well as the NW Mesoproterozoic Namaqua-Natal basement. This source from the north has not been documented in previous studies of the lEF, however its significance, especially in the light of the very few measurements in this study, can only be tested via more robust regional studies in the broad vicinity of Maphutseng. The north-easterly palaeoflows in uEF of Quthing fit well the overall uEF regional patterns. These NE directed drainage patterns point toward a SW provenance source, which coincides with the originally suggested reworked sedimentary older Karoo strata and Cape Supergroup sources.

As previously stated, the youngest (single grain) maximum depositional ages of the majority of uEF samples do not follow the consistently younging up single zircon age trends of other lEF and Clarens samples. This inconsistency is the result of a general lack of younger grain inputs in the uEF. The aforementioned increased aridity and pervasive depositional hiatuses throughout the uEF

resulted in dominantly pedogenically altered loessic-type units that comprised of concentrated recycled sediments, in conjunction with the pervasive depositional hiatus-type setting, ultimately diluting the younger grain source inputs. Unsurprisingly, the stratigraphically lowest uEF sample, sampled from one of the rare few channelised fluvial deposits (FA 2), situated ~17 m above the last lEF sandstone unit, shows evidence for a consistent, Early Jurassic grain input. This sample provides a Sinemurian youngest single grain maximum age of 197.8 Ma (Fig. 38; 39). This facies-dependent grain compositional bias reiterates and highlights the important role basinal tectonism and resultant varying facies deposits have on detrital material input (Catuneanu et al., 1998; Bordy et al., 2004a, b, c; 2005).

The lEF-uEF contact at Maphusteng is distinguished by the relatively sudden detrital composition and architectural change from basal multi-storey fluvial channel dominated successions in the lEF to directly overlying fine-grained, pedogenically altered floodplain deposits in the uEF. The sudden change in lithofacies, architectural elements, grain size and lack of discernable erosional surface, define a paraconformity. This intra-formational contact at Maphutseng is likely to be the local manifestation of the previously proposed 2nd order paraconformity presented by Bordy et al. (2004a, c) in their regional study based on lithostratigraphic grounds. Bordy et al. (2004a, c) attributed this unconformity at the lEF-uEF contact to foreland basin tectonics and ascribed the associated distinct changes in facies architecture, provenance and pedogenic alteration to tectonics, as well as palaeoclimatic changes (aridification as mentioned earlier in this section).

A radiometrically dated representative sample (Map4) was extracted from the uppermost surface of the thick, regionally extensive, FA 2 sandstone unit directly underlying the uEF-lEF contact at Maphutseng. This marker unit significantly provides a Rhaetian (Late Triassic) youngest maximum single zircon age of 206.5 Ma. Comparatively, the lowermost uEF sample, taken ~17 m above the lEF-uEF contact, displays a youngest maximum age set well within the Early Jurassic Sinemurian (197.8 Ma). This 8.7 Ma 'jump' in relative ages over a vertical stratigraphic distance of ~17 m verifies the

presence of a stratigraphic gap, which is interpreted as the aforementioned lEF-uEF contact 2nd order regional paraconformity. The lowermost uEF youngest single grain derived maximum depositional age (197.8 Ma) additionally verifies that the majority of uEF sediment deposition occurred within the Early Jurassic; and compares well with previously determined bio- and magnetostratigraphic correlations of the uEF (e.g., Kitching and Raath, 1984; Olsen and Galton, 1984; Lucas and Hancox, 2001; Knoll, 2004; Knoll, 2005; Sciscio et al., 2017a).
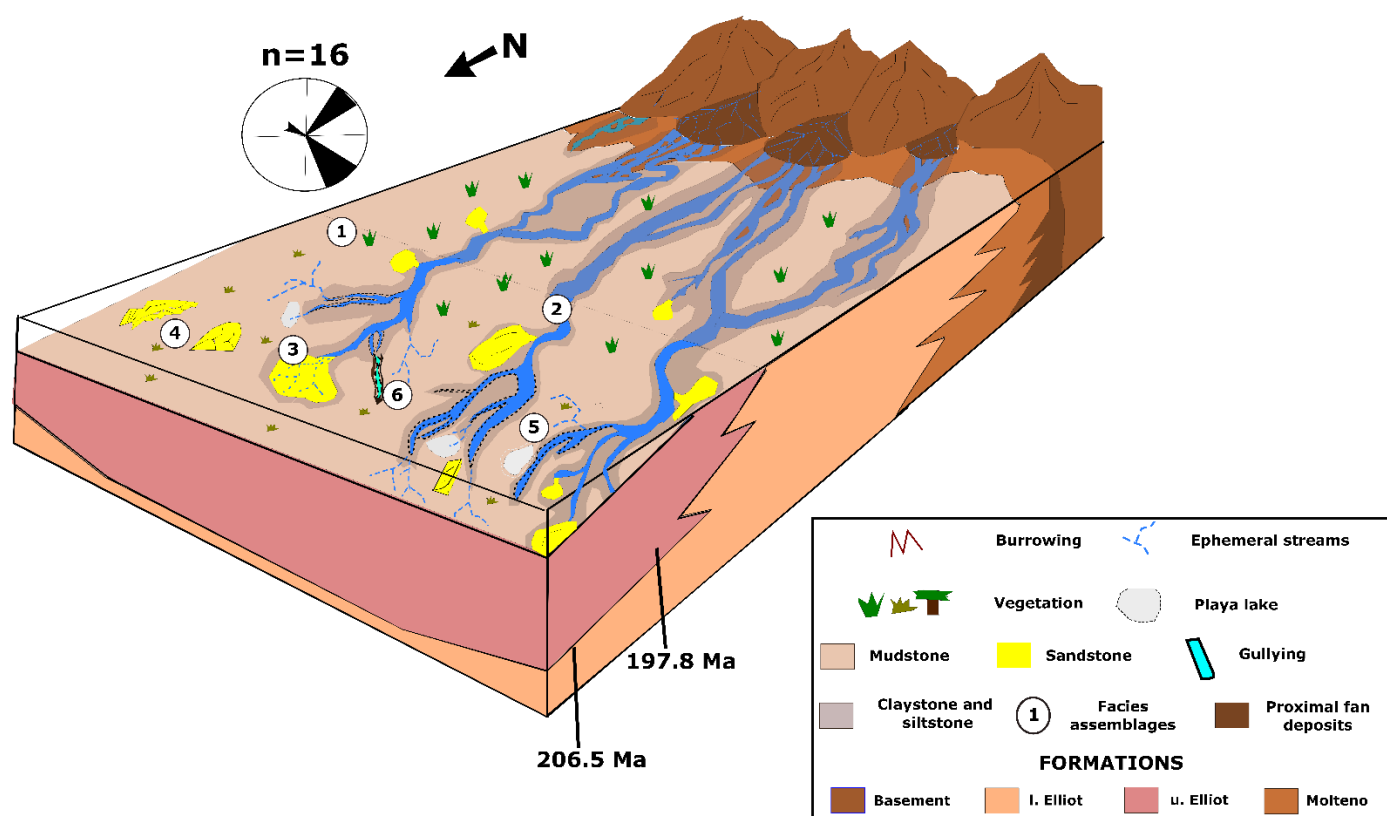
Fig. 41: Schematic model illustrating a localised palaeoenvironmental reconstruction of the FA 1 fluvial dominated deposition in the uEF (pink). The diagram highlights the tectonically driven transition from the meandering fluvial FA 2 dominant lEF units (above the orange coloured block) to the increasingly arid, ephemeral fluvial, pedogenically altered fines dominated uEF units (above the pink coloured block). Note: the multivariate uEF palaeocurrent readings included in the attached rose-diagram as well as the youngest single grain depositional temporal constraints. Illustration not to scale.

5.1.3   Clarens Formation

The Clarens Formation is an aeolian sequence, interbedded with fluvial 'wet' interdune facies, and shows similar repetitive upward coarsening successions at all three study sites of this investigation. The reoccurrence of these upward coarsening successions is indicative of the mobility between interdune and dune areas. Arguably, the most distinguishing feature of the Clarens Formation are the thick (>2 m) wedge-shaped intercalated aeolian dune sets (FA 4). These dune sets,

originally classified under Facies 4 of Eriksson (1981; 1983; 1986), consist of fine- to medium-grained cross-bedded wedge sets and indicate down-wind migration of dunes. These dune sets host palaeocurrent wind rippled surfaces with vertebrate trackways and semi-horizontal burrows. Interbedded massive to cross-bedded tabular sheets, similar to the aeolian loessic LS and unconfined ephemeral flash flood elements (FA 5 and 2) of the uEF, are interspersed throughout the aeolian dune (FA 4) sets. These LS and relatively unconfined ribbon CH sheets are similar to Eriksson's (1979; 1986) wadi type Facies 2 deposition.

Finely planar laminated to massive distinctly 'white weathered' claystone/siltstone lenses interbedded with the FA 4 aeolian dune sets represent shallow (water-depth: ~2 m) playa lakes (FA 5; Fig. 42; Briere, 2000). These ephemeral playa lakes illustrate the 'wet' interdune phase deposition in the Clarens Formation. Desiccation cracks, shallow water ripples and calcretized palaeosol markers are frequently associated with these interdune deposits and illustrate the gradual drying of these lakes. These FA 5 playa lake deposits tend to pinch out over lateral distances of <2 m; however, Clarens exposures of this study interestingly displayed a seemingly 'continuous', thick playa claystone unit at the basal Clarens. This laterally persistent basal bed formed a relatively sharp basal contact with the underlying uEF FA 1 fines and gradually coarsened up toward the first basal FA 4 dune bed sets. The sharp basal contact between the massive, pedogenically altered FA 1 uEF fines and overlying finely laminated 'whitish' claystone/siltstone beds was interpreted as the regionally pervasive Elliot-Clarens Formation contact. The presumed regional lateral continuity of the basal upward coarsening playa deposits was later found to comprise of an amalgamation of individual FA 5 lenses, each with limited individual lateral extents. These basal Clarens playa beds illustrate a distinct semi-arid to arid palaeoclimatic transition phase. The sudden shift from upward fining dominated, pedogenically-rich fines dominated underlying uEF deposits, to coarsening upward 'wet' interdune and FA 4 aeolian dune dominated deposits also illustrate an increase in the regional basin palaeorelief (Fig. 42). The progressive aridification and steepening of the regional palaeoslope is explained by the final tectonic unloading stage of the CFB, as suggested by Bordy et al. (2004a, b,

c; 2005). The tectonic forcing of the slope gradient change occurred as a result of the cessation of the subduction to the south of the Karoo Basin and initiation of extention, which eventualy lead to the break-up of Gondwana (Bordy et al. 2004a).

Similar to the rest of the basin, the Clarens Formation exhibits thickness variations throughout the study areas (4 outcrops in total). While it is tempting to link these thickness variations to local basinal palaeorelief changes rooted in continental marginal instabilities (early rifting), the localised nature of this study limits such interpretations. Furthermore, it was noted that the thicknesses of aeolian dune (FA 4) facies units is roughly inversely proportional to interdune (FA 5) facies units. The Clarens outcrop at Traverse 4 displays an ~9 m thick 'wet' interdune deposit and only ~2 m thick FA 4 aeolian sandstone bed; whereas comparatively, the Clarens outcrop at Traverse 3 displays ~43 m of FA 4 aeolian sandstone deposits and only ~6 m of FA 5 deposits. Similar to the overall thickness variations of the Formation, while the four Clarens outcrops analysed in this study present a unique relationship between total Formation thickness and relative abundance of facies, further testing of this relationship needs to be done regionally. Eriksson (1979; 1981; 1983; 1986) also noted variations in the thickness and spatial distribution of the aeolian and interdune facies in the Natal Drakensberg Clarens Formation, which he attributed to proximal and distal dominated alluvial fan deposition, respectively. Moreover, the early rifting as a tectonic influence on depositional patterns was proposed by Holzförster (2007), which tends to offer an additional and reasonable explanation for intrabasinal palaeorelief variations. Although this study is relatively localised, it, in association with Eriksson (1986) and Holzförster (2007), supports a dynamic tectonically- and climatically-driven depositional model that ought to be tested in future focused studies.

Palaeocurrent trends show a general SSW to NNE wind flow direction at the Moyeni and Masitise sites, respectively, and a NE to SW flow direction in Maphutseng. Previous palaeocurrent analyses of the Clarens have shown that although mean palaeocurrents flow from west to east (Beukes, 1970; Visser, 1984; Eriksson, 1986; Holzförster, 2007), a great deal of variability is noted

138

throughout some of the Clarens exposures (Beukes, 1970; Eriksson, 1986). This variability is evident in the palaeocurrent disparity between the adjacent Moyeni and Masitise localities and further northward Maphutseng locality. A general coarsening up trend is noted throughout the 4 Clarens Formation exposures of this study, with lithofacies grading from FA 5 basal 'wet' interdune deposits, up to pervasively mobile aeolian dune set dominated sandstone beds, indicating a potentially early initial Clarens aridification in SW Lesotho (Fig. 42).

The Clarens Formation detrital zircon samples (uEF-Clarens contact included) host a consistent clustering of Early Jurassic grains. This affirms the positive correlation between the flexural subsidence (coarsening upward sequences) and a constant younger grain source input. The youngest maximum (single grain) age of the uppermost uEF-Clarens Formation contact is set firmly within the Early Jurassic (Pliensbachian) at 190.5 Ma (Fig. 38). The uppermost unit of Clarens sample (Clarens-Drakensberg basalts contact) displays a Pliensbachian youngest maximum single grain age of 186.7 Ma (Fig. 38). This maximum single grain age of the uppermost Clarens exposures falls well below the age of the capping Drakensberg basalts known to have extruded at 183 ±1 Ma (Duncan et al., 1997). The Early Jurassic youngest maximum single grain and average depositional ages for the uEF-Clarens contact (190.5 Ma and 194.5 Ma, respectively) correlates well with the ~195-190 Ma magnetostratigraphically derived uEF-Clarens contact age constraints suggested in Sciscio et al. (2017a) (Fig. 39).
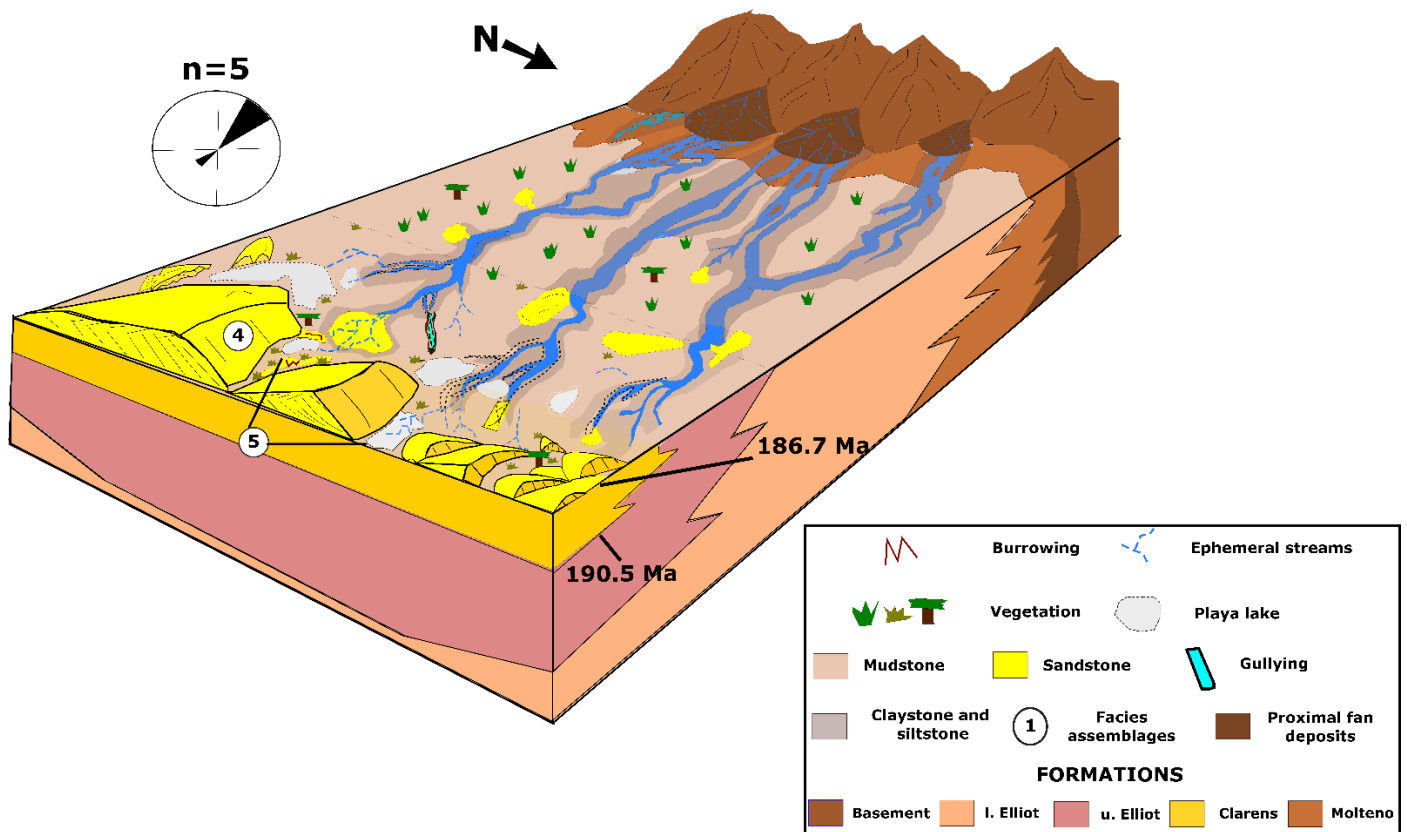
Fig. 42: Schematic model illustrating a localised palaeoenvironmental reconstruction of the FA 4 (aeolian dunal) and FA 5 (interdune) dominated deposition of the Clarens Formation (yellow block). The general coarsening up trend is illustrated by the transition from the basal 'wet' interdune dominant deposition (FA 5) to the increasingly more dominant aeolian dune sandstone units (FA 4). This signifies the final phase of retro-arc foreland basin unloading. Note: Clarens Formation palaeocurrent readings included in the attached rose-diagram as well as youngest single grain depositional temporal constraints. Illustration not to scale.

5.2   TJB and ETE

The actual stratigraphic positioning of the Triassic-Jurassic Boundary (TJB; 201.3 ±0.2 Ma) and

associated end-Triassic Extinction event (ETE; 201.6 ±0.015 Ma) in southern Africa is unresolved

(Blackburn et al., 2013; Cohen et al., 2013; Wotzlaw et al., 2015; Lindström et al., 2017). Globally,

the ETE and TJB positions are constantly shifted as new diagnostic geochronological analyses further

refine these geological events that, among others, resulted in the evolutionary radiation of

Dinosauria (Brusatte et al., 2008; Mc Phee et al., 2017). Southern African biostratigraphic correlative

studies of the Elliot exposures in Lesotho and South Africa initially suggested the TJB and ETE were

represented by the intra-formational continental red-bed succession, with the TJB (201.4 Ma)

located at the *Euseklosaurus* and *Massospondylus* biozones contact (Kitching and Raath, 1984; Olsen

and Galton, 1984; Smith et al., 1993). This remained the most likely TJB location for over three

decades, until a relatively recent globally correlative magnetostratigraphic investigation by Sciscio et al. (2017a) refined the TJB and ETE stratigrahic positions. Sciscio et al. (2017a) suggested that although the ETE may have coincided with the unconformable lEF-uEF stratigraphic contact, the TJB is more likely positioned in the lowermost uEF, but could not provide further age control due to lacking absolute ages. Resultantly, Sciscio et al. (2017a) expressed the need for a geochronological input, which is where this study plays an important role.

The temporal framework established in this study cannot determine the precise local or regional position of the ETE and TJB, due to the limitation of the dating method and available samples. It does, however, present a ~10 Ma stratigraphic gap between the uppermost lEF (206.5 Ma) and the lowermost uEF samples (197.8 Ma). This temporal gap provides sufficient time for the generation of a paraconformity at the lEF-uEF contact, initially suggested and regionally demonstrated by Bordy et al. (2004a, b, c), and confirmed by this study (Fig. 43). It is important to note that the 197.8 Ma age is not the oldest uEF Maphutseng strata; the age of those basal uEF mudstones still needs to be determined and can turn out to be anything from latest Rhaetian to Hettangian.

Considering that the age of the TJB is constrained to 201.3 ±0.2 Ma (Pálfy et al., 2000; Cohen et al., 2013; Blackburn et al., 2013; Kent et al., 2017), the TJB in SW Lesotho falls within the aforementioned stratigraphic gap at the lEF-uEF contact (Pálfy et al., 2000; Blackburn et al., 2013; Kent et al., 2017; Fig. 43). Further focused geochronological refinement is required to determine the true duration of the stratigraphic gap at the lEF-uEF contact and further refine the positions of the ETE and TJB in southern Africa. The stratigraphic positioning of the TJB in this study tends to concur with the older biostratigraphic-based *Euskelosaurus* and *Massospondylus* biozones contact interpretations by Kitching and Raath (1984), Olsen and Galton (1984) and Smith et al. (1993) and contradicts the magnetostratigraphically-derived placement of the TJB within the lower part of the uEF by Sciscio et al. (2017a).
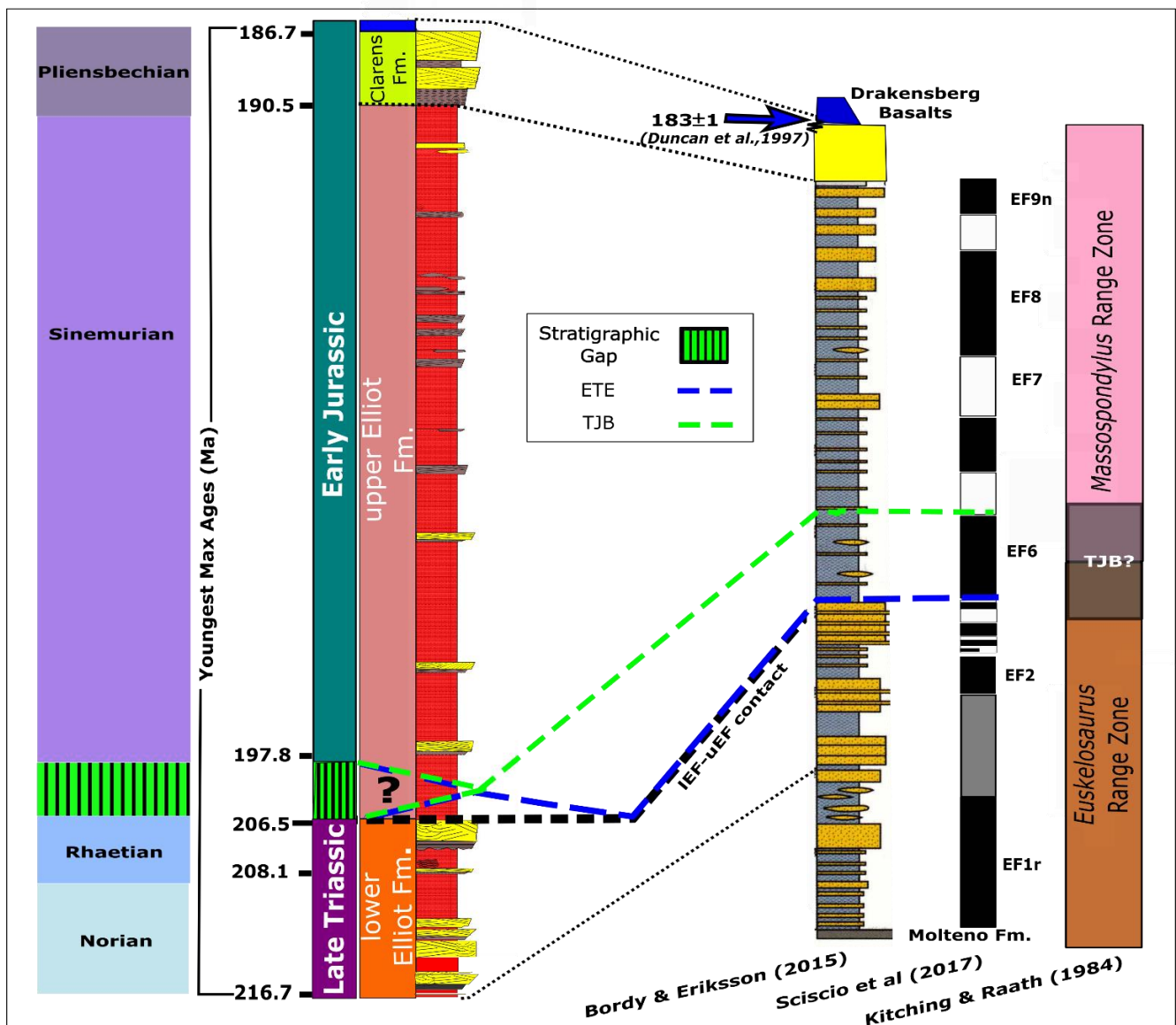
Fig. 43: Composite of previous (right) regional Elliot lithostratigraphic (Bordy and Eriksson,2015), biostratigraphic (Kitching and Raath, 1984) and magnetostratigraphy (Sciscio et al., 2017a) interpretations compared to the localised composite geochronological (youngest maximum single grain ages) and regional lithostratigraphic correlations attained from this study (left). The TJB (green), ETE (blue) and lEF-uEF contact (black) lines comparatively illustrate their relative, varying stratigraphic positions within the Elliot Formation. Interestingly, the implied geochronological maximum depositional ages and stratigraphic interpretation attained suggest a ~10 Ma stratigraphic gap (refer to image key) at the contact between the last lEF sandstone marker unit (dated at 206.5 Ma) and the overlying mudstone successions of the uEF (youngest age is Early Jurassic 197.8 Ma). The local ETE and TJB would fall within this gap (206.5-197.8 Ma) at the paraconformable lEF-uEF contact.

5.3   Ages of the fossil/trackway sites

In addition to providing a robust localised rate of deposition for the Elliot and Clarens

formations for the 3 study sites in the Elliot and Clarens formations, this study additionally presents

more direct absolute ages of 3 well-known ichnite-bearing sites. Although a biostratigraphic

reanalysis was not the aim or focus of this study, these absolute ages offer new insight into

142

ichnofaunal diversity, timing of local biozonation schemes in SW Lesotho and aid further global correlative investigations.

Sample Map2 represents the Late Triassic Rhaetian age (208.1 Ma) of the Maphutseng trackway site (Fig. 38). This new detrital geochronology at Maphutseng not only assigns, for the first time, an absolute age for the Maphutseng ichnofossil site, but also refines the famous underlying Maphutseng dinosaur bonebed to an absolute maximum youngest age of 208.1 Ma. Previously, based on biostratigraphic consideration, this rich fossil material was assigned a Carnian age by Gauffre (1993; 1996 [Unpublished]). The Cambrian (502.4 Ma) youngest single grain age obtained from the lower Moyeni trackway site (sample Q2) in Quthing presents an old, recycled source dominated deposition, typical of the loessic uEF units. This age individually only offers a maximum depositional age; however, the underlying, ~12 m below the trackway surface, Sinemurian sample Q1 offers an Early Jurassic (197.8 Ma) maximum depositional correlative age (Fig. 38). This new maximum depositional age constraint aids in constraining the *Neotrisauropus*-type, *Moyenisauropus*-type, *Episcopopustype*-type and chirotheroid-type trackways to the Early Jurassic Sinemurian (Ellenberger, 1970; Smith et al., 2009; Wilson et al., 2009; Marsicano et al., 2009). It additionally aids in resolving the 'Triassic' chirotheroid tracks hosted in an Early Jurassic unit-disparity noted by Smith et al. (2009), confirming the Early Jurassic lower Moyeni surface age and incorrect inference of a Triassic restricted chirotheroid age.

Furthermore, the Masitise cavehouse tridactyl dinosaur trackway site sample (Mas1), provided a Sinemurian youngest maximum single grain age of 196.4 Ma (Early Jurassic). In addition to dinosaur ichnites, Masitise and Moyeni (Quthing) are also renowned for hosting *Massospondylus* remains and two *Lesothosaurus* skulls in the upper Elliot Formation units below and above the respective trackway surfaces (Knoll, 2002a, b; Smith et al., 2009). Although the exact location of the fossils was not recorded, the additional maximum Early Jurassic age constraints provide additional temporal refinement to the local *Massospondylus* and *Lesothosaurus* remains.

6   CONCLUSION

The main purpose of this study was to provide a robust temporal framework for 3 ichnite-bearing study sites in the Upper Triassic-Lower Jurassic Elliot and Clarens formations of the upper Stromberg Group in SW Lesotho. The lack of radiometric age constraints hampered global and regional correlative bio-, litho- and magnetostratigraphic interpretations, particularly with regard to the stratigraphic positions of the TJB and ETE global turnover events (e.g., Ellenberger, 1970; Kitching and Raath, 1984; Olsen and Galton, 1984; Knoll and Battail, 2001; Lucas and Hancox, 2001; Bordy et al., 2004a, b, c, d; Knoll, 2004; Knoll, 2005; Smith et al., 2009; Wilson et al., 2009; Bordy and Eriksson, 2015; McPhee et al., 2017; Sciscio et al., 2017a). This study, aided by geochronological and in-depth localised stratigraphic analyses, aimed to refine not only the position of the ichnite bearing surfaces, but also that of the ETE and TJB within the Triassic-Jurassic Stromberg units and the duration of the temporal gap at lEF-uEF contact. The temporal, lithofacies and palaeocurrent focused data assimilation of this study additionally aided in contextualising localised interpretations of this palaeoclimatic trend, basinal tectonism and provenance dynamics.

Lithofacies and architectural element analysis of this study showed that:

- The lEF at Maphutseng comprised predominantly of perennial channelised, multi-storey, asymmterical, meandering fluvial FA 2 units, interbedded with associated FA 3 and FA 1 units (Fig. 40).

- The uEF in Maphutseng and Quthing comprised of dominantly pedogenically altered FA 1 FF units interbedded with minor channelised FA 2 deposits, increasingly abundant unconfined ephemeral flood-sheets (FA 2/5) and interbedded FA 3 overbank deposits (Fig. 41). The uEF was also typified by an increased abundance of aridity markers, including: unconfined ephemeral sheet flows, intensive pedogenic alteration, rubefication, aeolian loessic units, rare aeolian dunes (FA4), playa lakes, desiccation cracks and calcretized beds. Thus,

illustrating a palaeoclimatic shift from a lEF meandering fluvial dominated system to a semi-arid to arid flashflood dominated river and lake system.

- The overlying Clarens Formation, studied at all three localities, exhibited evidence for the final palaeoclimatic shift from the semi-arid fluvio-lacustine systems in the uppermost uEF to an arid, aeolian dominated setting. The Clarens exposures comprise predominantly of interfingering cross-bedded aeolian dune wedges (FA 4) and 'wet' interdune tabular laminated sandsheets and playa-lake lenses (FA 5; Fig. 42).

- The uppermost lEF meandering fluvial marker unit abruptly transitioned at the lEF-uEF contact to a thick unit of pedogenically altered, loessic floodplain fines (FA 1), denoting the basal uEF (Fig. 41). This confirmed the presence of the 2nd order regional paraconformity initially suggested by Bordy et al. (2004a, c).

This study highlighted smaller-scale intra-basinal facies and architectural variations, which suggest a possibly more dynamic tectonically-driven depositional model than the currently suggested one of transtentional distal overfilled phase Stormberg depo-centre uniformity (Catuneanu et al., 1998; Tankard et al., 2009). Notwithstanding the low number of palaeocurrent measurements obtained in this study, the local undulating palaeorelief is largely indicated by the palaeocurrent flow patterns and geochronologically derived detrital grain provenance variations. These proposed intra-basinal palaeorelief variabilities point toward a more complex sediment dispersal model for the Stormberg basin; however, due to the localised nature of this study, more definite interpretations are impossible.

The consistent youngest single grain and average maximum age constraints offered by the detrital zircon geochronology allowed for the construction of a youngest maximum single grain age temporal framework (Fig. 38; 39). The resultant depositional timeline (youngest single grain; average maximum unit ages) ranged from the Late Triassic Norian to Rhaetian for the lEF (216.7-206.5 Ma; 213.1 Ma), to the Early Jurassic Sinemurian (197.8 Ma) lower uEF, that extended up to the

Sinemurian-Pliensbachian (190.5 Ma; 194.5 Ma) basal Clarens contact (Fig. 39). A distinct age difference of the uppermost lEF (206.5 Ma) and lowermost uEF (197.8 Ma), dated in this study suggest a distinct age gap between the units. Although these samples do not come from only one site (Maphutseng), if proven valid on a regional scale with additonal dating work, the age gap, first quantified in this study, could support the presence of a regional unconformity at the lEF-uEF contact. Most excitingly, this study puts forward the first geochronolgical age for the uppermost Clarens Formation at Quthing (and within the Karoo Basin in southern Africa), having established an Early Jurassic mid-Pliensbachian (186.7 Ma) age at the Clarens-Drakensberg basalt contact (Fig. 39).

The detrital zircon geochronology utilized within this study additionally offered the first view of detrital grain population distributions within the Elliot and Clarens formations. Similar to the palaeoenvironmental interpretations, these grain age distributions offered new insights into a more diverse provenance model than originally interpreted from palaeodrainage, petrographic and lithostratigraphic studies (e.g., Eriksson, 1981; 1985; Cole, 1992; Catuneanu et al., 1998; Bordy et al., 2004b). Detrital grain clusterings of all samples displayed a good overall genetic correlation with one another (Fig. 35). All samples hosted similar Cambrian-Neoproterozoic, Neoproterozoic-Mesoproterozoic, and Jurassic-Permian major age cluster peaks (listed in order of decreasing abundance). More minor peaks occurred within the Late Neoproterozoic, Silurian-Ordovician and Archean. The dominance of older grains (>400.0 Ma) were noted throughout the samples; which, in association with loessic material and detrital grain morphologies (rounded and fragmented grains) suggested a major recycled source. Older, shared zircon populations indicate significant sediment recycling from the Cape Supergroup (Fourie et al., 2011) and older, pre-Stormberg units of the Karoo Supergroup (Craddock and Thomas, 2011; Walters, 2017 [Unpublished]; Viglietti et al., 2018).

The minor input of relatively euhedral, oscillatory zoned, prismatic grains suggested a more direct source input from primary magmatic sources. The youngest subset of Triassic to Jurassic grains were likely sourced directly (source to sink) from distal Patagonian igneous events (Fig. 34).

146

The distinct lack of younger Jurassic grain inputs into the uEF units was linked to the dominantly loessic nature of the units. The loessic units comprised of concentrated inputs of recycled sedimentary material; which, in addition to the pervasive pedogenic alteration of the uEF sediments, likely limited younger grain source inputs.

The temporal constraints of the previously undated Upper Triassic to Lower Jurassic Stormberg Group presented within this study, although localised, will aid both regional and global biostratigraphic, magnetostratigraphic and lithostratigraphic interpretations. It also offers the first geochronolgical age determinations of 3 well-known ichnite-bearing sites within the Elliot and Clarens formations, a succession known to host the TJB and ETE. These important ichnite-bearing sites are dated as follows: 502.4 Ma (Cambrian) at lower Moyeni (Quthing), 196.4 Ma (Early Sinemurian) at Masitise, and 208.1 Ma (Early Rhaetian) at Maphutseng.

Further intensive regional geochronological studies are suggested to bolster this localised framework of SW Lesotho, to provide more precise temporal constraints and enhance the correlation of these units with global counterparts. The localised, temporally constrained depositional reconstructions and detrital zircon-based provenance model (Fig. 34) of this study, in conjunction with previous palaeodrainage and provenance models, ultimately aid to further refine and contextualize depositional mechanisms and rates for these palaeoecologically vital southern African Triassic-Jurassic beds (i.e. Bordy et al., 2004a, b, d; Smith et al., 2009; Eriksson, 1986). The novel results of this study will additionally aid further global and local biostratigraphic investigations regarding the position of the TJB and ETE, evolutionary patterns and turnover rates in the early Mesozoic of southern Gondwana.

7   REFERENCES

Abrahams, M., Bordy, E. M., Sciscio, L. & Knoll, F., 2017. Scampering, trotting, walking tridactyl bipedal dinosaurs in southern Africa: ichnological account of a Lower Jurassic palaeosurface (upper Elliot Formation, Roma Valley) in Lesotho. *Historical Biology,* 29(7), pp. 958-975.

Allen, J. R. L., 1965. A review of the origin and character of recent alluvial sediments. *Sedimentology,* Volume 5, pp. 89-191.

Allen, J. R. L., 1968. The nature and origin of bed-form hierarchies. *Sedimentology,* 10(3), pp. 161-182.

Allen, J. R. L., 1970. A quantitative model of grain size and sedimentary structure in lateral deposits. *Geol. J.,* Volume 7, pp. 129-146.

Allen, J. R. L., 1978. Studies in fluviatile sedimentation: an exploratory quantitative model for the architecture of avulsion-controlled alluvial suites. *Sedimentary Geology,* Volume 21, pp. 129-147.

Allen, J. R. L., 1983. Studies in fluviatile sedimentation: Bars, bar-complexes and sandstone sheets (low sinuosity braided streams) in the Brownstones (L. Devonian), Welsh Borders. *Sediment. Geol.,* Volume 33, pp. 237-293.

Amidon, W., Burbank, D. & Gehrels, G., 2005b. Construction of detrital mineral populations: insights from mixing of U-Pb zircon ages in Himalayan rivers. *Basin Research,* Volume 17, pp. 463-485.

Amidon, W. H., Burbank, D. W. & Gehrels, G. E., 2005a. U–Pb zircon ages as a sediment mixing tracer in the Nepal Himalaya. *Earth and Planetary Science Letters,* Volume 235, pp. 244-260.

Andersen, T., Elburg, M. A., van Niekerk, H. S. & Ueckermann, H., 2018. Successive sedimentary recycling regimes in southwestern Gondwana: Evidence from detrital zircons in Neoproterozoic to Cambrian sedimentary rocks in southern Africa. *Earth-Science Reviews,* Volume 181, pp. 43-60.

Anderson, J. M. & Anderson, H. M., 1983. *Palaeoflora of southern Africa: Molteno Formation (Triassic), Vol. 1 : Part 1, Introduction, Part 2, Dicroidium.* Rotterdam: Balkema.

Anderson, J. M. & Anderson, H. M., 1993. Terrestrial flora and fauna of the Gondwana Triassic: Part 1–Occurrences. In: S. G. Lucas & M. Morales, eds. *The Nonmarine Triassic.* s.l.:Bull. New. Mexico Mus. Nat. Hist. (3), pp. 3-12.

Anderson, J. M. & Anderson, H. M., 1995. The Molteno Formation: window onto Late Triassic floral diversity. In: D. D. Pant, ed. *Proceedings of the international conference on global environment and diversification of plants through geological time.* Allahabad: Society of Indian Plant Taxonomists, pp. 27-40.

Anderson, J. M., Anderson, H. M. & Cruickshank, A. R., 1998. Late Triassic ecosystems of the Molteno/Lower Elliot biome of southern Africa. *Palaeontology,* Volume 41, pp. 387-421.

Apaldetti, C., Martinez, R. N., Alcober, O. A. & Pol, D., 2011. A new basal Sauropodomorph (Dinosauria: Saurischia) from Quebrada del Barro Formation (Marayes-El Carrizal Basin), Northwestern Argentina. *PLoS ONE,* 6(11), p. e26964.

Astin, T. R., 1990. The Devonian lacustrine sediments of Orkney, Scotland; implications for climate cyclicity, basin structure and maturation history. *Geol. Soc. Lond.,* Volume 147, pp. 141-151.

Astin, T. R. & Rogers, D. A., 1991. Subaqueous shrinkage cracks in the Devonian of Scotland reinterpreted. *J. Sed. Petrol.,* Volume 61, pp. 850-859.

Bangert, B., Stollhofen, H., Lorenz, V. & Armstrong, R. L., 1999. The geochronology and signifi cance of ash-fall tuffs in the glaciogenic Carboniferous-Permian Dwyka Group of Namibia and South Africa. *Journal of African Earth Sciences,* Volume 29, pp. 33-49.

Bann, K. L. et al., 2008. Ichnological and sedimentologic signatures of mixed wave- and storm-dominantd deltaic deposits: Examples from the Early Permian Sydney Basin, Australia. In: G. Hampson, R. Steel, P. Burgess & R. Dalrymple, eds. *Recent advances in models of siliciclastic shallow-marine stratigraphy.* s.l.:SSEPM Special Publications, 90, pp. 293-332.

Barbolini, N., 2014. Palynostratigraphy of the South African Karoo Supergroup and correlations with coeval Gondwanan successions. *[Unpublished PhD Thesis].*

Barrett, P. M., McGowan, A. J. & Page, V., 2009. Dinosaur diversity and the rock record. *Proceedings of the Royal Society B: Biological Sciences,* Volume 276, pp. 2667-2674.

Barthelemy, R., 1976. *Photogeology Lesotho. Project Findings and Recommendations.* New York: UNOTC.

Barthelemy, R. & Dempster, A. M., 1975. *Geological interpretation of the ERTS-I satellite imagery of Lesotho and possible relations between lineaments and kimberlite pipe emplacement,* Ann Arbor (USA): Proceedings of 10th Intenational Symposium for Remote Sensing.

Beckinsale, R. P. & Richardson, L., 1964. Recent findings on the physical development of the lower Severn valley. *Geographical Journal,* Volume 130, pp. 87-105.

Beerling, D. J. & Berner, R. A., 2002. Biogeochemical constraints on the Triassic-Jurassic boundary carbon cycle event. *Global Biogeochemical Cycles,* 16(3), pp. 10-1-10-13.

Belcher, R. W. & Kisters, A. F. M., 2003. Lithostratigraphic correlations in the western branch of the Pan-African Saldania belt, South Africa: the Malmesbury Group revisited. *South African Journal of Geology,* 106(4), pp. 327-342.

Bernard, H. A. & Major, C. F. J., 1963. *Recent meander belt deposits of the Brazos River; an alluvial "sand" model.* s.l.:American Association of Petroleum Geologists Bulletin, v. 47.

Beukes, N. J., 1970. Stratigraphy and sedlmentology of the Cave Sandstone Stage, Karoo System. *2nd International Gondwana Symposium. Proceedings and Papers,* pp. 321-342.

Blackburn, T. J. et al., 2013. Zircon U-Pb geochronology links the end-Triassic extinction with the Central Atlantic Magmatic Province. *Science,* Volume 340, pp. 941-945.

Blatt, H., Middleton, G. & Murray, R., 1972. *Origin of sedimentary rocks.* New Jersey : Prentice Hall Inc., New Jersey.

Blewett, S. & Phillips, D., 2016. An overview of Cape Fold Belt geochronology: implications for sediment provenance and the timing of orogenesis. In: B. Linol & M. J. de Wit, eds. *Origin and Evolution of the Cape Mountains and Karoo Basin.* Switzerland: Springer International Publishing, pp. 45-55.

Blomeier, D. et al., 2003. Facies analysis of the old Red Sandstone of Spitsbergen (Wood Bay Formation): Reconstruction of the depositional environments and implications of basin development. *Facies,* 49(1), pp. 151-174.

Bond, G., 1965. Some new fossil localities in the Karoo System of Rhodesia. *Arnoldia,* 2(11), pp. 1-4.

Bordy, E. M. & Abrahams, M., 2016. Geochemistry of the Pronksberg bentonite in the upper Elliot Formation (Early Jurassic), Eastern Cape, South Africa. In: B. Linol & M. de Wit, eds. *Origin and Evolution of the Cape Mountains and Karoo Basin: Geo-biohistory.* s.l.:s.n., pp. 119-127.

Bordy, E. M., Abrahams, M. & Sciscio, L., 2017. The Subeng vertebrate tracks: stratigraphy, sedimentology and a digital archive of a historic Upper Triassic palaeosurface (lower Elliot Formation), Leribe, Lesotho (southern Africa). *Bollettino della Società Paleontologica Italiana,* Volume 56, pp. 181-198.

Bordy, E. M. & Catuneanu, O., 2001. Sedimentology of the upper Karoo fluvial strata in the Tuli Basin, South Africa. *Journal of African Earth Sciences,* Volume 33, pp. 605-629.

Bordy, E. M. & Eriksson, P., 2015. Lithostratigraphy of the Elliot Formation (Karoo Supergroup), South Africa. *South African Journal of Geology,* 118(3), pp. 311-316.

Bordy, E. M., Hancox, J. P. & Rubidge, B. S., 2004a. Fluvial style variations in the Late Triassic–Early Jurassic Elliot formation, main Karoo Basin, South Africa. *Journal of African Earth Sciences,* Volume 38, pp. 383-400.

Bordy, E. M., Hancox, J. P. & Rubidge, B. S., 2004b. Provenance study of the Late Triassic - Early Jurassic Elliot Formation, main Karoo Basin, South Africa. *Geological Society of South Africa,* Volume 107, pp. 587-602.

Bordy, E. M., Hancox, J. P. & Rubidge, B. S., 2004d. Basin development during the deposition of the Elliot Formation (Late Triassic - Early Jurassic) Karoo Supergroup, South Africa. *Geological Society of South Africa ,* Volume 107, pp. 397-412.

Bordy, E. M., Hancox, P. J. & Rubidge, B. S., 2004c. A description of the sedimentology and palaeontology of the Late Triassic–Early Jurassic Elliot Formation in Lesotho. *Palaeont. afr.,* Volume 40, pp. 43-58.

Bordy, E. M. & Head, H., 2018 (In Press). Lithostratigraphy of the Clarens Formation (Stormberg Group, Karoo Supergroup), South Africa. *South African Journal of Geology,* 121(1).

Bordy, E. M. H. P. J. &. R. B. S., 2005. The contact of the Molteno and Elliot formations through the main Karoo Basin, South Africa: a second-order sequence boundary. *South African Journal of Geology,* 108(3), pp. 351-364.

Bordy, E. M. et al., 2017b. First Lower Jurassic vertebrate burrow from southern Africa (upper Elliot Formation, Karoo Basin, South Africa). *Palaeogeography, Palaeoclimatology, Palaeoecology,* Volume 468, pp. 362-372.

Bordy, E. M., van Gend, J., McPhee, B. & Tucker, R. T., 2015. *Maphutseng fossil heritage; Strtigraphic context of the dinosaur trackways and bone-bed in the upper Triassic- lower Jurassic Elliot Formation (Lesotho) [Poster].* El Jadida, 1st International Congress on Continental Ichnology.

Borg, S. G., DePaolo, D. J. & Smith, B. M., 1990. Isotopic structure and tectonics of the central Transantarctic Mountains. *Journal of Geophysical Research,* Volume 95, pp. 6647-6667.

Botha, B. J. V., 1968. The stratigraphy of the Red Beds Stage, Karoo System, at Elliot, C. P.. *Transactions of the Geological Society of South Africa,* Volume 71, pp. 101-113.

Bridge, J. S., 1984. Large-scale facies sequences in alluvial overbank environments. *J. Sed. Res.,* Volume 54, pp. 583-588.

Bridge, J. S. & Demicco, R. V., 2008. *Earth surface processes, landforms and sediment deposits.* Cambridge: Cambridge University Press.

Bridge, J. S. & Leeder, M. R., 1979. A simulation model of alluvial stratigraphy. *Sedimentology,* 26(5), pp. 617-644.

Briere, P. R., 2000. Playa, playa lake, sabkha: Proposed definitions for old terms. *Journal of Arid Environments,* 45(1), pp. 1-7.

Brookfield, M. E., 1977. The origin of bounding surfaces in ancient aeolian sandstones. *Sedimentology,* 24(3), pp. 303-332.

Brusatte, S. L., Benton, M. J., Ruta, M. & Lloyd, G. T., 2008. The first 50 Myr of dinosaur evolution: macroevolutionary pattern and morphological disparity. *Biology Letters,* 4(6), pp. 733-736.

Bull, W. B., 1997. Discontinuous ephemeral streams. *Geomorphology,* Volume 19, pp. 227-276.

Butler, R. J., 2005. The "fabrosaurid" ornithischian dinosaurs of the upper Elliot Formation (Lower Jurassic) of South Africa and Lesotho. *Zoological Journal of the Linnean Society,* Volume 145, p. 175–218.

Cairncross, B., Anderson, J. M. & Anderson, H. M., 1995. Palaeoecology of the Triassic Molteno Formation, Karoo Basin, South Africa- sedimentological and palaeontological evidence. *S. Afr. J. Geol.,* Volume 98, pp. 452-478.

Catuneanu, O., 2002. Sequence stratigraphy of clastic systems: concepts, merits, and pitfalls. *Journal of African Earth Sciences,* 35(1), pp. 1-43.

Catuneanu, O., 2004. Retroarc foreland systems—evolution through time. *Journal of African Earth Sciences,* Volume 38, pp. 225-242.

Catuneanu, O. et al., 2009. Towards the standardization of sequence stratigraphy. *Papers in the Earth and Atmospheric Sciences,* Volume 238.

Catuneanu, O. & Elango, H. N., 2001. Tectonic control on fluvial styles: the Balfour Formation of the Karoo Basin, South Africa. *Sedimentary Geology,* Volume 140, pp. 291-313.

Catuneanu, O. et al., 2011. Sequence stratigraphy: methodology and nomenclature. *Newsletters on Stratigraphy,* 44(3), pp. 173-245.

Catuneanu, O., Hancox, P. J. & Rubidge, B. S., 1998. Reciprocal flexural behaviour and contrasting stratigraphies: a new basin development model for the Karoo retroarc foreland system, South Africa. *Basin Research,* Volume 10, pp. 417-439.

Catuneanu, O. et al., 2005. The Karoo basins of south-central Africa. *Journal of African Earth Sciences,* Volume 43, pp. 211-253.

Cawood, P. A., Hawkesworth, C. J. & Dhuime, B., 2012. Detrital zircon record and tectonic setting. *Geology,* 40(10), pp. 875-878.

Cawood, P. A. & Nemchin, A. A., 2001. Source regions for Laurentian margin sediments: Constraints from U/Pb dating of detrital zircon in the Newfoundland Appalachians. *Geological Society of America Bulletin,* Volume 113, pp. 1234-1246.

Cawood, P. A. et al., 2007. Sedimentary basin and detrital zircon record along east Laurentia and Baltica during assembly and breakup of Rodinia. *Journal of the Geological Society,* 164(2), pp. 257-275.

Cecil, C. B. & Dulong, F. T., 2003. Precipitation models for sediment supply in warm climates. *Climate Controls on Stratigraphy,* Volume 77, pp. 21-27.

Christie, A. D. M., 1981. Stratigraphy and sedimentology of the Molteno Formation in the Elliot and Indwe area, Cape Province. *(Unpublished, MSc Thesis), University of Natal, Durban.*

Cohen, K. M., Finney, S. C., Gibbard, P. L. & Fan, J. X., 2013. The ICS International Chronostratigraphic Chart (updated). Volume 36, pp. 199-204.

Colbert, E. H., 1958. Tetrapod extinctions at the end of the Triassic Period. *Proceedings of the National Academy of Sciences of the United States of America,* 44(9), p. 973.

Cole, D. I., 1992. Evolution and development of the Karoo Basin. In: M. J. de Wit & I. G. D. Ransome, eds. *Inversion tectonics of the Cape Fold Belt, Karoo and Cretaceous Basins of Southern Africa.* Rotterdam: Balkema, pp. 87-100.

Coleman, J. M., 1969. Brahmaputra River: Channel processes and sedimentation. *Sedimentary Geology,* Volume 3, pp. 129-239.

Color, M., 2009. *Geological Rock-Color Chart.* Grand Rapids: X-Rite.

Coney, L. et al., 2007. Geochemical and mineralogical investigation of the Permian-Triassic boundary in the continental realm of the southern Karoo Basin, South Africa. *Palaeoworld,* Volume 16, pp. 67-104.

Cooper, M. J., 1982. A Mid-Permian to earliest Jurassic tetrapod biostratigraphy and its significance. *Arnoldia Zimb.,* 9(7), pp. 77-104.

Craddock, J. & Thomas, R., 2011. Detrital zircon provenance ages of the "Dwyka Tillite"in South Africa and the Falkland Islands. *GeoSynthesis,* pp. 33-34.

Croke, J. C., 1991. *Floodplain variability in the Glenmalure Valley, southeast Leinster, Ireland.* s.l.:Unpublished PhD Thesis, National University of Ireland.

Da Silva, L. C. et al., 2000. U-Pb SHRIMP and Sm-Nd age constraints on the timing and sources of the Pan-African Cape Granite Suite, South Africa. *Journal of African Earth Sciences,* 30(4), pp. 795-815.

Day, M. O. et al., 2015. Youngest dinocephalian fossils extend the Tapinocephalus Zone, Karoo Basin, South Africa. *S. Afr. J. Sci.,* 111(3/4), pp. 1-5.

de Wit, M. J. et al., 1992. Formation of an Archaean continent. *Nature,* Volume 357, pp. 553-562.

de Wit, M. J., Jeffery, M., Nicolaysen, L. O. N. & Bergh, H., 1988. Explanatory notes on the Geologic Map of Gondwana. *American Association Petroleum Geology (Tulsa).*

de Wit, M. J. & Ransome, I. G. D., 1992. Regional inversion tectonics along the southern margin of Gondwana. In: M. J. de Wit & I. G. D. Ransome, eds. *Inversion Tectonics of the Cape Fold Belt, Karoo and Cretaceous Basins of Southern Africa.* Rotterdam: Balkema, pp. 15-21.

DeCelles, P. G., Carrapa, B. & Gehrels, G. E., 2007. Detrital zircon U-Pb ages provide provenance and chronostratigraphic information from Eocene synorogenic deposits in northwestern Argentina. *Geology,* 35(4), pp. 323-326.

Deenen, M. H. et al., 2010. A new chronology for the end-Triassic mass extinction. *Earth and Planetary Science Letters,* 291(1), pp. 113-125.

Dickinson, W. R. & Gehrels, G. E., 2009. Use of U-Pb ages of detrital zircons to infer maximum depositional ages of strata: A test against a Colorado Plateau Mesozoic database. *Earth and Planetary Science Letters,* 288(1), pp. 115-125.

Donovan, R. N., 1975. Devonian lacustrine limestones at the margin of the Orcadian Basin, Scotland. *J. Geol. Soc. Lond.,* Volume 131, pp. 489-510.

Du Toit, A. I., 1939. *The Geology of South Africa.* Edinburgh: Oliver and Boyd.

Du Toit, A. L., 1954. *The Geology of South Africa.* 3 ed. Edinburgh, United Kingdom: Oliver and Boyd.

Duncan, R. et al., 1997. The timing and duration of the Karoo igneous event, southern Gondwana. *Journal of Geophysical Research, Vol. 102, no. B8,* pp. 18,127-18,138.

Eberth, D. A. & Miall, A. D., 1991. Stratigraphy, sedimentology and evolution of a vertebrate-bearing, braided to anastomosed fluvial system, Cutler Formation (Permian-Pennsylvanian), north-central New Mexico. *Sedimentary Geology,* 72(3), pp. 225-252.

Eglington, B. M., 2006. Evolution of the Namaqua-Natal Belt, southern Africa –A geochronological and isotope geochemical review. *Journal of African Sciences,* Volume 46, pp. 93-111.

Ellenberger, F. et al., 1964. The Stormberg Series of Basutoland (South Africa). *In: Report of 22nd session of the International Geological Congress,* pp. 320-330.

Ellenberger, F., Ellenberger, P., Fabre, J. & Mendrez, C., 1963. Deux nouvelles dalles a pistes de verte´bre´s fossiles de´couvertes au Basutoland (Afrique du Sud). *C R Somm Se´ance Soc Ge´ol France,* pp. 315-317.

Ellenberger, F., Ellenberger, P. & Ginsburg, L., 1967. The appearance and evolution of dinosaurs in the Trias and Lias: a comparison between South African Upper Karoo and western Europe based on vertebrate footprints. *International Symposium on Gondwana Geology, Mar del Plata: UNESCO,* pp. 333-354.

Ellenberger, P., 1970. Les niveaux paléontologiques de première apparition des mammifères primordiaux en Afrique du Sud et leur ichnologie. Establissement de zones stratigraphique détaillées dans le Stormberg du Lesotho (Afrique du Sud) (Trias superior a Jurassique). *Proceedings and Papers of the second Gondwana Symposium,* pp. 343-370.

Ellenberger, P., 1972. Contribution à la classification des pistes de vertébrés du Trias: les types du Stormberg d'Afrique du Sud (I partie). *Paleovertebrata, Mémoire Extraordinaire,* pp. 1-117.

Ellenberger, P., 1974. Contribution à la classification des pistes de Vertébrés du Trias: les types du Stormberg d'Afrique du Sud (II partie). *Paleovertebrata, Mémoire Extraordinaire,* pp. 1-201.

Ellenberger, P. & Ellenberger, F., 1956. Le gisement de Dinosauriens de Maphutseng. *Compte-Rendu Sommaire De La Société Géologique De France,* Volume 8, pp. 99-101.

Eriksson, P., 1985. The depositional palaeoenvironment of the Elliot Formation in the Natal Drakensberg and north-eastern Orange Free State. *Transactions of the Geological Society South Africa,* Volume 88, pp. 19-26.

Eriksson, P. G., 1979. Mesozoic sheetflow and playa sediments of the Clarens Formation in the Kamberg area of the Natal Drakensberg. *Transactions of the Geological Society of South Africa,* Volume 83, pp. 257-258.

Eriksson, P. G., 1981. A palaeoenvironmental analysis of the Clarens Formation in the Natal Drakensberg. *Transactions of the Geological Society of South Africa,* Volume 84, pp. 7-18.

Eriksson, P. G., 1983. *Palaeoenvironmental Study of the Molteno, Elliot and Clarens Formations in the Natal Drakensberg and Northeastern Orange Free State.* s.l.:Ph.D. Thesis, University of Natal.

Eriksson, P. G., 1986. Aeolian dune and alluvial fan deposits in the Clarens Formation of the Natal Drakensberg. *Transactions of the Geological Society of South Africa,* Volume 89, pp. 389-394.

Eriksson, P. G., McCourt, S. & Snyman, C. P., 1994. A note on the petrography of upper Karoo sandstones in the Natal Drakensberg: implications for the Clarens Formation palaeoenvironment. *Transactions of the Geological Society of South Africa,* Volume 97, pp. 101-105.

Erwin, D. H., 1998. The end and the beginning: Recoveries from mass extinctions. *Trends in Ecology & Evolution,* 13(9), pp. 344-349.

Farrell, K. J., 1987. Sedimentology and facies architecture of overbank deposits of the Mississippi River, False River region, Louisiana. In: F. G. Ethridge, R. M. Flores & M. D. Harvey, eds. *Recent Developments in Fluvial Sedimentology.* s.l.:Soc. Econ. Palaeontol. Mineral. Spec. Publ., 39, pp. 111-121.

Fielding, C. F., 1999. Varieties of Fluvial Form: the relevance to geologists of an expanded reality. In: A. J. Miller & A. Gupta, eds. *Varieties of Fluvial Form.* Chichester: John Wiley and Sons Ltd., pp. 497-504.

Fielding, C. R., 2006. Upper flow regime sheets, lenses and scour fills: Extending the range of architectural elements for fluvial sediment bodies. *Sedimentary Geology,* 190(1), pp. 227-240.

Fildani, A., Cope, T. D., Graham, S. A. & Wooden, J. L., 2003. Initiation of the Magallanes foreland basin: Timing of the southernmost Patagonian Andes orogeny revised by detrital zircon provenance analysis. *Geology,* Volume 31, pp. 1081-1084.

Fildani, A. et al., 2007. Age controls on the Tanqua and Laingsburg deep-water systems: New insights on the evolution and sedimentary fi ll of the Karoo Basin, South Africa. *Journal of Sedimentary Research,* Volume 77, pp. 901-908.

Fildani, A. et al., 2009. U-Pb zircon ages from the southwestern Karoo Basin, South Africa: Implications for the Permian-Triassic boundary. *Geology,* Volume 37, pp. 719-722.

Flint, S. S. et al., 2011. Depositional architecture and sequence stratigraphy of the Karoo basin floor to shelf edge succession, Laingsburg depocentre, South Africa. *Marine and Petroleum Geology,* Volume 28, pp. 658-674.

Foden, J., Elburg, M. A., Dougherty-Page, J. & Burtt, A., 2006. The timing and duration of the Delamerian Orogeny: correlation with the Ross Orogen and implications for Gondwana assembly. *The Journal of Geology,* Volume 114, pp. 189-210.

Fourie, P. H. et al., 2011. Provenance and reconnaissance study of detrital zircons of the Palaeozoic Cape Supergroup in South Africa: revealing the interaction of the Kalahari and Rı́o de la Plata cratons. *Int J Earth Sci,* Volume 100, pp. 527-541.

Frazier, D. E. & Osanik, A., 1961. Point-bar deposits, Old River Locksite, Louisiana. *Gulf Coast Assoc. Geol. Soc. Trans.,* Volume 11, pp. 127-137.

Frei, D. & Gerdes, A., 2009. Precise and accurate in situ U–Pb dating of zircon with high sample throughput by automated LA-SF-ICPMS. *Chemical Geology,* Volume 261, pp. 261-270.

Friend, P. F., 1983. Towards the field classification of alluvial architecture or sequence. In: J. D. Collinson & J. Lewin, eds. *Modern and ancient fluvial systems.* s.l.:International Association of Sedimentologists Special Publication, pp. 345-354.

Frimmel, H. E., Zartman, R. E. & Spath, A., 2001. The Richtersveld Igneous Complex, South Africa: U-Pb Zircon and Geochemical Evidence for the Beginning of Neoproterozoic Continental Breakup. *The Journal of Geology,* Volume 109, pp. 493-508.

Galli, M. T., Jadoul, F., Bernasconi, S. M. & Weissert, H., 2005. Anomalies in global carbon cycling and extinction at the Triassic/Jurassic boundary: evidence from a marine C-isotope record. *Palaeogeography, Palaeoclimatology, Palaeoecology,* Volume 16, pp. 203-214.

Galloway, W. E., 1981. Depositional architecture of Cenozoic Gulf Coastal Plain fluvial systems. In: F. G. Ethridge & R. M. Flores, eds. *Recent and Ancient Nonmarine Depositional Environments.* s.l.:Soc. Econ. Palaeontol. Mineral. Spec. Publ., 31, pp. 127-156.

Gärtner, A. et al., 2013. Morphology of zircon crystal grains in sediments – characteristics, classifications, definitions. *Geologica Saxonica,* Volume 59, pp. 65-73.

Gastaldo, R. A. et al., 2015. Is the vertebrate-defined Permian-Triassic boundary in the Karoo Basin, South Africa, the terrestrial expression of the end-Permian marine event?. *Geology,* 43(10), pp. 939-942.

Gauffre, F. X., 1993. Biochronostratigraphy of the lower Elliot Formation (southern Africa) and preliminary results on the Maphutseng Dinosaur (Saurishcia: Prosauropoda) from the same Formation of Lesotho. In: S. G. Lucas & M. Morales, eds. *The Nonmarine Triassic.* s.l.:New Mexico Museum of Natural History & Science Bulletin, 3, pp. 147-149.

Gauffre, F. X., 1996. *Phylogénie des dinosaures prosauropodes et étude d'un prosauropode du Trias supérieur d'Afrique australe.* s.l.:[PhD Thesis].

Gehrels, G. E., 2000. Introduction to detrital zircon studies of Paleozoic and Triassic. In: M. Soreghan & G. E. Gehrels, eds. *Paleozoic and Triassic Paleogeography and Tectonics of Western Nevada and Northern California.* s.l.:Geological Society of America Special Paper 347, pp. 1-17.

Gibling, M. R., 2006. Width and thickness of fluvial channel bodies and valley fills in the geological record: a literature compilation and classification. *Journal of Sedimentary Research,* Volume 76, pp. 731-770.

Glennie, K. W. 1., 1972. Permian Rotliegendes of northwest Europe interpreted in light of modern desert sedimentation studies. *American Association of Petroleum Geologists Bulletin,* Volume 56, pp. 1048-1071.

Glennie, K. W., 1970. *Desert sedimentary environments, Volume 14.* 1 ed. s.l.:Elsevier Science.

Gow, C. E. & Latimer, E. M., 1999. Preliminary report of dinosaur tracks in Qwa Qwa, South Africa. *Palaeontologia Africana,* Volume 35, pp. 41-43.

Grab, S. W. & Deschamps, C. L., 2004. Geomorphological and geoecological controls and processes following gully development in alpine mires, Lesotho. *Arctic, Antarctic, and Alpine Research,* 36(1), pp. 49-58.

Gradstein, F. M., Ogg, J. G., Schmitz, M. D. & Ogg, G. M., 2012. *The Geologic Time Scale 2012.* 1 ed. Boston: Elsevier.

Gradstein, F., Ogg, J. & Smith, A., 2004. *A Geological Time Scale.* Cambridge: Cambridge University Press.

Gresse, P. G., Chemale Junior, F., Da Silva, L. C. & Hartmann, L. A., 1996. Late- to post-orogenic basins of the Pan-African – Brasiliano collision orogen in southern Africa and southern Brazil. *Basin Research,* Volume 8, pp. 157-171.

Gresse, P. G., Theron, J. N., Fitch, F. J. & Miller, J. A., 1992. Tectonic inversion and radiometric resetting of the basement in the Cape Fold Belt. In: M. J. de Wit & I. G. D. Ransome, eds. *Inversion tectonics of the Cape Fold Belt, Karoo and Cretaceous Basins of Southern Africa.* Rotterdam: Balkema, pp. 217-228.

Gresse, P., Von Veh, M. & Frimmel, H., 2006. Namibian (Neoproterozoic) to early Cambrian successions. In: M. Johnson, C. R. Anhaeusser & R. J. Thomas, eds. *The Geology of South Africa.* s.l.:Geological Society of South Africa, Council For Geoscience, pp. 395-420.

Groenewald, P. B., Grantham, G. H. & Watkeys, M. K., 1991. Geological evidence for a Proterozoic to Mesozoic link between southeastern Africa and Dronning Maud Land, Antarctica. *Journal of the Geological Society,* Volume 148, pp. 1115-1123.

Hälbich, I. W., 1983. A geodynamic model for the Cape Fold Belt. In: N. Rast & F. M. Delany, eds. *Geodynamics of the Cape Fold Belt. Vol. 12..* Rotterdam: Geological Society South Africa, pp. 77-184.

Hallam, A., 2002. How catastrophic was the end-Triassic mass extinction?. *Lethalia,* Volume 35, pp. 147-157.

Hallam, A. & Wignall, P. B., 1999. Mass extinctions and sea-level changes. *Earth-Science Reviews,* Volume 48, pp. 217-250.

Hampton, B. A. & Horton, B. K., 2007. Sheetflow fluvial processes in a rapidly subsiding basin, Altiplano plateau, Bolivia. *Sedimentology,* Volume 54, pp. 1121-1147.

Hancox, P. J., 1998. *A Stratigraphic, Sedimentological and Paleoenvironmental synthesis of the Beaufort-Molteno contact in the Karoo Basin.* Johannesburg: Unpublished PhD thesis, University of the Witwatersrand.

Hancox, P. J. & Götz, A. E., 2014. South Africa's coalfields - A 2014 perspective. *International Journal of Coal Geology,* Volume 132, pp. 170-254.

Hancox, P. J. & Rubidge, B. S., 1996. The first specimen of the Mid-Triassic dicynodont Angonisaurus from the Karoo of South Africa, implications for the dating and biostratigraphy of the Cynognathus Assemblage Zone, Upper Beaufort Group. *South African Journal of Science,* Volume 92, pp. 391-392.

Hansma, J. et al., 2016. The timing of the Cape Orogeny: New 40Ar/39Ar age constraints on the deformation and cooling of the Cape Fold Belt, South Africa. *Gondwana Research,* Volume 32, pp. 122-137.

Hanson, E. K. et al., 2009. Cretaceous erosion in central South Africa: evidence from upper-crustal xenoltihs in kimberlite diatremes. *South African Journal of Geology,* Volume 112, pp. 125-140.

Harms, J. C., MacKenzie, D. B. & McCubbin, D. G., 1963. Stratification in modern sands of the Red River, Louisiana. *Journal Geology,* 71(5), pp. 566-580.

Harms, J. C., Southard, J. B., Spearing, D. R. & G, W. R., 1975. *Depositional environments as interpreted from primary sedimentary structures and stratification sequences.* s.l.:Society for Sedimentary Geology (SEPM) Short Course 2.

Harms, J. C., Southard, J. B. & Walker, R. G., 1982. *Structures and sequences in clastic rocks.* 9 ed. s.l.:Society for Sedimentary Geology (SEPM) Short Course.

Haughton, S. H., 1924. The fauna and stratigraphy of the Stormberg Series. *Ann. S. Afr. Mus.,* Volume 12, pp. 323-495.

Haughton, S. H., 1969. *Geological history of southern Africa.* Johannesburg: Geological Society of South Africa.

Hellstrom, J., Paton, C., Woodhead, J. & Hergt, J., 2008. Iolite: Software for spatially resolved LA-(quad and MC) ICPMS analysis. In: P. Sylvester, ed. *Laser Ablation ICP–MS in the Earth Sciences: Current Practices and Outstanding Issues.* Quebec: Mineralogical Association of Canada short course series, pp. 343-348.

Hesselbo, S. P., Jenkyns, H. C., Duarte, L. V. & Oliveira, L. C. V., 2007. Carbon-isotope record of the Early Jurassic (Toarcian) oceanic anoxic event from fossil wood and marine carbonate (Lusitanian Basin, Portugal). *Earth Planet. Sci. Lett.,* Volume 253, pp. 455-470.

Hesselbo, S. P., Robinson, S. A., Surlyk, F. & Piasecki, S., 2002. Terrestrial and marine extinction at the Triassic-Jurassic boudary synchronized with major carbon-cycle perturbation: A link to initiation of massive volcanism?. *Geological Society of America,* 30(3), pp. 251-254.

Hickson, T. A., Sheets, B. A., Paola, C. & Kelberer, M., 2005. Experimental Test of Tectonic Controls on Three-Dimensional Alluvial Facies Architecture. *Journal of Sedimentary Research,* 75(4), pp. 710-722.

Hillebrandt, A. v. & Krystyn, L., 2009. On the oldest Jurassic ammonites of Europe (Northern Calcareous Alps, Austria) and their global significance. *N. Jb. Geol. Paläont. Abh.,* Volume 253/2-3, pp. 163-195.

Hirst, J. P. P., 1991. Variations in alluvial architecture across the Oligo-Miocene Huesca fluvial system, Ebro Basin, Spain. In: A. D. Miall & N. Tyler, eds. *The three-dimensional facies architecture of terrigenous clastic sediments and its implications for hydrocarbon discovery and recovery.* s.l.:SEPM, Concepts in Sedimentology and Palaeontology, 3, pp. 111-121.

Hogg, S. E., 1982. Sheetfloods, Sheetwash, Sheetflow, or ...?. *Earth Science Reviews,* Volume 18, pp. 59-76.

Holzförster, F., 2007. Lithology and depositional environments of the Lower Jurassic Clarens Formation in the eastern Cape, South Africa. *South African Journal of Geology,* Volume 110, pp. 543-560.

Hüsing, S. K. et al., 2014. Astronomically-calibrated magnetostratigraphy of the Lower Jurassic marine successions at St. Audries Bay and East Quantoxhead (Hettangian-Sinemurian; Somerset (UK). *Palaeogeography Palaeoclimatology Palaeoecology,* Volume 403, pp. 43-56.

Ireland, T. R. & Williams, I. S., 2003. Considerations in zircon geochronology by SIMS. *Reviews in Mineralogy and Geochemistry,* 53(1), pp. 215-241.

Irmis, R. B., 2011. Evaluating hypotheses for the early diversification of dinosaurs. *Earth and Environmental Science Transactions of the Royal Society of Edinburgh,* Volume 101, pp. 397-426.

Isbell, J. L., Cole, D. I. & Catuneanu, O., 2008. Carboniferous - Permian glaciation in the main Karoo Basin, South Africa: Stratigraphy, depositional controls, and glacial dynamics. In: C. R. Fielding, T. D. Frank & J. L. Isbell, eds. *Resolving the Late Palaeozoic Ice age in Time and Space.* s.l.:Geological Society of America Special Paper (441), pp. 71-82.

Jackson, R. G., 1975. Velocity-bedform-texture patterns of meander bends in the lower Wabash River of Illinois and Indiana. *Geological Society of America Bulletin,* Volume 86, pp. 1511-1522.

Jackson, S., Pearson, N. J., Griffin, W. L. & Belousova, E. A., 2004. The application of laser ablation – inductively coupled plasma – mass spectrometry to in situ U–Pb zircon geochronology. *Chemical Geology,* Volume 211, pp. 47-69.

Johnson, M., 1991. Sandstone petrography, provenance and plate tectonic setting in Gondwana context of the south-eastern Cape Karoo Basin. *S. Afr. Tydskr. Geol.,* Volume 94, pp. 137-154.

Johnson, M. R., 1966. Stratigraphy and sedimentology of the Cape and Karoo sequences in the Eastern Cape Province. *Unpublished MSc thesis.*

Johnson, M. R., 1976. *Stratigraphy and Sedimentology of the Cape and Karoo Sequences in the Eastern Cape Province.* Grahamstown: Unpublished Ph.D. Thesis, Rhodes University.

Johnson, M. R., 1994. *Lexicon of South African Stratigraphy. Part 1: Phanerozoic Units.* Pretoria: South African Committee for Stratigraphy Publication: Council for Geoscience.

Johnson, M. R. & Le Roux, F. G., 1994. *The geology of the Grahamstown area.* s.l.:Geological Survey of South Africa - Geology.

Johnson, M. R. et al., 1996. Stratigraphy of the Karoo Supergroup in southern Africa: an overview. *Journal of African Earth Sciences,* 23(1), pp. 3-15.

Johnson, M. R. et al., 1997. The Foreland Karoo Basin, South Africa. In: R. C. Selly, ed. *Sedimentary Basins of the World, vol. 3.* Amsterdam: Elsevier Science, pp. 269-317.

Johnson, M. R. et al., 2006. Sedimentary Rocks of the Karoo Supergroup. In: M. Johnson, C. Anhaeusser & R. Thomas, eds. *Geology of South Africa.* Johannesburg, Pretoria: Geological Society of South Africa, Council of Geoscience, pp. 461-499.

Jones, J. V. et al., 2009. Age, provenance, and tectonic setting of Paleoproterozoic quartzite successions in the southwestern United States. *Geological Society of America Bulletin,* 121(1-2), pp. 247-264.

Jourdan, F. et al., 2005. Karoo Large Igneous Province: brevity, origin, and relation to mass extinction questioned by new 40Ar/39Ar age data. *Geology,* Volume 33, pp. 745-748.

Jourdan, F. et al., 2007. Distinct brief major events in the Karoo large igneous province clarified by new 40 Ar/39 Ar ages on the Lesotho basalts. *Lithos,* 98(1), pp. 195-209.

Kay, S. M., Ramos, V. A., Mpodozis, C. & Sruoga, P., 1989. Late Palaeozoic to Jurassic silicic magmatism at the Gondwana margin: analogy to the Middle Proterozoic in North America?. *Geology,* Volume 17, pp. 324-328.

Kelly, S. B. & Olsen, H., 1993. Terminal fans—a review with references to Devonian examples. *Sedimentary Geology,* Volume 85, pp. 339-374.

Kent, D. V. et al., 2014. Age constraints on the dispersal of dinosaurs in the Late Triassic from magnetochronology of the Los Colorados Formation (Argentina). *Proceedings of the National Academy of Sciences,* Volume 111, p. 7958–7963.

Kent, D. V., Olsen, P. E. & Muttoni, G., 2017. Astrochronostratigraphic polarity time scale (APTS) for the Late Triassic and Early Jurassic from continental sediments and correlation with standard marine stages. *Earth Science Reviews,* Volume 166, pp. 153-180.

Kirkland, J. I., Milner, A. R. C., Olsen, P. E. & Hargrave, J. E., 2014. The Whitmore Point Member of the Moenave Formation in its type area in northern Arizona and its age and correlation with the section in St. George, Utah: evidence for two major lacustrine sequences, Utah. *Geol. Assoc.,* Volume 43.

Kitching, J. W., 1977. The distribution of the Karoo vertebrate fauna. *Mem. Bernard Price Institute for Palaeontological Research, University of the Witwatersrand,* Volume 1, p. 131.

Kitching, J. W., 1979. Preliminary report on a clutch of six dinosaurian eggs from the Upper Triassic Elliot Formation, northern Orange Free State. *Palaeont. afr.,* Volume 22, pp. 41-45.

Kitching, J. W. & Raath, M. A., 1984. Fossils from the Elliot and Clarens Formations (Karoo Sequence) of the Northeastern Cape, Orange Free State and Lesotho, and a suggested biozonation based on tetrapods. *Palaeont. afr.,* Volume 25, pp. 111-125.

Knoll, F., 2002a. Les Fabrosauridae Galton, 1972 (Dinosauria : Ornthischia) : répartition géographique et stratigraphique ; systématique et phylogénie. *Thèse Dr., Mus. natl. Hist. Nat.,* p. 243.

Knoll, F., 2002b. New field works in the Upper Triassic-Lower Jurassic of Lesotho : preliminary results. *Journal of Vertebrate Paleontology,* 22(3), p. 75a.

Knoll, F., 2004. Review of the tetrapod fauna of the "Lower Stormberg Group" of the main Karoo Basin (southern Africa): Implication for the age of the Lower Elliot Formation. *Bulletin de la Societe géologique de France,* 175(1), pp. 73-83.

Knoll, F., 2005. The tetrapod fauna of the Upper Elliot and Clarens formations in the main Karoo Basin (South Africa and Lesotho). *Bulletin de la Société géologique de France,* 176(1), pp. 81-91.

Knoll, F. & Battail, B., 2001. New ornithischian remains from the Upper Elliot Formation (Lower Jurassic) of Lesotho and stratigraphical distribution of southern African fabrosaurids. *Geobios,* 34(4), pp. 415-421.

Kocurek, G. & Dott, R. H., 1981. Distinctions and Uses of Stratification Types in the Interpretation of Eolian Sand. *Journal of Sedimentary Petrology,* Volume 51, pp. 579-595.

Krönera, A. et al., 1999. Single zircon ages for granitoid gneisses in the Central Zone of the Limpopo Belt, Southern Africa and geodynamic significance. *Precambrian Research,* 93(4), pp. 299-337.

Lanci, L., Tohver, E., Wilson, A. & Flint, S., 2013. Upper Permian magnetic stratigraphy of the lower Beaufort Group,Karoo Basin. *Earth and Planetary Science Letters,* Volume 375, pp. 123-134.

Langer, M. C., Ezcurra, M. D., Bittencourt, J. S. & Novas, F. E., 2010. The origin and early evolution of dinosaurs. *Biological Reviews,* Volume 85, pp. 55-110.

Lawton, T. F. & Bradford, B. A., 2011. Correlation and provenance of Upper Cretaceous (Campanian) fluvial strata, Utah, USA, from zircon U-Pb geochronology and petrography. *Journal of Sedimentary Research,* 81(7), pp. 495-512.

Le Roux, J. S., 1974. *Palaeogeologiese en palaeogeografiese aspekte van die Etage Rooilae van die Sisteem Karoo.* Bloemfontein: PhD thesis, University Orange Free State.

Leith, M. J., 1970. *Geological well completion report of borehole SP 1/69 (Unpublished),* Johanneburg: Rep. Southern Oil Explor. Corp..

Leopold, L. B. & Wolman, M. G., 1957. River channel patterns: braided, meandering, and straight. *U.S Geological Survey Professional Paper,* Volume 282-B, pp. 39-85.

Lindeque, A. d. W. M. J. R. T. W. M. &. C. L., 2011. Deep crustal profile across the southern Karoo Basin and Beattie Magnetic Anomaly, South Africa: an integrated interpretation with tectonic implications. *South African Journal of Geology,* 114(3-4), pp. 265-292.

Lindström, S. et al., 2012. No causal link between terrestrial ecosystem change and methane release during the end-Triassic mass extinction. *Geology,* 40(6), pp. 531-534.

Lindström, S. et al., 2017. A new correlation of Triassic–Jurassic boundary successions in NW Europe, Nevada and Peru, and the Central Atlantic Magmatic Province: A time-line for the end-Triassic mass extinction. *Palaeogeography, Palaeoclimatology, Palaeoecology,* Volume 478, pp. 80-102.

Lock, B. E., 1978. The Cape Fold Belt of South Africa; tectonic control of sedimentation. *Proceedings (London) Geologists Association,* Volume 89, pp. 263-281.

Lock, B. E., 1980. Flat-plate subduction and the Cape Fold Belt of South Africa. *Geology,* Volume 8, pp. 35-39.

Lowe, D. R., 1975. Water escape structures in coarse-grained sediments. *Sedimentology,* 22(2), pp. 157-204.

Lucas, S. G. & Hancox, J. P., 2001. Tetrapod-based correlation of the non-marine Upper Triassic of southern Africa. *Albertiana,* Volume 25, pp. 5-9.

Lucas, S. G. et al., 2006. Triassic-Jurassic stratigraphic distribution of the theropod footprint ichnogenus Eubrontes. *SCIENCE Bulletin,* Volume 37, pp. 86-92.

Lucas, S. G. & Tanner, L. H., 2007. The nonmarine Triassic–Jurassic boundary in the Newark Supergroup of eastern North America. *Earth-Science Reviews,* Volume 84, pp. 1-20.

Ludwig, K., 2003. *Isoplot/Ex version 3: a Geochronological toolkit for Microsoft Excel.* Berkeley: Geochronology Centre.

Ludwig, K. R., 2009. *User's Manual for Isoplot 3.70. A Geochronological Toolkit for Microsoft Excel.* 4 ed. s.l.:Berkley Geochronology Centre Special Publication.

Macklin, M. G., 1985. Floodplain sedimentation in the Upper Axe Valley, Mendip, England. *Trans. Inst. Br. Geogr. New Ser.,* Volume 10, pp. 235-244.

MacRae, C. S., 1988. Palynostratigraphic correlation between the Lower Karoo sequence of the Waterberg and Pafuri coal-bearing basins and the Hammanskraal plant and macrofossil locality, Republic of South Africa. *Mem. Geol. Surv. S. Africa,* Volume 75, pp. 1-217.

Mange, M. A. & Maurer, H. F. W., 1992. Heavy minerals in the study of sediments: their application and limitations. In: *Heavy Minerals in Colour.* Dordrecht: Springer.

Margolis, S. & Krinsley, D., 1971. Submicroscopic frosting on eolian and subaqueous quartz sand grains. *Geol. Soc. Am. Bull.,* Volume 82, pp. 3395-3406.

Marsh, J. S., Hooper, P. R., Rehacek, J. & Duncan, A. R., 1997. Stratigraphy and age of Karoo basalts of Lesotho and implications for correlations within the Karoo Igneous Province. In: J. J. Mahoney & M. F. Coffin, eds. *Large Igenous Provinces: Continental, Oceanic and Planetary Flood Volcanism, Geophysical Monograph, vol. 100.* Washington, DC: American Geophysical Union, pp. 247-272.

Marsicano, C. A., Wilson, J. A. & Smith, R. M. H., 2009. A Temnospondyl trackway from the early Mesozoic of western Gondwana and its implications for basal tetrapod locomotion. *PLoS One,* 9(8), p. e103255.

Martínez, R. N. et al., 2015. A new Late Triassic vertebrate assemblage from northwestern Argentina. *Ameghiniana,* Volume 52, pp. 379-390.

Marzoli, A. et al., 2004. Synchrony of the Central Atlantic magmatic province and the Triassic-Jurassic boundary climatic and biotic crisis. *Geology,* 32(11), pp. 973-976.

Mattinson, J. M., 2010. Analysis of the relative decay constants of 235U and 238U by multi-step CA-TIMS measurements of closed-system natural zircon samples. *Chemical Geology,* Volume 275, pp. 186-198.

McKay, M. P. et al., 2015. U-PB zircon tuff geochronology from the Karoo Basin, South Africa: implications of zircon recycling on stratigraphic age controls. *International Geology Review,* 57(4), pp. 393-410.

McPhee, B. W. et al., 2015. A new basal sauropod from the pre-Toarcian Jurassic of South Africa: evidence of niche-partitioning at the sauropodomorph–sauropod boundary?. *Scientific Reports,* Volume 5, p. 13224.

McPhee, B. W., Bordy, E. M., Sciscio, L. & Choiniere, J. N., 2017. The sauropodomorph biostratigraphy of the Elliot Formation of southern Africa: Tracking the evolution of Sauropodomorpha across the Triassic–Jurassic boundary. *Acta Palaeontologica Polonica,* Volume 62, pp. 1-25.

McPhee, B. W., Yates, A. M., Choiniere, J. N. & Abdala, F., 2014. The complete anatomy and phylogenetic relationships of Antetonitrus ingenipes (Sauropodiformes, Dinosauria): implications for the origins of Sauropoda. *Zoological Journal of the Linnean Society,* Volume 171, pp. 151-205.

Merriman, R. J., Highley, D. E. & Cameron, D. G., 2003. Definition and characteristics of very-fine grained sedimentary rocks: clay mudstone, shale and slate. In: R. J. Merriman, D. E. Highley & D. G. Cameron, eds. *British Geological Survey Commissioned Report.* Nottingham: Bristish Geological Survey, pp. 1-14.

Miall, A. D., 1977. A review of the braided river depositional environment. *Earth-Science Reviews,* 13(1), pp. 1-62.

Miall, A. D., 1985. Architectural-element analysis: a new method of facies analysis applied to fluvial deposits. *Earth Science Reviews,* Volume 22, pp. 261-308.

Miall, A. D., 1991. Hierarchies of architectural units in terrigenous clastic rocks, and their relationship to sedimentation rate. In: A. D. Miall & N. Tyler, eds. *The three-dimensional facies architecture of terrigenous clastic sediments and its implications for hydrocarbon discovery and recovery.* s.l.: Society of Economic Paleontologists and Mineralogists, Concepts in Sedimentology and Paleontology 3, pp. 6-12.

Miall, A. D., 1996. *The Geology of Fluvial Deposits.* Oxford: Blackwell Scientific Publications.

Miall, A. D., 1997. *The Geology of Stratigraphic Sequences.* Berlin, Heidelberg, New York, London, Paris, Tokyo, Hong Kong: Springer-Verlag.

Miall, A. D., 2014. The Facies and Architecture of Fluvial Systems. In: *Fluvial Depositional Systems.* s.l.:Springer International Publishing, pp. 9-68.

Millard, C., Hajek, E. & Edmonds, D. A., 2017. Evaluating controls on crevasse-splay size: implications for floodplain-basin filling. *Journal of Sedimentary Research,* 87(7), pp. 722-739.

Millard, C. L., 2013. *Evaluating controls on crevasse-splay growth in modern and ancient fluvial systems.* s.l.:Unpublished MSc thesis, The Pennsylvania State University.

Mjøs, R., Walderhaug, O. & Prestholm, E., 1993. Crevasse splay sandstone geometries in the Middle Jurassic Ravenscar Group of Yorkshire, UK. *Spec. Publs Int. Ass. Sediment.,* Volume 17, pp. 167-184.

Moodley, A., 2015. The sedimentary petrology of carbonate nodules in the Elliot Formation, Karoo Supergroup, main Karoo Basin (South Africa). *(Unpublished MSc Thesis) University of Cape Town .*

Nanson, G. C., 1980. Point-bar and flood plain formation of the meandering Beatton River, northeastern British Columbia, Canada. *Sedimentology,* Volume 27, pp. 3-30.

Nanson, G. C. & Croke, J. C., 1992. A genetic classification of floodplains. *Geomorphology,* 4(6), pp. 459-486.

Nanson, G. C., Rust, B. R. & Taylor, G., 1986. Coexistent mud braids and anastomosing channels in an aridzone river: Cooper creek, central Australia. *Geology,* Volume 14, pp. 175-178.

Nanson, G. C., Young, R. W., Price, D. M. & Rust, B. R., 1988. Stratigraphy, sedimentology and Late Quaternary chronology of the Channel Country of Western Queensland. In: R. F. Warner, ed. *Fluvial Geomorphology of Australia.* Sydney: Academic Press, pp. 151-175.

Nasdala, L. et al., 2008. Zircon M257–a homogeneous natural reference material for the ion microprobe U-Pb analysis of zircon. *Geostandards and Geoanalytical Research,* Volume 32, pp. 247-265.

Nemec, W. & Muszyński, A., 1982. Volcaniclastic alluvial aprons in the Tertiary of Sofia district (Bulgaria). *Ann. Geol. Soc. Pol.,* Volume 52, pp. 239-303.

Neveling, J., 2004. *Stratigraphic and sedimentological investigation of the contact between the Lystrosaurus and the Cynognathus Assemblage Zones (Beaufort Group: Karoo Supergroup).* 137 ed. Pretoria: Council for Geoscience, Bulletin.

Newell, N. D., 1963. Crises in the history of life. *Scientific American,* Volume 208, pp. 76-93.

Newell, N. D., 1967. Revolutions in the history of life. In: C. C. J. Albritton, ed. *Uniformity and simplicity.* s.l.:Geological Society of America Special Paper, 89, pp. 63-91.

Nichols, G., 1999. Sedimentology and Stratigraphy. In: *Sedimentology and Stratigraphy.* Oxford: Wiley-Blackwell, p. 419.

O'Brien, P. E. & Wells, A. T., 1986. A small, alluvial crevasse splay. *J. Sed. Res.,* Volume 56, pp. 876-879.

Oberthu¨r, T., Davis, D. W., Blenkinsop, T. G. & Ho¨hndorf, A., 2002. Precise U–Pb mineral ages, Rb–Sr and Sm–Nd systematics for the Great Dyke, Zimbabwe—constraints on late Archean events in the Zimbabwe craton and Limpopo belt. *Precambrian Research,* Volume 113, pp. 293-305.

Olsen, P. E. & Galton, P. M., 1977. Triassic-Jurassic tetrapod extinctions; Are they real?. *Science,* Volume 197, pp. 983-986.

Olsen, P. E. & Galton, P. M., 1984. A review of the reptile and amphibian assemblages from the Stormberg of South Africa, with special emphasis on the footprints and the age of the Stormberg. *Palaeont. afr.,* Volume 25, pp. 87-100.

Olsen, P. E. et al., 2002a. Ascent of dinosaurs linked to an Iridium anomaly at the Triassic-Jurassic Boundary. *Science,* Volume 296, p. 13051307.

Olsen, P. E., Kent, D. V. & Whiteside, J. H., 2011. Implications of the Newark Supergroup-based astrochronology and geomagnetic polarity time scale (Newark-APTS) for the tempo and mode of the early diversification of the Dinosauria. *Earth and Environmental Science Transactions of the Royal Society of Edinburgh,* Volume 101, pp. 201-229.

Olsen, P. E. et al., 2002b. Continental Triassic-Jurassic boundary in central Pangea: Recent progress and discussion of an Ir anomaly. *Geological Society of America,* Volume 356, pp. 505-522.

Olsen, P. E., McCune, A. R. & Thomson, K. S., 1982. Correlation of the early Mesozoic Newark Supergroup by vertebrates, principally fishes. *Amer. J. Sci.,* Volume 282, pp. 1-44.

Olsen, P. E., Shubin, N. H. & Anders, M. H., 1987. New Early Jurassic tetrapod assemblages constrain Triassic–Jurassic tetrapod extinction event. *Science,* Volume 237, pp. 1025-1029.

Olsen, P. E. & Sues, H. D., 1986. Correlation of the continental Late Triassic and Early Jurassic sediments, and patterns of the Triassic-Jurassic tetrapod transition. In: K. Padian, ed. *The beginning of the age of dinosaurs; Faunal change across the Triassic-Jurassic boundary.* New York: Cambridge University Press, pp. 321-351.

Ottone, E. G. et al., 2014. A new Late Triassic age for the Puesto Viejo Group (San Rafael depocenter, Argentina): SHRIMP U–Pb zircon dating and biostratigraphic correlations across southern Gondwana. *Journal of South Amercian Earth Sciences,* Volume 56, pp. 186-199.

Pálfy, J., 2008. The quest for refined calibration of the Jurassic time-scale. *Proceedings of the Geologists' Association,* Volume 119, pp. 85-95.

Pálfy, J. et al., 2001. Carbon isotope anomaly and other geochemical changes at the Triassic-Jurassic boundary from a marine section in Hungary. *Geology,* 29(11), pp. 1047-1050.

Pálfy, J. et al., 2007. Triassic-Jurassic boundary events inferred from integrated stratigraphy of the Csővár section, Hungary. *Palaeogeography Palaeoclimatology Palaeoecology,* Volume 244, pp. 11-33.

Pálfy, J. et al., 2000. Timing the end-Triassic mass extinction: first on land, then in the sea?. *Geology,* Volume 28, pp. 39-42.

Pankhurst, R. J., Rapela, C. W. & Fanning, C. M., 2000. Age and origin of coeval TTG, I- and S-type granites in the Famatinian belt of NW Argentina. *Transactions of the Royal Society of EdinburghL Earth Sciences,* Volume 91, pp. 151-168.

Pankhurst, R. J., Rapela, C. W., Fanning, C. M. & Márquez, M., 2006. Gondwanide continental collision and the origin of Patagonia. *Earth-Science Reviews,* Volume 76, pp. 235-257.

Pankhurst, R. J. et al., 2014. The Gondwana connections of northern Patagonia. *Journal of the Geological Society,* Volume 171, pp. 313-328.

Pankhurst, R. J., Rapela, C. W. & Marquez, M. J., 1993. Geochronologia y petrogenesis de los granitoides Jurasicos del Noreste del Macizo del Deseado. *XII Congreso Geologico Argentino y II Congreso de Exploracion de Hidrocarburos,* pp. 134-141.

Pankhurst, R. J. et al., 1998. The Famatinian magmatic arc in the southern Sierras Pampeanas. In: R. J. Pankhurst & C. W. Rapela, eds. *The Proto-Andean Margin of Gondwana.* London: Special Publication of the Geological Society 142, pp. 343-367.

Paton, C. et al., 2010. Improved laser ablation U-Pb zircon geochronology through robust downhole fractionation correction. *Geochemistry, Geophysics, Geosystems,* Volume 11, p. Q0AA06.

Paton, D. A., Macdonald, D. I. M. & Underhill, J. R., 2006. Applicability of thin or thick skinned structural models in a region of multiple inversion episodes; southern South Africa. *Journal of Structural Geology,* Volume 28, pp. 1933-1947.

Pierce, E. L. et al., 2014. A comparison of detrital U–Pb zircon, 40Ar/39Ar hornblende, 40Ar/39Ar biotite ages in marine sediments off East Antarctica: Implications for the geology of subglacial terrains and provenance studies. *Earth-Science Reviews,* Volume 138, pp. 156-178.

Potter, P. E. & Pettijohn, F. J., 1977. *Palaeocurrents and basin analysis.* 2nd ed. Berlin: Springer-Verlag.

Pranter, M. J., Cole, R. D., Panjaitan, H. & Sommer, N. K., 2009. Sandstone-body dimensions in a lower coastal-plain depositional setting: Lower Williams Fork Formation, Coal Canyon, Piceance Basin, Colorado. *AAPG Bulletin,* 93(10), pp. 1379-1401.

Pupin, J. P., 1980. Zircon and granite petrology. *Contributions to Mineralogy and Petrology,* Volume 73, pp. 207-220.

Pysklywec, R. N. & Mitrovica, J. X., 1999. The role of subduction-induced subsidence in the evolution of the Karoo Basin. *The Journal of Geology,* Volume 107, pp. 155-164.

Raath, M. A., Kitching, J. W., Shone, R. W. & Rossouw, G. W., 1990. Dinosaur tracks in Triassic Molteno sediments: The earliest evidence of dinosaurs in South Africa?. *Palaeont. afr.,* Volume 27, pp. 89-95.

Rampino, M. R. & Stothers, R. B., 1988. Flood basalt volcanism during the past 250 million years. *Science,* Volume 241, pp. 663-668.

Rapela, C. W., Pankhurst, R., Fanning, C. M. & Grecco, L. E., 2003. Basement evolution of the Sierra de la Ventana Fold Belt: New evidence for Cambrian continental rifting along the southern margin of Gondwana. *Journal of the Geological Society,* Volume 160, pp. 613-628.

Raup, D. M. & Sepkoski, J. J., 1982. Mass Extinctions in the Marine Fossil Record. *Science,* 215(4539), pp. 1501-1503.

Ray, S. & Chinsamy-Turan, A., 2002. A theropod tooth from the Late Triassic of southern Africa. *Journal of Biosciences,* 27(3), pp. 295-298.

Reid, D. L., 1997. Sm–Nd age and REE geochemistry of Proterozoic arc-related igneous rocks in the Richtersveld Subprovince, Namaqua Mobile Belt, southern Africa. *Journal of African Earth Science,* Volume 24, pp. 621-633.

Reinech, H. E. & Singh, I. S., 1973. *Depositional Sedimentary Environments.* New York: Springer-Verlag.

Reineck, H. E. & Singh, I. B., 1980. *Depositional sedimentary environments with reference to terrigenous clastics.* 2 ed. Berlin-Heidelberg-New York: Springer-Verlag.

Richoz, S. et al., 2012. Hydrogen sulphide poisoning of shallow seas following the end-Triassic extinction. *Nature Geoscience,* Volume 5, pp. 662-667.

Rieck, E. F., 1973. Fossil insects from the Upper Permian of Natal, South Africa. *Annual Natal Museum,* Volume 21, pp. 513-532.

Rieck, E. F., 1974. Upper Triassic insects from the Molteno 'Formation', South Africa. *Palaeont. afr.,* Volume 16, pp. 17-23.

Rieck, E. F., 1976a. An unusual mayfly (Insecta: Ephemeroptera) from the Triassic of South Africa. *Palaeont. afr.,* Volume 19, pp. 149-151.

Rieck, E. F., 1976b. A new collection of insects from the Upper Triassic of South Africa. *Ann. Natal Mus.,* 22(3), pp. 791 -820.

Rieck, E. F., 1976c. An immature fossil insect from the Upper Permian of Natal. *Ann. Natal Mus.,* Volume 22, pp. 271-274.

Riley, T. R. e. a., 2004. U-Pb zircon (SHRIMP) ages for the Lebombo rhyolites, South Africa: refining the duration of Karoo volcanism. *Journal of the Geological Society, London,* pp. 547-550.

Riley, T. R. et al., 2016. Early Jurassic magmatism on the Antarctic Peninsula and potential correlation with the Subcordilleran plutonic belt of Patagonia. *Journal of the Geological Society,* Volume 174, pp. 365-376.

Robinson, A. C., Ducea, M. & Lapen, T. J., 2012. Detrital zircon and isotopic constraints on the crustal architecture and tectonic evolution of the northern Pamir. *Tectonics,* Volume 31, p. TC2016.

Rocha-Campos, A. C. et al., 2011. 30 million years of Permian volcanism recorded in the Choiyoi igneous province (W Argentina) and their source for younger ash fall deposits in the Paraná Basin: SHRIMP U-Pb zircon geochronology evidence. *Gondwana Research,* Volume 19, pp. 509-523.

Rozendaal, A., Gresse, P. G., Scheepers, R. & Le Roux, J. P., 1999. Neoproterozoic to Early Cambrian crustal evolution of the Pan-African Saldania Belt, South Africa. *Precambrian Research,* Volume 97, pp. 303-323.

Rubidge, B. S., 2005. Re-uniting lost continents – Fossil reptiles from the ancient Karoo and their wanderlust. *South African Journal of Geology,* 108(3), pp. 135-172.

Rubidge, B. S. et al., 2013. High-precision temporal calibration of Late Permian vertebrate biostratigraphy: U-Pb zircon constraints from the Karoo Supergroup, South Africa. *GEOLOGY,* 41(3), pp. 363-366.

Rubidge, B. S., Hancox, P. J. & Catuneanu, O., 2000. Sequence analysis of the Ecca-Beaufort contact in the southern Karoo of South Africa. *South African Journal of Geology,* 103(1), pp. 81-96.

Rubidge, B. S. et al., 1995. An introduction to the biozonation of the Beaufort Group. In: B. S. Rubidge, ed. *Biostratigraphy of the Beaufort Group (Karoo Supergroup).* Pretoria: SACS Biostratigraphic Series 1, pp. 1-2.

Rust, B. R., 1978. A classification of alluvial channel systems. In: A. D. Miall, ed. *Fluvial Sedimentology.* s.l.:Can. Soc. Petrol. Geol., Calgary, Mem., 5, pp. 187-198.

Rust, I. C., 1959. On the sedimentation of the Molteno Sandstone in the vicinity of Molteno, Cape Province. *Ann. Univ. Stellenbosch,* Volume 37, pp. 167-223.

Rust, I. C., 1975. Tectonic and sedimentary framework of Gondwana Basins in southern Africa. *Third Gondwana Symposium,* Volume 5, pp. 554-564.

Rydgren, B., 1988. A Geomorphological Approach to Soil Erosion Studies in Lesotho. *Geografiska Annaler,* Volume 70A, pp. 255-262.

Sarti, G., Zanchetta, G., Mazza, P. & Grassi, R., 2001. Sedimentological and palaeontological features of an ancient alluvial plain in the Lucca Basin (Central Italy). *Eclogae geol. Helv.,* Volume 94, pp. 107-117.

Scheepers, R. & Armstrong, R., 2002. New U-Pb SHRIMP zircon ages of the Cape Granite Suite: implications for the magmatic evolution of the Saldania Belt. *South African Journal of Geology,* 105(3), pp. 241-156.

Schmieder, M. et al., 2010. A Rhaetian 40Ar/39Ar age for the Rochechouart impact structure (France) and implications for the latest Triassic sedimentary record. *Meteoritics & Planetary Science,* 45(8), pp. 1225-1242.

Schmitz, G. & Rooyani, F., 1987. Geological Evolution. In: G. Schmitz & F. Rooyani, eds. *Lesotho Geology, Geomorphology, Soils.* The National Universiy of Lesotho: Morija Printing Works-Lesotho, pp. 3-66.

Schoene, B., 2014. U–Th–Pb Geochronology. In: H. Holland & K. Turekian, eds. *Treatise on Geochemistry 2nd Edition.* s.l.:Elsevier, pp. 341-370.

Schoene, B. et al., 2010. Correlating the end-Triassic mass extinction and flood basalt volcanism at the 100 ka level. *Geology,* 38(5), pp. 387-390.

Schumm, S. A., 1981. Evolution and response to the fluvial system, sedimentological implications. In: F. G. Ethridge & R. M. Flores, eds. *Recent and Ancient Nonmarine Environments: Models for Exploration.* s.l.:SEPM, Special Publication, 31, pp. 19-29.

Schumm, S. A., 1985. Patterns of alluvial rivers. *Annual Review of Earth and Planetary Sciences,* Volume 13, pp. 5-27.

Schwertmann, U., 1993. Relations between iron oxides, soil color, and soil formation. In: J. M. Bigham & E. J. Ciolkosz, eds. *Soil Color.* s.l.:SSSA Special Publication 31, pp. 51-69.

Schwertmann, U. & Taylor, R. M., 1989. Iron oxides. In: J. B. Dixon & S. B. Weed, eds. *Minerals in Soil Environments.* Madison, Wisconsin, USA: Soil Science Society of America, pp. 379-438.

Sciscio, L., 2015. *Position of the Triassic-Jurassic boundary in South Africa and Lesotho: A multidisciplinary approach aimed at improving the chronostratigraphy and biostratigraphy of the Elliot Formation, Stormberg Group.* s.l.:University of Cape Town [Unpublished PhD].

Sciscio, L. et al., 2017b. The first megatheropod tracks from the Lower Jurassic upper Elliot Formation, Karoo Basin, Lesotho. *PLoS ONE,* 12(10), p. e0185941.

Sciscio, L., Bordy, E. M., Reid, M. & Abrahams, M., 2016. Sedimentology and ichnology of the Mafube dinosaur track site (Lower Jurassic, eastern Free State, South Africa): a report on footprint preservation and palaeoenvironment. *PeerJ,* Volume 4:e2285.

Sciscio, L., de Kock, M., Bordy, E. M. & Knoll, F., 2017a. Magnetostratigraphy across the Triassic-Jurassic boundary in the main Karoo Basin. *Gondwana Research,* Volume 51, pp. 177-192.

Sepkoski, J. J., 1982. Mass extinctions in the Phanerozoic oceans: a review. *Geological Society of America Special Papers,* Volume 190, pp. 283-290.

Sertich, J. J. W. & Loewen, M. A., 2010. A new basal sauropodomorph Dinosaur from the Lower Jurassic Navajo Sandstone of Southern Utah. *PLoS ONE,* 5(3), p. e9789.

Singh, I. B., 1972. On the bedding in the natural-levee and the point-bar deposits of the Gomti River, Uttar Pradesh, India. *Sedimentary Geology,* 7(4), pp. 309-317.

Sláma, J. K. J. C. D. C. J. L. et al., 2008. Plešovice zircon—a new natural reference material for U–Pb and Hf isotopic microanalysis. *Chemical Geology,* Volume 249, pp. 1-35.

Smith, D. G., 1983. Anastomosed fluvial deposits: modern examples from Western Canada . In: J. D. Collinson & J. Lewin, eds. *Modern and Ancient Fluvial Systems.* s.l.:Int. Assoc. Sedimentol. Spec. Publ., 6, pp. 155-168.

Smith, N. D., Cross, T. A., Dufficy, J. P. & Clough, S. R., 1989. Anatomy of an avulsion. *Sedimentology,* Volume 36, pp. 1-23.

Smith, R. & Kitching, J., 1997. Sedimentology and vertebrate taphonomy of the Tritylodon Acme Zone: a reworked palaeosol in the Lower Jurassic Elliot Formation, Karoo Supergroup, South Africa. *Palaeogeography, Palaeoclimatology, Palaeoecology,* Volume 131, pp. 29-50.

Smith, R. M. H., 1987. Morphology and depositional history of exhumed Permian point bars in the southwestern Karoo. *South African Journal of Sedimentary Petrology,* Volume 57, pp. 19-29.

Smith, R. M. H., 1990. A review of the stratigraphy and sedimentary environments of the Karoo basin of South Africa. *Journal of African Earth Sciences,* Volume 10, pp. 117-137.

Smith, R. M. H., 1995. Changing fluvial environments across the Permian-Triassic boundary in the Karoo Basin, South Africa and possible causes of tetrapod extinctions. *Palaeogeography Palaeoclimatology Palaeoecology,* Volume 117, pp. 81-104.

Smith, R. M. H., Eriksson, P. G. & Botha, W. J., 1993. A review of the stratigraphy and sedimentary environments of the Karoo-aged basins of Southern Africa. *Journal of African Earth Sciences (and the Middle East),* 16(1-2), pp. 143-169.

Smith, R. M., Marsicano, C. A. & Wilson, J. A., 2009. Sedimentology and paleoecology of a diverse Early Jurassic tetrapod tracksite in Lesotho, southern Africa.. *Palaios, 24 (10),* pp. 672-684.

Sneh, A., 1983. Desert stream sequences in the Sinai Peninsula. *Journal of sedimentary Petrology,* Volume 53, pp. 1271-1279.

Southard, J. B., 1971. Representation of bed configurations in depth-velocity-size diagrams. *Journal of Sedimentary Research,* Volume 41, pp. 903-915.

Spencer, C. J., Kirkland, C. L. & Taylor, R. J. M., 2016. Strategies towards statistically robust interpretations of in situ U–Pb zircon geochronology. *Geoscience Frontiers,* 7(4), pp. 581-589.

Stacey, J. S. & Kramers, J. D., 1975. Approximation of terrestrial lead isotope evolution by a 2-Stage Model. *Earth and Planetary Science Letters,* 26(2), pp. 207-221.

Stear, W. M., 1983. Morphological characteristics of ephemeral stream channel and overbank splay sandstone bodies in the Permian Lower Beaufort Group, Karoo Basin, South Africa. In: J. D. Collinson & J. Lewin, eds. *Modern and Ancient Fluvial Systems.* s.l.:Special Publications International Association of Sedimentologists (6), pp. 405-420.

Stear, W. M., 1985. Comparison of bedform distribution and dynamics of modern and ancient sandy ephemeral flood deposits in the southwestern Karoo region, South Africa. *Sedimentary Geology,* Volume 45, pp. 209-230.

Stockley, G. M., 1947. *Report on the geology of Basutoland.* Maseru: Government Printer.

Stollhofen, H., Stanistreet, I. G., Bangert, B. & Grill, H., 2000. Tuffs, tectonism and glacially related sea-level changes, Carboniferous-Permian, southern Namibia. *Palaeogeography, Palaeoclimatology, Palaeoecology,* Volume 161, pp. 127-150.

Streel, M. & Theron, J. N., 1999. The Devonian-Carboniferous boundary in South Africa and the age of the earliest episode of the Dwyka glaciation: New palynological result. *Episodes,* 22(1), pp. 41-44.

Suarez, C. A. et al., 2017. A chronostratigraphic assessment of the Moenave Formation, USA using C-isotope chemostratigraphy and detrital zircon geochronology: Implications for the terrestrial end Triassic extinction. *Earth and Planetary Science Letters,* Volume 475, pp. 83-93.

Surpless, K. D., Graham, S. A., Covault, J. A. & Wooden, J. L., 2006. Does the Great Valley Group contain Jurassic strata? Reevaluation of the age and early evolution of a classic forearc basin. *Geology,* Volume 34, pp. 21-24.

Tankard, A. J. et al., 1982. *Crustal Evolution of Southern Africa-3.8 billion years of earth history.* New York: Springer-Verlag.

Tankard, A. J. et al., 2012. Geodynamic interpretation of the Cape and Karoo Basins, South Africa. In: D. G. Roberts & A. W. Bally, eds. *Regional Geology and Tectonics: Phanerozoic Passive Margins, Cratonic Basins and Global Tectonic Maps.* s.l.:Elsevier, pp. 868-945.

Tankard, A. et al., 2009. Tectonic evolution of the Cape and Karoo basins of South Africa. *Marine and Petroleum Geology,* 26(8), pp. 1379-1412.

Tanner, L. H., Hubert, J. F., Coffey, B. P. & McInerney, D. P., 2001. Stability of atmospheric CO2 levels across the Triassic/Jurassic boundary. *Nature,* Volume 411, pp. 675-677.

Tanner, L. H., Kyte, F. T. & Walker, A. E., 2008. Multiple Ir anomalies in uppermost Triassic to Jurassic-age strata of the Blomidon Formation, Fundy basin, eastern Canada. *Earth Planetary Science Letters,* Volume 274, pp. 103-111.

Tanner, L. H., Lucas, S. G. & Chapman, M. G., 2004. Assessing the record and causes of Late Triassic extinctions. *Earth-Science Reviews,* Volume 65, pp. 103-139.

Tanner, W. F., 1967. Ripple mark indices and their uses. *Sedimentology,* 9(2), pp. 89-104.

Tasch, P., 1984. Biostratigraphy and palaeontology of some conchostracan-bearing beds in southern Africa. *Palaeont. afr,* Volume 25, pp. 61-85.

Thomas, R. J., Cornell, D. H., Moore, J. M. & Jacobs, J., 1994. Crustal evolution of the Namaqua-Natal Metamorphic Province, southern Africa. *South African Journal of Geology,* 97(1), pp. 8-14.

Tucker, M. E., 2011. *Sedimentary rocks in the field: a practical guide.* 4th ed. Sussex: Wiley Blackwell, 275pp.

Tucker, R. T., 2014. *Stratigraphy, Sedimentation and Age of the Upper Cretaceous Winton Formation, central-western Queensland, Australia: Implications for regional palaeogeography, palaeoenvironments and Gondwanan palaeontology.* s.l.:Unpublished PhD Thesis, James Cook University.

Tucker, R. T. et al., 2013. Detrital zircon age constraints for the Winton Formation, Queensland: Contextualizing Australia's Late Cretaceous dinosaur faunas. *Gondwana Research,* 24(2), pp. 767-779.

Tunbridge, I. P., 1981. Sandy high-energy flood sedimentation—some criteria for recognition, with an example from the Devonian of S.W. England. *Sedimentary Geology,* Volume 28, pp. 79-95.

Tunbridge, I. P., 1984. Facies model for a sandy ephemeral stream and clay playa complex; the Middle Devonian Trentishoe Formation of North Devon, U.K.. *Sedimentology,* 31(5), pp. 697-715.

Turner, B. R., 1969. The stratigraphy and sedimentological history of the Molteno stage in part of the North East Cape Province. *(Unpublished MSc Thesis) Univerity of the Witwatersrand, Johannesburg,* pp. 203-204.

Turner, B. R., 1975. Statistical appraisal of Molteno (Triassic) sedimentary cycles from the upper part of the Karoo (Gondwana) system in South Africa. *Journal of Sedimentary Petrology,* Volume 45, pp. 95-104.

Turner, B. R., 1978. Trace fossils from the Upper Triassic fluviatile Molteno Formation of the Karoo (Gondwana) Supergroup, Lesotho. *Journal of Palaeontology,* Volume 52, pp. 959-963.

Turner, B. R., 1981. The occurrence and stratigraphic significance of bone-bearing mudstone pellet conglomerates from the Beaufort Group in the Jansenville District, Cape Province, South Africa. *Palaeontologia Africana,* Volume 24, pp. 63-73.

Turner, B. R., 1983. Braidplain deposition of the Upper Triassic Molteno Formation in the main Karoo (Gondwana} Basin, South Africa. *Sedlmentology,* Volume 30, pp. 77-89.

Turner, B. R., 1985. Uranium mineralization in the Karoo Basin, South Africa. *Economic Geology,* Volume 80, pp. 256-269.

Turner, B. R., 1986. Tectonic and climatic controls on continental depositlonal facies in the Karoo Basin of northern Natal, South Africa. *Sedimentary Geology,* Volume 48, pp. 231-257.

Turner, B. R., 1999. Tectonostratigraphical development of the Upper Karoo foreland basin orogenic unloading versus thermally-induced Gondwana rifting. *Journal of African Earth Sciences,* 28(1), pp. 215-238.

Turner, P., 1980. Ancient Aeolian Red Beds. In: *Developments in Sedimentology (29); Continental Red Beds.* Amsterdam-Oxford-New York: Elsevier, pp. 105-107.

Valencio, D. A., Mendía, J. E. & Vilas, J. E., 1975. Palaeomagnetism and K-Ar ages of triassic igneous rocks from the Ischigualasto-Ischichuca Basin and Puesto Viejo Formation, Argentina. *Earth and Planetary Science Letters,* 26(3), pp. 319-330.

van Breeman, N., 1988. Long-term chemical, mineralogical and morphological effects of iron-redox processes in periodically flooded soils. In: J. Stucki, B. Goodman & U. Schwertmann, eds. *Iron in Soils and Clay Minerals.* s.l.:NATO ASI Series, D. Reidel Publishing Company.

van Dijk, D. E., 1978. Trackways in the Stormberg. *Palaeontologia africana,* Volume 21, pp. 113-120.

van Dijk, D. E., Hobday, D. K. & Tankard, A. J., 1978. Permo-Triassic lacustrine deposits in the Eastern Karoo Basin, Natal, South Africa. In: A. Matter & M. E. Tucker, eds. *Modern and ancient lake sediments.* s.l.:Special Publications International Association of Sedimentologists, 2, pp. 225-239.

van Vuuren, C. J., 1972. *Geological well completion report of the Swartberg (SW1/67) borehole (Unpublished),* s.l.: Rep. Southern Oil Explor. Corp.

Van Zijl, G. M., 2010. An investigation of the soil properties controlling gully erosion in a sub-catchment in Maphutseng, Lesotho. *University of Stellenbosch [Unpublished MSc Thesis].*

Veevers, J. J., Powell, C., Collinson, J. W. & López-Gamundi, O. R., 1994. Synthesis. In: J. J. Veevers & C. Powell, eds. *Permian-Triassic Pangean Basins and Foldbelts along the Panthalassan Margin of Gondwanaland.* s.l.:Geological Society of America Memoir, 184, pp. 223-279.

Viglietti, P. A., Frei, D., Rubidge, B. S. & Smith, R. M. H., 2018. U-Pb detrital zircon dates and provenance data from the Beaufort Group (Karoo Supergroup) reflect sedimentary recycling and air-

fall tuff deposition in the Permo-Triassic Karoo foreland basin. *Journal of African Earth Sciences,* Volume 143, pp. 59-66.

Visser, J. N. J., 1984. A review of the Stormberg Group and Drakensberg Volcanics in southern Africa. *Palaeontologia Africana,* Volume 25, pp. 5-27.

Visser, J. N. J., 1986. Lateral lithofacies relationships in the glacigene Dwyka Formation in the western and central parts of the Karoo Basin. *Transactions of the Geological Society of South Africa,* Volume 89, pp. 373-383.

Visser, J. N. J., 1989. The Permo-Carboniferous Dwyka Formation of southern Africa: deposition by a predominantly subpolar marine ice sheet. *Palaeogeography, Palaeoclimatology, Palaeoecology,* Volume 70, pp. 377-391.

Visser, J. N. J., 1990. The age of the late Palaeozoic glucagon deposits in southern Africa. *South African Journal of Geology,* Volume 93, pp. 366-375.

Visser, J. N. J., 1991. Self-destructive collapse of the Permo-Carboniferous marine ice sheet in the Karoo Basin: evidence from the southern Karoo. *South African Journal of Geology,* Volume 94, pp. 255-262.

Visser, J. N. J., 1992. Deposition of the Early to Late Permian Whitehill Formation during a sea-level high stand in a juvenile foreland basin. *Transactions of the Geological Society of South Africa,* Volume 95, pp. 181-193.

Visser, J. N. J. & Botha, B. J. V., 1980. Meander channel, point bar, crevasse splay and aeolian deposits from the Elliot Formation in Barkly Pass, North-Eastern Cape. *Transactions of the Geological Society of South Africa,* Volume 83, pp. 55-62.

Visser, J. N. J. & Loock, J. C., 1978. Water depth in the main Karoo Basin, South Africa, during Ecca (Permian) sedimentation. *Transaction of the Geological Society of South Africa,* Volume 81, pp. 185-191.

Vorster, C., 2013. *Laser ablation ICP-MS age determination of detrital zircon populations in the Phanerozoic Cape and Lower Karoo Supergroups (South Africa) and correlatives in Argentina.* s.l.:University of Johannesburg [Unpublished PhD Thesis].

Walker, R. G., 1976. Facies Models 3. Sandy Fluvial Systems. *Journal of the Geological Association of Canada,* 3(2), pp. 101-109.

Walters, S. W., 2017. *Reanalysis of cryptic sedimentological relationships involving the southern Karoo Ripon Formation and the southwestern Karoo Vischkuil/Laingsburg Formations of the Ecca Group: Implications for basin and palaeoenvironmental reconstruction.* s.l.:University of Stellenbosch [Unpublished MSc Thesis].

Ward, P. D. et al., 2001. Sudden productivity collapse associated with the Triassic-Jurassic Boundary mass extinction. *SCIENCE,* Volume 292, pp. 1148-1151.

Warren, A. & Damiani, R., 1999. Stereospondyl amphibians from the Elliot Formation of South Africa. *Palaeont. afr.,* Volume 35, pp. 45-54.

Werner, M., 2006. *The stratigraphy, sedimentology, and age of the Late Palaeozoic Mesosaurus inland sea, SW Gondwana—New Implications from studies on sediments and altered pyroclastic*

layers of the Dwyka and Ecca Group (Lower Karoo Supergroup) in Southern Namibia. s.l.:University of Würzburg [Unpblished PhD thesis].

Whiteside, J. H. et al., 2010. Compound-specific carbon isotopes from Earth's largest flood basalt eruptions directly linked to the end-Triassic mass extinction. *PNAS,* 107(15), pp. 6721-6725.

Wignall, P., 2005. The link between Large Igneous Province eruptions and mass extinctions. *Elements,* 1(5), pp. 293-297.

Wignall, P. B., 2001. Large igneous provinces and mass extinctions. *Earth-Sciences Reviews,* Volume 53, pp. 1-33.

Williams, I. S. & Claesson, S., 1987. Isotopic evidence for the Precambrian provenance and Caledonian metamorphism of high grade paragneisses from the Seve Nappes, Scandinavian Caledonides: Ion microprobe zircon U-Th-Pb. *Contributions to Mineralogy and Petrology,* Volume 97, pp. 205-217.

Wilson, J. A., Marsicano, C. A. & Smith, R. M. H., 2009. Dynamic locomotor capabilities revealed by early dinosaur trackmakers from southern Africa. *PLoS ONE,* 4(10), p. e7331.

Winter, H. d. l. R., 1984. Tectonostratigraphy, as applied to the analysis of South African Phanerozoic basins. *Trans. Geol. Soc. S. Afr.,* Volume 87, pp. 169-179.

Woodford, A. C. & Chevallier, L., 2002. Regional characterization and mapping of Karoo fractured aquifer systems - an integrated approach using a geographical information system and digital processing. *Water Research Commission Report,* Volume 653/1/02.

Wotzlaw, J. F. et al., 2014. Towards accurate numerical calibration of the Late Triassic: High-precision U-Pb geochronology constraints on the duration of the Rhaetian. *Geology,* 42(7), pp. 571-574.

Yates, A. M., 2003. The species taxonomy of the sauropodomorph dinosaurs from the Löwenstein Formation (Norian, Late Triassic) of Germany. *Palaeontology,* Volume 46, pp. 317-337.

Yates, A. M., 2005. A new theropod dinosaur from the Early Jurassic of South Africa and its implications for the early evolution of theropods. *Palaeontologia Africana,* Volume 41, pp. 105-122.

Yates, A. M., 2007a. The first complete skull of the Triassic dinosaur Melanorosaurus Haughton (Sauropodomorpha: Anchisauria). *Special Papers in Paleontology,* Volume 77, pp. 9-55.

Yates, A. M., 2007b. Solving a dinosaurian puzzle: the identity of Aliwalia rex Galton, Historical Biology. *An International Journal of Paleobiology,* 19(1), pp. 93-123.

Yates, A. M. et al., 2010. A new transitional sauropodomorph dinosaur from the Early Jurassic of South Africa and the evolution of sauropod feeding and quadrupedalism. *Proceedings of the Royal Society B: Biological Sciences,* Volume 277, pp. 787-794.

Yates, A. M. & Kitching, J. W., 2003. The earliest known sauropod dinosaur and the first steps towards sauropod locomotion. *Proceedings of the Royal Society of London. Series B: Biological Sciences,* Volume 270, pp. 1753-1758.

Zeigler, K. E., Kelley, S. & Geissman, J. W., 2008. Revisions to stratigraphic nomenclature of the Upper Triassic Chinle Group in New Mexico: new insights from geologic mapping, sedimentology, and magnetostratigraphic/paleomagnetic data. *Rocky Mt Geol.,* Volume 43, pp. 121-141.